

**EVALUATION OF BASE ISOLATION AND SOIL STRUCTURE
INTERACTION EFFECTS ON SEISMIC RESPONSE OF BRIDGES**

A Dissertation

by

WENTAO DAI

Submitted to the Office of Graduate Studies of
Texas A&M University
in partial fulfillment of the requirements for the degree of

DOCTOR OF PHILOSOPHY

August 2005

Major Subject: Civil Engineering

**EVALUATION OF BASE ISOLATION AND SOIL STRUCTURE
INTERACTION EFFECTS ON SEISMIC RESPONSE OF BRIDGES**

A Dissertation

by

WENTAO DAI

Submitted to the Office of Graduate Studies of
Texas A&M University
in partial fulfillment of the requirements for the degree of

DOCTOR OF PHILOSOPHY

Approved by:

Chair of Committee,	Jose M. Roësset
Committee Members,	Charles P Aubeny
	Giovanna Biscontin
	James D Murff
	Chii-Der (Steve) Suh
Head of Department,	David Rosowsky

August 2005

Major Subject: Civil Engineering

ABSTRACT

Evaluation of Base Isolation and Soil Structure Interaction Effects on Seismic Response of Bridges. (August 2005)

Wentao Dai, B. En., Tongji University, China;

M.S., Tongji University, China

Chair of Advisory Committee: Dr. Jose M. Roësset

A continuous formulation to calculate the dynamic stiffness matrix of structural members with distributed masses is presented in detail and verified with some simple examples.

The dynamic model of a specific bridge (the Marga-Marga bridge in Chile) was developed using this formulation, and the model was then used to obtain the transfer functions of the motions at different points of the bridge due to seismic excitation. The model included rubber pads, used for base isolation, as additional members. The transfer functions were obtained with and without rubber pads to investigate their effect.

The dynamic stiffness of complete pile foundations was calculated by a semi-analytical solution with Poulos' assumption. General observations on group effects under various conditions were obtained from the result of these studies. The dynamic stiffness of the pile foundations for the Marga-Marga bridge was then obtained and used to study the soil structure interaction effects on the seismic response of the bridge.

Records obtained during a real earthquake were examined and interpreted in light of the results from all these analyses. Finally, conclusions and recommendations on future studies are presented.

*To Everybody
In My Dreams!*

ACKNOWLEDGMENTS

I would like to express my cordial gratitude to Dr. Jose M. Roësset, the chair of my committee. He taught and gave me much during my 3 year study at Texas A&M University. He is a model for me, for he has demonstrated to me how to become a professional and successful researcher, as well as a complete man with integrity.

I also want to extend my thanks to Dr. Charles Aubeny, Dr. Giovanna Biscontin and Dr. Don Murff. Their encouragement and suggestions helped me very much with my research.

The information and knowledge I learned from Dr. Steve Suh's courses enlightened me during my research. I extend sincere appreciation to him, and I wish I could learn more from him.

I am also indebted to my family and friends for their enduring support.

TABLE OF CONTENTS

	Page
ABSTRACT.....	iii
DEDICATION.....	iv
ACKNOWLEDGMENTS.....	v
TABLE OF CONTENTS.....	vi
LIST OF FIGURES.....	viii
LIST OF TABLES.....	xviii
 CHAPTER	
I DESCRIPTION OF PROBLEM.....	1
1.1 Objective.....	1
1.2 Base Isolation.....	1
1.3 Soil Structure Interaction (SSI).....	3
1.4 Marga-Marga Bridge.....	5
1.5 Previous Studies.....	6
1.6 Outline of Research.....	6
1.7 Dissertation Outline.....	7
II STRUCTURAL FORMULATION.....	8
2.1 Dynamic Stiffness Matrix of a Prismatic Member.....	8
2.2 Verification of the Program Spfram.for.....	18
2.3 Program Bridge.for.....	21
III DYNAMIC STIFFNESS OF PILE FOUNDATIONS.....	37
3.1 Formulation of Dynamic Stiffness of Pile Groups.....	37
3.2 Results.....	42
IV DYNAMIC STIFFNESS OF FOUNDATIONS OF MARGA-MARGA BRIDGE'S PIERS.....	71

CHAPTER	Page
4.1 Introduction.....	71
4.2 Dimensions of Pile Groups and Soil Properties.....	72
4.3 Dynamic Stiffness of Pile Foundations.....	76
4.4 Dynamic Stiffness with Reduced Soil Shear Modulus.....	88
 V EFFECT OF RUBBER PADS' STIFFNESS.....	 97
5.1 Properties of Structure.....	97
5.2 Numbering of Structure.....	103
5.3 Results.....	104
5.4 Conclusions.....	120
 VI EFFECT OF SOIL STRUCTURE INTERACTION.....	 122
6.1 Assumptions.....	122
6.2 Loads.....	123
6.3 Results.....	124
6.4 Conclusions.....	141
 VII CONCLUSIONS AND RECOMMENDATIONS.....	 142
7.1 General Observations.....	142
7.2 Data from a Real Earthquake.....	143
7.3 Recommendations for Future Studies.....	149
 REFERENCES.....	 150
 APPENDIX.....	 157
 VITA.....	 173

LIST OF FIGURES

FIGURE	Page
I.1 Normal Rubber Bearing (NRB) (Made of Alternating Layers of Rubber and Steel).....	2
I.2 The Marga-Marga Bridge.....	5
II.1 A Beam Pinned at Two Ends.....	19
II.2 Overview of the Marga-Marga Bridge in Chile.....	21
II.3 Cross Section of the Bridge.....	22
II.4 Nodal and Element Number of a Bridge with Rubber Pads.....	23
II.5 Nodal and Element Number of a Bridge without Rubber Pads.....	23
II.6 Forces and Displacements Transformation of Deck Members.....	24
II.7 Stiffness Matrix Transformation of Deck Members.....	26
II.8 Displacement at Node 11 in X Direction due to X Motion at Node 1.....	29
II.9 Displacement at Node 11 in Y Direction due to Y Motion at Node 1.....	29
II.10 Displacement at Node 11 in Z Direction due to Z Motion at Node 1.....	30
II.11 Displacement at Node 12 in X Direction due to X Motion at Node 4.....	30
II.12 Displacement at Node 12 in Y Direction due to Y Motion at Node 4.....	31
II.13 Displacement at Node 12 in Z Direction due to Z Motion at Node 4.....	31
III.1 Interaction of Two Piles in Horizontally Layered Soil Deposit.....	39
III.2 Definition of Equivalent Area for Pile Groups.....	43
III.3 Static Group Reduction Factors ($E_p/E_s=1000$).....	45
III.4 Effect of E_p/E_s on Group Factors (No Threshold Distance).....	46

FIGURE	Page
III.5 Static Stiffness Comparison ($E_S = \text{Constant} = 5E7 \text{ N/m}^2$, $H = 40\text{m}$).....	47
III.6 Effect of Number of Piles on Normalized Real Coefficients (k_1) ($E_P/E_S = 1000$, 2% Material Damping, No Threshold Distance, End Bearing Piles).....	48
III.7 A Single Degree of Freedom System.....	49
III.8 Least Square Fit of the Real Stiffness Coefficients.....	49
III.9 Equivalent Mass from Least Square Fit ($E_P = 1000E_S = 5E10$, 2% Material Damping, No Threshold Distance, End Bearing Piles).....	50
III.10 Effect of S_{\max} on Real Stiffness Coefficients of a 6 by 6 Pile Group ($E_P = 1000E_S = 5E10$, 2% Material Damping, End Bearing Piles).....	51
III.11 Effect of Number of Pile on Normalized Imaginary Coefficients (c_1) ($E_P/E_S = 1000$, 2% Material Damping, No Threshold Distance, End Bearing Piles)	52
III.12 Effect of E_P/E_S on Normalized Imaginary Coefficients (c_1) of Single Pile ($E_S = \text{Constant} = 5E7$, 2% Material Damping, No Threshold Distance, End Bearing Piles)	53
III.13 Effect of S_{\max} on Imaginary Stiffness Coefficients of a 6 by 6 Pile Group ($E_P = 1000E_S = 5E10$, 2% Material Damping, End Bearing Piles)	53
III.14 Effect of S_{\max} on Equivalent Dashpot Constant of a 6 by 6 Pile Group ($E_P = 1000E_S = 5E10$, 2% Material Damping, End Bearing Piles)	54
III.15 Vertical Static Group Factors for Vertical Stiffness ($E_P/E_S = 1000$, Floating Piles).....	55
III.16 Vertical Static Group Factors for Vertical Stiffness ($E_P/E_S = 1000$, End Bearing Piles).....	56
III.17 Effect of E_P/E_S on Vertical Group Factors (No Threshold Distance, Floating Piles)	57
III.18 Effect of E_P/E_S on Vertical Group Factors (No Threshold Distance, End Bearing Piles)	57

FIGURE	Page
III.19 Effect of Number of Piles on Real Coefficients ($E_P=1000E_S=5E10$, 2% Material Damping, No Threshold Distance, Floating Piles)	58
III.20 LSF of Equivalent Mass of Vertical Stiffness.....	59
III.21 Equivalent Mass with Number of Piles.....	60
III.22 Effect of Threshold Distance on Real Coefficients of 6 by 6 Pile Groups ($E_P=1000E_S=5E10$, 2% Material Damping, Floating Piles).....	60
III.23 Effect of Number of Piles on Imaginary Coefficients ($E_P=1000E_S=5E10$, 2% Material Damping, No Threshold Distance, Floating Piles).....	60
III.24 Effect of E_P/E_S on Imaginary Coefficients of Single Piles ($E_S=Constant$ $=5E10$, 2% Material Damping, No Threshold Distance, Floating Piles)....	62
III.25 Static Group Reduction Factor for Rocking Stiffness ($E_P/E_S=1000$, Floating Piles)	63
III.26 Static Group Reduction Factor for Rocking Stiffness ($E_P/E_S=1000$, End Bearing Piles).....	64
III.27 Effect of E_P/E_S on Static Group Factor (No Threshold Distance, Floating Piles)	65
III.28 Effect of E_P/E_S on Static Group Factor (No Threshold Distance, End Bearing Piles).....	65
III.29 Effect of Number of Piles on Real Coefficients ($E_P=1000E_S=5E10$, 2% Material Damping, No Threshold Distance, Floating Piles).....	66
III.30 Least Square Fit of Equivalent Inertia of Rotation of Rocking Stiffness....	67
III.31 Equivalent Inertia of Rotation with Number of Piles.....	68
III.32 Effect of Limit Distance on Real Coefficients of 6 by 6 Pile Groups ($E_P=1000E_S=5E10$, 2% Material Damping, Floating Piles).....	69
III.33 Effect of Number of Piles on Imaginary Coefficients ($E_P=1000E_S=5E10$, 2% Material Damping, No Threshold Distance, Floating Piles).....	70

FIGURE	Page
III.34 Effect of E_p/E_s on Imaginary Coefficients of 2 by 2 Pile Groups (2% Material Damping, No Threshold Distance, Floating Piles).....	70
IV.1 Piers and Pile Groups of Marga-Marga Bridge.....	71
IV.2 A Pier and Its Pile Foundation.....	72
IV.3 Dimensions of Cap and Pile Spacing.....	73
IV.4 Real Part of Horizontal Stiffness in Y Direction.....	77
IV.5 Imaginary Part of Horizontal Stiffness in Y Direction.....	77
IV.6 Real Part of Horizontal Stiffness in X Direction.....	78
IV.7 Imaginary Part of Horizontal Stiffness in X Direction.....	78
IV.8 Real Part of Horizontal Stiffness of an Equivalent Surface Mat.....	79
IV.9 Imaginary Part of Horizontal Stiffness of an Equivalent Surface Mat.....	79
IV.10 Real Part of Vertical Stiffness.....	80
IV.11 Imaginary Part of Vertical Stiffness.....	82
IV.12 Real Part of Vertical Stiffness of an Equivalent Surface Mat.....	82
IV.13 Imaginary Part of Vertical Stiffness of an Equivalent Surface Mat.....	83
IV.14 Real Part of Rocking Stiffness around X Axis.....	83
IV.15 Imaginary Part of Rocking Stiffness around X Axis.....	84
IV.16 Real Part of Rocking Stiffness around Y Axis.....	84
IV.17 Imaginary Part of Rocking Stiffness around Y Axis.....	85
IV.18 Real Part of Rocking Stiffness around X Axis of an Equivalent Surface Mat.....	85
IV.19 Imaginary Part of Rocking Stiffness around X Axis of an Equivalent Surface Mat.....	86

FIGURE	Page
IV.20 Real Part of Rocking Stiffness around Y Axis of an Equivalent Surface Mat.....	86
IV.21 Imaginary Part of Rocking Stiffness around Y Axis of an Equivalent Surface Mat.....	87
IV.22 Stiffness of Surface Mat of Pier #1 & Pier #7.....	88
IV.23 New Real Part of Horizontal Stiffness in X Direction.....	91
IV.24 New Imaginary Part of Horizontal Stiffness in X Direction.....	91
IV.25 New Real Part of Horizontal Stiffness in Y Direction.....	92
IV.26 New Imaginary Part of Horizontal Stiffness in Y Direction.....	92
IV.27 New Real Part of Vertical Stiffness.....	93
IV.28 New Imaginary Part of Vertical Stiffness.....	93
IV.29 New Real Part of Rocking Stiffness around X Axis.....	94
IV.30 New Imaginary Part of Rocking Stiffness around X Axis.....	94
IV.31 New Real Part of Rocking Stiffness around Y Axis.....	95
IV.32 New Imaginary Part of Rocking Stiffness around Y Axis.....	95
IV.33 New Stiffness of Surface Mat under Pier #1 & Pier #7.....	96
V.1 Overview of Marga-Marga Bridge.....	97
V.2 Cross Section of Deck.....	98
V.3 Transverse View of Pier and Its Dimensions.....	99
V.4 Cross Section of Pier.....	100
V.5 Rubber Pads on Top of Pier.....	101
V.6 Elements and Nodal Numbering of Marga-Marga Bridge (without Rubber Pads).....	103

FIGURE	Page
V.7 Elements and Nodal Numbering of Marga-Marga Bridge (with Rubber Pads).....	104
V.8 Displacement in X Direction at Top of Pier 4 due to Unit Motion at Base of All Piers (without Rubber Pads).....	106
V.9 Displacement in X Direction due to Unit Motion at Base of All Piers (with Rubber Pads, $G = 6.0 \times 10^6$ Pa, Free Deck).....	107
V.10 Displacement in X Direction due to Unit Motion at Base of Pier 4 (with Rubber Pads, $G = 6.0 \times 10^6$ Pa, Free Deck).....	108
V.11 Displacement in X Direction due to Unit Motion at Base of All Piers (with Rubber Pads, $G = 1.8 \times 10^6$ Pa, Free Deck).....	109
V.12 Displacement in X Direction due to Unit Motion at Base of All Piers (with Rubber Pads, $G = 1.0 \times 10^6$ Pa, Free Deck).....	109
V.13 Displacement in X Direction due to Unit Motion at Base of All Piers (with Rubber Pads, $G = 6.0 \times 10^6$ Pa, Constrained Deck).....	111
V.14 Displacement in X Direction due to Unit Motion at Base of Pier 4 (with Rubber Pads, $G = 6.0 \times 10^6$ Pa, Constrained Deck).....	111
V.15 Displacement in X Direction due to Unit Motion at Base of All Piers (with Rubber Pads, $G = 1.8 \times 10^6$ Pa, Constrained Deck).....	112
V.16 Displacement in X Direction due to Unit Motion at Base of All Piers (with Rubber Pads, $G = 1.0 \times 10^6$ Pa, Constrained Deck).....	112
V.17 Displacement in Y Direction at Top of Pier 4 due to Unit Motion at Base of All Piers (without Rubber Pads).....	113
V.18 Displacement in Y Direction due to Unit Motion at Base of All Piers (with Rubber Pads, $G = 6.0 \times 10^6$ Pa, Free Deck).....	114
V.19 Displacement in Y Direction due to Unit Motion at Base of All Piers (with Rubber Pads, $G = 1.8 \times 10^6$ Pa, Free Deck).....	115

FIGURE	Page
V.20 Displacement in Y Direction due to Unit Motion at Base of All Piers (with Rubber Pads, $G = 1.0 \times 10^6$ Pa, Free Deck).....	115
V.21 Displacement in Y Direction due to Unit Motion at Base of All Piers (with Rubber Pads, $G = 6.0 \times 10^6$ Pa, Constrained Deck).....	116
V.22 Displacement in Y Direction due to Unit Motion at Base of All Piers (with Rubber Pads, $G = 1.8 \times 10^6$ Pa, Constrained Deck).....	117
V.23 Displacement in Y Direction due to Unit Motion at Base of All Piers (with Rubber Pads, $G = 1.0 \times 10^6$ Pa, Constrained Deck).....	117
V.24 Displacement in Z Direction at Top of Pier 4 due to Unit Motion at Base of All Piers (without Rubber Pads).....	118
V.25 Displacement in Z Direction due to Unit Motion at Base of All Piers (with Rubber Pads, $E = 1.8 \times 10^9$ Pa, Free Deck).....	119
V.26 Displacement in Z Direction due to Unit Motion at Base of All Piers (with Rubber Pads, $E = 1.8 \times 10^9$ Pa, Free Deck).....	120
VI.1 Displacement in X Direction at Top of Pier 4 due to Unit Motion at Base of All Foundations (without Rubber Pads).....	124
VI.2 Displacement in X Direction due to Unit Motion at Base of All Foundations (with Rubber Pads, $G = 6.0 \times 10^6$ Pa, Free Deck).....	126
VI.3 Displacement in X Direction due to Unit Motion at Base of Foundation under Pier 4 (with Rubber Pads, $G = 6.0 \times 10^6$ Pa, Free Deck).....	127
VI.4 Displacement in X Direction due to Unit Motion at Base of All Foundations (with Rubber Pads, $G = 1.8 \times 10^6$ Pa, Free Deck).....	127
VI.5 Displacement in X Direction due to Unit Motion at Base of All Foundations (with Rubber Pads, $G = 1.0 \times 10^6$ Pa, Free Deck).....	128
VI.6 Displacement in X Direction due to Unit Motion at Base of All Foundations (with Rubber Pads, $G = 6.0 \times 10^6$ Pa, Constrained Deck).....	128

FIGURE	Page
VI.7 Displacement in X Direction due to Unit Motion at Base of the Foundation under Pier 4 (with Rubber Pads, $G = 6.0 \times 10^6$ Pa, Constrained Deck).....	129
VI.8 Displacement in X Direction due to Unit Motion at Base of All Foundations (with Rubber Pads, $G = 1.8 \times 10^6$ Pa, Constrained Deck).....	129
VI.9 Displacement in X Direction due to Unit Motion at Base of All Foundations (with Rubber Pads, $G = 1.0 \times 10^6$ Pa, Constrained Deck).....	130
VI.10 Motion of the Base of Pier 4 When All Foundations Are Excited in the X Direction (Free Deck).....	130
VI.11 Motion of the Base of Pier 4 When All Foundations Are Excited in the X Direction (Constrained Deck).....	131
VI.12 Displacement in Y Direction at Top of Pier 4 due to Unit Motion at Base of All Foundations (without Rubber Pads).....	132
VI.13 Displacement in Y Direction due to Unit Motion at Base of All Foundations (with Rubber Pads, $G = 6.0 \times 10^6$ Pa, Free Deck).....	133
VI.14 Displacement in Y Direction due to Unit Motion at Base of All Foundations (with Rubber Pads, $G = 1.8 \times 10^6$ Pa, Free Deck).....	134
VI.15 Displacement in Y Direction due to Unit Motion at Base of All Foundations (with Rubber Pads, $G = 1.0 \times 10^6$ Pa, Free Deck).....	134
VI.16 Displacement in Y Direction due to Unit Motion at Base of All Foundations (with Rubber Pads, $G = 6.0 \times 10^6$ Pa, Constrained Deck).....	135
VI.17 Displacement in Y Direction due to Unit Motion at Base of All Foundations (with Rubber Pads, $G = 1.8 \times 10^6$ Pa, Constrained Deck).....	135
VI.18 Displacement in Y Direction due to Unit Motion at Base of All Foundations (with Rubber Pads, $G = 1.0 \times 10^6$ Pa, Constrained Deck).....	136
VI.19 Motion of the Base of Pier 4 When All Foundations Are Excited in the Y Direction (Free Deck).....	136

FIGURE	Page
VI.20 Motion of the Base of Pier 4 When All Foundations Are Excited in the Y Direction (Constrained Deck).....	137
VI.21 Displacement in Z Direction at Top of Pier 4 due to Unit Motion at Bottom of All Foundations (without Rubber Pads).....	138
VI.22 Displacement in Z Direction due to Unit Motion at Base of All Foundations (with Rubber Pads, $E = 6.0 \times 10^9$ Pa, Free Deck).....	138
VI.23 Displacement in Z Direction due to Unit Motion at Base of All Foundations (with Rubber Pads, $E = 6.0 \times 10^9$ Pa, Free Deck).....	139
VII.1 FFT of Recorded Longitudinal (X) Motion of Marga-Marga Bridge during the Earthquake of July 24, 2001.....	145
VII.2 FFT of Recorded Transverse (Y) Motion of Marga-Marga Bridge during the Earthquake of July 24, 2001.....	145
VII.3 FFT of Recorded Vertical (Z) Motion of Marga-Marga Bridge during the Earthquake of July 24, 2001.....	148
VII.4 One-dimensional Horizontal Soil Amplification of the Soil Deposit.....	148
A.1 The 1 st Mode Shape of the Bridge in Figure II.5.....	157
A.2 The 2 nd Mode Shape of the Bridge in Figure II.5.....	158
A.3 The 3 rd Mode Shape of the Bridge in Figure II.5.....	158
A.4 The 4 th Mode Shape of the Bridge in Figure II.5.....	159
A.5 The 5 th Mode Shape of the Bridge in Figure II.5.....	159
A.6 The 6 th Mode Shape of the Bridge in Figure II.5.....	160
A.7 The 7 th Mode Shape of the Bridge in Figure II.5.....	160
A.8 The 8 th Mode Shape of the Bridge in Figure II.5.....	161
A.9 The 9 th Mode Shape of the Bridge in Figure II.5.....	161
A.10 The 10 th Mode Shape of the Bridge in Figure II.5.....	162

FIGURE	Page
A.11 The 11 th Mode Shape of the Bridge in Figure II.5.....	162
A.12 The 12 th Mode Shape of the Bridge in Figure II.5.....	163
A.13 The 13 th Mode Shape of the Bridge in Figure II.5.....	163
A.14 The 14 th Mode Shape of the Bridge in Figure II.5.....	164
A.15 The 15 th Mode Shape of the Bridge in Figure II.5.....	164
A.16 The 16 th Mode Shape of the Bridge in Figure II.5.....	165
A.17 The 17 th Mode Shape of the Bridge in Figure II.5.....	165
A.18 The 18 th Mode Shape of the Bridge in Figure II.5.....	166
A.19 The 19 th Mode Shape of the Bridge in Figure II.5.....	166
A.20 The 20 th Mode Shape of the Bridge in Figure II.5.....	167
A.21 The 21 st Mode Shape of the Bridge in Figure II.5.....	167
A.22 The 22 nd Mode Shape of the Bridge in Figure II.5.....	168
A.23 The 23 rd Mode Shape of the Bridge in Figure II.5.....	168
A.24 The 24 th Mode Shape of the Bridge in Figure II.5.....	169
A.25 The 25 th Mode Shape of the Bridge in Figure II.5.....	169
A.26 The 26 th Mode Shape of the Bridge in Figure II.5.....	170
A.27 The 27 th Mode Shape of the Bridge in Figure II.5.....	170
A.28 The 28 th Mode Shape of the Bridge in Figure II.5.....	171
A.29 The 29 th Mode Shape of the Bridge in Figure II.5.....	171
A.30 The 30 th Mode Shape of the Bridge in Figure II.5.....	172

LIST OF TABLES

TABLE	Page
II.1	Natural Frequencies for Different Values of Axial Load..... 20
II.2	Natural Frequencies and Mode Shapes Description of the Bridge in Figure II.5 (from ABAQUS) (Length of each segment is 0.05m)..... 33
II.3	Natural Frequencies and Mode Shapes Description of the Bridge in Figure II.5 (from ABAQUS) (Each member is considered as one segment, which is 10~14m-long)..... 34
II.4	Natural Frequencies and Mode Shapes Description of the Bridge in Figure II.5 (from ABAQUS) (Each member is considered as two segments, which is 5~7m-long)..... 35
II.5	Natural Frequencies and Mode Shapes Description of the Bridge in Figure II.5 (from ABAQUS) (Each member is about 3m-long)..... 36
IV.1	Dimension of the Pier and Cap..... 73
IV.2	Length and Diameter of Piles..... 74
IV.3	Soil Properties for Pier #2..... 74
IV.4	Soil Properties for Pier #3 and #4..... 75
IV.5	Soil Properties for Pier #5..... 75
IV.6	Soil Properties for Pier #6..... 76
IV.7	Reduced Soil Properties for Pier #2..... 89
IV.8	Reduced Soil Properties for Pier #3 and #4..... 89
IV.9	Reduced Soil Properties for Pier #5..... 89
IV.10	Reduced Soil Properties for Pier #6..... 90
V.1	Natural Frequencies of Marga-Marga Bridge from Former Studies..... 105
VI.1	Effect of SSI on Peaks of Transfer Function in Longitudinal Direction..... 125

TABLE	Page
VI.2 Effect of SSI on Peaks of Transfer Function in Transverse Direction.....	132
VI.3 Effect of SSI on Peaks of Transfer Function in Longitudinal Direction (with New Soil Properties).....	140
VI.4 Effect of SSI on Peaks of Transfer Function in Transverse Direction (with New Soil Properties).....	140

CHAPTER I

DESCRIPTION OF PROBLEM

1.1 Objective

The purpose of this work is to evaluate the effectiveness and efficiency of base isolation on the seismic response of bridges and the potential importance of soil-structure interaction effects. The dynamic stiffness of the complete system, including the structure, the foundations and the isolation pads, is obtained in the frequency domain. The transfer functions of the motions at some points on the bridge due to motions at the base of all the piers or only one pier are calculated to examine the frequency response characteristics of the system.

The objective of this research is to evaluate through some parametric studies the effects of base isolation and soil structure interaction on the seismic response of bridges, with application to a particular bridge, the Marga-Marga bridge, in Chile, for which data were available, in order to use realistic parameters. This bridge uses hard rubber pads at the abutments and on top of each pier for base isolation and has pile foundations for five of its seven piers.

1.2 Base Isolation

Although I-Elastomeric bearings were first used in 1969 in Italy, base isolation techniques were not widely used in civil structures to resist lateral forces before the 1990's. Since the first design provisions appeared in the 1991 Uniform Building Code (UBC), the use of base isolators as a part of a structure in addition to conventional

This dissertation follows the style and format of the *Journal of Geotechnical and Environmental Engineering, ASCE*.

materials (steel, concrete, etc.) has become more and more popular in severe seismic hazard areas, and now base isolation plays an important part in the area of structural control.

Extensive research has been done on the effect of base isolation on bridges since the 1990's, when the technique started to be widely used to protect bridges from the effect of seismic motions. Tan et al. (1993, 1996, 2000), Chaudhary et al. (1998, 2000, 2001a, 2001b, 2002a), Shinozuka et al. (2001) and Crouse and McGuire (2001) worked on the system identification of base isolated bridges, in some cases considering the effect of soil structure interaction. Park et al. (2002), Chaudhary et al. (2002b) and Su et al. (1989, 1990) used real earthquake records to investigate the behavior of base isolated bridges and compared the performance of different kinds of base isolators.

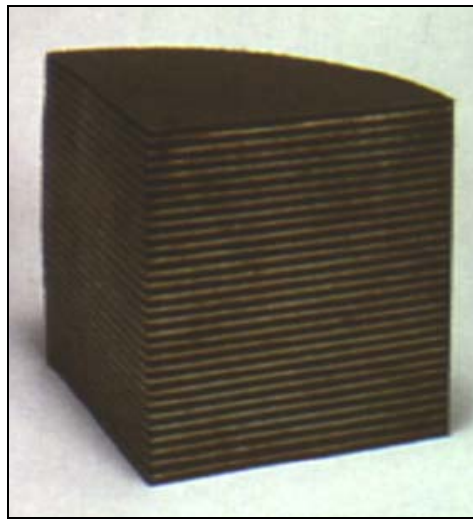


Figure I.1 Normal Rubber Bearing (NRB)
(Made of Alternating Layers of Rubber and Steel)

The base isolators used in the Marga-Marga bridge are Normal Rubber Bearings (NRB). As shown in Figure I.1, they are made of alternating layers of steel and rubber to achieve

a low horizontal stiffness with a high vertical stiffness, to provide a uniform transfer of vertical load from the girder to the piers but to mitigate the horizontal load transfer from the piers to the girder during the earthquake. The NRBs can extend the natural period of the structure as well as absorb the earthquake energy through their hysteretic damping (Skinner et al. 1993).

There have been many models proposed by researchers to study the behavior of the isolated structure or of the bearings by themselves. Most of them have been nonlinear models in the time domain to perform time history analysis. In some linear models, each rubber layer of the bearing has been considered to be linear, homogeneous and isotropic and treated as an equivalent column to calculate its stiffness matrix using beam theory (Haringx, 1949). All rubber and steel layers were then combined to get the stiffness matrix of the bearing pad and the matrix was then condensed to relate only end forces and displacements (Chang, 2002). Seki et al. (1987), Takayama et al. (1990), Billings (1993) and Matsuda (1999, 2001) developed two- or three-dimensional finite element models of the NRBs to investigate the internal stress-strain relationship under large deformations and gave some recommendations on the value of the hysteretic damping. In this research, the whole rubber pad will be considered as an equivalent structural member to evaluate its dynamic stiffness in the same way as for the structural members, using Timoshenko beam theory.

1.3 Soil Structure Interaction (SSI)

The conventional design method of a building or a bridge assumes that the foundations are fixed. The internal forces in the structural members, including the forces transferred from the base columns or the piers to the foundation, are calculated, and the strength of the foundation and settlements of the subsoil are then estimated. The problem is that the settlement of the foundation will change the internal forces in the superstructure. The

stiffness of the foundation should be incorporated in the model of the structure to perform a soil structure interaction analysis.

The effects of soil structure interaction (SSI) on the dynamic response of bridges have been extensively studied. The superstructures were normally discretized into structural members with concentrated or consistent mass matrices, while the foundations could be modeled using different methods. The simplest model is to use Winkler's assumption to model the soils as springs to support spread footings or piles (Crouse et al. 1987; Casas, 1997; Mylonakis et al. 1997; McGuire et al. 1998; Hutchinson et al. 2004). With this model the effect of inertia forces of the soil and the radiation damping were not included. Other researchers (Levine and Scott, 1989; Spyrakos, 1990; Spyrakos and Loannidis, 2003; Harada et al. 1994; Makins et al. 1994, 1996; Chaudhry and Prakash, 1998; Tongaokar and Jangid, 2003) modeled the soils or piles as a single degree freedom with coefficients for the mass, spring and dashpot, as recommended by Wolf (1988). Iwasaki et al. (1984) and Takemiya (1985) simplified the subsoil into a one-dimensional soil column to calculate its dynamic stiffness. Finite element (Kuribaya and Iida, 1974; Yamada and Kawano, 1979; Dendrou et al. 1984; Zheng and Takeda, 1995; Consolazio et al. 2003) or Boundary element formulations (Betti, 1995; Guin and Banerjee, 1998) were also widely used in the modeling of the soils and piles. Crouse and Price (1993), Takemiya and Yamada (1981) and Saadeghvaziri et al. (2000) used analytical or semi-analytical formulations similar to the one used in this research. Lee and Dasgupta (1984) modeled the soil under the piers with nonlinear finite elements and the outer region with an analytical frequency dependent stiffness. Other studies concentrated on the nonlinear soil behavior (Hino and Tanabe, 1986; Zechlin and Chai, 1998; Carrubba et al. 2003).

In this work, the dynamic stiffness of pile groups is investigated using an Elastodynamic solution with Poulos' method (1971) in the frequency domain. The dynamic stiffness of the surface foundations for the piers without pile foundations was calculated

using also an Elasto-dynamic solution. After combining the dynamic stiffness of the structure and the foundation, the effect of soil structure interaction is evaluated.

1.4 Marga-Marga Bridge

The Marga-Marga bridge, shown schematically in Figure I.2, is an actual bridge in Chile. The deck, which is 383 meters long, consists of 8 spans, all 50 meters long, except for the first one (connecting the south abutment and pier 1), which is 33 meters long. On top of each pier and of the two abutments are rubber pads (base isolators). The bridge has seven piers (P1~P7), five of them (P2~P6) with pile foundations. Each of the pile foundations consists of a 5 by 2 pile group (rows of 5 piles in the direction perpendicular to the figure and 2 in the longitudinal direction of the bridge). Piers P1 and P7 have surface mat foundations without any supporting piles. The bridge was instrumented after construction and a number of earthquake records were obtained.

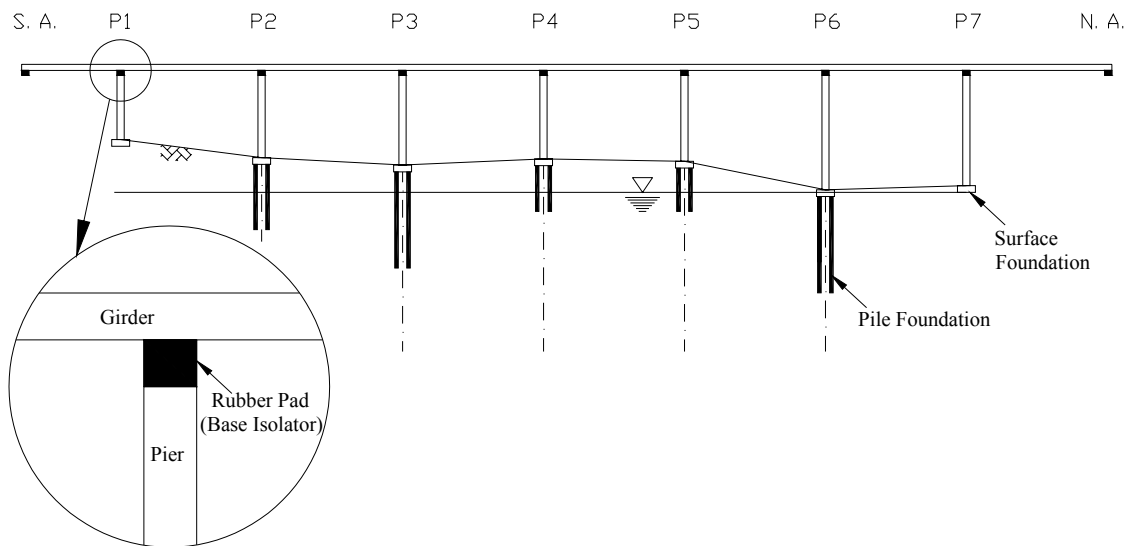


Figure I.2 The Marga-Marga Bridge

1.5 Previous Studies

Seismic analyses of the Marga-Marga bridge had been conducted by a number of students at the University of Chile. M.E. Segovia developed in 1997 a model to calculate the natural frequencies of the bridge with or without rubber pads; D. Romo (1999) develop in 1999 a different model using finite elements (shell elements), studying the effect of the boundary conditions at the two ends of the deck; Another finite element model has implemented by V.M. Daza in 2003 including soil structure interaction effects.

1.6 Outline of Research

The research conducted in this work consists of the following steps:

- Development of a computational model for a three-dimensional bridge structure with distributed masses in the frequency domain. This model includes the piers, girders and slab as well as the isolation pads. It will accept as input the dynamic stiffness of the foundations, computed separately, as functions of frequency. The model was implemented in a computer program and tested for accuracy;
- Determination of the dynamic stiffness terms for pile foundations. Some preliminary studies were conducted to investigate the nature and importance of group effects and the effect of limiting the interaction between piles when their separation exceeds a given distance. The program developed to determine the dynamic stiffness of pile groups was then used to compute the stiffness of the pile foundations of the Marga-Marga bridge. A separate program was used to compute the stiffness of the surface foundations of two piers;

- Parametric studies were conducted to assess the effectiveness of the base isolation assuming first rigid foundations, without soil structure interaction effects. The stiffness of the rubber pads was changed to study the effect of their properties on the seismic response of the bridge, looking at the transfer functions for the motions at various points due to unit motions at the base of the piers;
- The same type of studies were carried out including now soil structure interaction effects to assess their potential importance;

1.7 Dissertation Outline

The formulation of the structural model in the frequency domain is presented in Chapter II with some simple analyses to validate it. Chapter III discusses the dynamic stiffness of pile groups. The results for the foundations of the Marga-Marga bridge are included in Chapter IV. The effect of the stiffness of the rubber pads is investigated and reported in Chapter V while Chapter VI presents the studies on soil structure interaction effects. Conclusions and recommendations for further work are included in Chapter VII.

CHAPTER II

STRUCTURAL FORMULATION

2.1 Dynamic Stiffness Matrix of a Prismatic Member

The use of the dynamic stiffness matrices in the frequency domain for linear structural members with distributed masses provides a more efficient and accurate procedure for the dynamic analysis of frames than lumped or consistent mass matrices. The higher accuracy provided is a major consideration in the interpretation of dynamic non-destructive tests based on impact loads and wave propagation.

The dynamic stiffness matrix for linear structural members with distributed masses were first used by Latona (1969) and extended by Papaleontiou (1992) later to validate the accuracy of lumped and consistent mass matrices. Formulations for beam members and shell elements were then obtained by Kolousěk (1973), Banerjee and William (1985, 1994a, 1994b), Doyle (1989a, 1989b), Gopalakrishnan and Doyle (1994) and Yu and Roësset (2001). Chen and Sheu (1993, 1996), Yu (1995, 1996) and Yu and Roësset (1998) used these formulations to carry out some studies on structural dynamics, soil structure interaction and non-destructive testing. In this chapter, the derivation of the dynamic stiffness matrix associated with the exact continuous solution is carried out using the same approach followed to obtain the static stiffness matrix. The following paragraphs give the main steps of this approach deriving the dynamic stiffness matrix of a prismatic flexural member.

2.1.1 Dynamic Stiffness Matrix for Transverse Deflection

For the transverse behavior of a flexural member, the Timoshenko beam theory includes the shear deformation and rotational inertia of the beam. The governing equations in the frequency domain are

$$\left\{ \begin{array}{l} \frac{\partial \hat{M}}{\partial x} + \hat{V} = -\omega^2 \rho I \hat{\phi} \\ \frac{\partial \hat{Y}}{\partial x} = -\omega^2 \rho A \hat{v} \\ \hat{M} = EI \frac{\partial \hat{\phi}}{\partial x} \\ \hat{V} = \kappa GA \left(\frac{\partial \hat{v}}{\partial x} - \hat{\phi} \right) \\ \hat{Y} = \hat{V} + N \frac{\partial \hat{v}}{\partial x} \end{array} \right. \dots\dots\dots (II.1)$$

in which

ρ, E, G density, Young's modulus and shear modulus of the material;
 κ, I, A ...effective shear area coefficient, moment of inertia and area of the cross section;
 M, V, Y, ϕ, v bending moment, shear force, vertical force, bending rotation and transverse displacement of the cross section;
 $\hat{M}, \hat{V}, \hat{Y}, \hat{\phi}, \hat{v}$ M, V, Y, ϕ, v in frequency domain, respectively;
 N axial force.

In this case, to obtain a linear ordinary differential equation with constant coefficients, all the material properties and cross-section properties are assumed to be constant along the beam. These properties include ρ, E, G, κ, I, A and N .

After combining the above equations, we can get a governing equation with only one unknown- \hat{v} .

$$EI \left(1 + \frac{N}{\kappa GA} \right) \hat{v}^{IV} + \left[\frac{\omega^2 \rho A}{\kappa GA} EI - N + \omega^2 \rho I \left(1 + \frac{N}{\kappa GA} \right) \right] \hat{v}'' + \omega^2 \rho A \left(\frac{\omega^2 \rho I}{\kappa GA} - 1 \right) \hat{v} = 0$$

..... (II.2)

Solving this equation and finding \hat{v} as a function of x and ω , we can find \hat{M} , \hat{V} , \hat{Y} and $\hat{\phi}$ by substituting \hat{v} back into Equation II.1.

$$\text{Defining } \begin{cases} 2\beta = \frac{\omega^2 \rho A}{\kappa GA \left(1 + \frac{N}{\kappa GA}\right)} - \frac{N}{EI \left(1 + \frac{N}{\kappa GA}\right)} + \frac{\omega^2 \rho I}{EI} \\ \alpha^2 = \frac{\omega^2 \rho A}{EI \left(1 + \frac{N}{\kappa GA}\right)} \left(\frac{\omega^2 \rho I}{\kappa GA} - 1\right) \end{cases}$$

we get the characteristic equation $\bar{r}^4 + 2\beta\bar{r}^2 + \alpha^2 = 0 \dots\dots\dots$ (II.3)

It is convenient to express the solution of Equation II.3 for three different cases.

A. Static case without axial force, $\omega = 0$ and $N = 0$;

In this case, $2\beta = \alpha^2 = 0$. The governing equation becomes $EI\hat{v}^{IV} = 0$. The solution of this equation is $\hat{v} = C_1 + C_2x + C_3x^2 + C_4x^3$. From Equation II.1, the expressions for the bending moment, shear force, transverse force and bending rotation can be derived in terms of the transverse displacement \hat{v} . Since $\omega = N = 0$, the expressions are

$$\begin{cases} \hat{M} = EI\hat{v}'' \\ \hat{Y} = \hat{V} = EI\hat{v}''' \\ \hat{\phi} = \hat{v}' + \frac{EI}{\kappa GA}\hat{v}''' \end{cases} \dots\dots\dots$$
 (II.4)

The end displacements $\{\hat{u}\}$ of this case can be expressed in terms of the constants C_i .

$$\{\hat{u}\} = \begin{Bmatrix} \hat{v}_A \\ \hat{\phi}_A \\ \hat{v}_B \\ \hat{\phi}_B \end{Bmatrix} = \begin{Bmatrix} \hat{v}(0) \\ \hat{\phi}(0) \\ \hat{v}(L) \\ \hat{\phi}(L) \end{Bmatrix} = \begin{bmatrix} 1 & 0 & 0 & 0 \\ 0 & 1 & 0 & \frac{6EI}{\kappa GA} \\ 1 & L & L^2 & L^3 \\ 0 & 1 & 2L & 3L^2 + \frac{6EI}{\kappa GA} \end{bmatrix} \begin{Bmatrix} C_1 \\ C_2 \\ C_3 \\ C_4 \end{Bmatrix} = [T_1]\{C\}.$$

The end forces $\{\hat{F}\}$ can also be expressed in terms of the constants C_i .

$$\{\hat{F}\} = \begin{Bmatrix} \hat{Y}_A \\ \hat{M}_A \\ \hat{Y}_B \\ \hat{M}_B \end{Bmatrix} = \begin{Bmatrix} -\hat{Y}(0) \\ -\hat{M}(0) \\ \hat{Y}(L) \\ \hat{M}(L) \end{Bmatrix} = \begin{bmatrix} 0 & 0 & 0 & 6 \\ 0 & 0 & -2 & 0 \\ 0 & 0 & 0 & -6 \\ 0 & 0 & 2 & 6L \end{bmatrix} \begin{Bmatrix} C_1 \\ C_2 \\ C_3 \\ C_4 \end{Bmatrix} = [T_2]\{C\}.$$

The computation of the stiffness matrix $[S_f]$ can be carried out numerically as

$$\{\hat{F}\} = [T_2]\{C\} = [T_2][T_1]^{-1}\{\hat{u}\} = [S_f]\{\hat{u}\}$$

$$[S_f] = [T_2][T_1]^{-1}$$

The result can be written in explicit form as

$$[S_f] = \frac{EI}{1+2\eta} \begin{bmatrix} \frac{12}{L^3} & \frac{6}{L^2} & -\frac{12}{L^3} & \frac{6}{L^2} \\ \frac{6}{L^2} & \frac{2(2+\eta)}{L} & -\frac{6}{L^2} & \frac{2(1-\eta)}{L} \\ -\frac{12}{L^3} & -\frac{6}{L^2} & \frac{12}{L^3} & -\frac{6}{L^2} \\ \frac{6}{L^2} & \frac{2(1-\eta)}{L} & -\frac{6}{L^2} & \frac{2(2+\eta)}{L} \end{bmatrix} \dots \dots \dots (II.5)$$

$$\text{in which } \eta = \frac{6EI}{\kappa GAL^2}.$$

B. For static case with axial force, $\omega = 0$ and $N \neq 0$;

In this case, $\alpha^2 = 0$, but $2\beta = \frac{-N}{EI\left(1 + \frac{N}{\kappa GA}\right)} \neq 0$. The governing equation becomes

$$EI\left(1 + \frac{N}{\kappa GA}\right)\hat{v}^{IV} - N\hat{v}'' = 0.$$

The solution to this equation is $\hat{v} = C_1 + C_2x + C_3e^{r_1x} + C_4e^{r_2x}$, in which $r_1 = -r_2 = \sqrt{-2\beta}$. The expressions of bending moment, shear force, transverse force and bending rotation in the frequency domain are

$$\begin{cases} \hat{M} = EI\left(1 + \frac{N}{\kappa GA}\right)\hat{v}'' \\ \hat{V} = -EI\left(1 + \frac{N}{\kappa GA}\right)\hat{v}''' \\ \hat{Y} = \hat{V} + N\hat{v}' = N\hat{v}' - EI\left(1 + \frac{N}{\kappa GA}\right)\hat{v}''' \\ \hat{\phi} = \hat{v}' + \frac{EI}{\kappa GA}\left(1 + \frac{N}{\kappa GA}\right)\hat{v}''' \end{cases} \dots\dots\dots (II.6)$$

The end displacements $\{\hat{u}\}$ and end forces $\{\hat{F}\}$ can be expressed in terms of the constants C_i .

$$\{\hat{u}\} = \begin{Bmatrix} \hat{v}_A \\ \hat{\phi}_A \\ \hat{v}_B \\ \hat{\phi}_B \end{Bmatrix} = \begin{Bmatrix} \hat{v}(0) \\ \hat{\phi}(0) \\ \hat{v}(L) \\ \hat{\phi}(L) \end{Bmatrix} = \begin{bmatrix} 1 & 0 & 1 & 1 \\ 0 & 1 & r_1\left(1 + \frac{N}{\kappa GA}\right) & r_2\left(1 + \frac{N}{\kappa GA}\right) \\ 1 & L & e^{r_1L} & e^{r_2L} \\ 0 & 1 & r_1\left(1 + \frac{N}{\kappa GA}\right)e^{r_1L} & r_2\left(1 + \frac{N}{\kappa GA}\right)e^{r_2L} \end{bmatrix} \begin{Bmatrix} C_1 \\ C_2 \\ C_3 \\ C_4 \end{Bmatrix} = [T_1]\{C\}$$

$$\begin{aligned} \{\hat{F}\} &= \begin{Bmatrix} \hat{Y}_A \\ \hat{M}_A \\ \hat{Y}_B \\ \hat{M}_B \end{Bmatrix} = \begin{Bmatrix} -\hat{Y}(0) \\ -\hat{M}(0) \\ \hat{Y}(L) \\ \hat{M}(L) \end{Bmatrix} = \begin{bmatrix} 0 & -N & 0 & 0 \\ 0 & 0 & -EI\left(1+\frac{N}{\kappa GA}\right)r_1^2 & -EI\left(1+\frac{N}{\kappa GA}\right)r_2^2 \\ 0 & N & 0 & 0 \\ 0 & 0 & EI\left(1+\frac{N}{\kappa GA}\right)r_1^2 e^{r_1 L} & EI\left(1+\frac{N}{\kappa GA}\right)r_2^2 e^{r_2 L} \end{bmatrix} \begin{Bmatrix} C_1 \\ C_2 \\ C_3 \\ C_4 \end{Bmatrix} \\ &= [T_2]\{C\} \end{aligned}$$

The computation of the stiffness matrix can be carried out numerically as before as $[S_f] = [T_2][T_1]^{-1}$.

C. Dynamic case with or without axial force, which means $\omega \neq 0$;

This is the most general case and neither α nor β are equal to zero, so the governing equation is the same as Equation II.2. The characteristic equation is $\bar{r}^4 + 2\beta\bar{r}^2 + \alpha^2 = 0$. The roots are

$$\begin{cases} r_1 = -r_2 = \sqrt{-\beta + \sqrt{\beta^2 - \alpha^2}} \\ r_3 = -r_4 = \sqrt{-\beta - \sqrt{\beta^2 - \alpha^2}} \end{cases}$$

α and β were defined in Equation II.3. Then the solution to the governing Equation II.2 can be written as $\hat{v} = C_1 e^{r_1 x} + C_2 e^{r_2 x} + C_3 e^{r_3 x} + C_4 e^{r_4 x}$.

Substituting \hat{v} into Equation II.1, the most general expressions for bending moment, shear force, transverse force and bending rotation become

$$\left\{ \begin{array}{l} \hat{M} = EI \left[\left(1 + \frac{N}{\kappa GA} \right) \hat{v}'' + \frac{\omega^2 \rho A}{\kappa GA} \hat{v} \right] \\ \hat{V} = -\frac{\kappa GA}{\kappa GA - \omega^2 \rho I} EI \left(1 + \frac{N}{\kappa GA} \right) \hat{v}''' - \kappa GA \left[\frac{1}{\kappa GA - \omega^2 \rho I} \left(\kappa GA + EI \frac{\omega^2 \rho A}{\kappa GA} \right) - 1 \right] \hat{v}' \quad \dots \text{(II.7)} \\ \hat{Y} = \hat{V} + N\hat{v}' \\ \hat{\phi} = \frac{1}{\kappa GA - \omega^2 \rho I} \left[\left(\kappa GA + EI \frac{\omega^2 \rho A}{\kappa GA} \right) \hat{v}' + EI \left(1 + \frac{N}{\kappa GA} \right) \hat{v}''' \right] \end{array} \right.$$

Equation II.7 can be simplified using the characteristic equation $\bar{r}^4 + 2\beta\bar{r}^2 + \alpha^2 = 0$ as

$$\left\{ \begin{array}{l} \hat{M} = EI \sum_{i=1}^4 \left[r_i^2 \left(1 + \frac{N}{\kappa GA} \right) + \frac{\omega^2 \rho A}{\kappa GA} \right] C_i e^{r_i x} \\ \hat{V} = \hat{Y} - N\hat{v}' = \sum_{i=1}^4 - \left(\frac{\omega^2 \rho A}{r_i} + Nr_i \right) C_i e^{r_i x} \\ \hat{Y} = \sum_{i=1}^4 - \frac{\omega^2 \rho A}{r_i} C_i e^{r_i x} \\ \hat{\phi} = \sum_{i=1}^4 \left[r_i \left(1 + \frac{N}{\kappa GA} \right) + \frac{\omega^2 \rho A}{\kappa GA r_i} \right] C_i e^{r_i x} \end{array} \right.$$

The end displacements $\{\hat{u}\}$ and end forces $\{\hat{F}\}$ can also be derived in the same way as before.

$$\{\hat{u}\} = \begin{Bmatrix} \hat{v}_A \\ \hat{\phi}_A \\ \hat{v}_B \\ \hat{\phi}_B \end{Bmatrix} = \begin{Bmatrix} \hat{v}(0) \\ \hat{\phi}(0) \\ \hat{v}(L) \\ \hat{\phi}(L) \end{Bmatrix} = \begin{bmatrix} 1 & 1 & 1 & 1 \\ R_1 & R_2 & R_3 & R_4 \\ e^{r_1 L} & e^{r_2 L} & e^{r_3 L} & e^{r_4 L} \\ R_1 e^{r_1 L} & R_2 e^{r_2 L} & R_3 e^{r_3 L} & R_4 e^{r_4 L} \end{bmatrix} \begin{Bmatrix} C_1 \\ C_2 \\ C_3 \\ C_4 \end{Bmatrix} = [T_1] \{C\}$$

$$\{\hat{F}\} = \begin{Bmatrix} \hat{Y}_A \\ \hat{M}_A \\ \hat{Y}_B \\ \hat{M}_B \end{Bmatrix} = \begin{Bmatrix} -\hat{Y}(0) \\ -\hat{M}(0) \\ \hat{Y}(L) \\ \hat{M}(L) \end{Bmatrix} = \begin{bmatrix} \frac{\omega^2 \rho A}{r_1} & \frac{\omega^2 \rho A}{r_2} & \frac{\omega^2 \rho A}{r_3} & \frac{\omega^2 \rho A}{r_4} \\ -EIR_1 r_1 & -EIR_2 r_2 & -EIR_3 r_3 & -EIR_4 r_4 \\ -\frac{\omega^2 \rho A}{r_1} e^{r_1 L} & -\frac{\omega^2 \rho A}{r_2} e^{r_2 L} & -\frac{\omega^2 \rho A}{r_3} e^{r_3 L} & -\frac{\omega^2 \rho A}{r_4} e^{r_4 L} \\ EIR_1 r_1 e^{r_1 L} & EIR_2 r_2 e^{r_2 L} & EIR_3 r_3 e^{r_3 L} & EIR_4 r_4 e^{r_4 L} \end{bmatrix} \begin{Bmatrix} C_1 \\ C_2 \\ C_3 \\ C_4 \end{Bmatrix}$$

$$= [T_2] \{C\}$$

in which $R_i = r_i \left(1 + \frac{N}{\kappa GA}\right) + \frac{\omega^2 \rho A}{\kappa GA r_i}$, ($i=1,2,3,4$). The computation of the stiffness

matrix can be carried out numerically again as $[S_f] = [T_2][T_1]^{-1}$.

The resulting stiffness matrices for case A and B can also be derived from the limit of

$[S_f]$ for this case as $\begin{cases} \omega \rightarrow 0 \\ N \rightarrow 0 \end{cases}$ and $\omega \rightarrow 0$, respectively.

In Equation II.7, if $\kappa GA = \omega^2 \rho I$, the denominators of \hat{V} and $\hat{\phi}$ will become zero. So for this special case, the governing equation becomes

$$EI \left(1 + \frac{N}{\kappa GA}\right) \hat{v}''' + (EA + \kappa GA) \hat{v}' = 0 \dots\dots\dots (II.8)$$

The corresponding characteristic equation is $EI \left(1 + \frac{N}{\kappa GA}\right) \bar{r}^3 + (EA + \kappa GA) \bar{r} = 0$

with roots $\begin{cases} r_1 = 0 \\ r_2 = -r_3 = \sqrt{\frac{EA + \kappa GA}{EI \left(1 + \frac{N}{\kappa GA}\right)}} \end{cases}$. The solution to the governing Equation II.8 can

be written as $\hat{v} = C_1 + C_2 e^{r_2 x} + C_3 e^{r_3 x}$.

Substituting \hat{v} into Equation II.1, the expressions for bending moment, shear force, transverse force and bending rotation can be written as

$$\left\{ \begin{aligned} \hat{M} &= EI \left[\left(1 + \frac{N}{\kappa GA} \right) \hat{v}'' + \frac{\omega^2 \rho A}{\kappa GA} \hat{v} \right] = EIC_1 + EI \sum_{i=2}^3 \left[r_i^2 \left(1 + \frac{N}{\kappa GA} \right) + \frac{\omega^2 \rho A}{\kappa GA} \right] e^{r_i x} \\ \hat{\phi} &= \left(1 + \frac{N}{\kappa GA} \right) \hat{v}' + \frac{\omega^2 \rho A}{\kappa GA} \int \hat{v} dx = \frac{\omega^2 \rho A}{\kappa GA} C_1 x + \sum_{i=2}^3 \left[r_i \left(1 + \frac{N}{\kappa GA} \right) + \frac{\omega^2 \rho A}{\kappa GA r_i} \right] e^{r_i x} + C_4 \\ \hat{V} &= -\kappa GA (\hat{\phi} - \hat{v}') = -\omega^2 \rho A C_1 x - \sum_{i=2}^3 \left(N r_i + \frac{\omega^2 \rho A}{r_i} \right) e^{r_i x} - \kappa GA C_4 \\ \hat{Y} &= \hat{V} + N \hat{v}' = -\omega^2 \rho A C_1 x - \sum_{i=2}^3 \frac{\omega^2 \rho A}{r_i} e^{r_i x} - \kappa GA C_4 \end{aligned} \right. \dots \text{(II.9)}$$

The end displacements and end forces are

$$\left\{ \hat{u} \right\} = \begin{Bmatrix} \hat{v}_A \\ \hat{\phi}_A \\ \hat{v}_B \\ \hat{\phi}_B \end{Bmatrix} = \begin{Bmatrix} \hat{v}(0) \\ \hat{\phi}(0) \\ \hat{v}(L) \\ \hat{\phi}(L) \end{Bmatrix} = \begin{bmatrix} 1 & 1 & 1 & 0 \\ 0 & R_2 & R_3 & 1 \\ 1 & e^{r_2 L} & e^{r_3 L} & 0 \\ L & R_2 e^{r_2 L} & R_3 e^{r_3 L} & 1 \end{bmatrix} \begin{Bmatrix} C_1 \\ C_2 \\ C_3 \\ C_4 \end{Bmatrix} = [T_1] \{C\}$$

$$\left\{ \hat{F} \right\} = \begin{Bmatrix} \hat{Y}_A \\ \hat{M}_A \\ \hat{Y}_B \\ \hat{M}_B \end{Bmatrix} = \begin{Bmatrix} -\hat{Y}(0) \\ -\hat{M}(0) \\ \hat{Y}(L) \\ \hat{M}(L) \end{Bmatrix} = \begin{bmatrix} 0 & \frac{\omega^2 \rho A}{r_2} & \frac{\omega^2 \rho A}{r_3} & \kappa GA \\ -EI & -EIR_2 r_2 & -EIR_3 r_3 & 0 \\ -\kappa GA L & -\frac{\omega^2 \rho A}{r_2} e^{r_2 L} & -\frac{\omega^2 \rho A}{r_3} e^{r_3 L} & -\kappa GA \\ EI & EIR_2 r_2 e^{r_2 L} & EIR_3 r_3 e^{r_3 L} & 0 \end{bmatrix} \begin{Bmatrix} C_1 \\ C_2 \\ C_3 \\ C_4 \end{Bmatrix} = [T_2] \{C\}$$

in which $R_i = r_i \left(1 + \frac{N}{\kappa GA} \right) + \frac{\omega^2 \rho A}{\kappa GA r_i}$, ($i=1,2,3,4$). The computation of the stiffness

matrix can be carried out numerically as $[S_f] = [T_2][T_1]^{-1}$.

2.1.2 Dynamic Stiffness Matrix for Axial and Torsional Vibrations

The basic governing equation for axial vibration in the frequency domain is

$$\frac{\partial^2 \hat{u}}{\partial x^2} + \frac{\omega^2 \rho A}{EA} \hat{u} = 0;$$

and for torsional vibration $\frac{\partial^2 \hat{\theta}}{\partial x^2} + \frac{\omega^2 \rho I_p}{GJ} \hat{\theta} = 0$ (II.10)

The derivation of the axial stiffness matrix is

A. If $\omega \neq 0$, then the characteristic equation of is $r^2 + \frac{\omega^2 \rho A}{EA} = 0$ with roots

$$r_1 = -r_2 = ia = i\sqrt{\frac{\omega^2 \rho A}{EA}}, \text{ and the solution to the governing equation is}$$

$$\hat{u} = C_1 e^{r_1 x} + C_2 e^{r_2 x}.$$

Following the same procedure as for the flexural member, the resulting stiffness matrix in the frequency domain can be written as

$$[S_a] = \frac{iaEA}{e^{iaL} - e^{-iaL}} \begin{bmatrix} e^{iaL} + e^{-iaL} & -2 \\ -2 & e^{iaL} + e^{-iaL} \end{bmatrix} = \frac{aEA}{\sin(aL)} \begin{bmatrix} \cos(aL) & -1 \\ -1 & \cos(aL) \end{bmatrix} \dots\dots\dots (II.11)$$

B. If $\omega = 0$, the solution to the governing Equation II.10 is $\hat{u} = C_1 + C_2 x$. Based on this solution, the stiffness matrix can be derived as

$$[S_a] = \frac{EA}{L} \begin{bmatrix} 1 & -1 \\ -1 & 1 \end{bmatrix} \dots\dots\dots (II.12)$$

This formula can also be derived computing the limit of Equation II.11 as $\omega \rightarrow 0$.

$$\begin{aligned}
[S_a]_{\omega=0} &= \lim_{a \rightarrow 0} \left(\frac{aEA}{\sin(aL)} \begin{bmatrix} \cos(aL) & -1 \\ -1 & \cos(aL) \end{bmatrix} \right) \\
&= \lim_{a \rightarrow 0} \left(\frac{aEA}{\sin(aL)} \begin{bmatrix} \cos(aL) & -1 \\ -1 & \cos(aL) \end{bmatrix} \right) \\
&= \lim_{a \rightarrow 0} \left(\frac{aEA}{\sin(aL)} \begin{bmatrix} \lim_{a \rightarrow 0} [\cos(aL)] & \lim_{a \rightarrow 0} (-1) \\ \lim_{a \rightarrow 0} (-1) & \lim_{a \rightarrow 0} [\cos(aL)] \end{bmatrix} \right) \\
&= \frac{EA}{L} \begin{bmatrix} 1 & -1 \\ -1 & 1 \end{bmatrix}
\end{aligned}$$

The torsional stiffness matrix can be obtained just changing EA and ρA into GJ and ρI_p in $[S_a]$, respectively.

After deriving the $[S_f]$, $[S_a]$ and $[S_T]$ matrices, they can be assembled to get the general stiffness matrix $[S]$ in three dimensions.

2.2 Verification of the Program Spfram.for

Using the formulation described above a FORTRAN program was implemented to perform dynamic analysis of three-dimensional frames. The program Spfram.for consists of two parts:

- subroutines to compute the stiffness matrix of a single member;
- subroutines to assemble the global stiffness matrix and solve the system of linear equations.

To test the program, a case was run to find the natural frequencies and buckling load of a beam comparing the results with the analytical solution.

For a three-dimensional beam pinned at two ends in one direction, as shown in Figure II.1, the natural frequencies and buckling load can be easily found analytically.



Figure II.1 A Beam Pinned at Two Ends

At end A, the rotation around the Z axis is free; at end B, the rotation around the Z axis and the displacement along the X axis are free. All other end displacements are constrained. The governing equation of this beam is also Equation II.2. The mode shapes (Eigen-functions) of this pinned beam are

$$\hat{v} = C_n \sin \frac{n\pi x}{L}, (n = 1, 2, \dots),$$

because they satisfy both the boundary conditions $\begin{cases} \hat{M}(x=0) = \hat{M}(x=L) = 0 \\ \hat{v}(x=0) = \hat{v}(x=L) = 0 \end{cases}$ and governing Equation II.2.

Substituting the first mode shape into Equation II.2 to find the first natural frequency and first buckling load, the resulting formula in implicit form is obtained

$$EI \left(1 + \frac{N}{\kappa GA} \right) \frac{\pi^4}{L^4} - \left[\frac{\omega^2 \rho A}{\kappa GA} EI - N + \omega^2 \rho I \left(1 + \frac{N}{\kappa GA} \right) \right] \frac{\pi^2}{L^2} + \omega^2 \rho A \left(\frac{\omega^2 \rho I}{\kappa GA} - 1 \right) = 0 \dots (II.13)$$

If we know the axial force N , we can compute the corresponding natural frequency ω from this equation. For a given frequency ω one can compute on the other hand the buckling load N .

For a rectangular-cross-section with $\left\{ \begin{array}{l} E = 1 \times 10^{10} \text{ Pa} , \nu = 0.25 , \rho = 1000 \text{ kg} / \text{m}^3 \\ A = 9 \text{ m}^2 , I_z = 2.25 \text{ m}^4 , L = 10 \text{ m} , \kappa = \frac{5}{6} \end{array} \right.$,

the natural frequencies corresponding to different values of the axial load are summarized in Table II.1.

Table II. 1 Natural Frequencies for Different Values of Axial Load

Axial Load (N)	Natural Frequency from Analytical Solution (HZ)	Natural Frequency from Program Spfram.for (HZ)
1000000000	28.8830	28.883
500000000	26.4246	26.425
0	23.7127	23.713
-500000000	20.6475	20.647
-1000000000	17.0395	17.039
-1500000000	12.4244	12.424
-2000000000	4.2881	4.288
-2067612136 (Buckling Load)	0	0.000

With program Spfram.for, a unit bending moment was applied at end B as shown in Figure II.1. The output provided the end rotations as a function of frequency for a given axial load. When the rotation at end B became infinite, the frequency was the natural frequency. The results from the program are also tabulated in Table II.1.

The results indicate that the program is working correctly.

2.3 Program Bridge.for

2.3.1 Introduction to the Program

The ultimate goal of this work was to study the seismic behavior of the Marga-Marga bridge (Figure II.2), assessing the effect of the isolation rubber pads between the girders and piers (Figure II.3) and the potential importance of soil structure interaction.

A second program Bridge.for was implemented to analyze a bridge under seismic loading in the frequency domain using the direct stiffness method. The program mainly consists of three parts:

- a main program to perform the nodal and element generation;
- subroutines to compute the stiffness matrix of the members;
- subroutines to assemble the global stiffness matrix and solve the linear equations.

The last two parts are identical to those of the Spfram.for program.

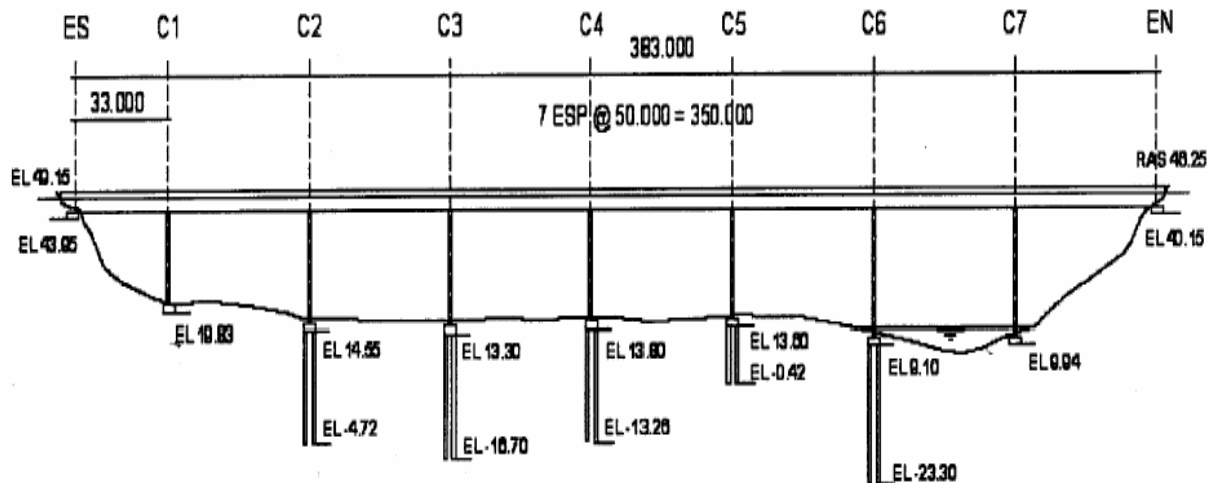


Figure II.2 Overview of the Marga-Marga Bridge in Chile

There are in general three kinds of structural members: deck, piers and rubber pads (Figures II.4 and II.5). To assess the effect of isolation pads the program allows including or omitting the rubber pads in order to compare the corresponding response.

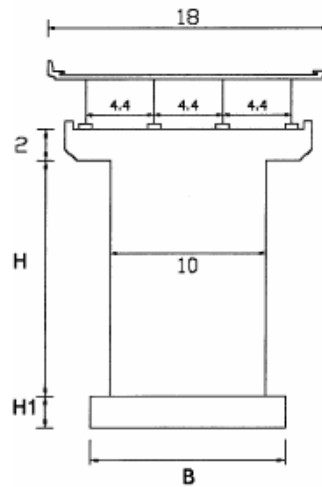


Figure II.3 Cross Section of the Bridge

If there are n piers, the deck will consist of $n + 1$ members, as shown in Figure II.2. If there are rubber pads, rubber pads are on the top of each pier. All the rubber pads on the top of one pier are regarded as one member in the program. In the program, each pier is divided into 3 members according to changes of the cross section to accommodate a situation as shown in Figure II.3, because the stiffness matrix derived before is only valid for prismatic members with constant cross section.

Figures II.4 and II.5 show the nodal and element numbers of the bridge for the cases with and without rubber pads. In the two figures, dashed lines represent the deck members, while continuous lines and solid lines represent the pier members and rubber pads, if they exist, respectively.

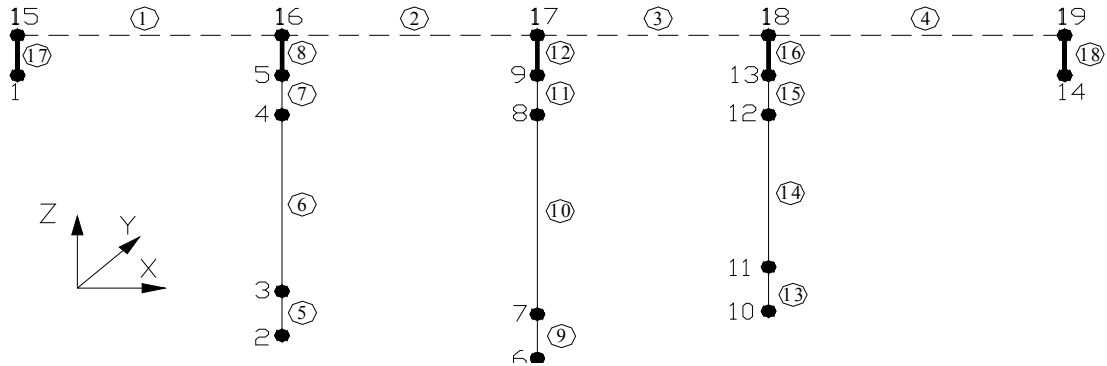


Figure II.4 Nodal and Element Number of a Bridge with Rubber Pads

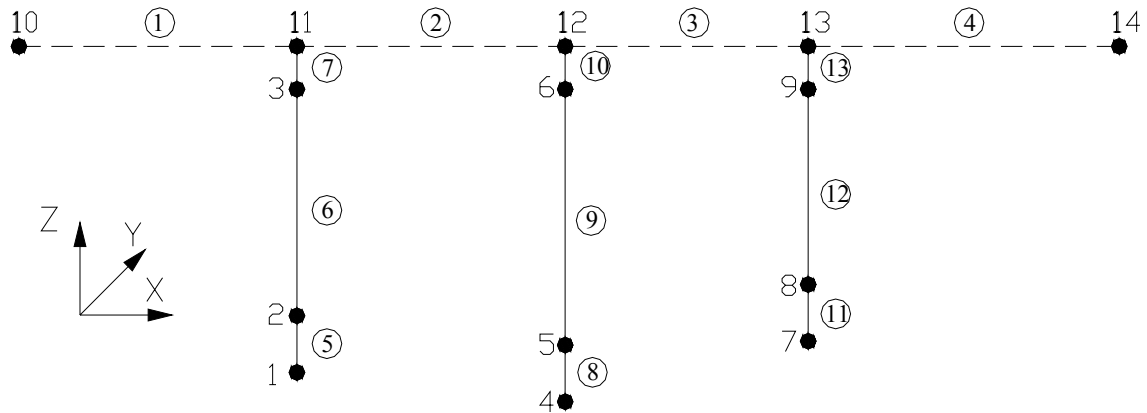


Figure II.5 Nodal and Element Number of a Bridge without Rubber Pads

2.3.2 Stiffness Matrix Transformation

The deck members consist of the deck itself and the steel girders. They are modeled as an equivalent member. The centroidal axis of these equivalent members will be at some vertical distance from the top of the piers or the rubber pads. To account for this eccentricity rigid links are assumed between the centroidal axis of the equivalent deck member and the top surface of the rubber pads (points A and A' in Figure II.6).

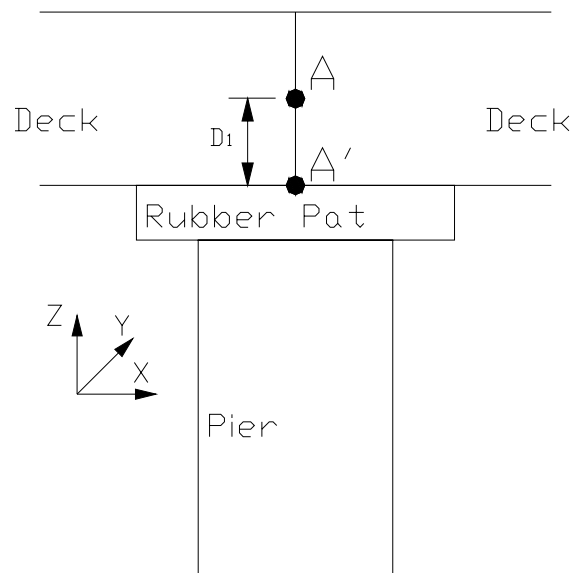


Figure II.6 Forces and Displacements Transformation of Deck Members

One way to incorporate the rigid links is to transform the stiffness matrix of the deck members. If we assume that the cross section cannot deform out of the plane, the relationship between the displacements at A and A' is

$$\begin{cases} u_A = u_{A'} + D_1 (\theta_y)_{A'} \\ v_A = v_{A'} - D_1 (\theta_x)_{A'} \\ w_A = w_{A'} \\ (\theta_x)_A = (\theta_x)_{A'} \\ (\theta_y)_A = (\theta_y)_{A'} \\ (\theta_z)_A = (\theta_z)_{A'} \end{cases}$$

The relationship in matrix form is

$$\begin{Bmatrix} u_A \\ v_A \\ w_A \\ (\theta_x)_A \\ (\theta_y)_A \\ (\theta_z)_A \end{Bmatrix} = \begin{bmatrix} 1 & 0 & 0 & 0 & D_1 & 0 \\ 0 & 1 & 0 & -D_1 & 0 & 0 \\ 0 & 0 & 1 & 0 & 0 & 0 \\ 0 & 0 & 0 & 1 & 0 & 0 \\ 0 & 0 & 0 & 0 & 1 & 0 \\ 0 & 0 & 0 & 0 & 0 & 1 \end{bmatrix} \begin{Bmatrix} u_{A'} \\ v_{A'} \\ w_{A'} \\ (\theta_x)_{A'} \\ (\theta_y)_{A'} \\ (\theta_z)_{A'} \end{Bmatrix} \dots\dots\dots (II.14)$$

$$\{U_A\} = [L_U]\{U_{A'}\}$$

where $[L_U]$ is the transformation matrix.

The transformation matrix for forces is derived in the same way as that of for displacements.

$$\begin{cases} (F_x)_A = (F_x)_{A'} \\ (F_y)_A = (F_y)_{A'} \\ (F_z)_A = (F_z)_{A'} \\ (M_x)_A = (M_x)_{A'} + D_1(F_y)_{A'} \\ (M_y)_A = (M_y)_{A'} - D_1(F_x)_{A'} \\ (M_z)_A = (M_z)_{A'} \end{cases}$$

$$\begin{Bmatrix} (F_x)_A \\ (F_y)_A \\ (F_z)_A \\ (M_x)_A \\ (M_y)_A \\ (M_z)_A \end{Bmatrix} = \begin{bmatrix} 1 & 0 & 0 & 0 & 0 & 0 \\ 0 & 1 & 0 & 0 & 0 & 0 \\ 0 & 0 & 1 & 0 & 0 & 0 \\ 0 & D_1 & 0 & 1 & 0 & 0 \\ -D_1 & 0 & 0 & 0 & 1 & 0 \\ 0 & 0 & 0 & 0 & 0 & 1 \end{bmatrix} \begin{Bmatrix} (F_x)_{A'} \\ (F_y)_{A'} \\ (F_z)_{A'} \\ (M_x)_{A'} \\ (M_y)_{A'} \\ (M_z)_{A'} \end{Bmatrix} \dots\dots\dots (II.15)$$

$$\{F_A\} = [L_F]\{F_{A'}\} \text{ or } \{F_{A'}\} = [L_F]^{-1}\{F_A\} = [L_U]^T\{F_A\} \text{ because } [L_F]^{-1} = [L_U]^T.$$

We can then derive the transformed stiffness matrix for a span member as below in Figure II.7.

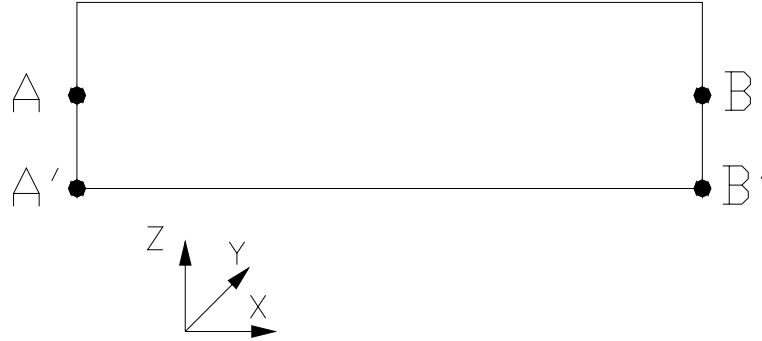


Figure II.7 Stiffness Matrix Transformation of Deck Members

$$\{U\} = \{u_A, v_A, w_A, (\theta_x)_A, (\theta_y)_A, (\theta_z)_A, u_B, v_B, w_B, (\theta_x)_B, (\theta_y)_B, (\theta_z)_B\}^T = \{U_A, U_B\}^T$$

$$\begin{aligned} \{F\} &= \{(F_x)_A, (F_y)_A, (F_z)_A, (M_x)_A, (M_y)_A, (M_z)_A, (F_x)_B, (F_y)_B, (F_z)_B, (M_x)_B, (M_y)_B, (M_z)_B\}^T \\ &= \{F_A, F_B\}^T \end{aligned}$$

$$\{U'\} = \{u_{A'}, v_{A'}, w_{A'}, (\theta_x)_{A'}, (\theta_y)_{A'}, (\theta_z)_{A'}, u_{B'}, v_{B'}, w_{B'}, (\theta_x)_{B'}, (\theta_y)_{B'}, (\theta_z)_{B'}\}^T = \{U_{A'}, U_{B'}\}^T$$

$$\begin{aligned} \{F'\} &= \{(F_x)_{A'}, (F_y)_{A'}, (F_z)_{A'}, (M_x)_{A'}, (M_y)_{A'}, (M_z)_{A'}, (F_x)_{B'}, (F_y)_{B'}, (F_z)_{B'}, (M_x)_{B'}, (M_y)_{B'}, (M_z)_{B'}\}^T \\ &= \{F_{A'}, F_{B'}\}^T \end{aligned}$$

$$\begin{aligned} \{F'\} &= \begin{bmatrix} [L_F]_A^{-1} & 0 \\ 0 & [L_F]_B^{-1} \end{bmatrix} \{F\} = \begin{bmatrix} [L_F]_A^{-1} & 0 \\ 0 & [L_F]_B^{-1} \end{bmatrix} [S] \{U\} \\ &= \begin{bmatrix} [L_F]_A^{-1} & 0 \\ 0 & [L_F]_B^{-1} \end{bmatrix} [S] \begin{bmatrix} [L_U]_A & 0 \\ 0 & [L_U]_B \end{bmatrix} \{U'\} = \begin{bmatrix} [L_U]_A^T & 0 \\ 0 & [L_U]_B^T \end{bmatrix} [S] \begin{bmatrix} [L_U]_A & 0 \\ 0 & [L_U]_B \end{bmatrix} \{U'\} \\ &= [S'] \{U'\} \end{aligned}$$

$$\text{Defining } [S] = \begin{bmatrix} S_{AA} & S_{AB} \\ S_{BA} & S_{BB} \end{bmatrix} \text{ and } [S'] = \begin{bmatrix} S_{A'A'} & S_{A'B'} \\ S_{B'A'} & S_{B'B'} \end{bmatrix},$$

$$\begin{cases} S_{A'A'} = [L_U]_A^T S_{AA} [L_U]_A \\ S_{A'B'} = [L_U]_A^T S_{AB} [L_U]_B \\ S_{B'A'} = [L_U]_B^T S_{BA} [L_U]_A \\ S_{B'B'} = [L_U]_B^T S_{BB} [L_U]_B \end{cases} \dots\dots\dots (II.16)$$

2.3.3 Program Bridge.for Verification

To validate the program runs were conducted for the bridge sketched in Figure II.5, without rubber pads and with 3 piers. The properties are

$$\begin{cases} \text{deck} \begin{cases} E = 1 \times 10^9 \text{ N} / \text{m}^2, \nu = 0.25, \rho = 1000 \text{ kg} / \text{m}^3, \mu = 0.01 \\ L = 10 \text{ m} / \text{span}, A = 2 \text{ m}^2, \kappa = 0.85, I_y = \frac{1}{6} \text{ m}^4, I_z = \frac{2}{3} \text{ m}^4, J = 0.46 \text{ m}^4 \end{cases} \\ \text{pier} \begin{cases} E = 1 \times 10^9 \text{ N} / \text{m}^2, \nu = 0.25, \rho = 1000 \text{ kg} / \text{m}^3, \mu = 0.01 \\ L = 14 \text{ m}, A = 2 \text{ m}^2, \kappa = 0.85, I_y = \frac{1}{6} \text{ m}^4, I_z = \frac{2}{3} \text{ m}^4, J = 0.46 \text{ m}^4 \end{cases} \end{cases}$$

And the displacement boundary conditions in this case are:

- the left end of the deck and the bottom of all piers are completely fixed, which means that all six possible displacements and rotations are constrained;
- the right end of the deck is also fixed except for the displacement in the x direction.

The excitations are unit harmonic motions at each of the supports in each of the three directions.

The same case was studied with the program ABAQUS to determine the natural frequencies and mode shapes. Because ABAQUS does not allow considering distributed masses each member was divided into a number of sub-elements (segments) to obtain comparable results to those of Bridge.for. In this case, the length of each segment is 0.05m.

The results are illustrated in Figures II.8, II.9 and II.10, which give the response (displacements) of node 11 in all three directions due to a unit excitation at node 1 in the same directions, respectively; and in Figures II.11, II.12 and II.13, showing the displacements of node 12 due to a unit excitation at node 4. In these figures, the peaks in the plots represent the natural frequencies from the program Bridge.for (for small values of damping ratio, as used in this case, the peaks are almost exactly the natural frequencies.), while the vertical dashed lines represent those calculated with the program ABAQUS using a very fine discretization of each member (0.05m/member).

As we can see, the natural frequencies from the two programs are almost identical, which indicates that the program Bridge.for gives the correct results. Table II.2 also gives the natural frequencies and a brief description of the corresponding mode shapes from ABAQUS, and the mode shapes are also shown in Appendix (Figures A.1~A.30).

In Figures II.8~II.13, some natural frequencies from ABAQUS do not correspond to any peaks in the plots. When referring to the mode shape corresponding to that natural frequency, one will find that in that mode, the displacement of node 11 has no components in that direction. For example, in Figure II.12, one cannot find the corresponding peaks to the 11th and 15th modes, because in these modes, the displacement of node 12 in the y direction is zero (in Figures A.11 & A.15 in Appendix).

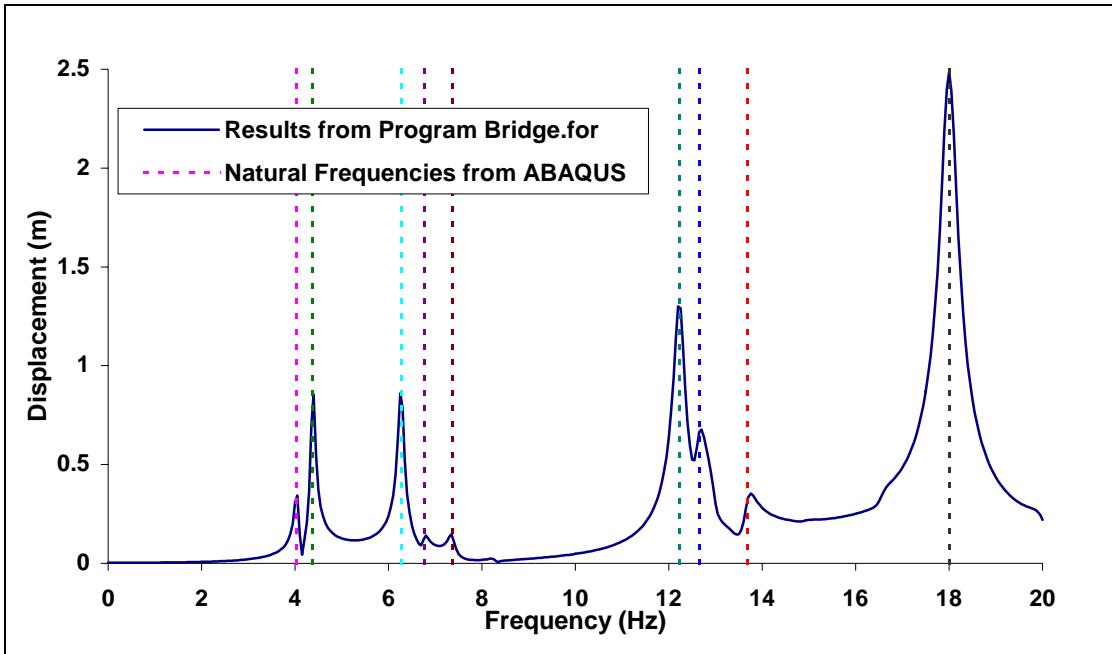


Figure II.8 Displacement at Node 11 in X Direction due to X Motion at Node 1

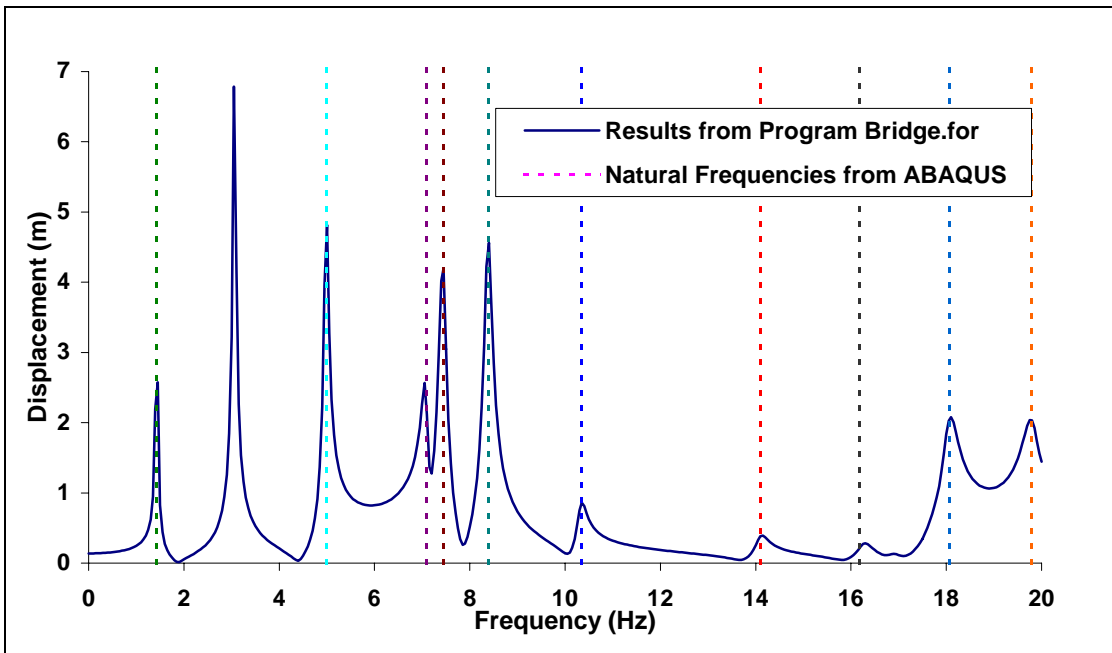


Figure II.9 Displacement at Node 11 in Y Direction due to Y Motion at Node 1

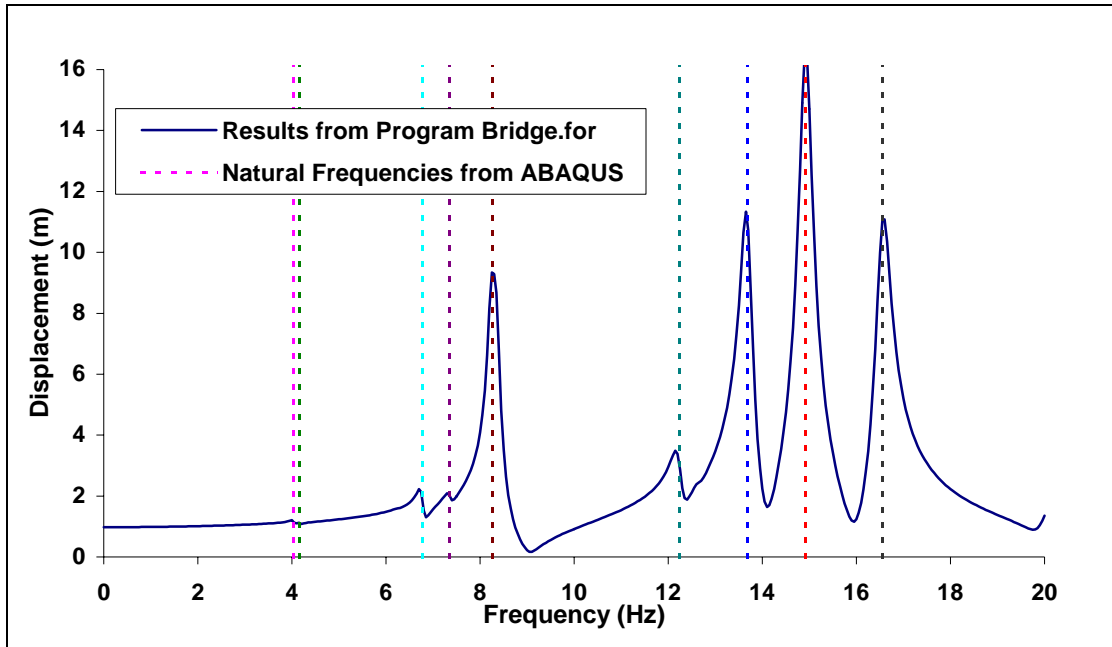


Figure II.10 Displacement at Node 11 in Z Direction due to Z Motion at Node 1

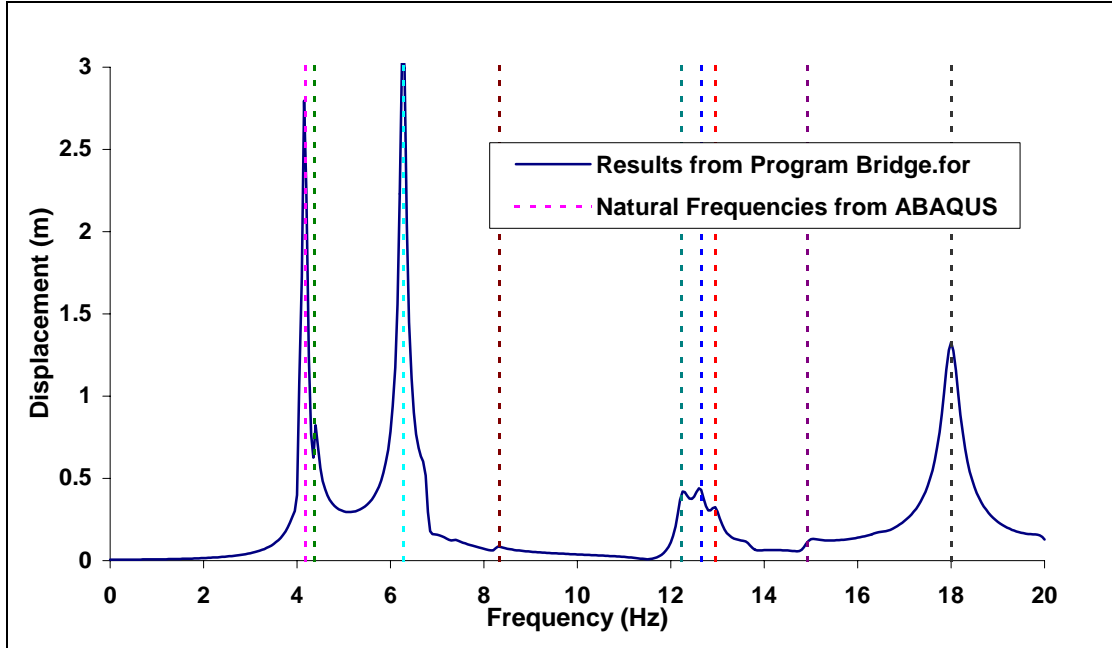


Figure II.11 Displacement at Node 12 in X Direction due to X Motion at Node 4

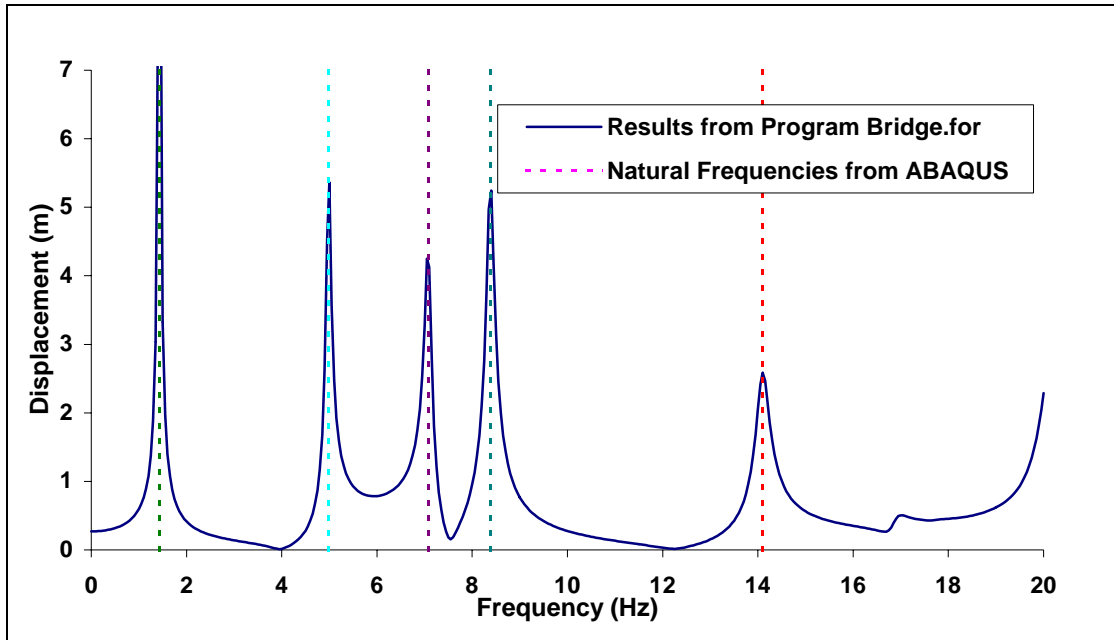


Figure II.12 Displacement at Node 12 in Y Direction due to Y Motion at Node 4

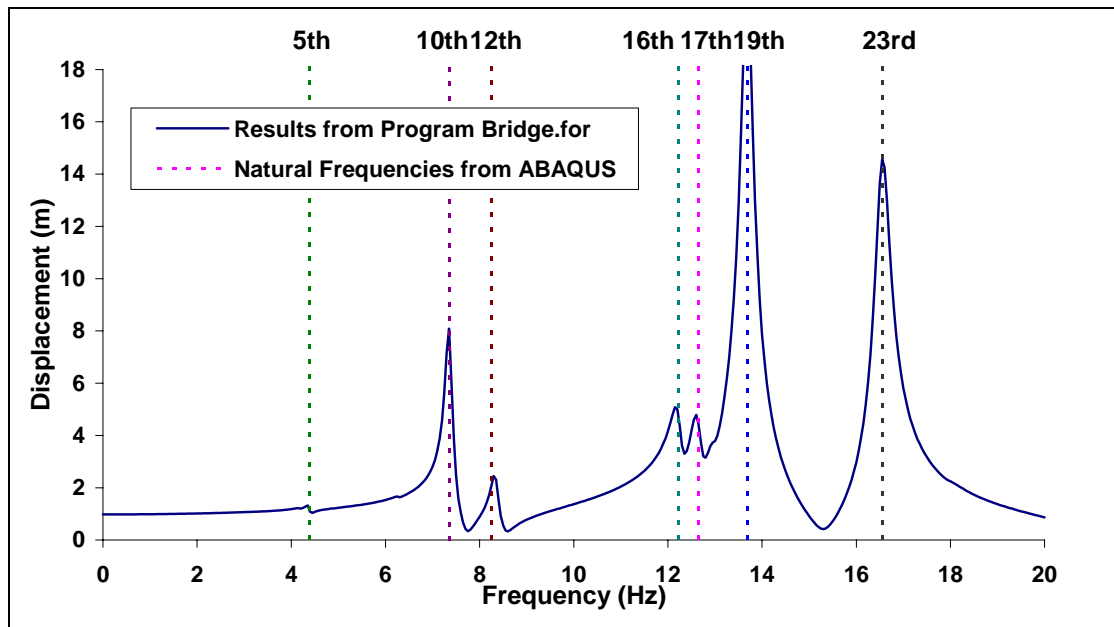


Figure II.13 Displacement at Node 12 in Z Direction due to Z Motion at Node 4

In the above analysis using ABAQUS, to get good results each member was divided into a number of very small 0.05m-long segments. But typically in engineering practice each member has one segment. Table II.3 gives the results obtained with this model using lumped masses at the joint. Comparing with Table II.2 which contains almost the exact solution, this model only gives a good approximation of the first two modes. From the 3rd mode on, the results are no longer reliable. The accuracy of the usual model would improve somewhat using consistent mass matrices.

Tables II.4 and II.5 list the natural frequencies obtained using lumped mass matrices and dividing each member into 2 segments (good accuracy for 10 or 15 modes) and dividing the members into 3m-long segments, which means each span is divided into 3 segments and pier into 5 segments. The approximation is then reasonable for the first 30 modes and the maximum error in the natural frequencies is about 3%.

**Table II. 2 Natural Frequencies and Mode Shapes Description of the Bridge in Figure II.5
(from ABAQUS, Length of each segment is 0.05m)**

Mode	Natural Frequency (Hz)	Mode Shape Description	Mode	Natural Frequency (Hz)	Mode Shape Description
1	1.4285	Transverse, in y direction; symmetric	16	12.235	Longitudinal & Axial, in x-z plane
2	3.0588	Transverse, in y direction; anti-symmetric	17	12.650	Longitudinal & Axial, in x-z plane
3	4.0408	Longitudinal, in x-z plane; anti-symmetric	18	12.964	Longitudinal & Axial, in x-z plane
4	4.1685	Longitudinal & Axial, mainly in x direction	19	13.686	Longitudinal & Axial, in x-z plane; symmetric
5	4.3829	Longitudinal & Axial, in x-z plane	20	14.106	Transverse, in y direction; symmetric
6	4.9865	Transverse, in y direction; symmetric	21	14.928	Longitudinal & Axial, in x-z plane
7	6.2708	Longitudinal & Axial, mainly in x direction	22	16.176	Transverse, in y direction; anti-symmetric
8	6.7674	Longitudinal, in x-z plane anti-symmetric	23	16.557	Longitudinal & Axial, in x-z plane; symmetric
9	7.0866	Transverse, in y direction symmetric	24	16.671	Transverse, in y direction; anti-symmetric
10	7.3603	Longitudinal & Axial, in x-z plane; symmetric	25	16.794	Transverse, in y direction; symmetric
11	7.4381	Transverse, in y direction; anti-symmetric	26	17.755	Transverse, in y direction; symmetric
12	8.2621	Longitudinal, in x-z plane; anti-symmetric	27	18.003	Longitudinal & Axial, mainly in x direction
13	8.3444	Longitudinal & Axial, in x-z plane; symmetric	28	18.070	Transverse, in y direction; anti-symmetric
14	8.3851	Transverse, in y direction; symmetric	29	19.796	Transverse, in y direction; anti-symmetric
15	10.333	Transverse, in y direction; anti-symmetric	30	20.035	Longitudinal, in x-z plane; anti-symmetric

**Table II. 3 Natural Frequencies and Mode Shapes Description of the Bridge in Figure II.5
(from ABAQUS, Each member is considered as one segment, which is 10~14m-long)**

Mode	Natural Frequency (Hz)	Mode Shape Description	Mode	Natural Frequency (Hz)	Mode Shape Description
1	1.3192	Transverse, in y direction; symmetric	16	37.202	Longitudinal & Axial, in x-z plane
2	3.9152	Transverse, in y direction; anti-symmetric	17	41.589	Transverse, in y direction; anti-symmetric
3	4.7401	Transverse, in y direction; symmetric	18	44.727	Longitudinal & Axial, in x-z plane, symmetric
4	4.0711	Longitudinal & Axial, in x-z plan	19	51.143	Longitudinal & Axial, in x-z plane
5	10.339	Longitudinal & Axial, in x-z plan, symmetric			
6	10.439	Longitudinal & Axial, in x-z plan, anti-symmetric			
7	10.609	Longitudinal & Axial, in x-z plan, symmetric			
8	14.304	Longitudinal & Axial, in x-z plan			
9	21.319	Transverse, in y direction; symmetric			
10	21.577	Transverse, in y direction; anti-symmetric			
11	22.702	Transverse, in y direction; anti-symmetric			
12	23.776	Transverse, in y direction; symmetric			
13	26.782	Longitudinal & Axial, in x-z plan			
14	27.754	Transverse, in y direction; anti-symmetric			
15	35.386	Transverse, in y direction; symmetric			

**Table II. 4 Natural Frequencies and Mode Shapes Description of the Bridge in Figure II.5
(from ABAQUS, Each member is considered as two segments, which is 5~7m-long)**

Mode	Natural Frequency (Hz)	Mode Shape Description	Mode	Natural Frequency (Hz)	Mode Shape Description
1	1.4020	Transverse, in y direction; symmetric	16	13.687	Longitudinal & Axial, in x-z plan, symmetric
2	3.0551	Transverse, in y direction; anti-symmetric	17	13.809	Transverse, in y direction symmetric
3	4.1865	Transverse, in y direction; anti-symmetric	18	14.435	Longitudinal & Axial, in x-z plan, anti-symmetric
4	4.3521	Longitudinal & Axial, mainly in x direction	19	14.833	Transverse, in y direction; anti-symmetric
5	4.5228	Longitudinal & Axial, in x-z plan	20	15.048	Transverse, in y direction; anti-symmetric
6	5.1644	Transverse, in y direction; symmetric	21	15.205	Longitudinal & Axial, in x-z plane, symmetric
7	5.9847	Longitudinal & Axial, mainly in x direction	22	15.241	Transverse, in y direction; symmetric
8	7.0123	Longitudinal & Axial, in x-z plan, anti-symmetric	23	16.490	Longitudinal & Axial, mainly in x direction
9	7.0705	Transverse, in y direction; symmetric	24	17.621	Transverse, in y direction; anti-symmetric
10	7.3389	Transverse, in y direction; anti-symmetric	25	18.861	Transverse, in y direction; symmetric
11	7.6540	Longitudinal & Axial, in x-z plan, symmetric	26	19.998	Transverse, in y direction; anti-symmetric
12	7.8519	Transverse, in y direction; symmetric	27	20.275	Transverse, in y direction; symmetric
13	8.5618	Longitudinal & Axial, in x-z plan, anti-symmetric	28	20.694	Transverse, in y direction; symmetric
14	8.6085	Longitudinal & Axial, in x-z plan, symmetric	29	21.011	Longitudinal & Axial, mainly in x direction
15	10.398	Transverse, in y direction; anti-symmetric	30	26.518	Longitudinal & Axial, mainly in x direction

**Table II. 5 Natural Frequencies and Mode Shapes Description of the Bridge in Figure II.5
(from ABAQUS, Each member is about 3m-long)**

Mode	Natural Frequency (Hz)	Mode Shape Description	Mode	Natural Frequency (Hz)	Mode Shape Description
1	1.4265	Transverse, in y direction; symmetric	16	12.571	Longitudinal & Axial, in x-z plane
2	3.0721	Transverse, in y direction; anti-symmetric	17	12.950	Longitudinal & Axial, in x-z plane
3	4.0973	Longitudinal, in x-z plane; anti-symmetric	18	13.345	Longitudinal & Axial, in x-z plane
4	4.2309	Longitudinal & Axial, mainly in x direction	19	13.874	Longitudinal & Axial, in x-z plane; symmetric
5	4.4585	Longitudinal & Axial, in x-z plane	20	14.180	Transverse, in y direction; symmetric
6	5.0452	Transverse, in y direction; symmetric	21	15.115	Longitudinal & Axial, in x-z plane
7	6.2748	Longitudinal & Axial, mainly in x direction	22	15.987	Transverse, in y direction; anti-symmetric
8	6.9318	Longitudinal, in x-z plane anti-symmetric	23	16.422	Transverse, in y direction; anti-symmetric
9	7.1017	Transverse, in y direction symmetric	24	16.584	Transverse, in y direction; symmetric
10	7.4487	Transverse, in y direction anti-symmetric	25	16.677	Longitudinal & Axial, in x-z plane; symmetric
11	7.5645	Longitudinal & Axial, in x-z plane; symmetric	26	17.812	Transverse, in y direction; symmetric
12	8.3428	Transverse, in y direction symmetric	27	17.930	Longitudinal & Axial, mainly in x direction
13	8.5337	Longitudinal & Axial, in x-z plane; anti-symmetric	28	18.251	Transverse, in y direction; anti-symmetric
14	8.6185	Longitudinal & Axial, in x-z plane; symmetric	29	19.398	Transverse, in y direction; anti-symmetric
15	10.420	Transverse, in y direction; anti-symmetric	30	19.896	Transverse, in y direction; symmetric

CHAPTER III

DYNAMIC STIFFNESS OF PILE FOUNDATIONS

The dynamic stiffness of pile foundations are obtained in this chapter using an Elasto-Dynamics solution assuming linear strain-stress behavior for both piles and soil. The formulation assumes also that the piles (end bearing or floating piles) are welded to the soil in a horizontally layered soil deposit of finite depth. The contact between the piles and the soil is assumed to be continuous in all three directions, without any slippage or gap. This guarantees that the equations are linear.

3.1 Formulation of Dynamic Stiffness of Pile Groups

The dynamic stiffness of pile groups or complete pile foundations has been investigated using an Elasto-Dynamic solution and assuming linear behavior in the frequency domain. Solutions were obtained, by Gomez (1982) for small pile groups (2 by 2, 3 by 3 or 4 by 4 piles) accounting for the complete interaction between all piles and enforcing compatibility of displacements between piles and surrounding soil in all three coordinate directions. Alternatively, one can get an approximate solution extending Poulos' Method (1971), originally presented for the static case, to the dynamic case. Gomez (1982) showed that the results of this approximation were in very good agreement with those of the more accurate formulation for these small groups. This approach is the one followed in the present study.

In this approach as shown in Figure III.1, one considers two piles (a cavity and a dot-dashed line) at a time neglecting the presence of the other piles. Applying unit forces along a cylindrical cavity in the soil deposit, corresponding to the space to be occupied by a pile, one can determine the displacements at various points along this cavity and along the axis of a second cavity, using a formulation in cylindrical coordinates (Kausel,

1974). These displacements provide a flexibility matrix for the soil. Its inverse is a dynamic stiffness matrix to which one adds the dynamic stiffness matrices of the 2 piles. The sum provides the dynamic stiffness matrix of the combined soil-piles system. Using this dynamic stiffness matrix and applying unit forces at the head of each pile or just condensing the matrix, one can get the head displacements of the piles.

$$\left. \begin{aligned} [K_{soil}]^{-1} &= [F_{soil}] = [d_{ij}]_{2n \times 2n} \\ ([K_{soil}] + [K_{pile}])\bar{U} &= \bar{P} \\ \bar{U} &= \begin{Bmatrix} U_h \\ U_r \end{Bmatrix} \\ \bar{P} &= \begin{Bmatrix} P_h \\ P_r \end{Bmatrix} \end{aligned} \right\} \Rightarrow \begin{bmatrix} K_{hh} & K_{hr} \\ K_{rh} & K_{rr} \end{bmatrix} \begin{Bmatrix} U_h \\ U_r \end{Bmatrix} = \begin{Bmatrix} P_h \\ P_r \end{Bmatrix}$$

$$\Rightarrow \begin{cases} U = U_h \\ P_r = \{0\} \\ U_r = -[K_{rr}]^{-1}[K_{rh}]U \\ P = P_h = [K_{hh}]U + [K_{hr}]U_r = ([K_{hh}] - [K_{hr}][K_{rr}]^{-1}[K_{rh}])U \end{cases} \dots\dots\dots (III.1)$$

where h denotes the pile head degrees of freedom and r denotes the remaining degrees of freedom;

$P = P_h = \begin{Bmatrix} P_1 \\ P_2 \end{Bmatrix}$ and $U = U_h = \begin{Bmatrix} u_1 \\ u_2 \end{Bmatrix}$ are the pile head forces and displacements.

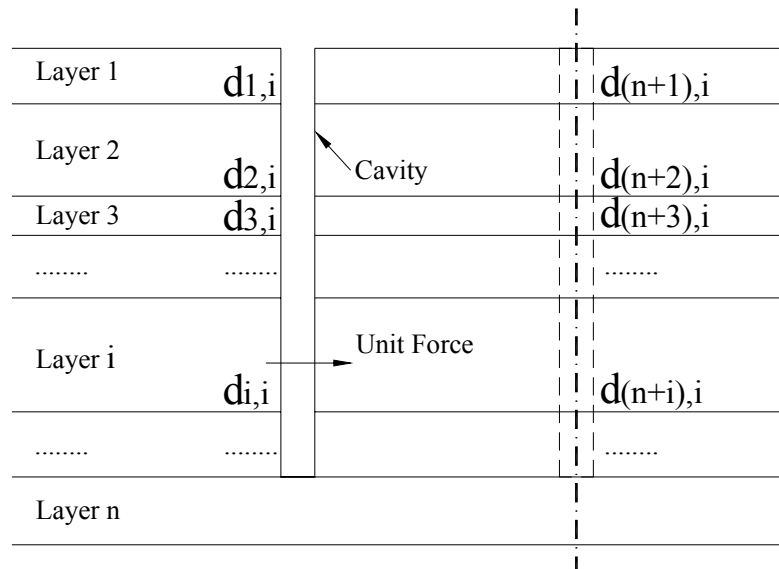


**Figure III.1 Interaction of Two Piles in Horizontally Layered Soil Deposit
(Displacements of Two Cavities at Each Layer due to Unit Force Applied at Layer i)**

Alternatively, we can write the last equation in Equation III.1 into the following form.

$$\begin{cases} u_1 = u_{1,1}P_1 + u_{1,2}P_2 = u_{1,1}(P_1 + \alpha_{1,2}P_2) \\ u_2 = u_{2,1}P_1 + u_{2,2}P_2 = u_{2,2}(\alpha_{2,1}P_1 + P_2) \end{cases} \dots\dots\dots (III.2)$$

where $u_{i,j}$ denotes the displacement at the head of pile i due to a unit force at the head of pile j ; $\alpha_{i,j} = \frac{u_{i,j}}{u_{i,i}}$ are the interaction coefficients; u_i and P_i are the head displacement and force for pile i ; and $i, j \in \{1, 2\}$.

The above procedure is known as Poulos' method.

This procedure can be used with horizontal or vertical forces, rocking (around an axis in the horizontal plane) or torsional moments (around the vertical axis). The coupling

between them is relatively small and always ignored in the following derivation. Furthermore, for a pile group with a rigid cap, rocking and torsional stiffness of a single pile can be neglected because they are much smaller than the contribution of the vertical or horizontal stiffness multiplied by the distance squared.

- Horizontal Stiffness of Pile Group

Defining

$$f = \begin{bmatrix} u_{1,1} & 0 \\ 0 & u_{2,2} \end{bmatrix}, A = \begin{bmatrix} 1 & \alpha_{1,2} \\ \alpha_{2,1} & 1 \end{bmatrix}, K = f^{-1} = \begin{bmatrix} 1/u_{1,1} & 0 \\ 0 & 1/u_{2,2} \end{bmatrix},$$

one can write

$$U = fAP = K^{-1}AP \text{ or } P = A^{-1}KU \dots\dots\dots(\text{III.3})$$

where $1/u_{i,i}$ denotes the pile head stiffness of pile i alone and U and P are horizontal displacements and forces at the pile heads. If the external horizontal force is applied on the top of the rigid cap, all the piles have the same horizontal displacement at their heads. The external force applied on the cap p_H can be

expressed as $p_H = \{1,1\} P = \{1,1\} A^{-1} K U = \{1,1\} A^{-1} K \begin{Bmatrix} 1 \\ 1 \end{Bmatrix} u_H = k_{Hg} u_H$ or

$$k_{Hg} = I^T A^{-1} K I, \text{ where } u_H \text{ is the horizontal displacement of the rigid cap and } I = \begin{Bmatrix} 1 \\ 1 \end{Bmatrix}.$$

Similarly, if the pile group consists of n piles, then

$$k_{Hg} = I^T A_H^{-1} K_H I \dots\dots\dots(\text{III.4})$$

where $I = \begin{Bmatrix} 1 \\ \dots \\ 1 \end{Bmatrix}_{n \times 1}$, $A_H = \begin{bmatrix} 1 & \dots & \alpha_{1,i} & \dots & \alpha_{1,n} \\ \dots & \dots & \dots & \dots & \dots \\ \alpha_{i,1} & \dots & 1 & \dots & \alpha_{i,n} \\ \dots & \dots & \dots & \dots & \dots \\ \alpha_{n,1} & \dots & \alpha_{n,i} & \dots & 1 \end{bmatrix}_{n \times n}$ and $K_H = \begin{bmatrix} \frac{1}{u_{1,1}} & \dots & 0 & \dots & 0 \\ \dots & \dots & \dots & \dots & \dots \\ 0 & \dots & \frac{1}{u_{i,i}} & \dots & 0 \\ \dots & \dots & \dots & \dots & \dots \\ 0 & \dots & 0 & \dots & \frac{1}{u_{n,n}} \end{bmatrix}_{n \times n}$.

- Vertical Stiffness of Pile Group

$$k_{Vg} = I^T A_V^{-1} K_V I \dots \dots \dots (III.5)$$

where A_V and K_V are similar to A_H and K_H but correspond to the vertical interaction coefficients and vertical stiffness of an individual pile.

- Rocking Stiffness of Pile Group

$$k_{Rg} = D^T A_V^{-1} K_V D \dots \dots \dots (III.6)$$

where $D = \begin{Bmatrix} d_1 \\ \dots \\ d_i \\ \dots \\ d_n \end{Bmatrix}_{n \times 1}$ and $d_i (i = 1, 2, \dots, n)$ is the horizontal distance between the pile i and

the center of the pile cross section.

3.2 Results

Computer programs were developed implementing the above formulation. Results were then obtained for pile groups of 2 by 2, 4 by 4, 6 by 6, 8 by 8 and 10 by 10 piles. The soil properties used in the study were:

$$\begin{cases} c_s = 100(m/s) \\ \nu = 0.25 \\ \rho_s = 2000(kg/m^3) \\ D_s = 0.02 \end{cases}$$

where

c_s shear wave velocity of soil deposit;
 ν Poisson's ratio of soil deposit;
 ρ_s mass density of soil deposit;
 D_s linear hysteretic damping of soil deposit.

The piles were assumed to have a radius of 0.5 meters, pile spacing of 3 meters, a mass density of 2500 kg/m³ and 2% damping. The modulus of elasticity of the piles was changed to investigate the effect of the E_p/E_s ratio. The depth of the soil deposit was assumed to be 40 meters in all cases. End bearing and floating piles were considered. The end bearing piles had a length of 40 meters, the same as the depth of the soil deposit, while the floating piles were 20 meters long.

3.2.1 Horizontal Stiffness

The horizontal stiffness of the pile groups was calculated accounting for the full interaction coefficients computed from the elastic analyses and assuming no interaction for pile spacings larger than a limiting value. The reason to use a limiting distance is

that, a number of field tests showed that the interaction coefficients obtained from an elastic solution may be too large and that almost no interaction was observed experimentally for a spacing of 10 or even 5 diameters. Approximate nonlinear analyses considering separation effects also indicate that the interaction decreases for large spacing. The dynamic horizontal stiffness of a foundation can be expressed as

$$K_{dynamic} = K_{real} + i \cdot K_{imaginary} = K_{real} + i\Omega C = K_{static} \left(k_1 + i \frac{\Omega \bar{R}}{c_s} c_1 \right) \dots\dots\dots (III.7)$$

in which

Ω forcing frequency;

C equivalent viscous dashpot;

$\bar{R} = \sqrt{A/\pi}$ equivalent radius of the pile group;

A equivalent area of the pile group (see Figure III.2);

c_s shear wave velocity of the soil deposit;

k_1, c_1 dynamic stiffness coefficients.

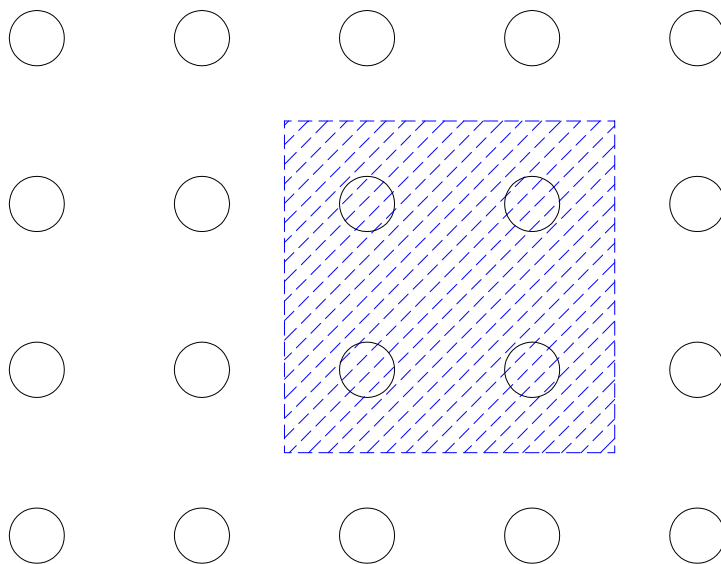


Figure III.2 Definition of Equivalent Area (Shaded Area) for Pile Groups

We first consider the variation of the static stiffness K_{static} for a pile group.

(1) Static Stiffness

Figure III.3 shows the static group factors for end bearing piles. The group factor is defined as the ratio of the group stiffness to that of a single pile multiplied by the total number of piles.

$$GF = \frac{K_G}{n \cdot K_s} \dots\dots\dots (III.8)$$

where $n = N^2$ for the case of N by N piles while K_G and K_s are static group stiffness and single pile stiffness, respectively.

The ratio of Young's modulus of the piles to that of the soil is 1000 for the results in Figure III.3. S_{max} is the threshold distance. From the figure we can conclude that, if no threshold distance is specified, the group factor is approximately inversely proportional to N , which implies that the static stiffness is proportional to N . This is very similar to the case of a rigid mat on an elastic foundation, whose horizontal stiffness is proportional to the radius and not to the area. When a threshold distance is imposed, the group factor decreases with increasing N initially but tends to become constant later, which implies that the horizontal stiffness increases proportionally to N initially and then proportionally to N^2 .

For floating piles 20 meters long, the group factors and the dynamic stiffness coefficients are almost exactly the same as those of 40 meters long end bearing piles. The reason is that the horizontal stiffness is only governed by the properties of the pile and soils near the surface (a few radii from the surface). So if the length of the pile is equal to or longer than 10 times its diameter, the horizontal stiffness will not change significantly when increasing the pile length.

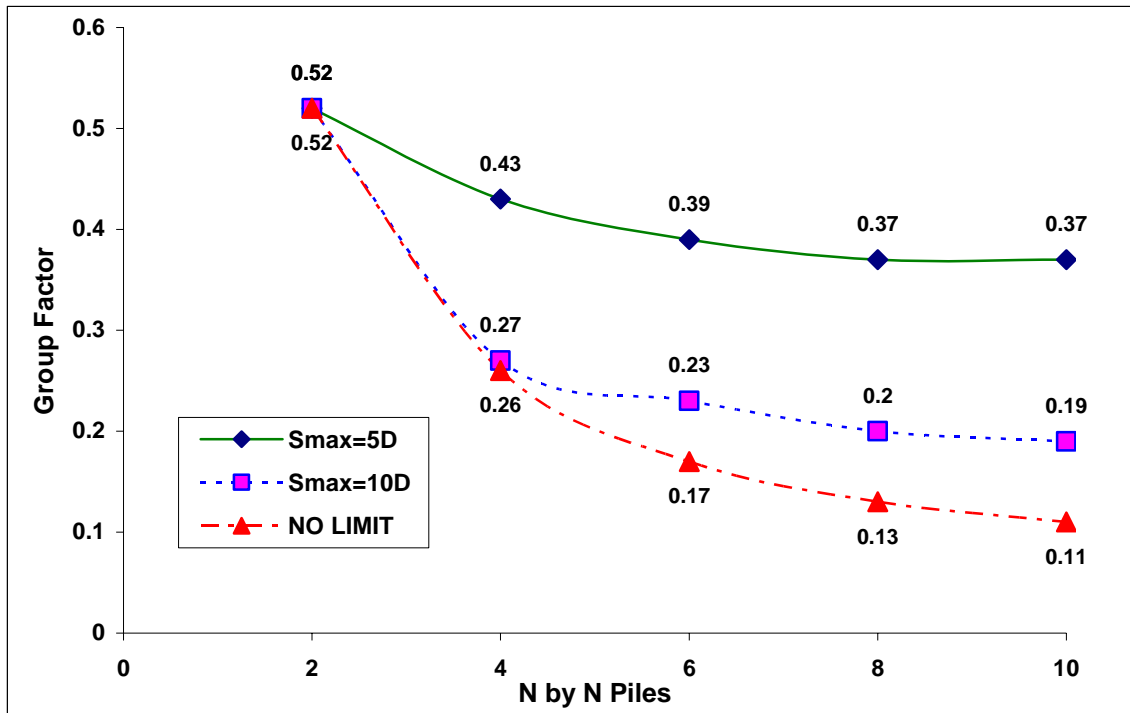


Figure III.3 Static Group Reduction Factors ($E_p/E_s=1000$)

The group factors will depend, of course, on the pile spacing and on the ratio of the Young's modulus of the pile to that of the soil. Basically, the group factor decreases with increasing E_p/E_s but only slightly. Figure III.4 shows the results for the case without threshold distance and values of E_p/E_s of 100, 500 and 1000, normally the range of practical interest. Similar variations were obtained for $S_{max} = 10D$ and $5D$.

To illustrate further the similarity between the horizontal static stiffness of a pile group when accounting for the full interaction coefficients (without a limit distance) and that of a rigid mat foundation with the same area (as defined in Figure III.2), results were obtained for circular mats with areas corresponding to the 2 by 2, 4 by 4, 6 by 6, 8 by 8 and 10 by 10 piles.

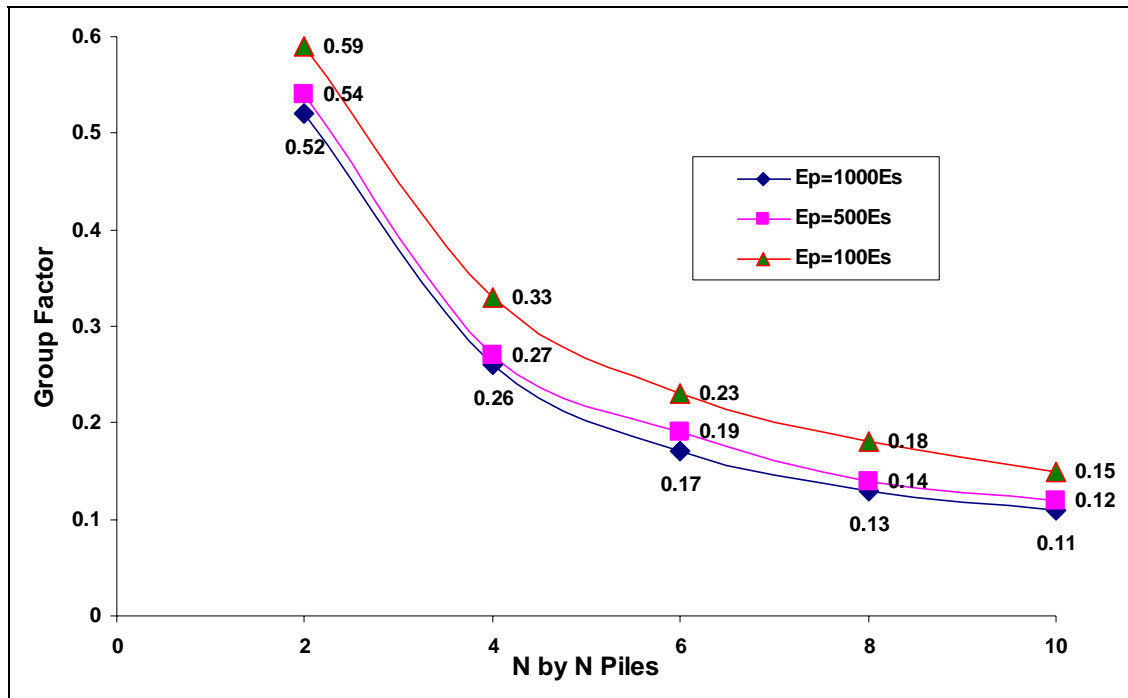


Figure III.4 Effect of E_p/E_s on Group Factors (No Threshold Distance)

For comparison purposes the stiffness of a mat was computed using the formula proposed by Elsabee and Morray (1977)

$$K_{static} = \frac{8GR_m}{2-\nu} \left(1 + \frac{1}{2} \frac{R_m}{H}\right) \left(1 + \frac{2}{3} \frac{E}{R_m}\right) \left(1 + \frac{5}{4} \frac{E}{H}\right)$$

where G is the shear modulus of the soil deposit, and H , R_m and E are the depth of the soil deposit, the radius of the mat and the depth of embedment. As shown in Figure III.5, for small E_p/E_s , say 100, the static group stiffness is very similar to that of a rigid surface mat with the same radius. For $E_p/E_s=500$, the static pile group stiffness is 15% higher than that of the rigid mat; for $E_p/E_s=1000$, it is 20~30% higher.

For embedded rigid mats, the static stiffness increases substantially even for a small value of embedment. Figure III.5 shows that if the rigid mat is embedded 1.5 meters its static stiffness is similar to that of a pile group with $E_p/E_s=500$.

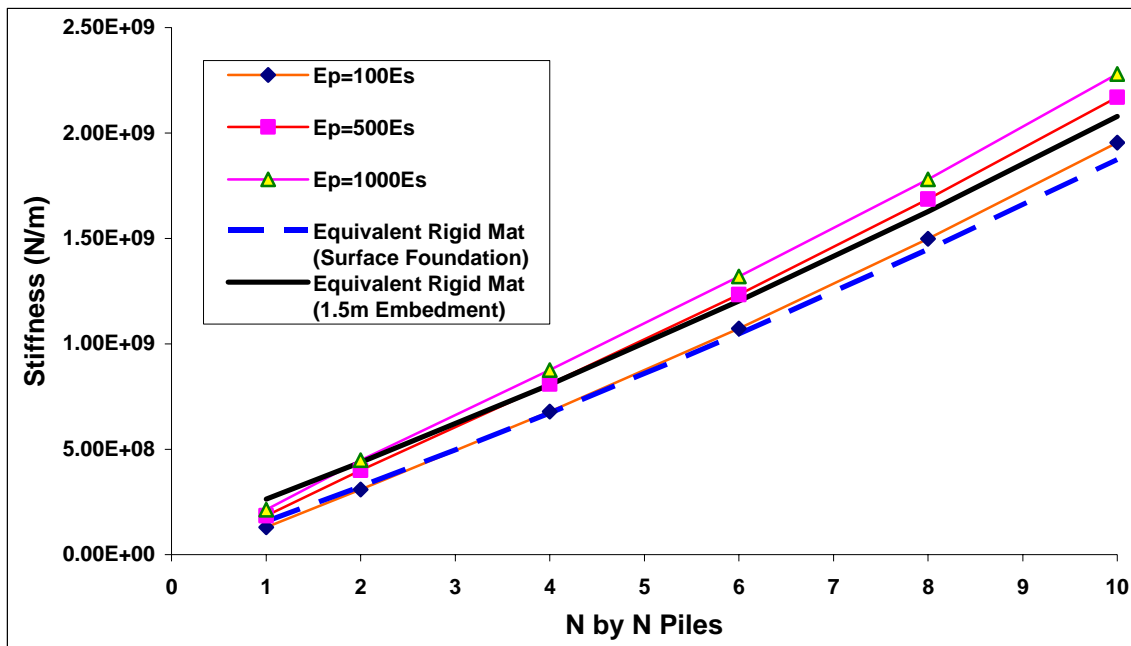


Figure III.5 Static Stiffness Comparison ($E_s=\text{Constant}=5E7 \text{ N/m}^2$, $H=40\text{m}$)

(2) Real and Imaginary Stiffness Coefficients

The real stiffness coefficient k_1 is nearly independent of frequency for a single pile, with a dip at the natural frequency of the soil deposit in shear (0.625 Hz in this case) and some small fluctuations around a horizontal line (with a value of 1) for higher frequencies. As the number of piles in the group increases the variation of k_1 with frequency becomes more pronounced, as illustrated in Figure III.6.

Basically, the real stiffness coefficients decrease with increasing frequency exhibiting a parabolic variation, especially for small groups (2 by 2, 4 by 4), which would indicate

that there is a soil mass entrapped between the piles vibrating in-phase with all the piles. For larger pile groups, the real coefficient k_1 oscillates around a second degree parabola. The larger the pile group the bigger the fluctuations, as shown in Figure III.6.

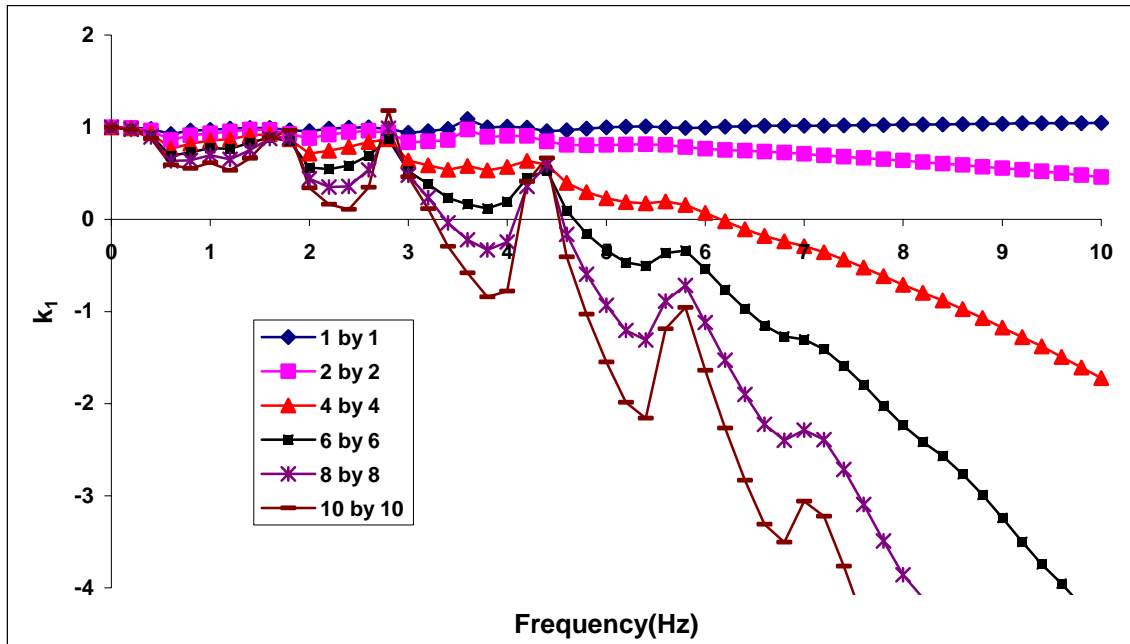


Figure III.6 Effect of Number of Piles on Normalized Real Coefficients (k_1)
($E_p/E_s=1000$, 2% Material Damping, No Threshold Distance, End Bearing Piles)

Using a second degree parabola to fit each curve in Figure III.6, an equivalent mass can be determined to simulate the pile-soil system as a single degree of freedom system. For a single degree of freedom system as shown in Figure III.7, the dynamic stiffness can be expressed as $K_{dynamic} = k - \omega^2 m + i\omega c$, in which k is the stiffness of the spring, m is the mass and c is the viscous damping constant of the dashpot. One can fit the real part stiffness coefficients k_1 of a pile group by an expression of the form $1 - \omega^2 b$ as shown in Figure III.8, and the equivalent mass is then $m_{eq} = K_{static} \cdot b$.

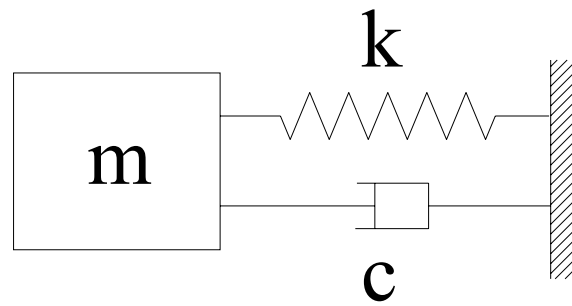


Figure III.7 A Single Degree of Freedom System

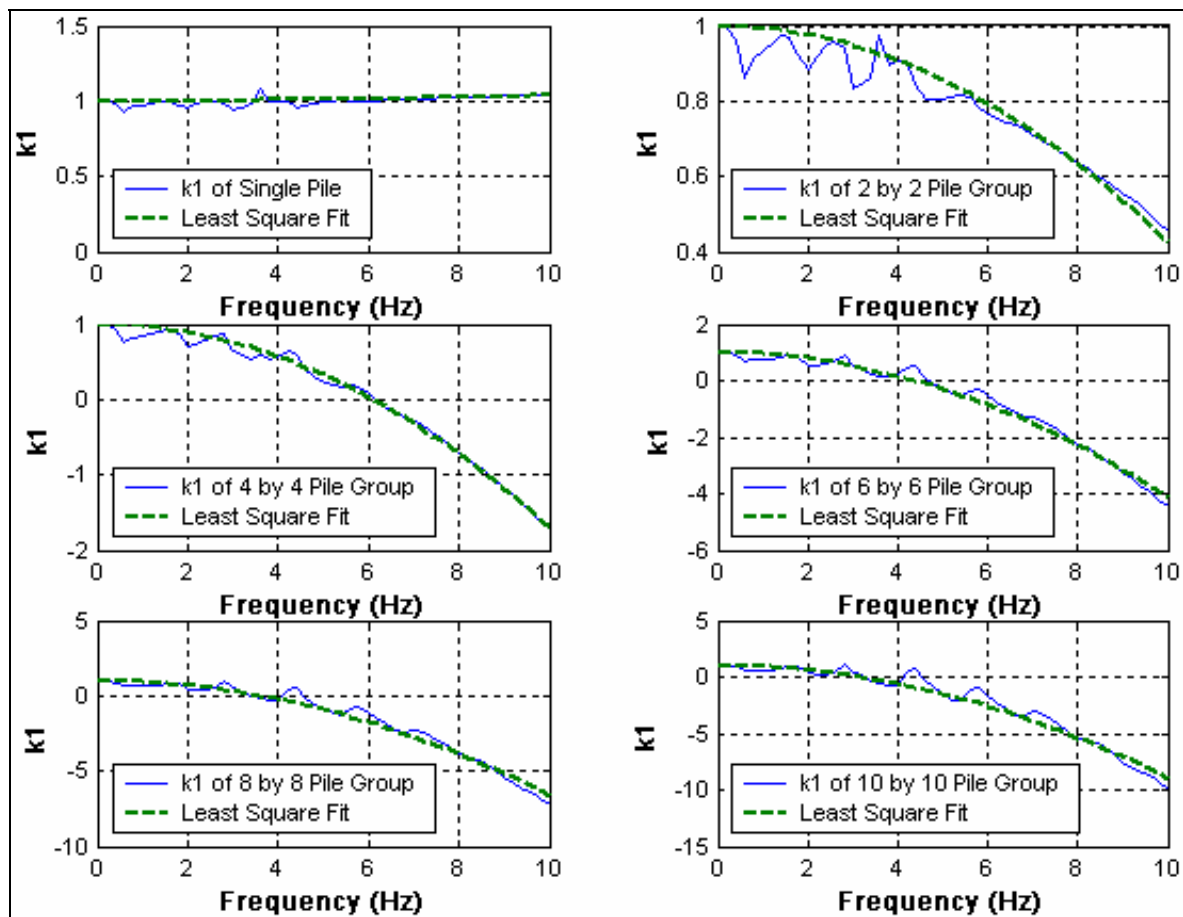


Figure III.8 Least Square Fit of the Real Stiffness Coefficients

Figure III.9 shows the equivalent mass resulting from a least squares fit as a function of the number of piles. Basically, it is a second degree parabola and proportional to $(N-1)^2$, which implies that the equivalent mass is almost proportional to the number of piles or the equivalent area defined in Figure III.2. The equivalent mass for a single pile is almost zero. Its real stiffness does not change very much with frequency, and it is normally assumed to be constant.

Figure III.10 shows the variation of the real stiffness coefficient k_1 with frequency for a 6 by 6 pile group when a limit (threshold) distance is imposed for the interaction coefficients. It can be seen that with the introduction of a limit distance the fluctuations decrease substantially, leading to a much smoother variation, and the curvature of the second degree parabola decreases also significantly, implying a smaller mass of the soil vibrating in phase with the foundation. The effect is relatively small for a threshold distance of 10 diameters but very pronounced for 5 diameters.

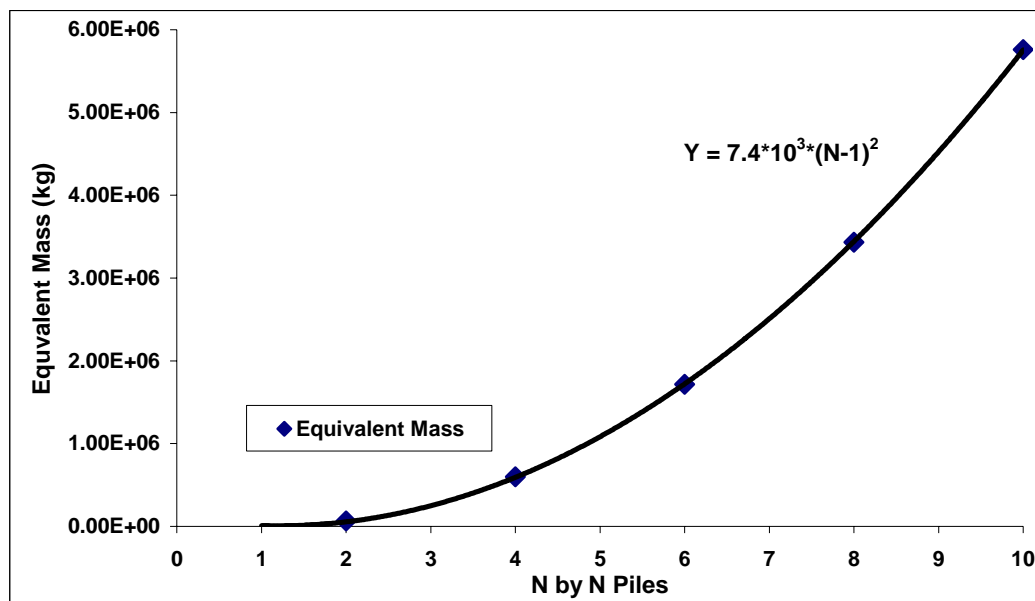


Figure III.9 Equivalent Mass from Least Square Fit

($E_p = 1000E_s = 5E10$, 2% Material Damping, No Threshold Distance, End Bearing Piles)

The imaginary stiffness coefficient c_I , representing the radiation damping, after subtracting the effect of the internal soil damping, should be zero below the fundamental shear frequency of the soil layer (0.625 Hz in this case), then jump suddenly and oscillate around a constant value. In reality, if there is some internal soil damping the jump is not sudden but there is a small amount of leakage of energy before the fundamental frequency.

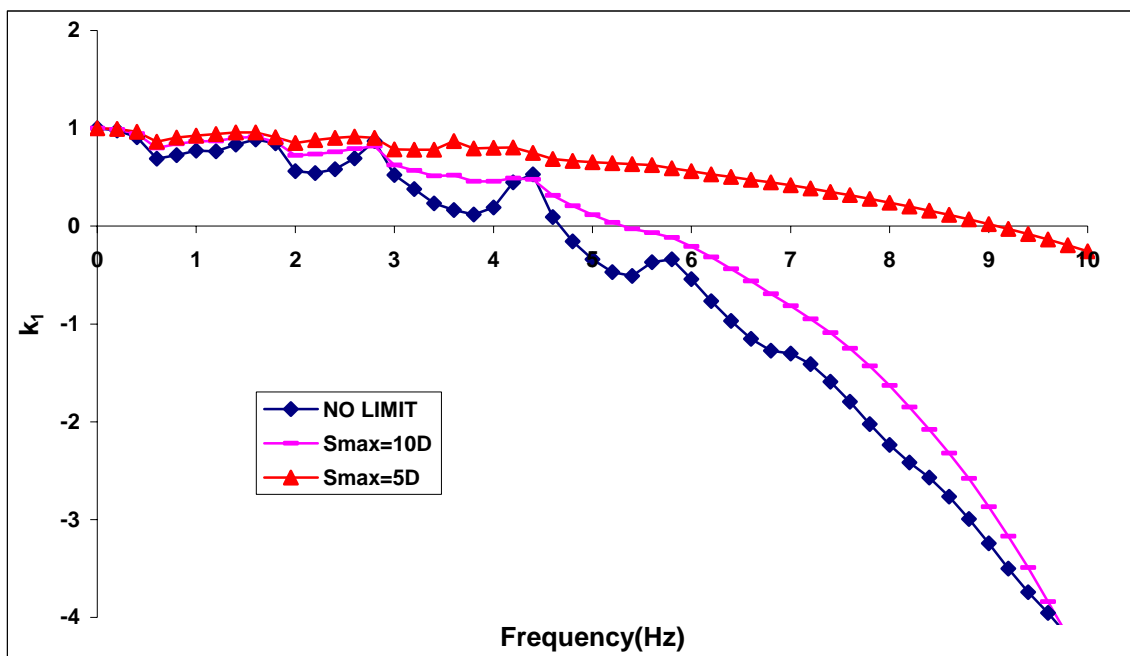


Figure III.10 Effect of S_{max} on Real Stiffness Coefficients of a 6 by 6 Pile Group
($E_p=1000E_s=5E10$, 2% Material Damping, End Bearing Piles)

Figure III.11 shows the variation of the coefficient c_I the number of piles for E_p/E_s equal to 1000. For frequencies larger than 1 the results oscillate around a value of approximately 0.7, the fluctuations increasing with increasing number of piles (as in the case of the real coefficient). For pile groups the coefficient c_I seems to continue to increase slightly with increasing frequency rather than oscillating around a constant value but use of this value should be reasonable over the range of frequencies of normal

interest. Figure III.12 shows the effect of the E_p/E_s ratio on the coefficient c_I for a single pile. It can be seen that c_I increases as the E_p/E_s ratio increases (as the soil became softer relative to the pile). When a limiting distance is imposed, neglecting the interaction coefficients beyond this distance, there will be less interaction between different piles in a group. So both the real and imaginary coefficients of pile groups will behave like those of a single pile, as previously discussed for the real coefficients (Figure III.10) and illustrated in Figure III.13 for c_I . The value of c_I above 1 Hz decreases significantly with decreasing value of the limiting distance. It should be noted, however, that since the equivalent dashpot is the product of the coefficient c_I by $\bar{R} \cdot K_{static} / c_s$ and the static stiffness, and the latter increases as the interaction coefficients are neglected, it would appear that the value of the dashpot is not affected much by the threshold distance (Figure III.14).

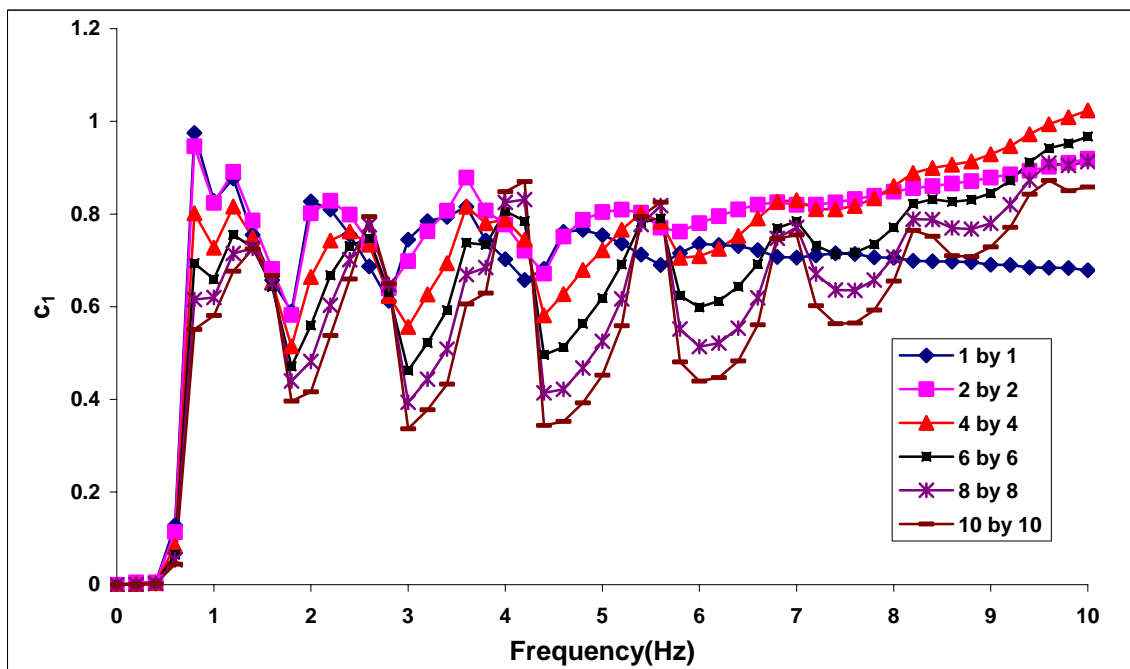


Figure III.11 Effect of Number of Pile on Normalized Imaginary Coefficients (c_I)
 ($E_p/E_s=1000$, 2% Material Damping, No Threshold Distance, End Bearing Piles)

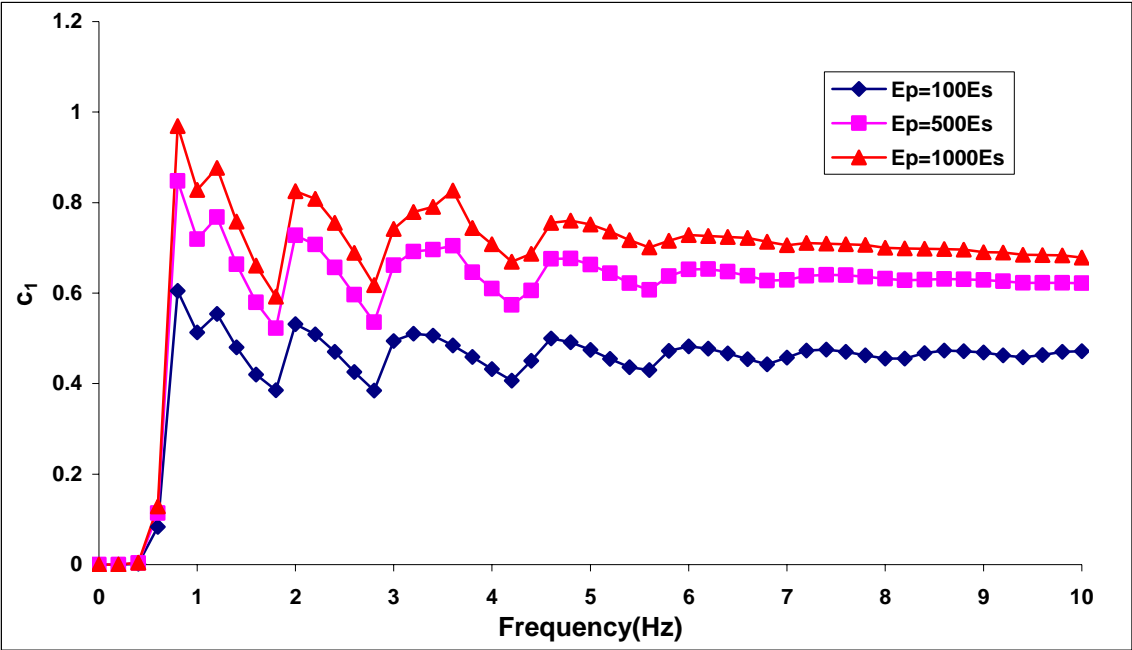


Figure III.12 Effect of E_p/E_s on Normalized Imaginary Coefficients (c_1) of Single Pile ($E_s=Constant=5E7$, 2% Material Damping, No Threshold Distance, End Bearing Piles)

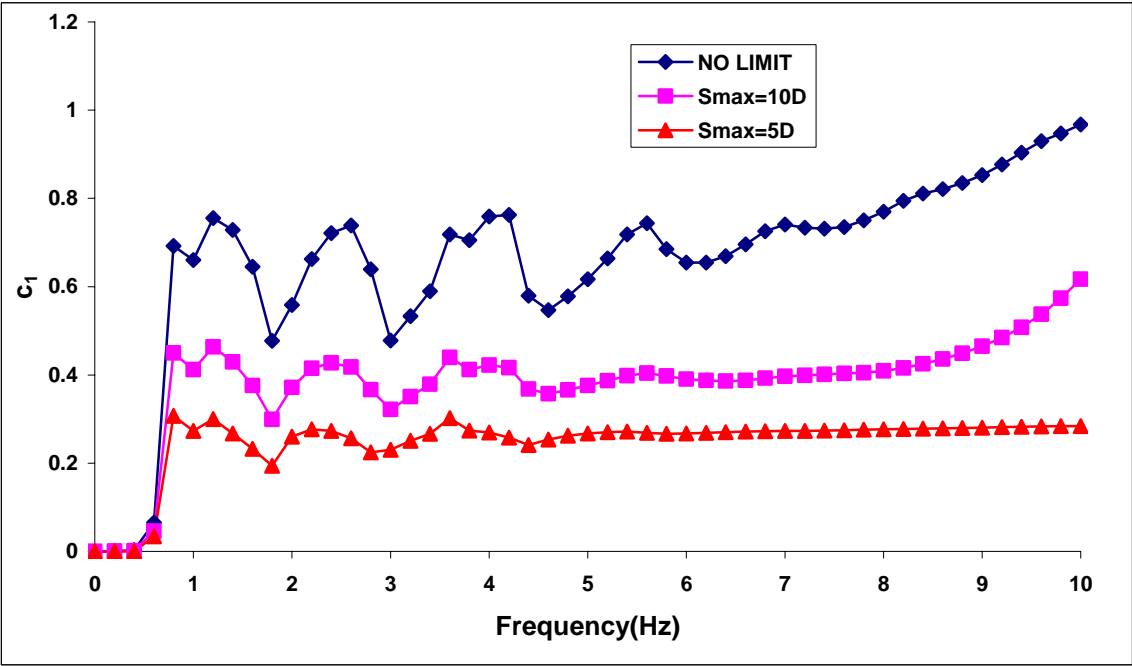


Figure III.13 Effect of S_{max} on Imaginary Stiffness Coefficients of a 6 by 6 Pile Group ($E_p=1000E_s=5E10$, 2% Material Damping, End Bearing Piles)

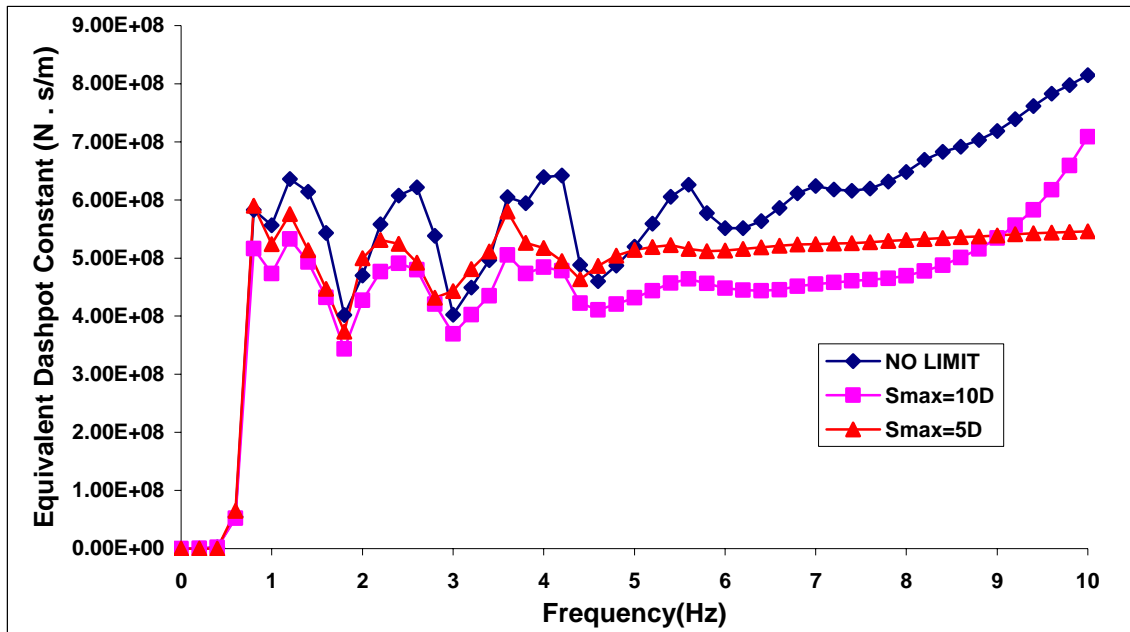


Figure III.14 Effect of S_{max} on Equivalent Dashpot Constant of a 6 by 6 Pile Group
($E_p=1000E_s=5E10$, 2% Material Damping, End Bearing Piles)

3.2.2 Vertical Stiffness

The vertical stiffness can also be expressed in the general form of Equation III.7. Unlike the horizontal cases in which the results are insensitive to the pile length and the tip conditions for most practical cases, the vertical stiffness is sensitive to the pile length and boundary conditions at the pile end, so in this section we consider primarily the vertical stiffness of floating piles and only that of end bearing piles for static loads.

(1) Static Stiffness

The group factor for the vertical stiffness is defined in the same way as for the horizontal stiffness by Equation III.8, except that K_G and K_S represent the static vertical group stiffness and static vertical stiffness of a single pile, respectively.

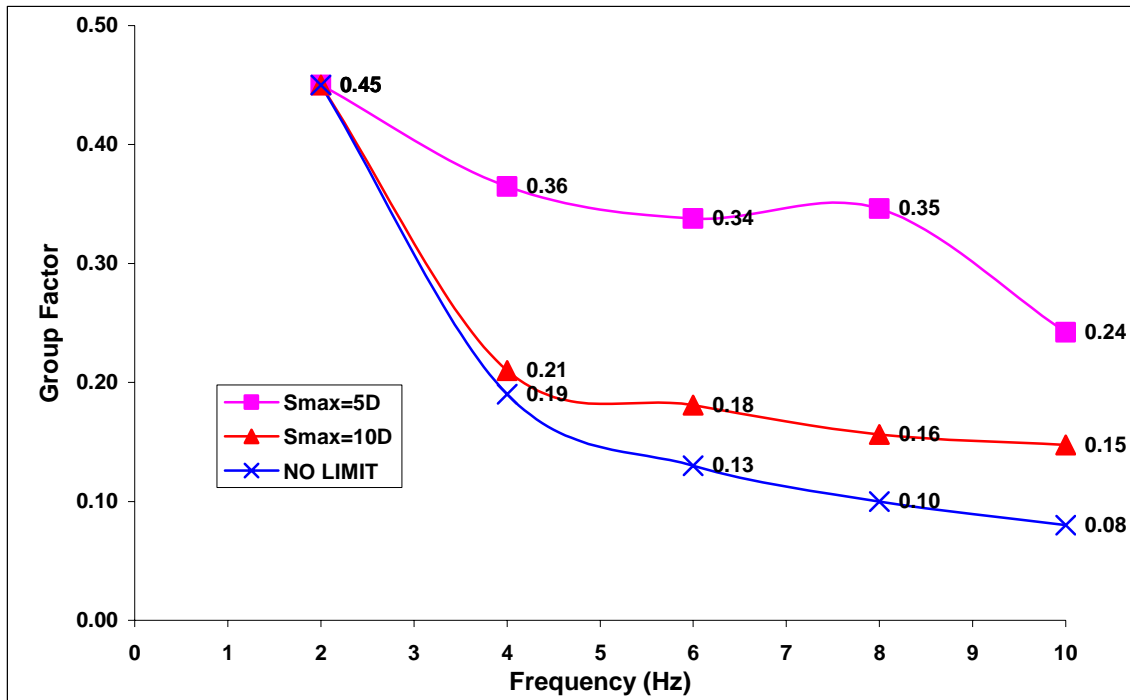


Figure III.15 Vertical Static Group Factors for Vertical Stiffness
($E_p/E_s=1000$, Floating Piles)

The vertical group factors of floating and end bearing piles are illustrated in Figures III.15 & III.16 with the ratio of Young's modulus of the piles to that of the soil (E_p/E_s) equal to 1000. The vertical group factors are much larger than $1/N$ for end bearing piles as shown in Figure III.16, but a little smaller than $1/N$ for floating piles as shown in Figure III.15. The reason is that, unlike the horizontal static stiffness, the vertical static stiffness will increase substantially as the pile length increases and rigid rock is reached. For end bearing piles there will be a lower bound for the vertical stiffness corresponding to a value of E_s equal to 0. In this case the total stiffness will be proportional to the number of piles.

The limiting distance has the same effect on vertical group factors as on the horizontal ones. The limit distance decreases the interaction between different piles in a pile group, so the group factors increase substantially. The vertical group factors of end bearing

piles are always much larger than those for floating piles (with or without limit distance), as could be expected. The results for floating piles and a limit distance of 5 diameters show an unexpected fluctuation.

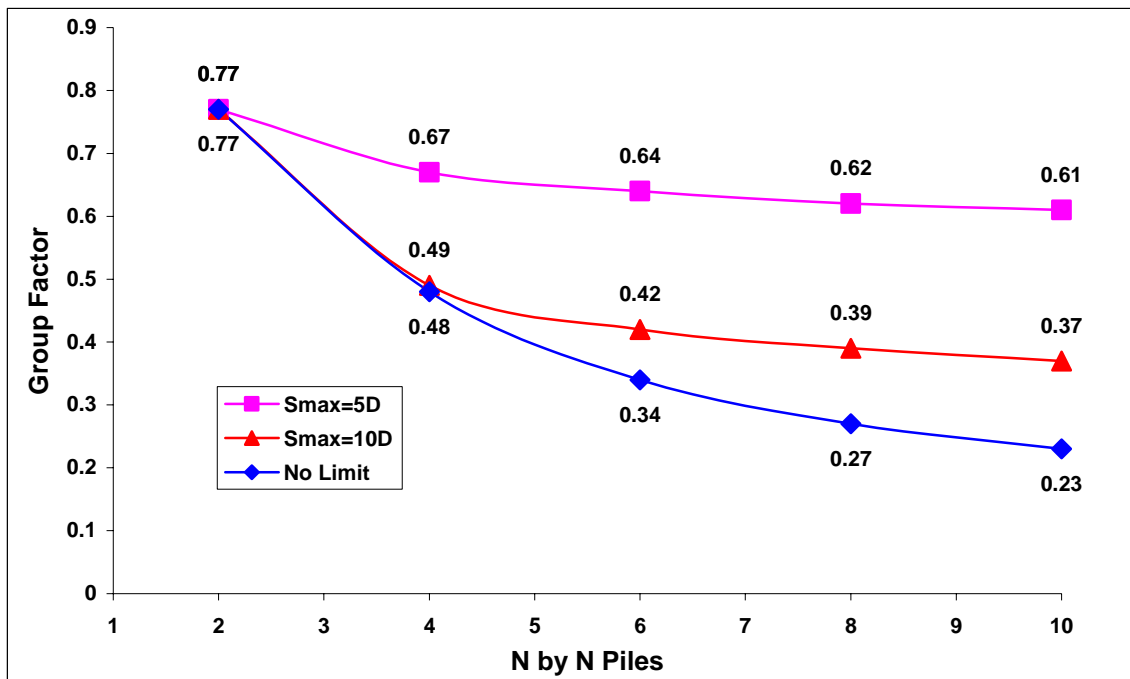


Figure III.16 Vertical Static Group Factors for Vertical Stiffness
($E_p/E_s=1000$, End Bearing Piles)

Other factors, like pile spacing and ratio of Young's modulus of the pile to that of the soil, will also have an effect on the vertical group factors. Figures III.17 & III.18 show the results when E_p/E_s varies from 100 to 1000, normally the range of engineering practice, without limit distance. The group factors decrease slightly with increasing E_p/E_s for both floating, while increase for end bearing piles.

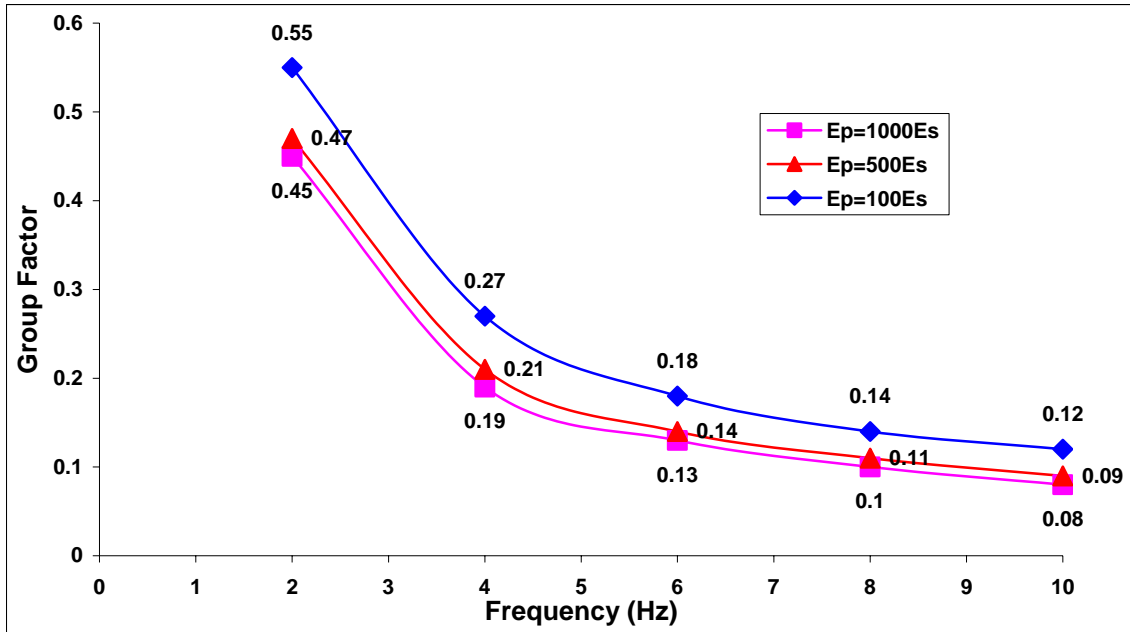


Figure III.17 Effect of E_p/E_s on Vertical Group Factors
(No Threshold Distance, Floating Piles)

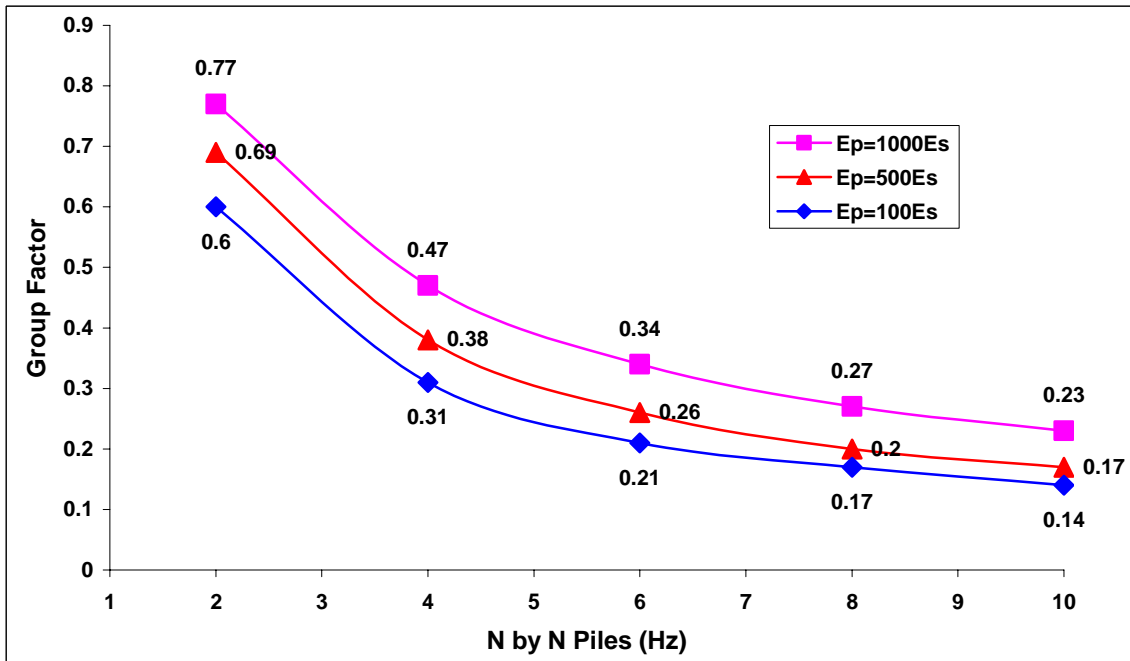


Figure III.18 Effect of E_p/E_s on Vertical Group Factors
(No Threshold Distance, End Bearing Piles)

(2) Real and Imaginary Stiffness Coefficients

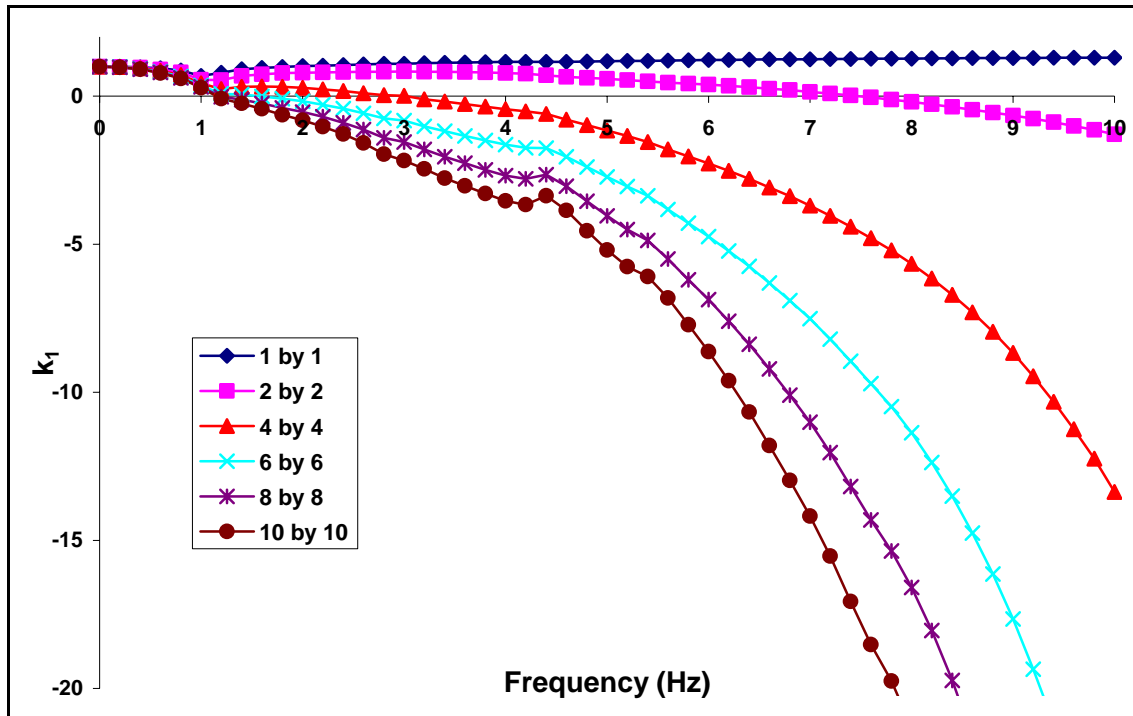


Figure III.19 Effect of Number of Piles on Real Coefficients
 ($E_p=1000E_s=5E10$, 2% Material Damping, No Threshold Distance, Floating Piles)

The real coefficient k_1 of a single pile is nearly a constant for all frequencies with a dip at the dilatational natural frequency of the soil deposit (about 1.0 Hz in this case) for the assumed Poisson's ratio of 0.25. As the number of piles increases the coefficient k_1 exhibits a parabolic variation with frequency like that of the horizontal stiffness, as illustrated in Figure III.19, but with smaller fluctuations around the second degree parabola.

Using the same method described earlier, one can find an equivalent mass for the vertical case. The results of LSF (Least Square Fit) for the vertical stiffness of floating

piles are shown in Figure III.20. For a single pile, the equivalent mass is essentially zero. As the number of piles increases, the equivalent mass increases and is proportional to $(N-1)^2$, as illustrated in Figure III.21, which suggests that the equivalent mass for vertical vibration of floating pile groups is proportional to the equivalent area (as for the horizontal case).

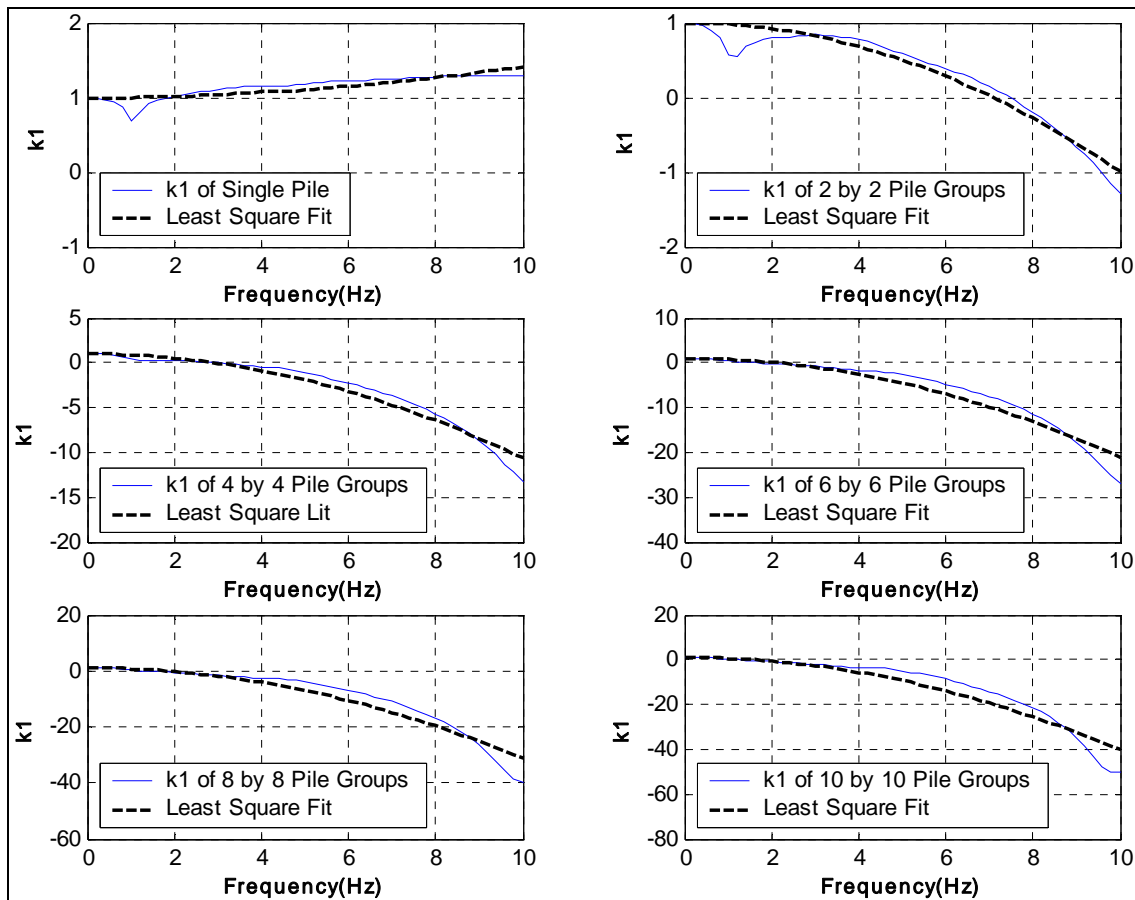


Figure III.20 LSF of Equivalent Mass of Vertical Stiffness

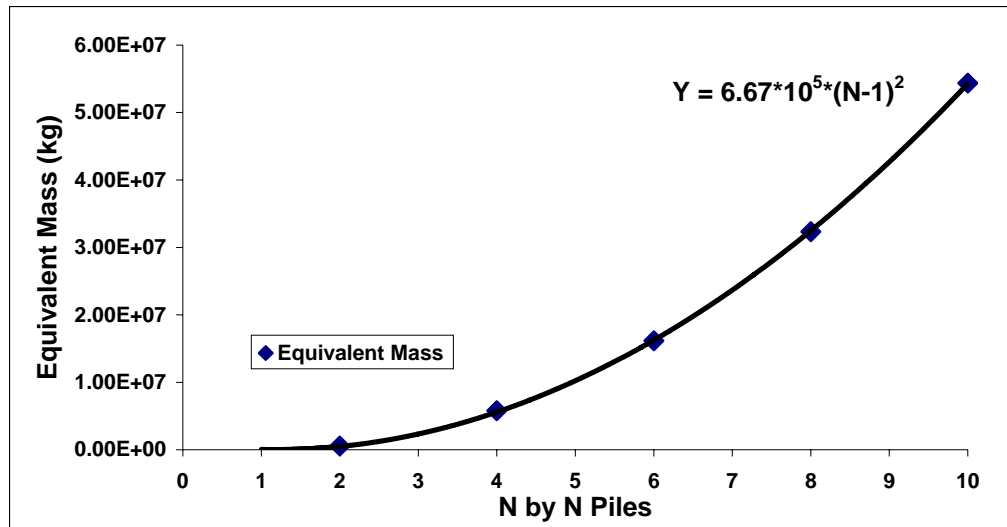


Figure III.21 Equivalent Mass with Number of Piles

Figure III.22 shows the variation of the real coefficient k_1 with frequency for a 6 by 6 pile group when a limit distance is imposed. It can be seen that the introduction of a limit distance of 5 or even 10 diameters will decrease the fluctuation, leading to a variation very similar to that of a smaller pile group with smaller equivalent mass, which results from the reduction of interaction between different piles.

The imaginary stiffness coefficients c_1 of floating piles for different number of piles, shown in Figure III.23, remain zero below the fundamental frequency in dilatation compression (about 1 Hz in this case), then jump suddenly and decrease to a constant value for a single pile, but are nearly a constant for pile groups in the normal range of interest. Figure III.24 shows the coefficients c_1 of single floating piles for different values of the E_p/E_s ratio. The coefficient c_1 for a single pile decreases with decreasing E_p/E_s .

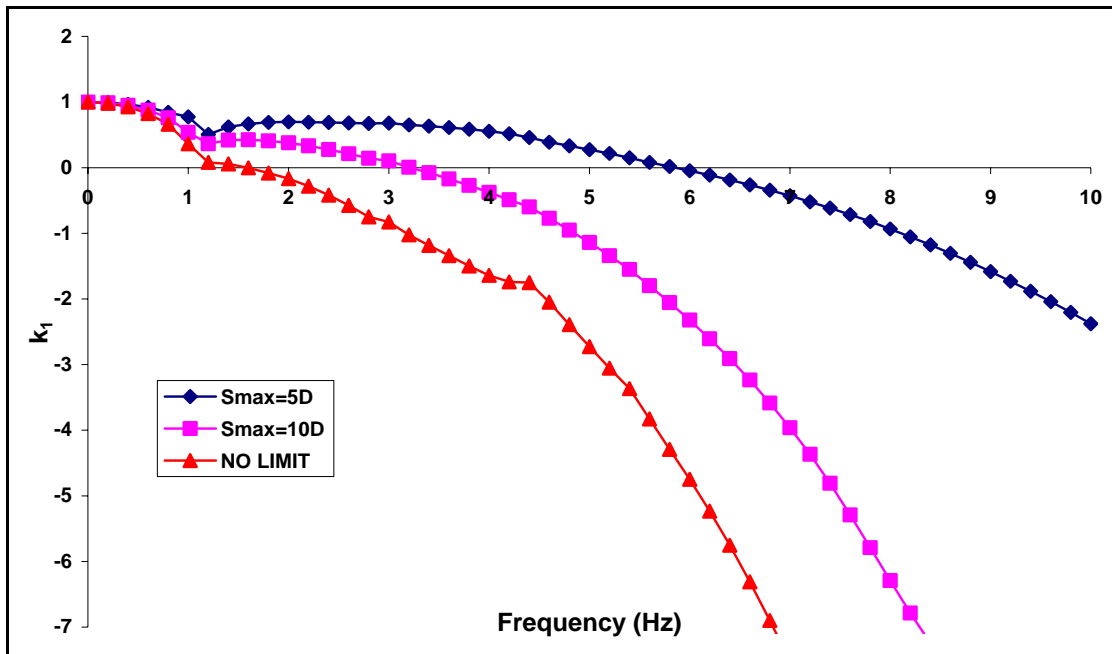


Figure III.22 Effect of Threshold Distance on Real Coefficients of 6 by 6 Pile Groups
($E_p=1000E_s=5E10$, 2% Material Damping, Floating Piles)

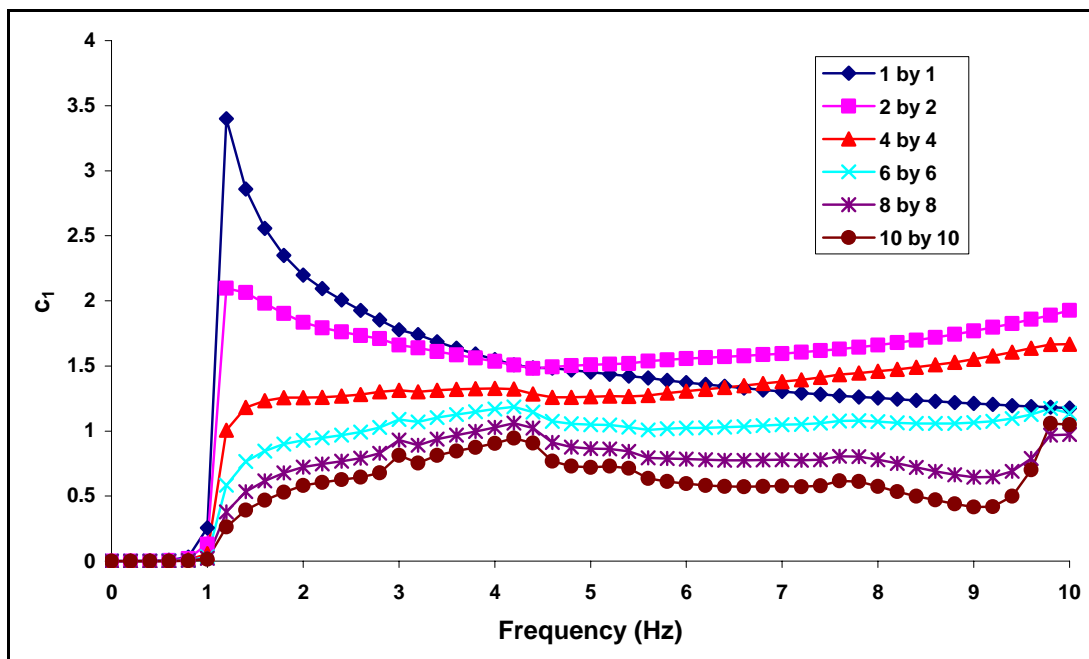


Figure III.23 Effect of Number of Piles on Imaginary Coefficients
($E_p=1000E_s=5E10$, 2% Material Damping, No Threshold Distance, Floating Piles)

The effect of imposing a limit distance on the interaction coefficients in the imaginary coefficient c_1 is similar to that discussed earlier for the horizontal case, the coefficient decreasing with decreasing limit distance. The same observations made earlier apply here. Although the coefficient decreases the static stiffness increases so that the equivalent dashpot may not change very much.

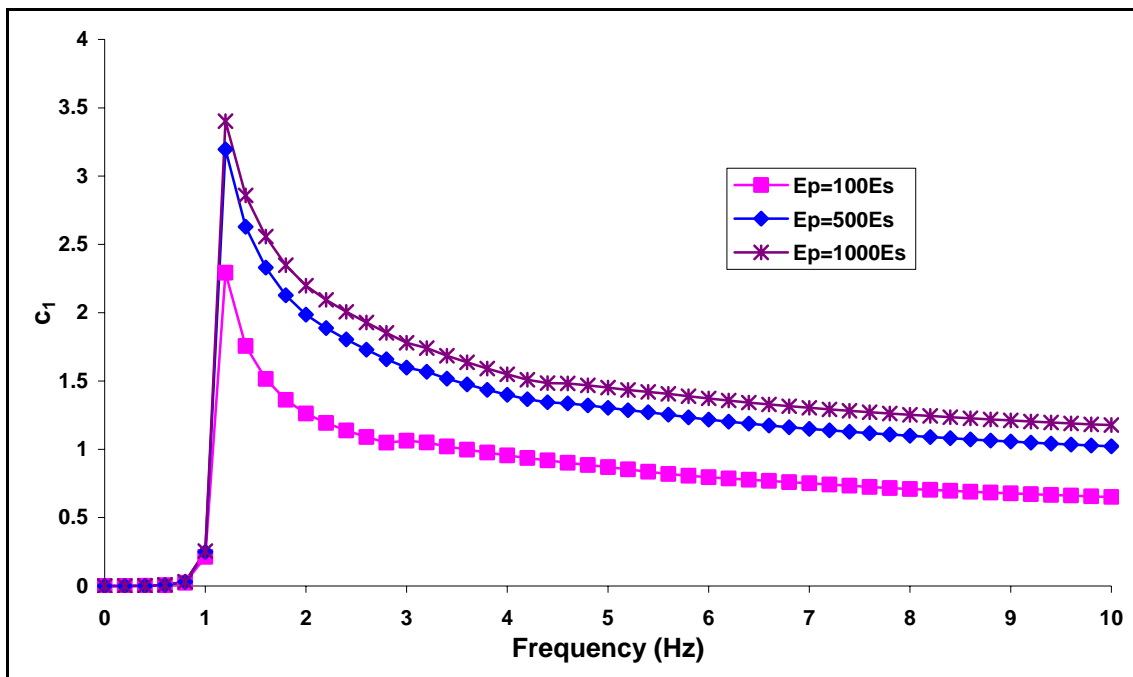


Figure III.24 Effect of E_p/E_s on Imaginary Coefficients of Single Piles
(E_s =Constant=5E10, 2% Material Damping, No Threshold Distance, Floating Piles)

3.2.3 Rocking Stiffness

As in the vertical case the rocking stiffness is affected significantly by the length and tip condition of the piles, since it is a function of the vertical stiffness of each pile. Only the dynamic case of floating piles is studied in this section. End bearing piles are considered for the static case for comparison purposes.

(1) Static Stiffness

The definition of the static group reduction factor the for rocking stiffness is

$$GF_{Rocking} = \frac{K_G}{K_S \cdot \sum_{i=1}^n d_i^2}$$

where

n number of piles;

d_i distance from i -th pile to the center of the pile group;

K_G static rocking stiffness of the pile group;

K_S static vertical stiffness of a single pile.

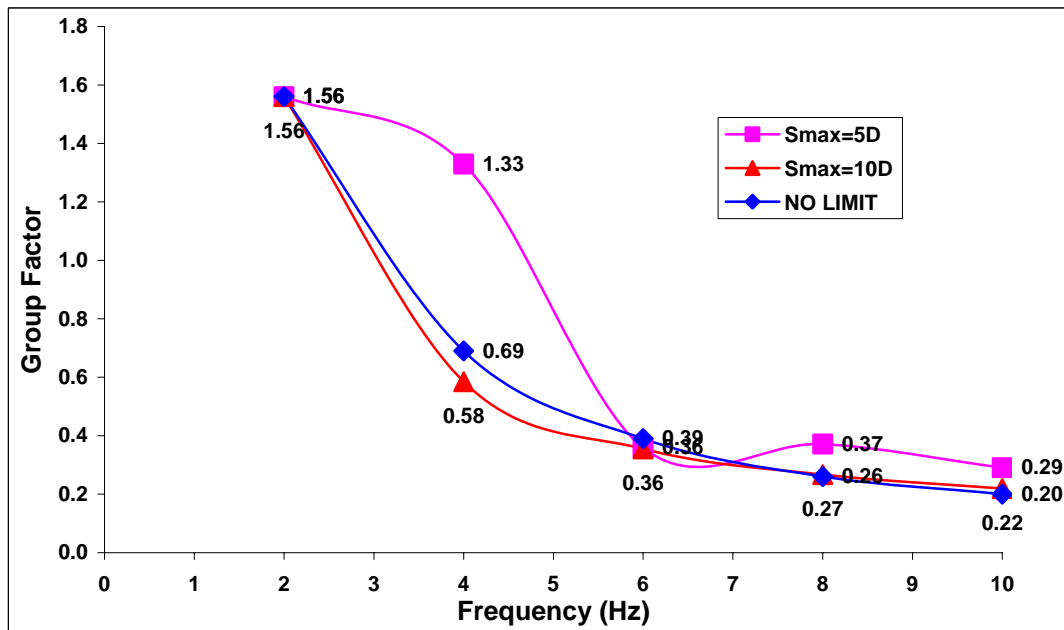


Figure III.25 Static Group Reduction Factor for Rocking Stiffness
($E_p/E_s=1000$, Floating Piles)

Figures III.25 & III.26 show the group factor for the rocking stiffness of floating piles and end bearing piles, respectively, with $E_p/E_s=1000$. The group factor is larger than 1 for 2 by 2 pile groups, which implies the interaction between piles will increase the group static stiffness, while smaller than 1 for pile groups larger than 4 by 4.

With the introduction of a limiting distance, the group factor of end bearing piles will decrease for smaller pile groups while increasing for larger groups. The group factor of floating piles for $S_{\max} = 10D$ is almost the same as that without limit distance, while that for $S_{\max} = 5D$ exhibits some unexpected fluctuations more pronounced for small pile groups.

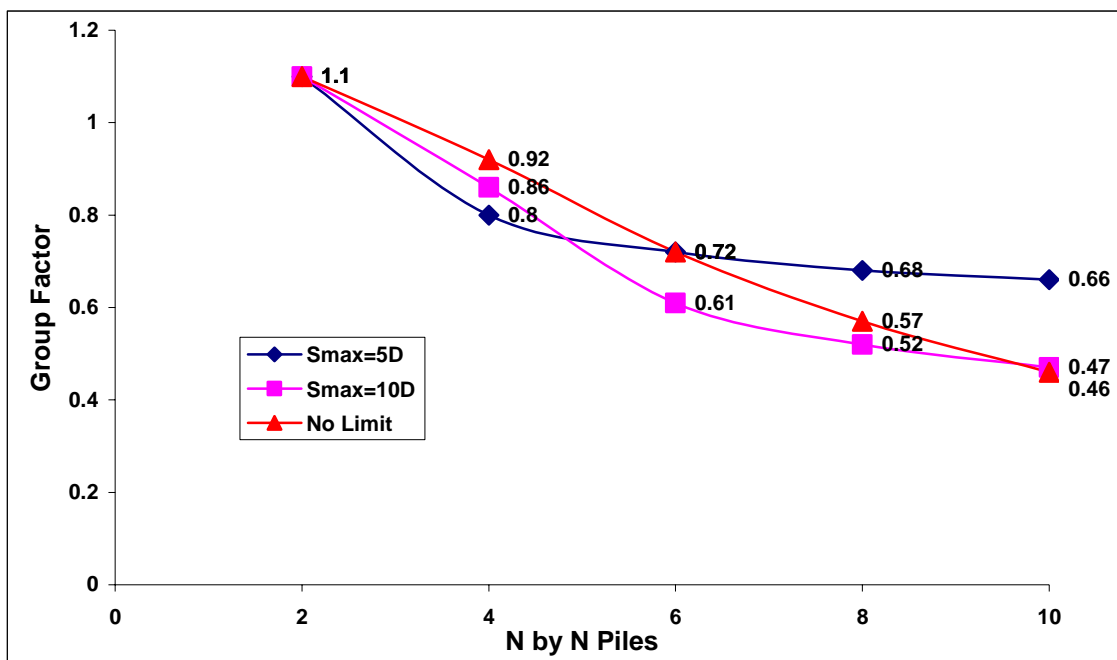


Figure III.26 Static Group Reduction Factor for Rocking Stiffness
($E_p/E_s=1000$, End Bearing Piles)

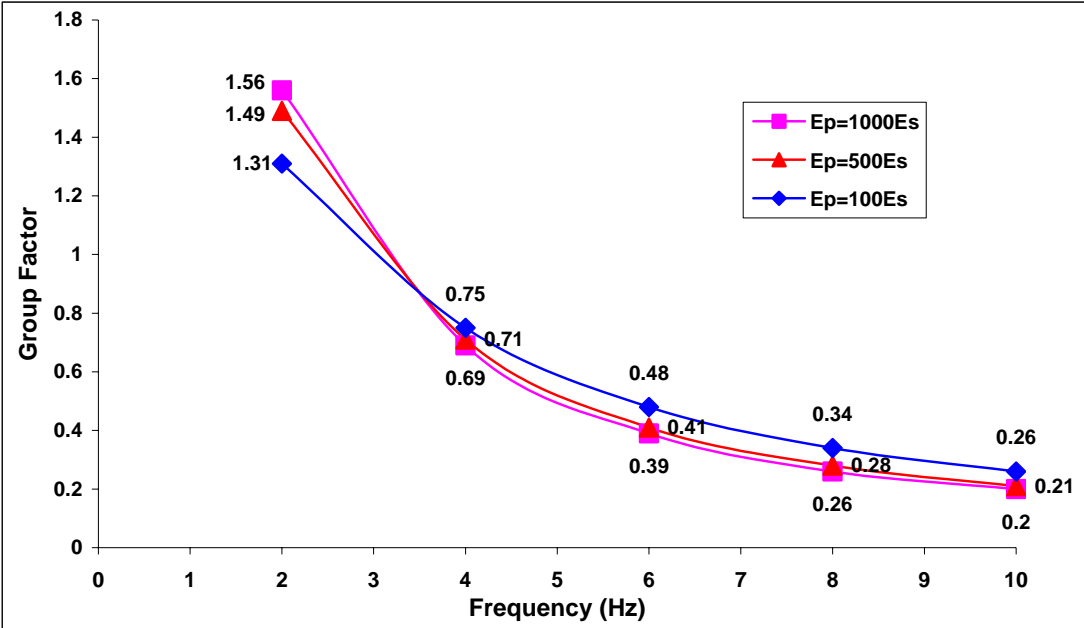


Figure III.27 Effect of E_p/E_s on Static Group Factor
(No Threshold Distance, Floating Piles)

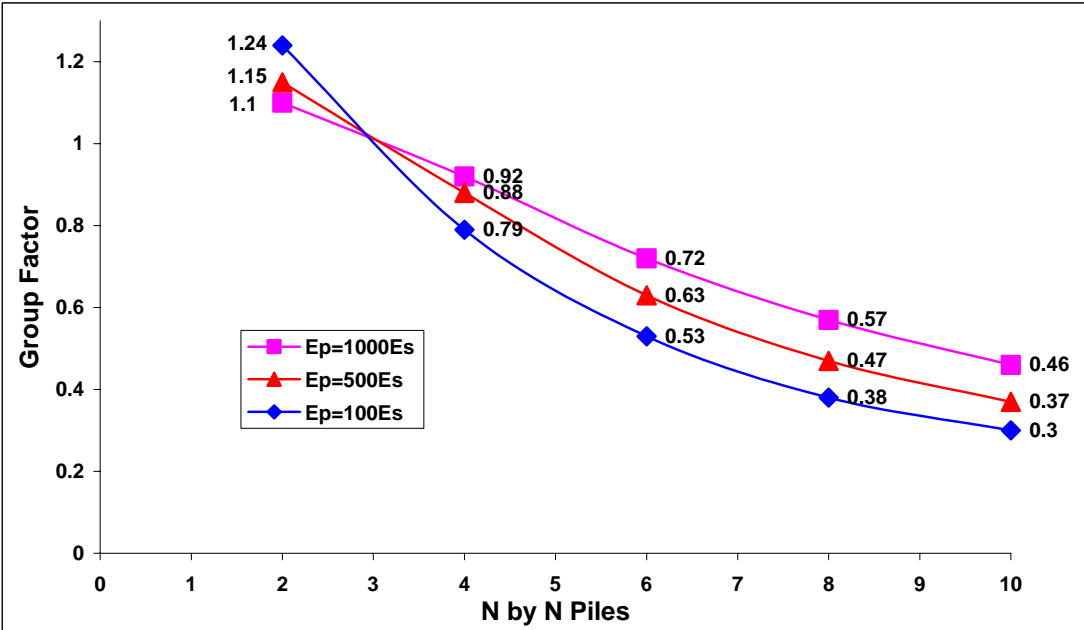


Figure III.28 Effect of E_p/E_s on Static Group Factor
(No Threshold Distance, End Bearing Piles)

The group factor also depends on other factors, like E_p/E_s , as shown in Figures III.27 & III.28. All curves in the two figures intersect at about $N = 3$ (It depends on pile spacing.). As E_p/E_s increases, the group factors decrease for 2 by 2 pile groups and increase for larger groups.

The group factors of end bearing piles are larger than those of floating piles for larger pile groups while smaller for 2 by 2 groups.

(2) Real and Imaginary Stiffness Coefficients

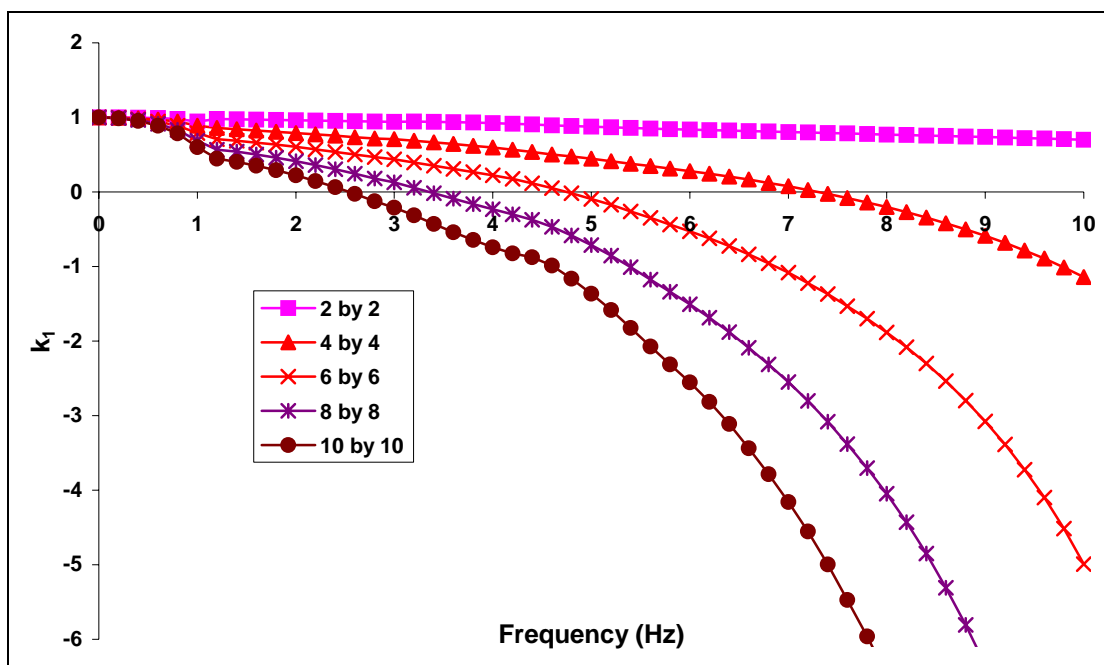


Figure III.29 Effect of Number of Piles on Real Coefficients

($E_p=1000E_s=5E10$, 2% Material Damping, No Threshold Distance, Floating Piles)

The real stiffness coefficient k_1 of the rocking stiffness, shown in Figure III.29, behaves like that of the single degree of freedom system in Figure III.7. Unlike the real

coefficient k_1 of the horizontal stiffness, k_1 of the rocking stiffness does not have large fluctuations even for large pile groups like 10 by 10. One can also fit (Least Square Fit) the coefficients k_1 by an expression of the form $1 - b \cdot \omega^2$ to find an equivalent mass moment of inertia ($I_{eq} = K_{static} \cdot b$), as in the case of horizontal and vertical stiffness.

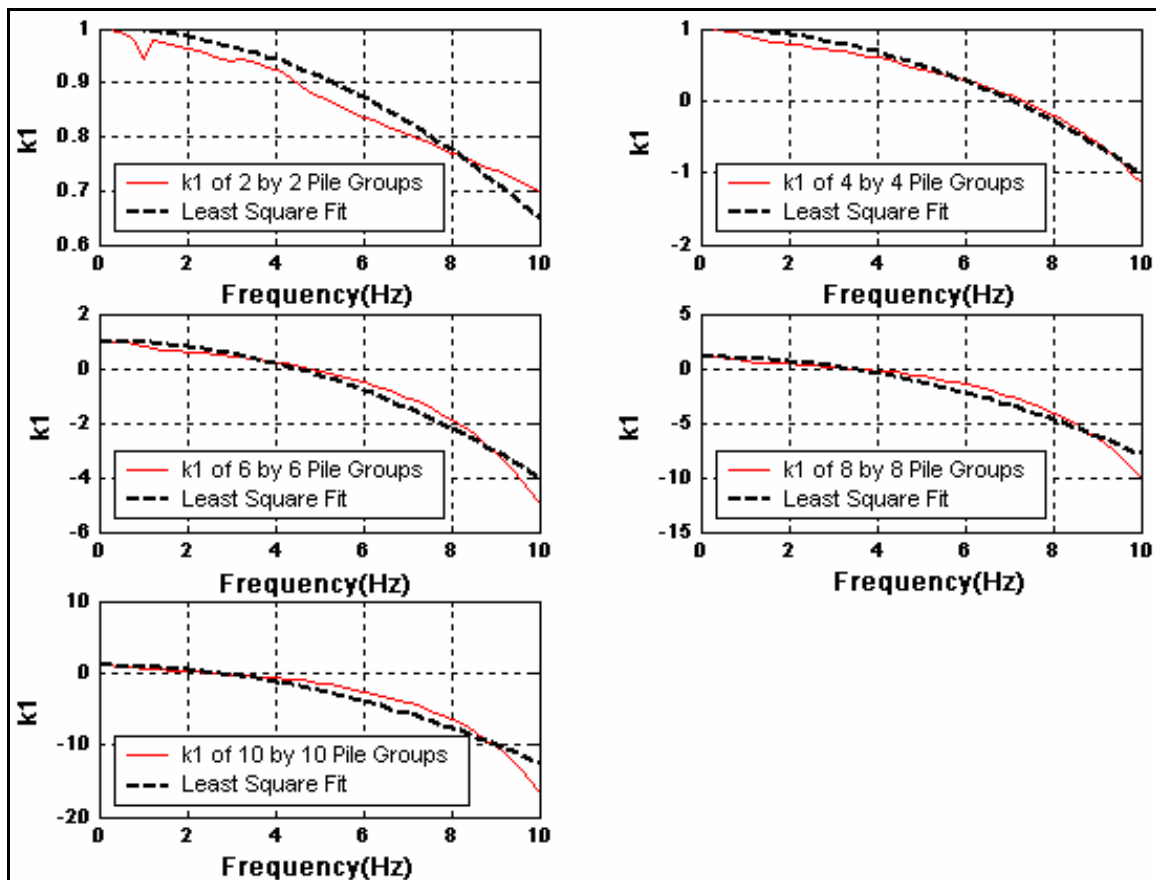


Figure III.30 Least Square Fit of Equivalent Inertia of Rotation of Rocking Stiffness

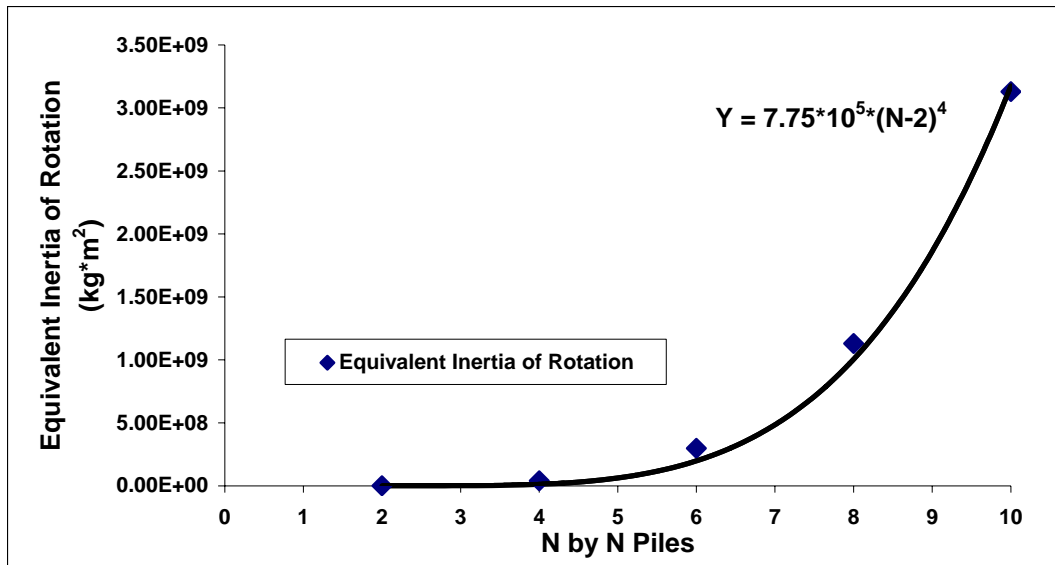


Figure III.31 Equivalent Inertia of Rotation with Number of Piles

Figure III.30 shows the results of the LSF (Least Square Fit) for the real coefficient k_1 . It can be seen that one can approximate the coefficient k_1 of the rocking stiffness by a second degree parabola of the form of $1 - b \cdot \omega^2$ and the equivalent moment of inertia is proportional to $(N - 2)^4$, as illustrated in Figure III.31. This is very similar to a cylindrical rigid mass, whose rotational inertia is proportional to the radius to the fourth order.

The introduction of a limiting distance will lead to an even smoother variation with frequency and decrease in the curvature of the second degree parabola, as illustrated in Figure III.32, indicating a smaller equivalent mass vibrating in phase with the foundation, but the reduction is not as marked as for the horizontal stiffness.

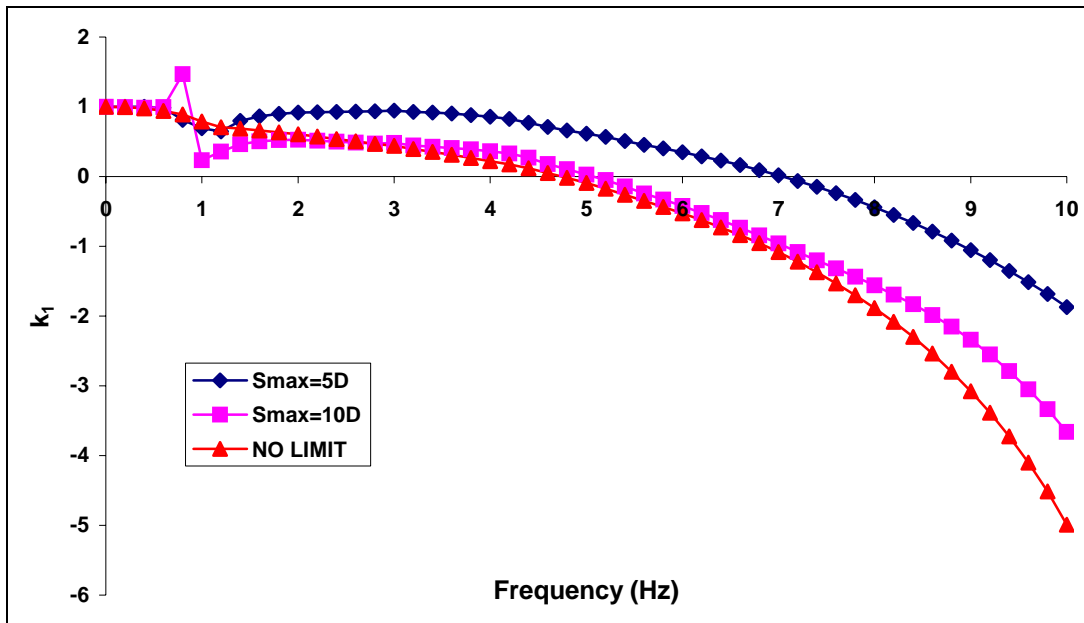


Figure III.32 Effect of Limit Distance on Real Coefficients of 6 by 6 Pile Groups
($E_p=1000E_s=5E10$, 2% Material Damping, Floating Piles)

Figure III.33 shows the imaginary coefficient c_1 of the rocking stiffness for different number of piles. The coefficient c_1 jumps at 1 Hz and keeps increasing slowly and smoothly for 2 by 2, 4 by 4 and 6 by 6 pile groups, while it oscillates around a constant (about 0.4 in this case) for 8 by 8 and 10 by 10 pile groups. It can be seen that the coefficient c_1 of a 2 by 2 pile group is much smaller than that of larger pile groups.

The effect of E_p/E_s on the imaginary coefficient c_1 for a 2 by 2 pile group is illustrated in Figure III.34. For E_p/E_s varying from 100 to 1000 in the normal range of engineering practice, c_1 increases a little bit for increasing E_p/E_s but the shape of the curves is very similar.

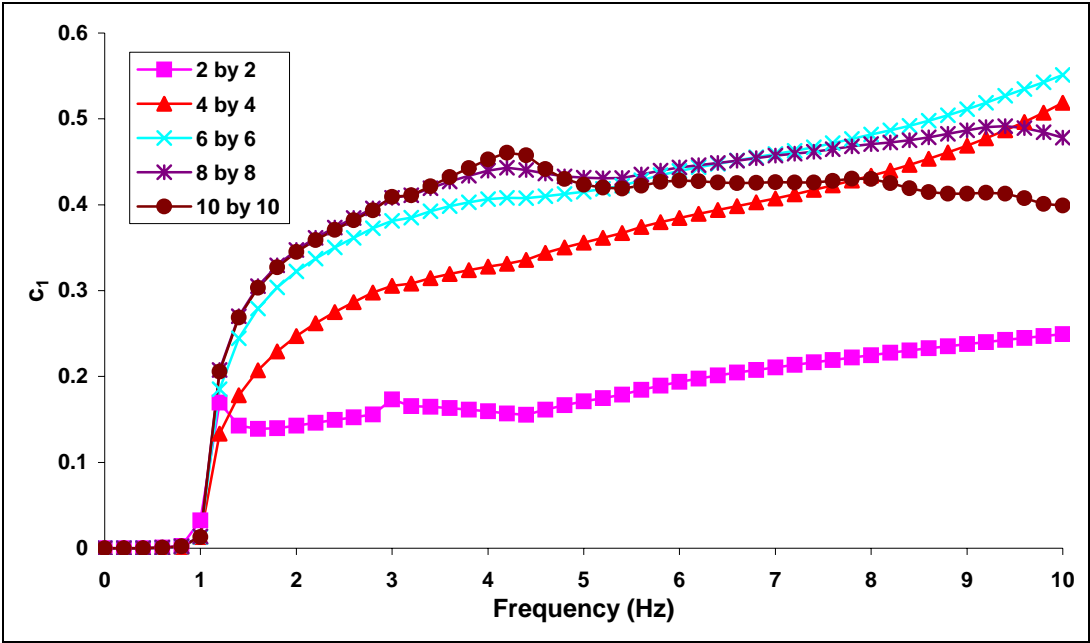


Figure III.33 Effect of Number of Piles on Imaginary Coefficients
($E_p=1000E_s=5E10$, 2% Material Damping, No Threshold Distance, Floating Piles)

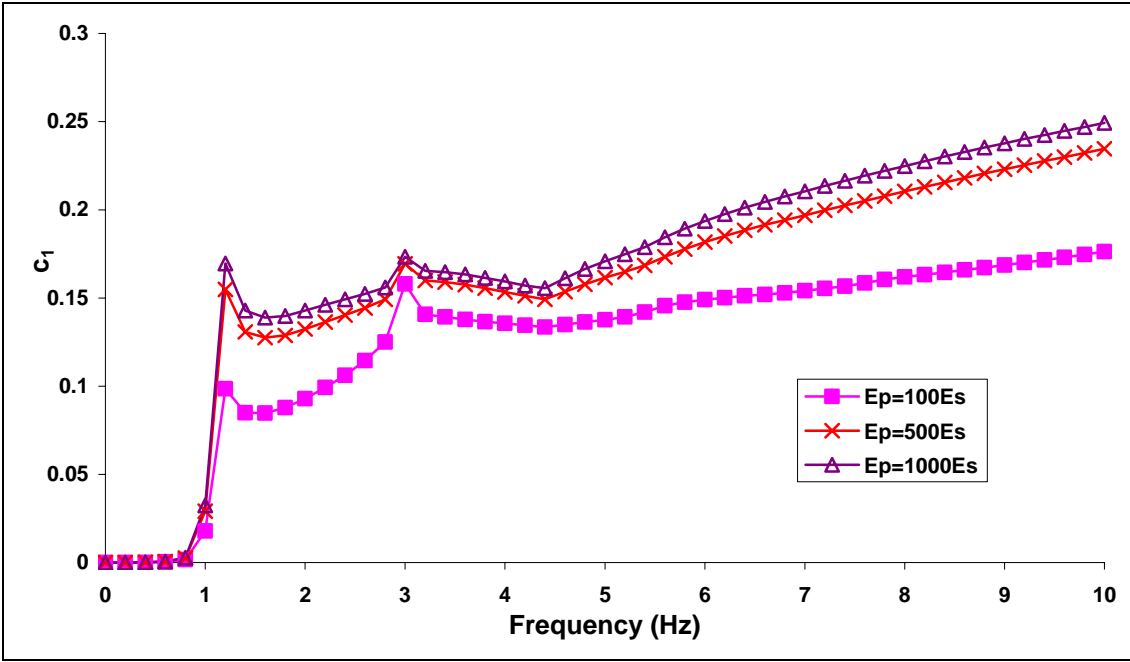


Figure III.34 Effect of E_p/E_s on Imaginary Coefficients of 2 by 2 Pile Groups
(2% Material Damping, No Threshold Distance, Floating Piles)

CHAPTER IV

DYNAMIC STIFFNESS OF FOUNDATIONS OF MARGA-MARGA BRIDGE'S PIERS

In this chapter, the procedures described in the previous one are applied to determine the dynamic stiffness of the pile foundations of piers P2 to P6 of the Marga-Marga bridge. The stiffness of the foundations for piers P1 and P7 were determined with an existing program for mat foundations.

4.1 Introduction

The Marga-Marga bridge, shown schematically in Figure IV.1, has seven piers (P1~P7), five of them (P2~P6) with pile foundations. Each of the pile foundations consists of a 5 by 2 pile group (rows of 5 piles in the direction perpendicular to the figure and 2 in the longitudinal direction of the bridge). Piers P1 and P7 have surface mat foundations without any supporting piles.

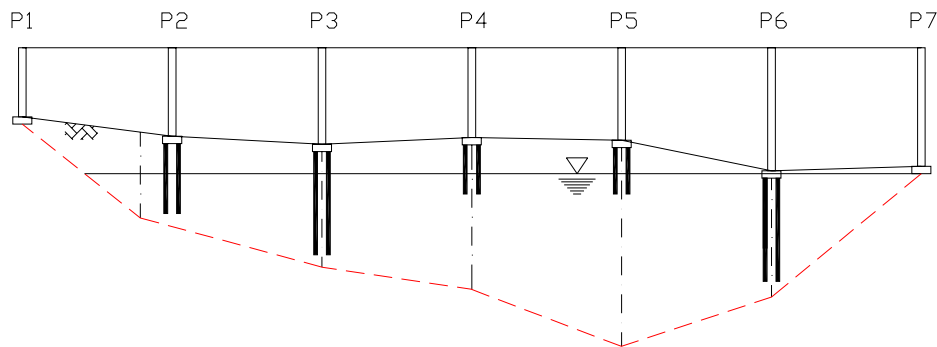


Figure IV. 1 Piers and Pile Groups of Marga-Marga Bridge

To calculate the stiffness of these pile groups, the interaction between two different pile groups was neglected, assuming each pile group embedded in a horizontal layered soil deposit extending to infinity in the two horizontal directions, based on the fact that the distance between pile groups is much larger than the horizontal dimension of the pile groups themselves.

4.2 Dimensions of the Pile Groups and Soil Properties

The dimensions of the piers and their pile foundations are illustrated in Figure IV.2 and Table IV.1. For piers P2~P6, which have pile foundations, the dimensions of the caps are the same, 13.5×5 m. The pile spacings in the x and y directions are 3 and 4 meters respectively, as illustrated in Figure IV.3. The length and diameter of the piles are listed in Table IV.2.

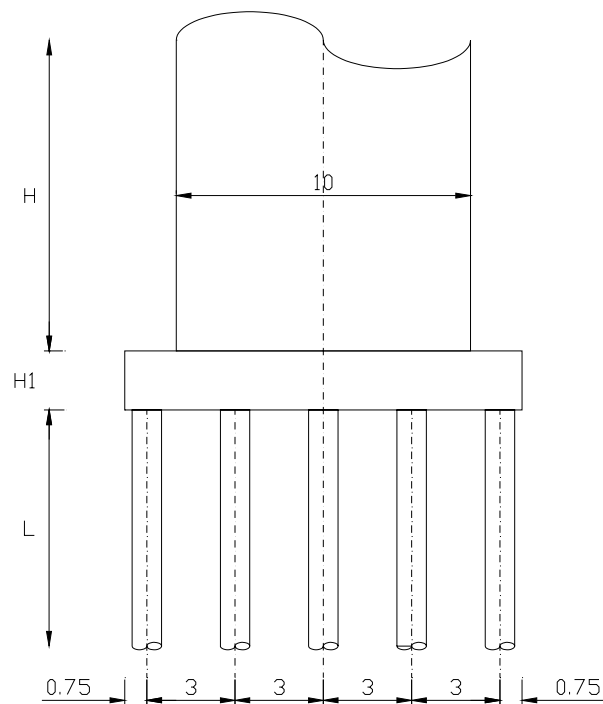
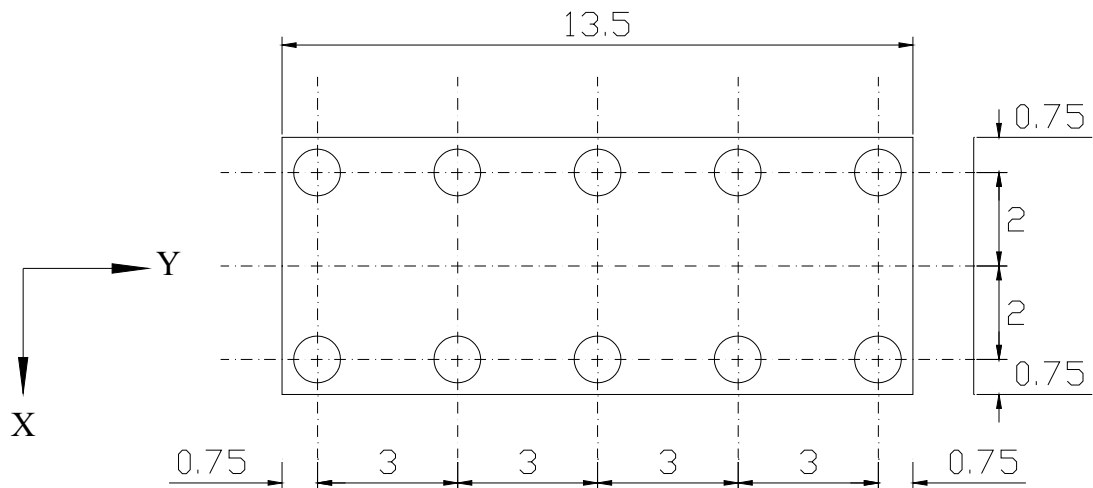


Figure IV. 2 A Pier and Its Pile Foundation

Table IV. 1 Dimension of the Pier and Cap

Pier #	H (m)	H1 (m)	Width of Cap (m)
1	21.865	1.5	10.5
2	26.317	2.0	13.5
3	27.138	2.0	13.5
4	26.260	2.0	13.5
5	26.082	2.0	13.5
6	30.154	2.0	13.5
7	30.086	1.5	10.5

**Figure IV. 3 Dimensions of Cap and Pile Spacing**

The soil properties under each pier, including the thickness of each layer and its shear wave velocity, are shown in Tables IV.3 to IV.6. The soil under the dashed line at the bottom of Figure IV.1 is assumed to have a shear wave velocity of 550 m/s, while the layers above the line have shear wave velocities in the range of 200~400 m/s. All the

soils are assumed to have a Poisson's ratio, mass density and internal damping of 0.25, 2000 kg/m³ and 5%, respectively.

Table IV. 2 Length and Diameter of Piles

Pier #	L (m)	Diameter (m)
2	19.50	1.0
3	30.00	1.0
4	15.06	1.0
5	14.02	1.0
6	31.70	1.0

Table IV. 3 Soil Properties for Pier #2

	Thickness (m)	Depth (m)	Shear Wave Velocity (m/s)
Layer 1	7.20	7.20	240
Layer 2	5.00	12.20	210
Layer 3	27.80	40.00	550
Layer 4	50.00	90.00	550

The piles are made of concrete with a Young's modulus of about 3×10^{10} Pa. The mass density and internal damping are assumed to be 2500kg/m³ and 5%, respectively. This represents an E_p/E_s ratio of 75 to 100, indicating a stiffer soil than the one normally encountered with pile foundations.

No limiting distance was used in the calculation of the dynamic stiffness terms.

Table IV. 4 Soil Properties for Pier #3 and #4

	Thickness (m)	Depth (m)	Shear Wave Velocity (m/s)
Layer 1	7.20	7.20	240
Layer 2	5.00	12.20	210
Layer 3	4.69	16.89	330
Layer 4	13.11	30.00	360
Layer 5	10.00	40.00	390
Layer 6	50.00	90.00	550

Table IV. 5 Soil Properties for Pier #5

	Thickness (m)	Depth (m)	Shear Wave Velocity (m/s)
Layer 1	7.20	7.20	240
Layer 2	5.00	12.20	310
Layer 3	4.69	16.89	330
Layer 4	13.11	30.00	360
Layer 5	10.00	40.00	390
Layer 6	50.00	90.00	550

Table IV. 6 Soil Properties for Pier #6

	Thickness (m)	Depth (m)	Shear Wave Velocity (m/s)
Layer 1	1.35	1.35	240
Layer 2	5.00	6.35	310
Layer 3	4.69	11.04	330
Layer 4	13.11	24.15	210
Layer 5	10.00	35.15	390
Layer 6	50.00	84.15	550

4.3 Dynamic Stiffness of Pile Foundations

The dynamic stiffness terms (real and imaginary parts) were computed by the programs described in the previous chapter using the data shown above. Figures IV.4 to IV.13 show the dynamic stiffness of the pile foundations P2~P6.

The real and imaginary parts of the horizontal dynamic stiffness in the X and Y directions are shown in Figures IV.4 to IV.7. The horizontal stiffness is similar in the two directions and slightly larger in the longitudinal direction of the bridge, because group effects are less important in this direction (only rows of 2 piles instead of 5). Since the horizontal stiffness depends only on the soil and pile properties near the surface, those of P3 and P4 are almost the same, though the length of the piles in the two groups is very different (P3 has piles 30m long but those of P4 are only 15.06m long).

The real part of the horizontal stiffness is nearly constant, with some oscillations. The real part of the horizontal stiffness for pier P6 is the largest of the five with an apparent dip at the fundamental natural frequency in shear (about 1.4 Hz in this case), which results from the stiffer soil near the surface (Table IV.6).

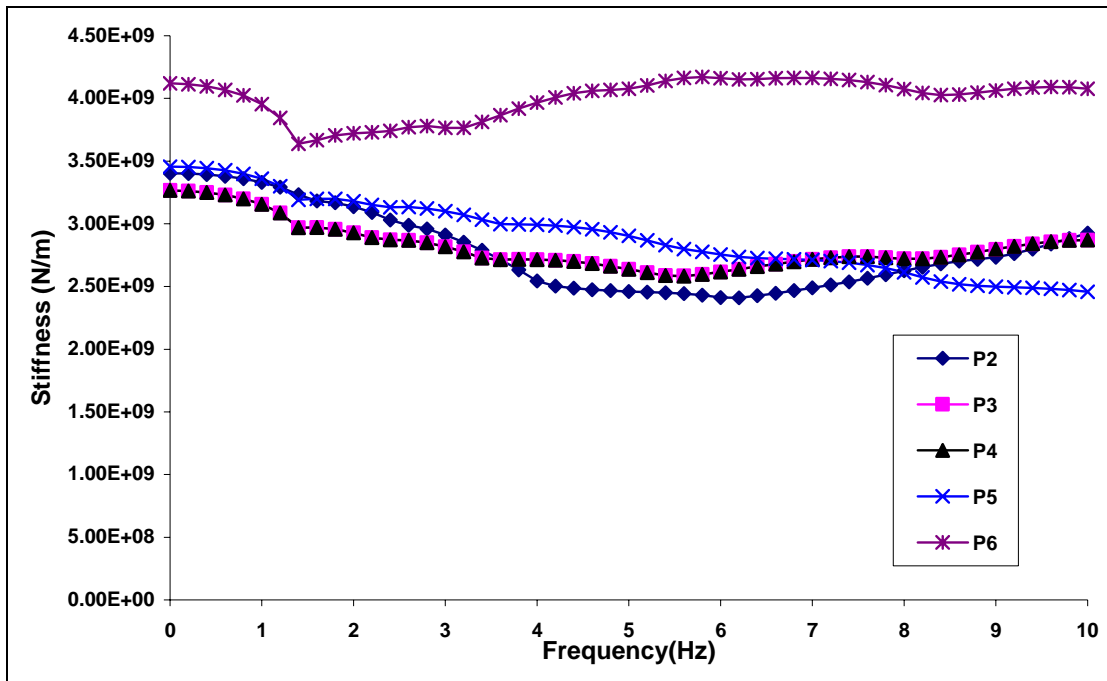


Figure IV. 4 Real Part of Horizontal Stiffness in Y Direction

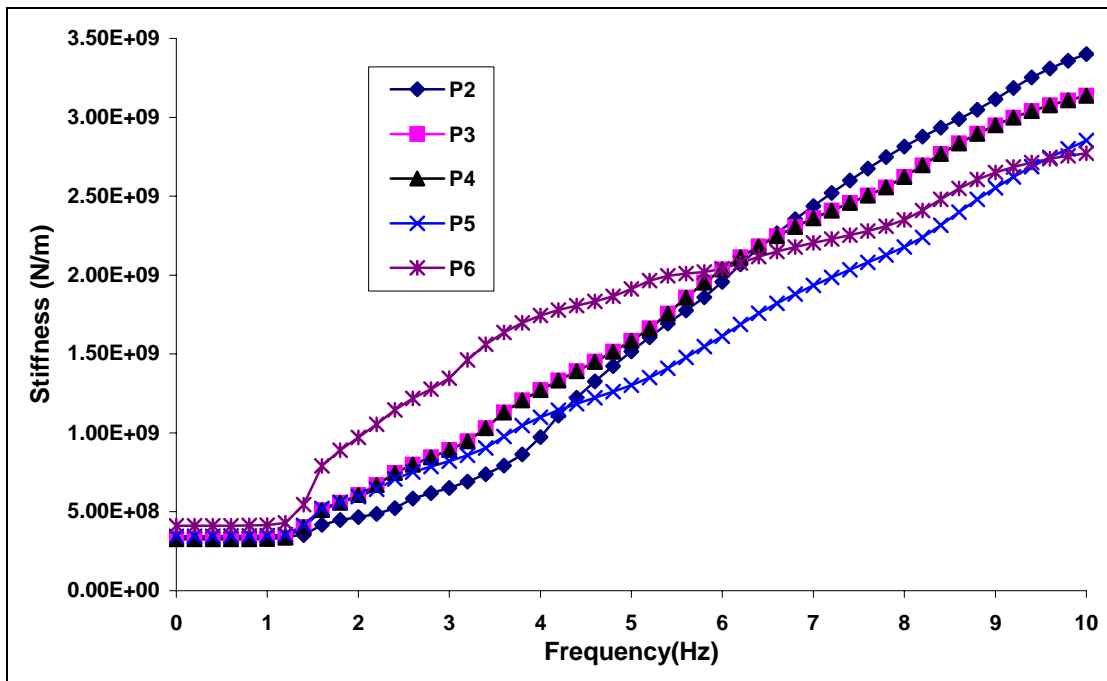


Figure IV. 5 Imaginary Part of Horizontal Stiffness in Y Direction

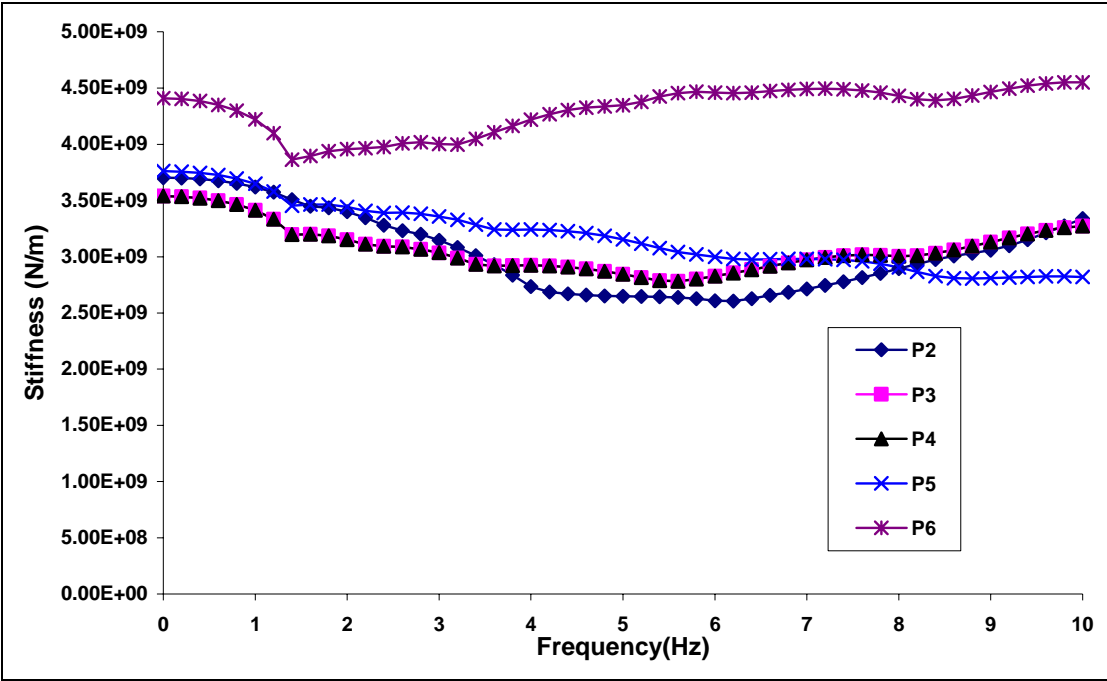


Figure IV. 6 Real Part of Horizontal Stiffness in X Direction

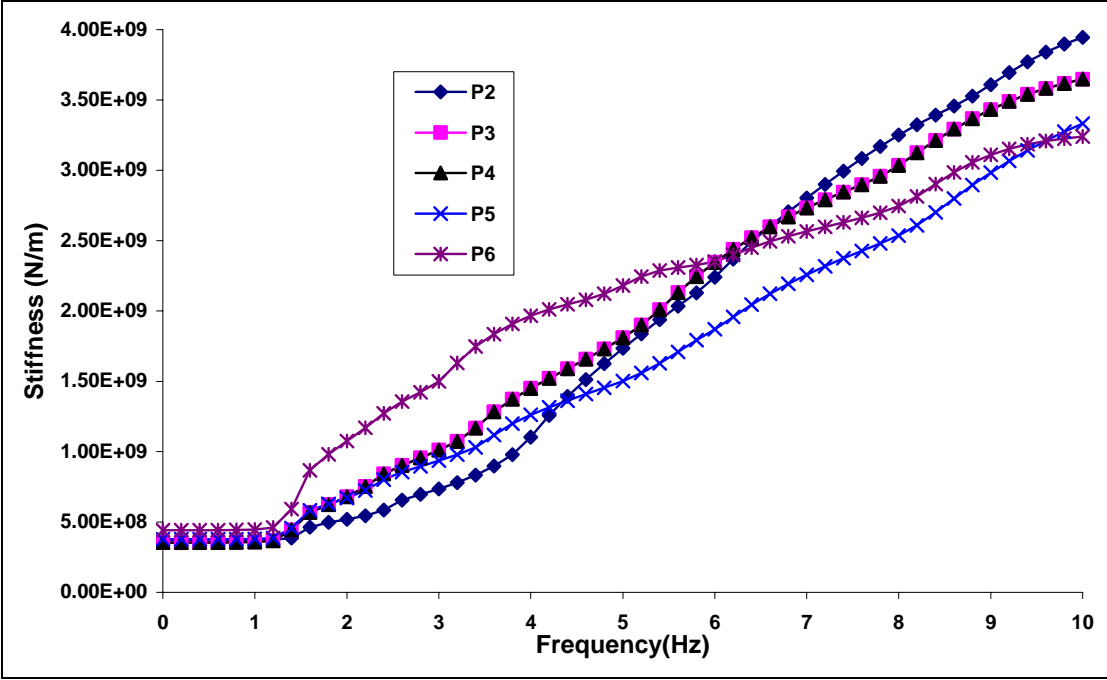


Figure IV. 7 Imaginary Part of Horizontal Stiffness in X Direction

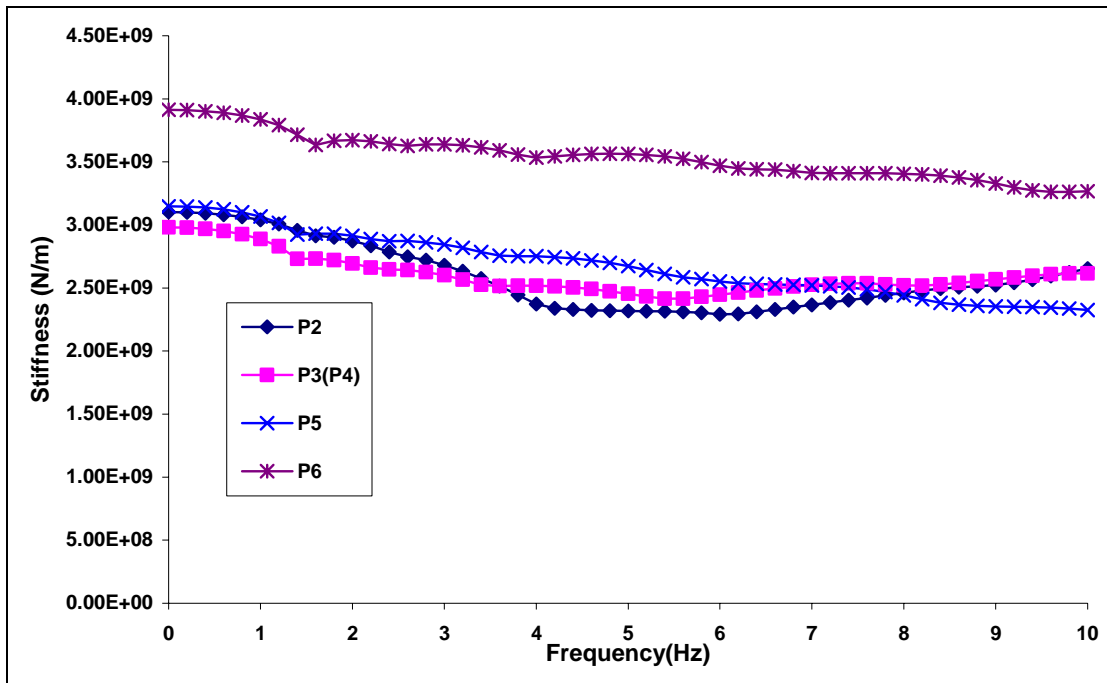


Figure IV. 8 Real Part of Horizontal Stiffness of an Equivalent Surface Mat

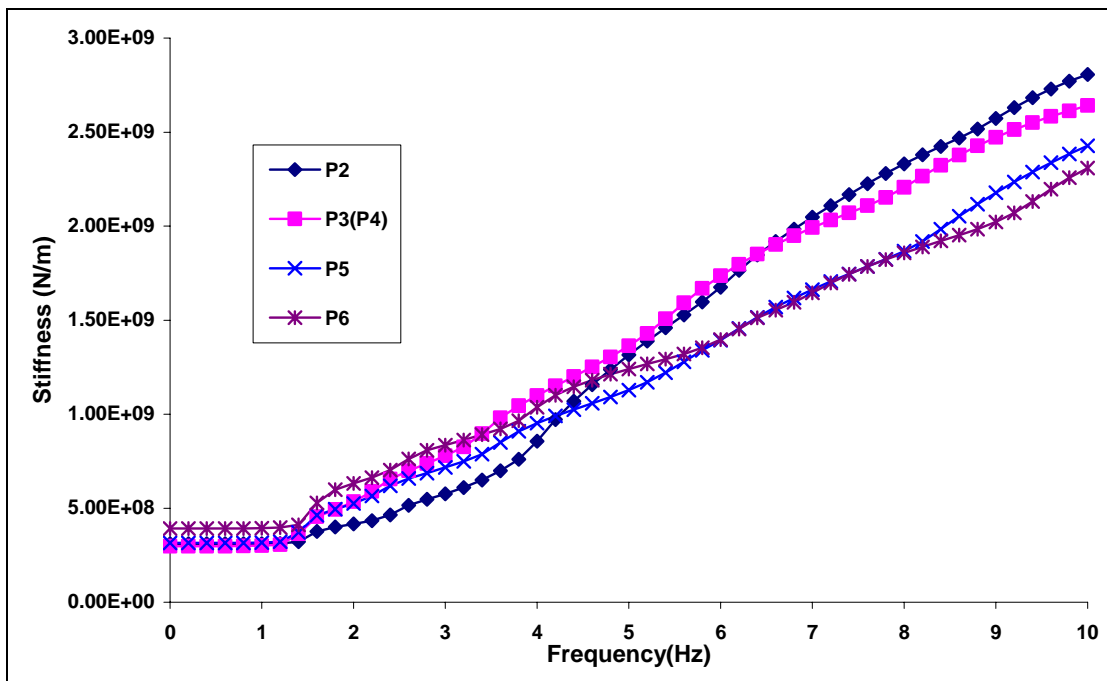


Figure IV. 9 Imaginary Part of Horizontal Stiffness of an Equivalent Surface Mat

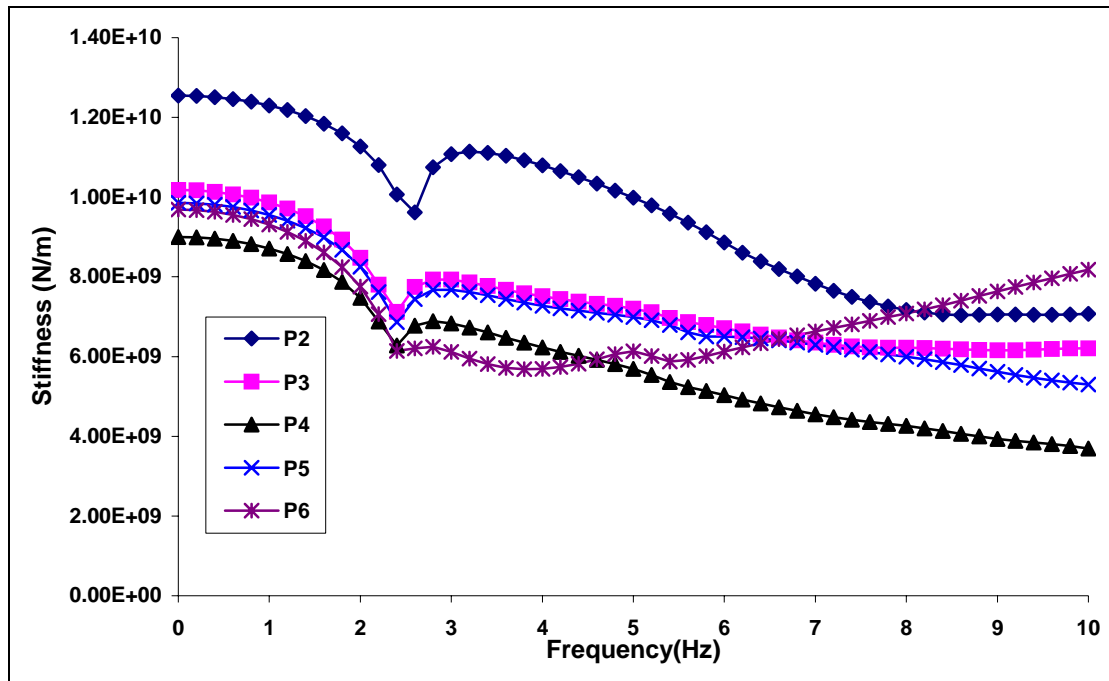


Figure IV. 10 Real Part of Vertical Stiffness

The imaginary parts are constant below the fundamental natural frequency in shear, with a value representing the effect of the internal (material) damping, then increase almost linearly with frequency.

As a matter of interest, Figures IV.8 & IV.9 show the horizontal stiffness for mat foundations representing the cap of the pile groups for each pier. It can be seen that the values are very similar to those of the pile foundations and just slightly smaller. In comparing these values, the rectangular mats are replaced by an equivalent circular foundation with the same area leading to the same value in both horizontal directions.

From the real parts of the vertical stiffness shown in Figure IV.10, one can identify the dilatational fundamental frequency (2.4 Hz in this case). Basically, the real part decreases slowly with frequency, except for P6. P2 has the largest static vertical stiffness because the distance to the hard material is the smallest. The variation of the imaginary

parts of the vertical stiffness with frequency, shown in Figure IV.11, is very similar to that of the horizontal stiffness with the difference in the threshold frequency for radiation damping (from 1.4 to 2.4 Hz).

Figures IV.12 & IV.13 show the vertical stiffness of the pile caps by themselves. As expected these values are much smaller than those of the pile groups by a factor of almost 2.5.

The rocking stiffness, illustrated in Figure IV.14 to IV.17, has a much smoother variation with frequency than either the horizontal or the vertical stiffness. It is hard to identify from the figures for the real part the fundamental frequencies of the soil. The real part decreases with frequency in the normal range of engineering practice. The real parts of P2 and P6 are larger than those of the other piers, which implies that the rocking stiffness is sensitive to both pile tip conditions and soil properties. The imaginary parts follow the same shape as those of the horizontal and vertical stiffness but they have less variation with frequency. As could be expected, the rocking stiffness around an axis perpendicular to the longitudinal direction of the bridge is smaller than the stiffness around the longitudinal axis by a factor of about 3.

Figures IV.18 to IV.21 show the rocking stiffness for the pile caps as surface foundations (without piles). The equivalent circular foundations had the radii selected so as to yield the same moment of inertia. Once again the pile foundations have a much larger stiffness by a factor of about 4.

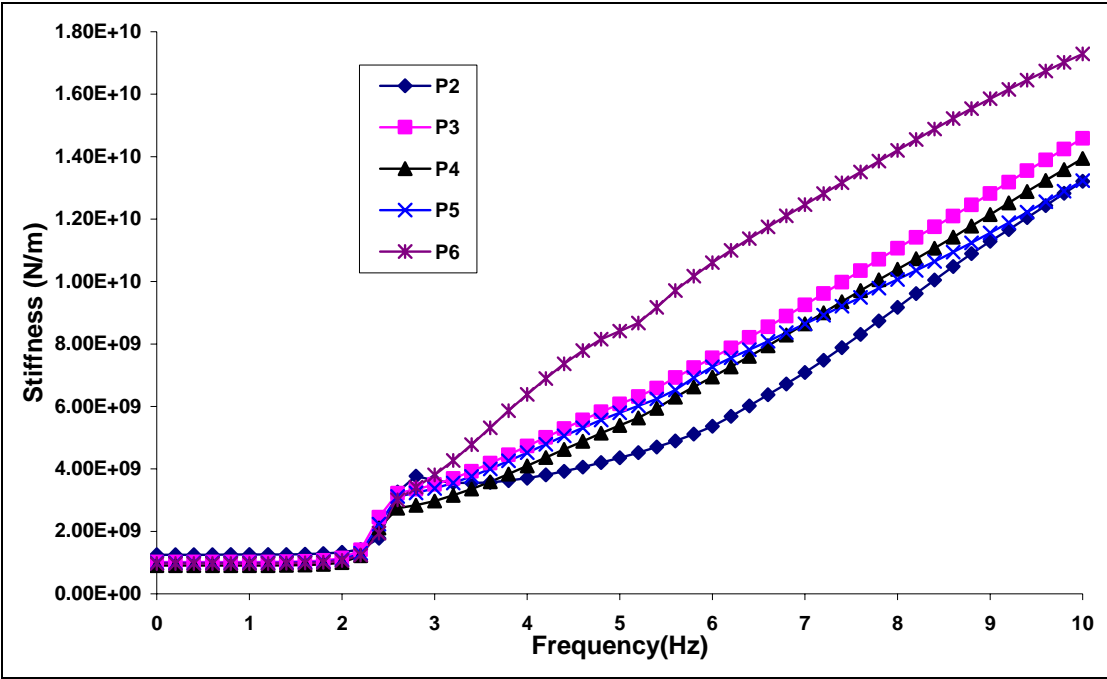


Figure IV. 11 Imaginary Part of Vertical Stiffness

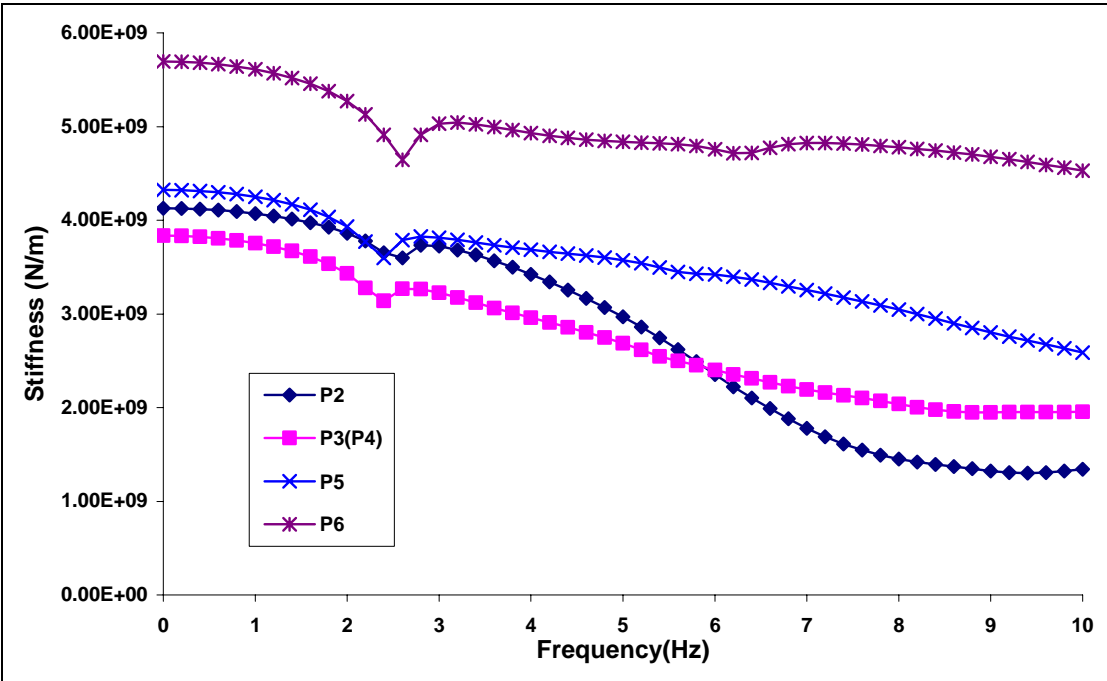


Figure IV. 12 Real Part of Vertical Stiffness of an Equivalent Surface Mat

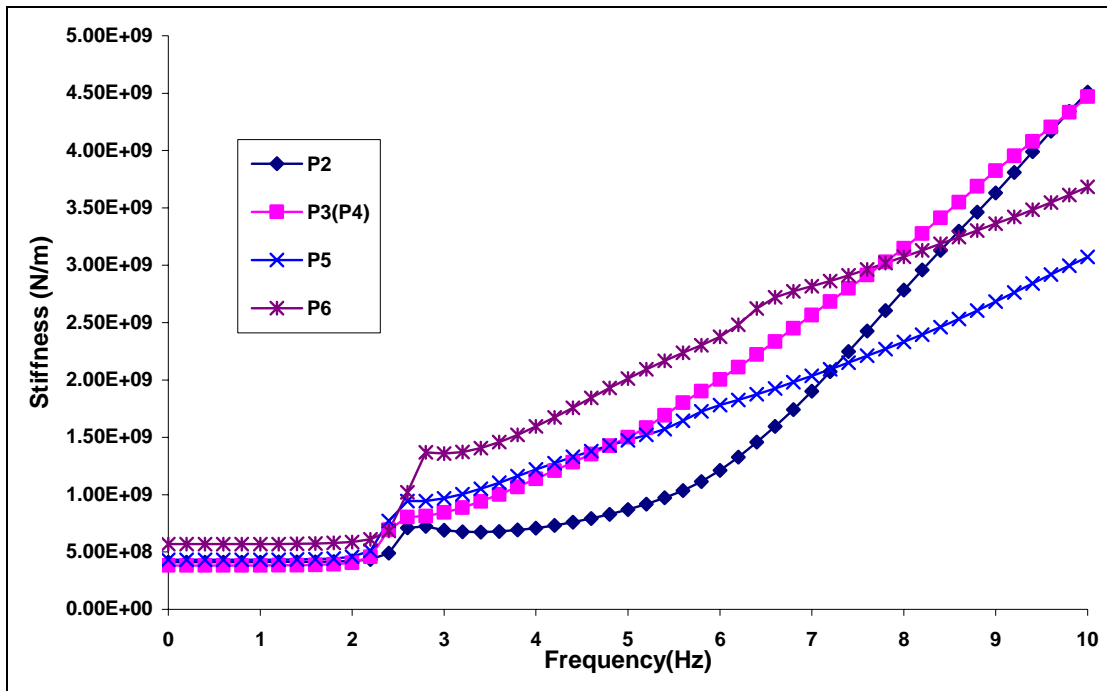


Figure IV. 13 Imaginary Part of Vertical Stiffness of an Equivalent Surface Mat

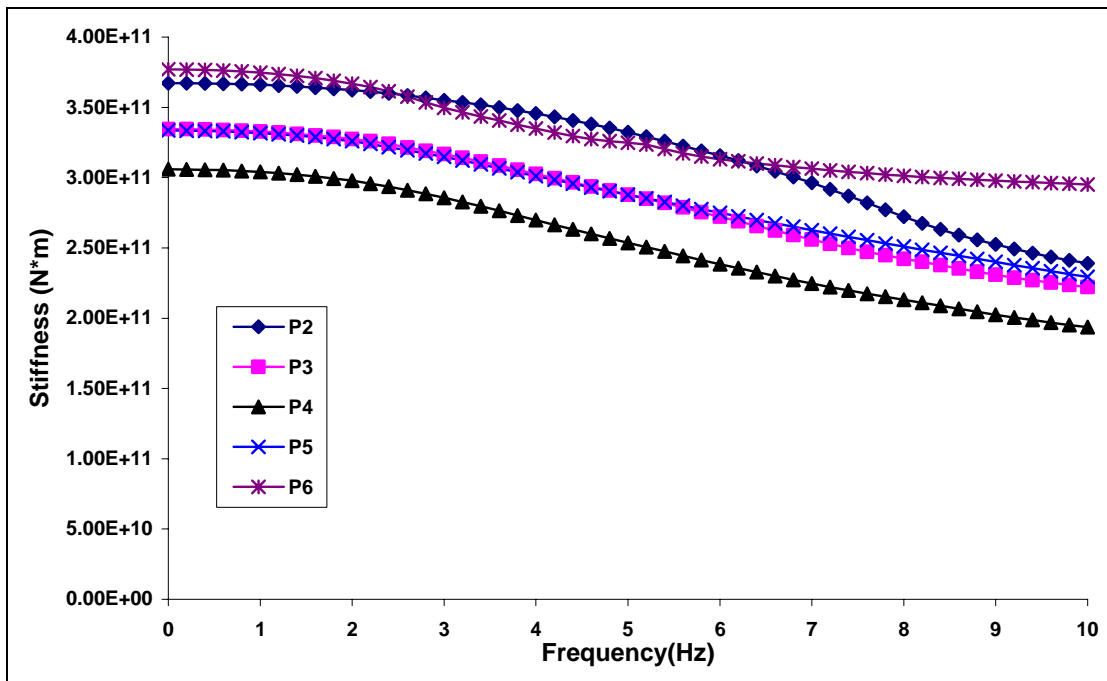


Figure IV. 14 Real Part of Rocking Stiffness around X Axis

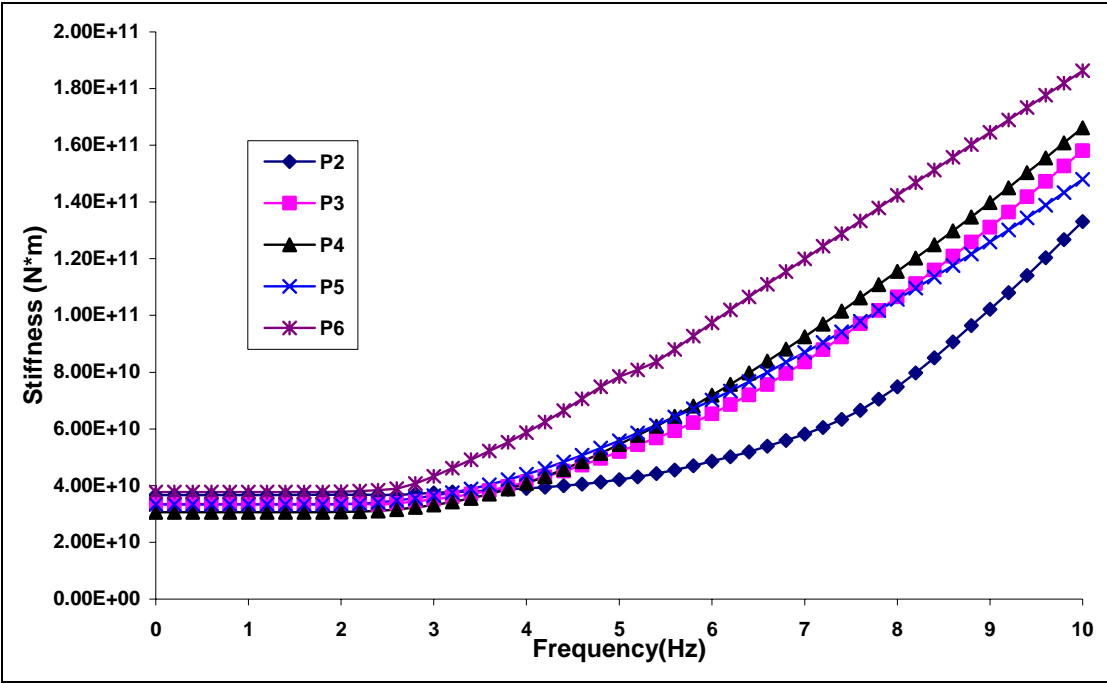


Figure IV. 15 Imaginary Part of Rocking Stiffness around X Axis

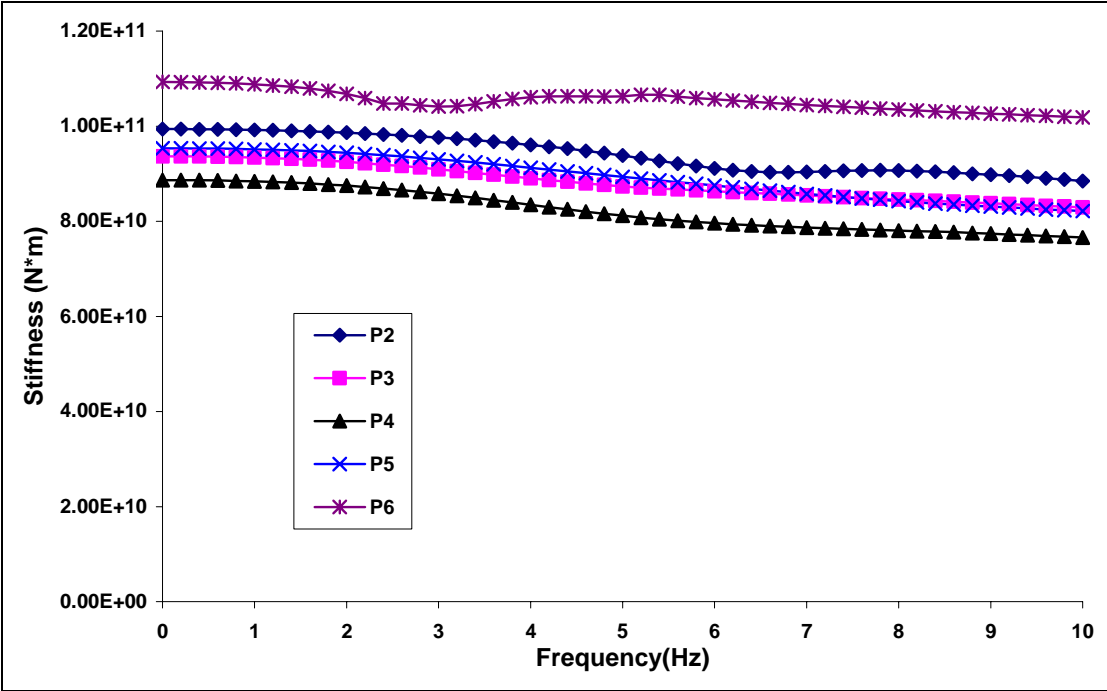


Figure IV. 16 Real Part of Rocking Stiffness around Y Axis

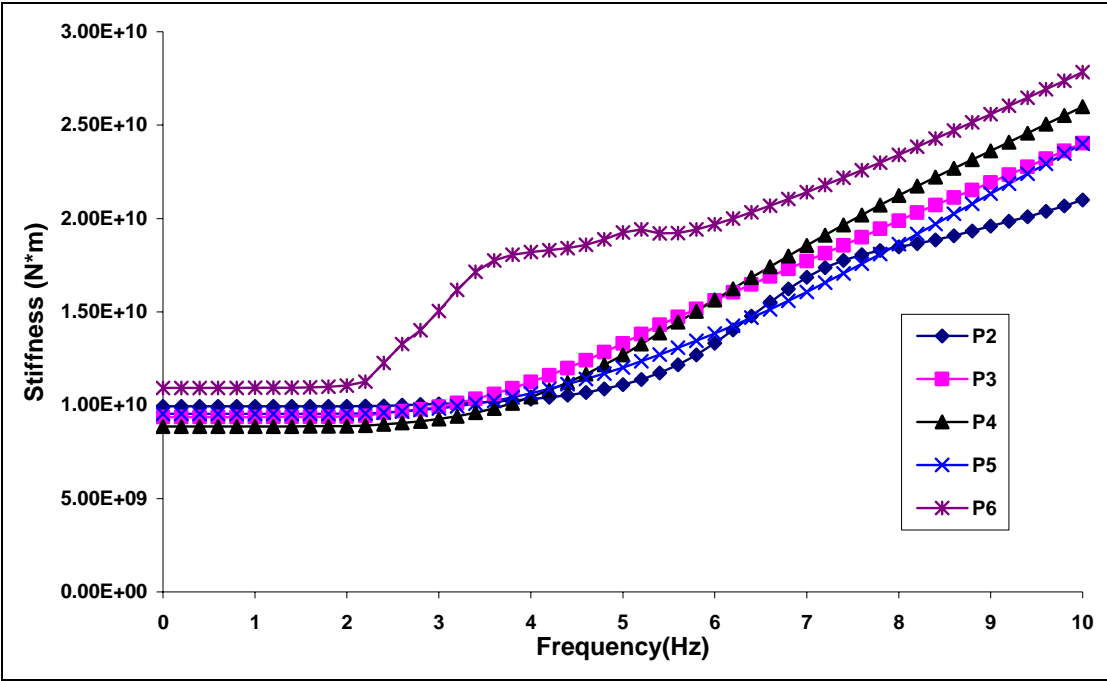


Figure IV. 17 Imaginary Part of Rocking Stiffness around Y Axis

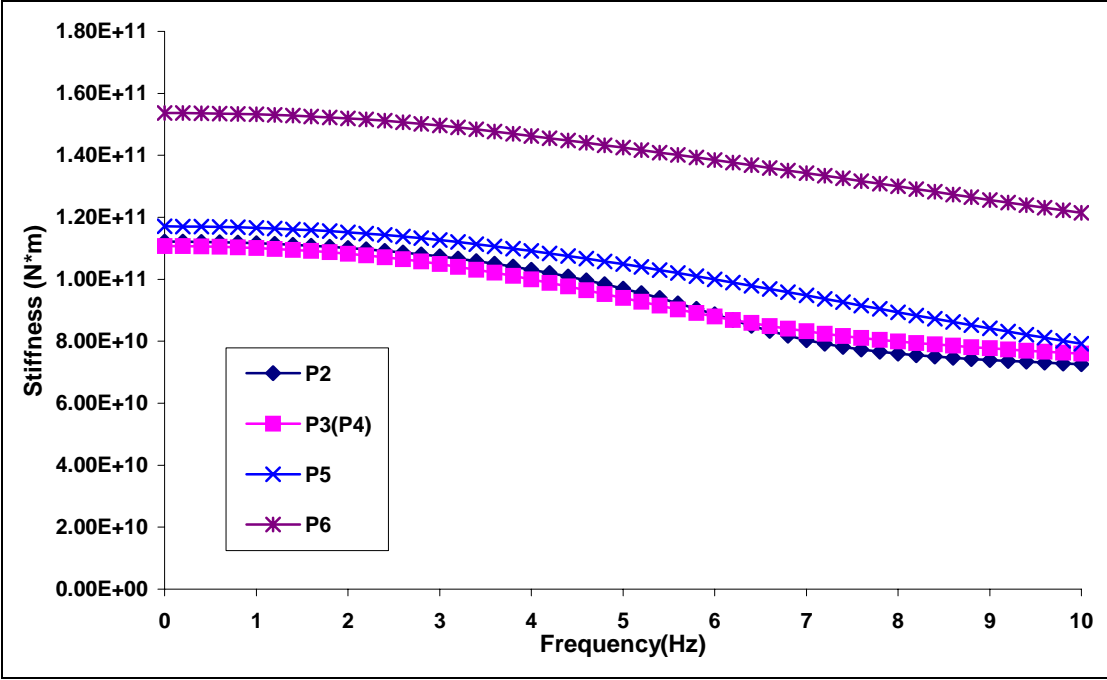


Figure IV. 18 Real Part of Rocking Stiffness around X Axis of an Equivalent Surface Mat

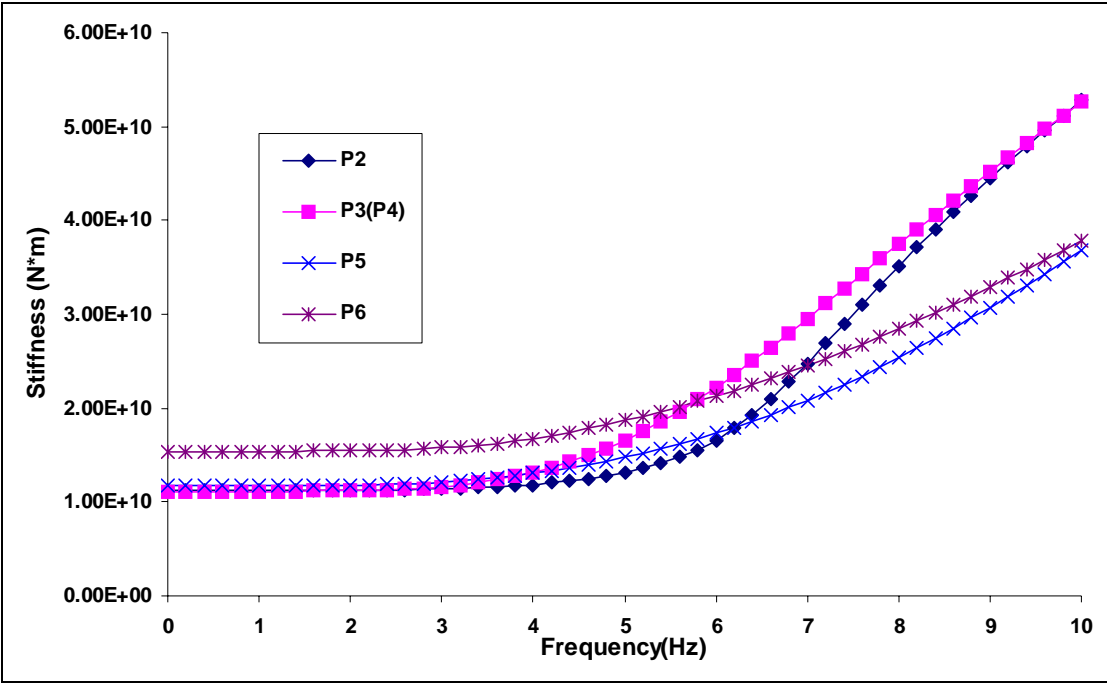


Figure IV. 19 Imaginary Part of Rocking Stiffness around X Axis of an Equivalent Surface Mat

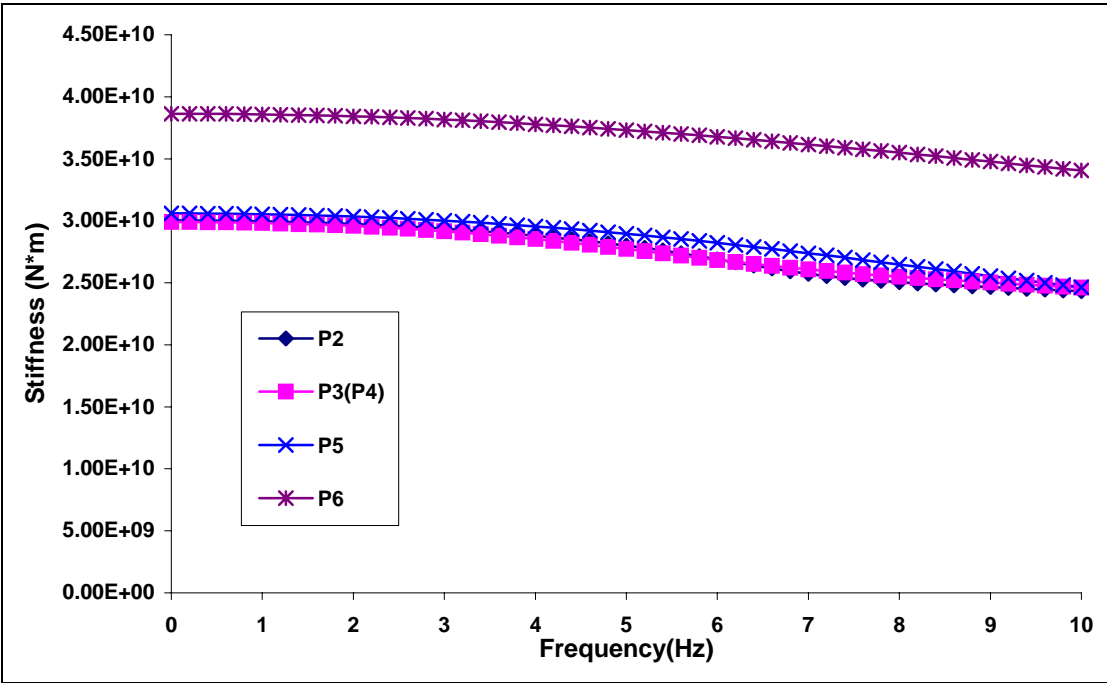


Figure IV. 20 Real Part of Rocking Stiffness around Y Axis of an Equivalent Surface Mat

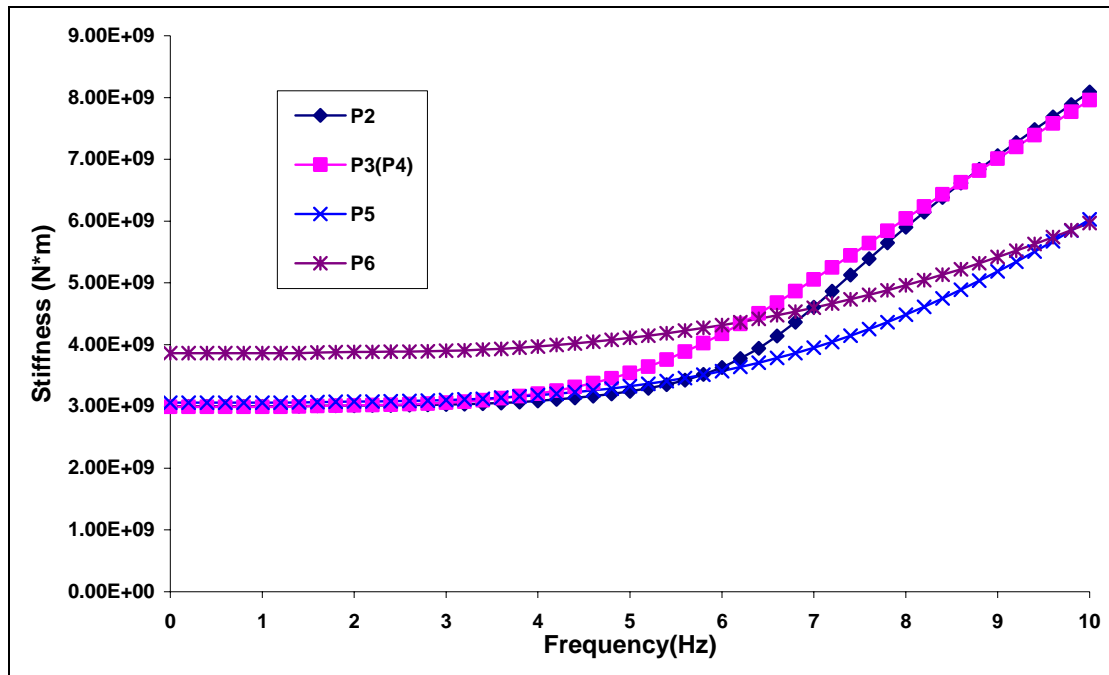


Figure IV. 21 Imaginary Part of Rocking Stiffness around Y Axis of an Equivalent Surface Mat

P1 and P7 only have surface mats without supporting piles. One can find an equivalent circular mat (having the same area as the rectangular mat shown in Figure IV.3) to calculate their horizontal stiffness (the same in the two directions) and vertical stiffness, while using a circle having the same moment of inertia as the rectangular mat to calculate the rocking stiffness. Results are shown in Figure IV.22, assuming that the subsoil is 90 meters deep with a shear wave velocity of 550m/s.

It can be seen that the natural frequency in shear is about 1.6 Hz and the dilatational natural frequency is about 2.5 Hz for this case.

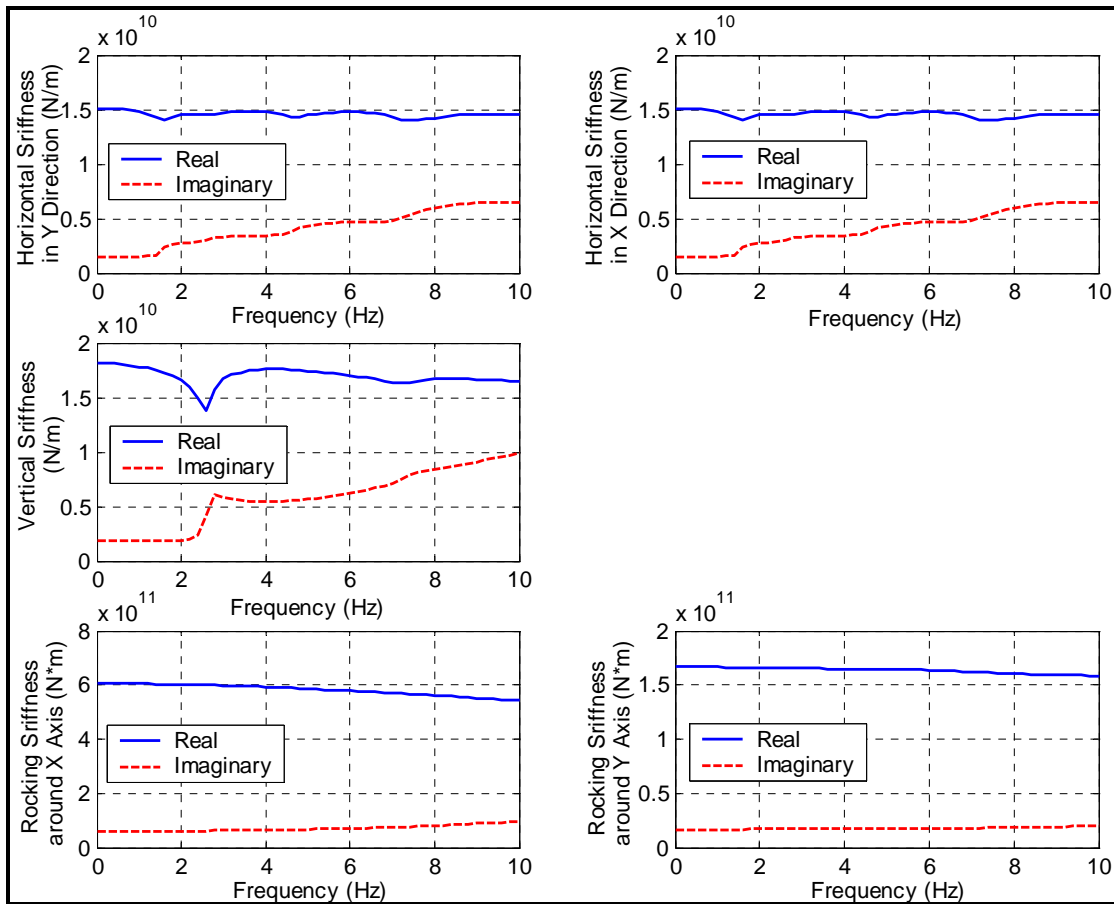


Figure IV. 22 Stiffness of Surface Mat of Pier #1 and Pier #7

4.4 Dynamic Stiffness with Reduced Soil Shear Modulus

To study further the potential SSI effects, the shear wave velocities were reduced over the top 12 meters to simulate some nonlinear soil behavior. Other properties of the soils are the same as used before. The foundation stiffness terms were calculated again for this case. The assumed properties and the calculated foundation stiffness are shown in Tables IV.7 - IV.10 and Figures IV.23 - IV.33.

Table IV. 7 Reduced Soil Properties for Pier #2

	Thickness (m)	Depth (m)	Shear Wave Velocity (m/s)
Layer 1	7.20	7.20	150
Layer 2	5.00	12.20	150
Layer 3	27.80	40.00	550
Layer 4	50.00	90.00	550

Table IV. 8 Reduced Soil Properties for Pier #3 and #4

	Thickness (m)	Depth (m)	Shear Wave Velocity (m/s)
Layer 1	7.20	7.20	150
Layer 2	5.00	12.20	150
Layer 3	4.69	16.89	330
Layer 4	13.11	30.00	360
Layer 5	10.00	40.00	390
Layer 6	50.00	90.00	550

Table IV. 9 Reduced Soil Properties for Pier #5

	Thickness (m)	Depth (m)	Shear Wave Velocity (m/s)
Layer 1	7.20	7.20	150
Layer 2	5.00	12.20	150
Layer 3	4.69	16.89	330
Layer 4	13.11	30.00	360
Layer 5	10.00	40.00	390
Layer 6	50.00	90.00	550

Table IV. 10 Reduced Soil Properties for Pier #6

	Thickness (m)	Depth (m)	Shear Wave Velocity (m/s)
Layer 1	1.35	1.35	150
Layer 2	5.00	6.35	150
Layer 3	4.69	11.04	150
Layer 4	13.11	24.15	210
Layer 5	10.00	35.15	390
Layer 6	50.00	84.15	550

The new horizontal stiffness in both directions decreases by 50% because it depends on the properties of the soil near the surface, while the new rocking stiffness decreases by about 20%~30%. Only the vertical stiffness is almost the same as before. The shapes of the curves of the dynamic stiffness with frequency are very similar to those obtained before. The natural frequency in shear has been reduced from 1.6Hz to 1.4Hz while the dilatational natural frequency is almost the same as before.

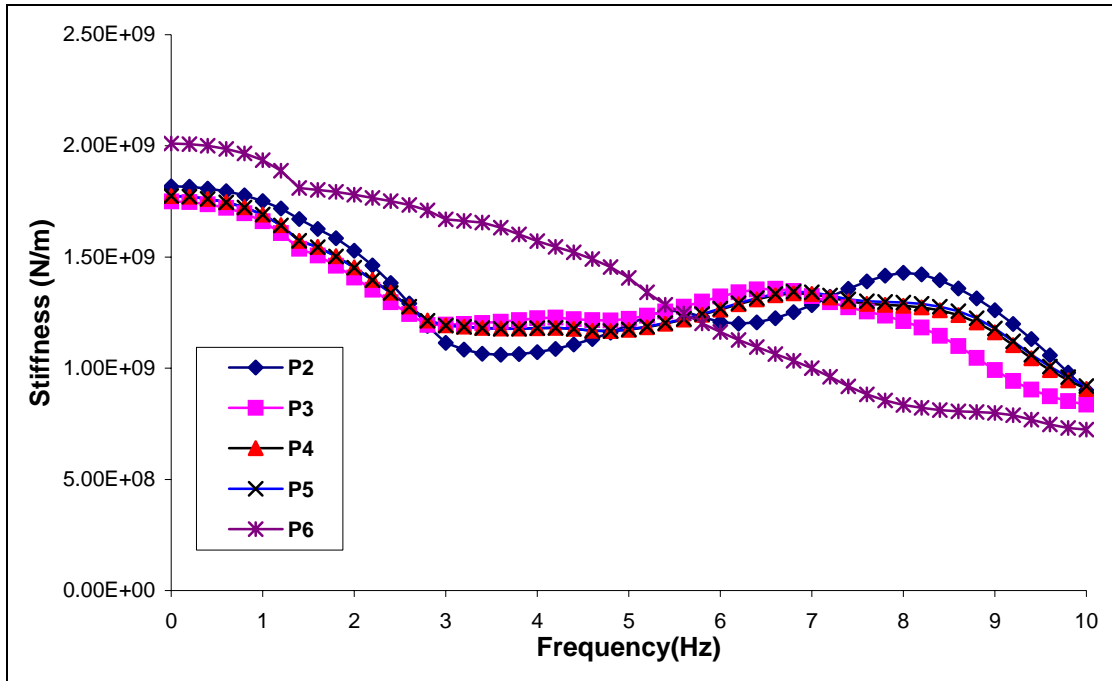


Figure IV. 23 New Real Part of Horizontal Stiffness in X Direction

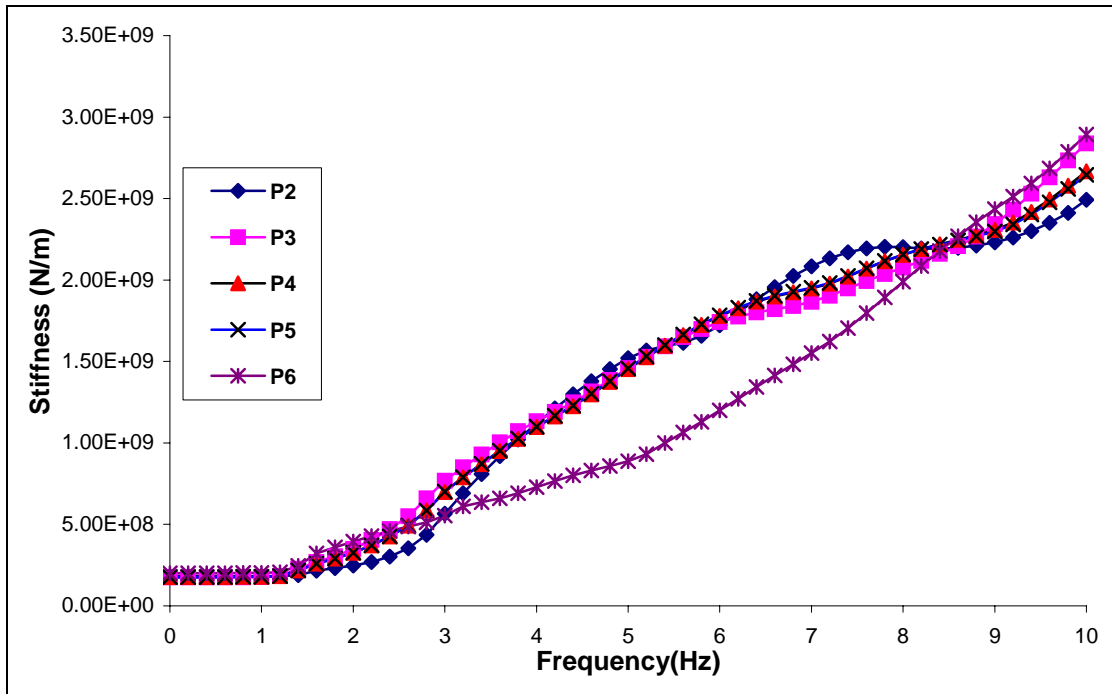


Figure IV. 24 New Imaginary Part of Horizontal Stiffness in X Direction

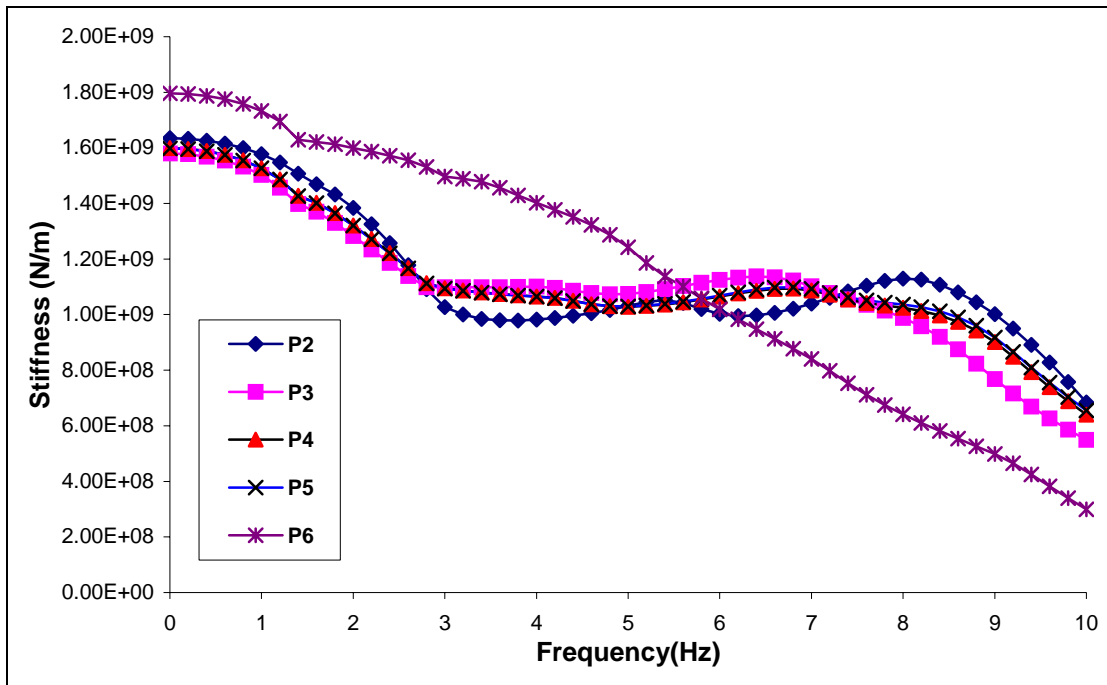


Figure IV. 25 New Real Part of Horizontal Stiffness in Y Direction

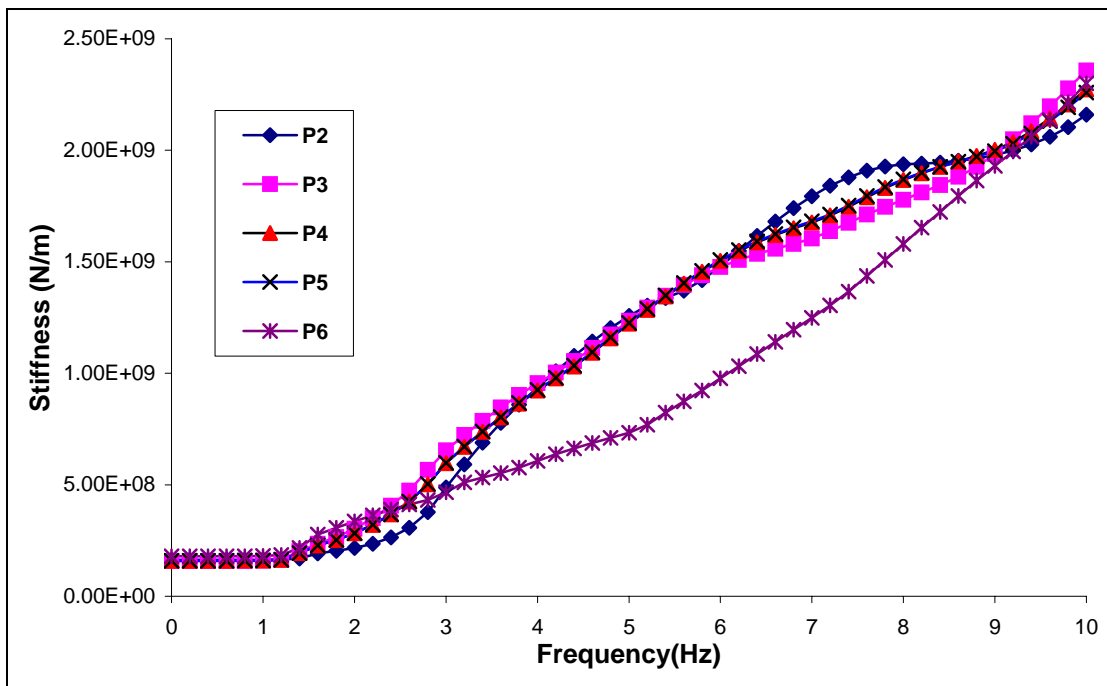


Figure IV. 26 New Imaginary Part of Horizontal Stiffness in Y Direction

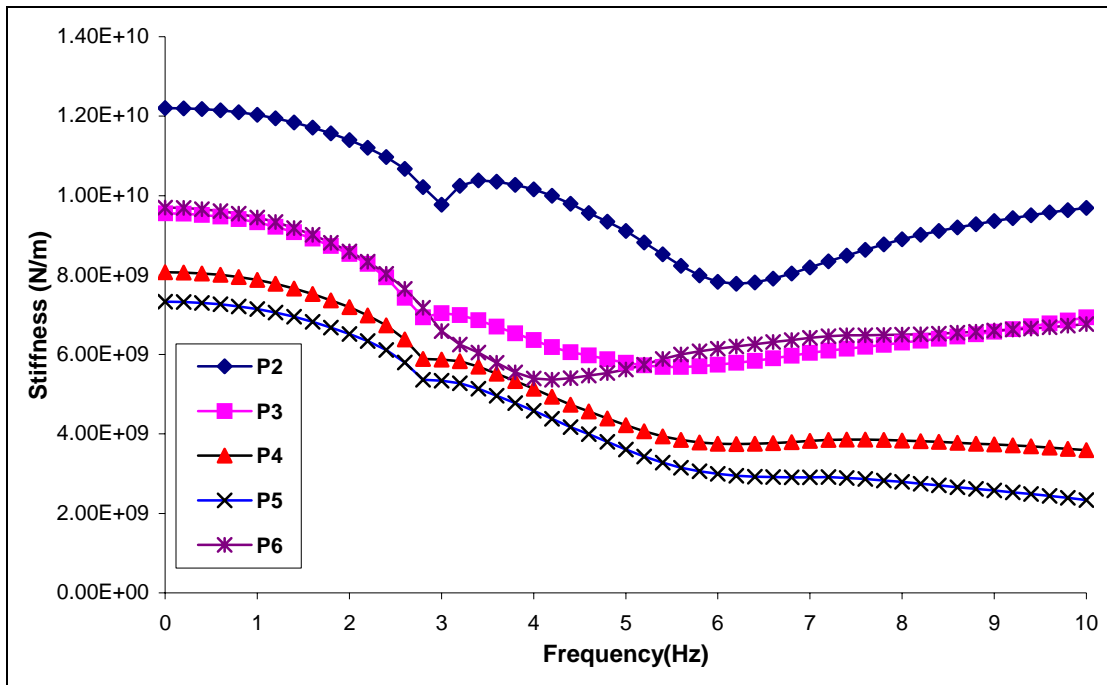


Figure IV. 27 New Real Part of Vertical Stiffness

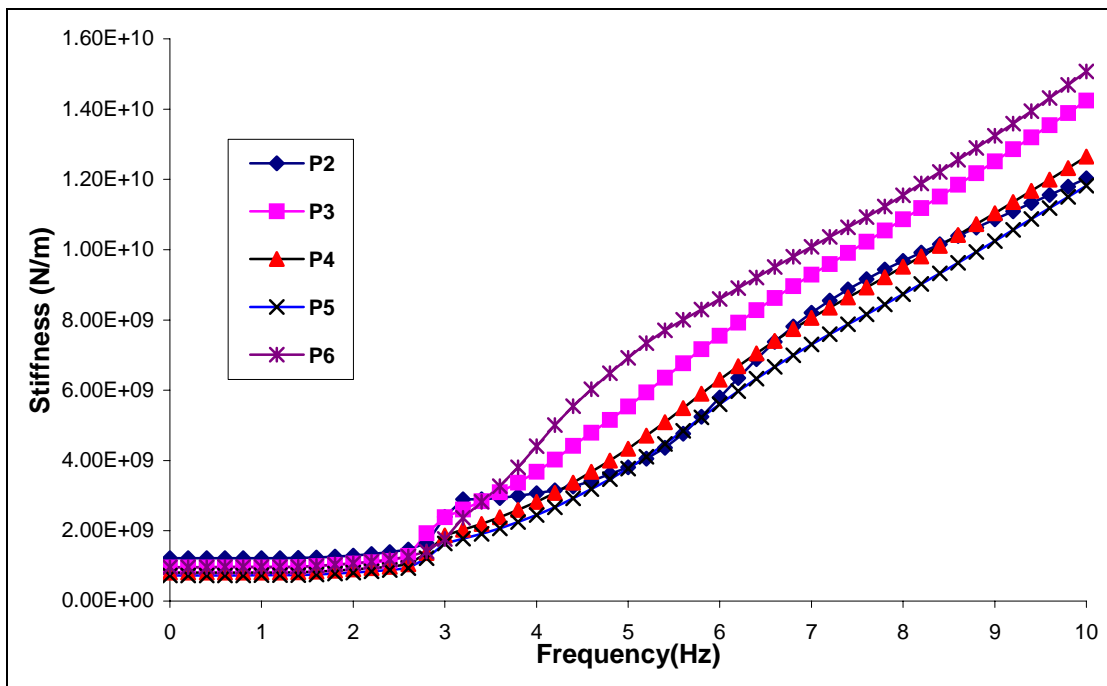


Figure IV. 28 New Imaginary Part of Vertical Stiffness

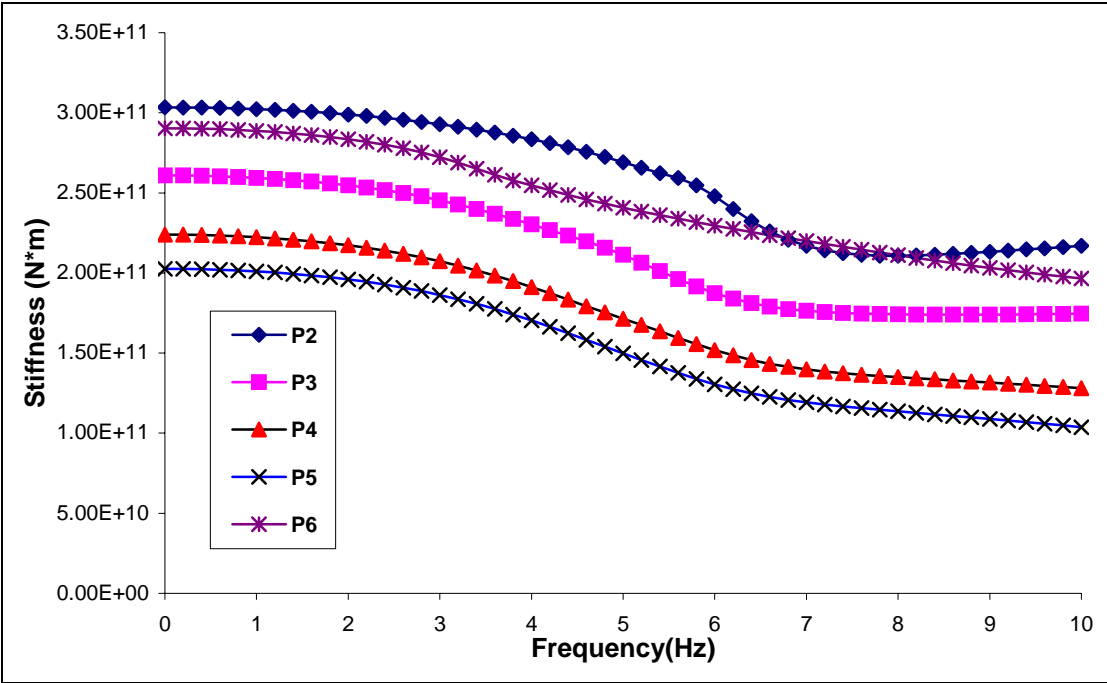


Figure IV. 29 New Real Part of Rocking Stiffness around X Axis

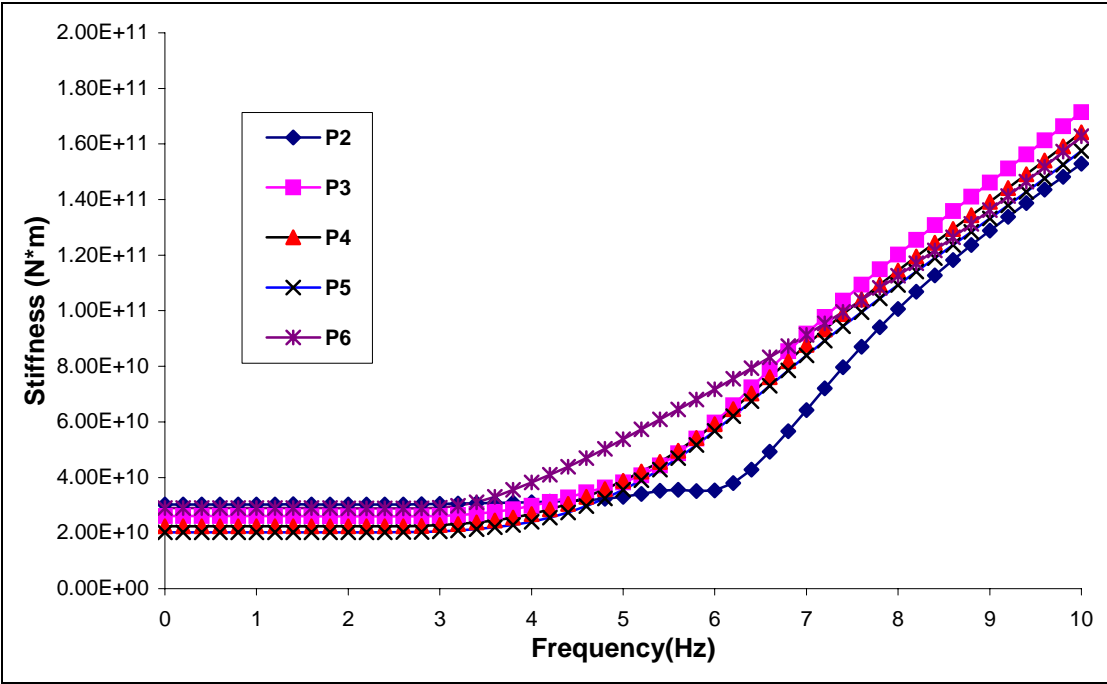


Figure IV. 30 New Imaginary Part of Rocking Stiffness around X Axis

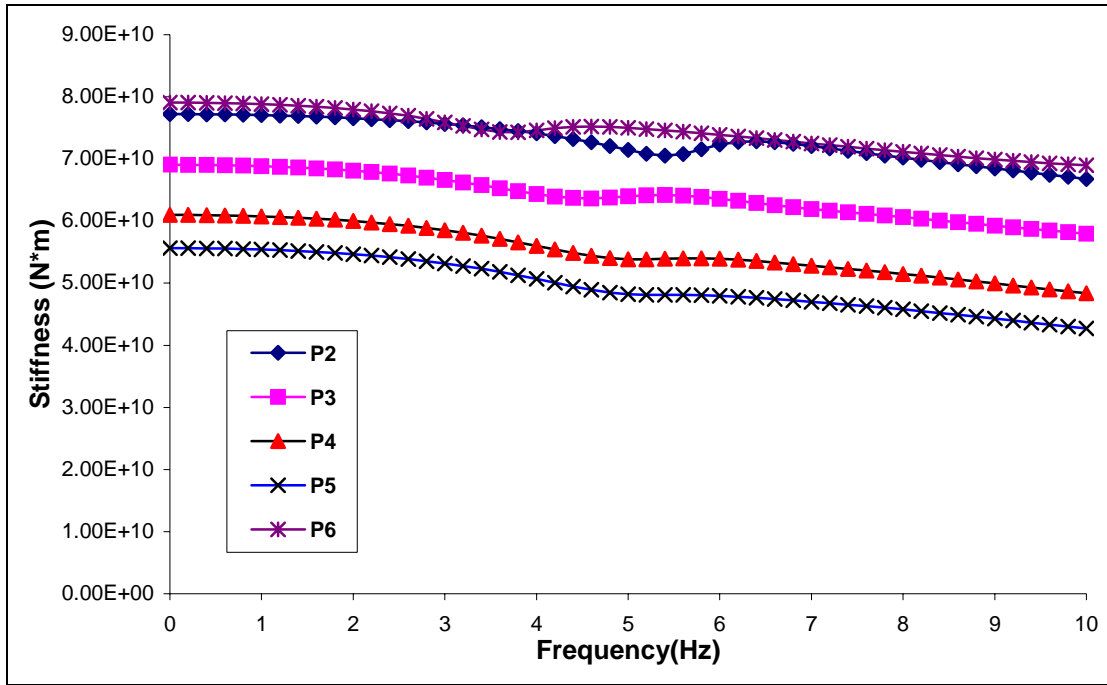


Figure IV. 31 New Real Part of Rocking Stiffness around Y Axis

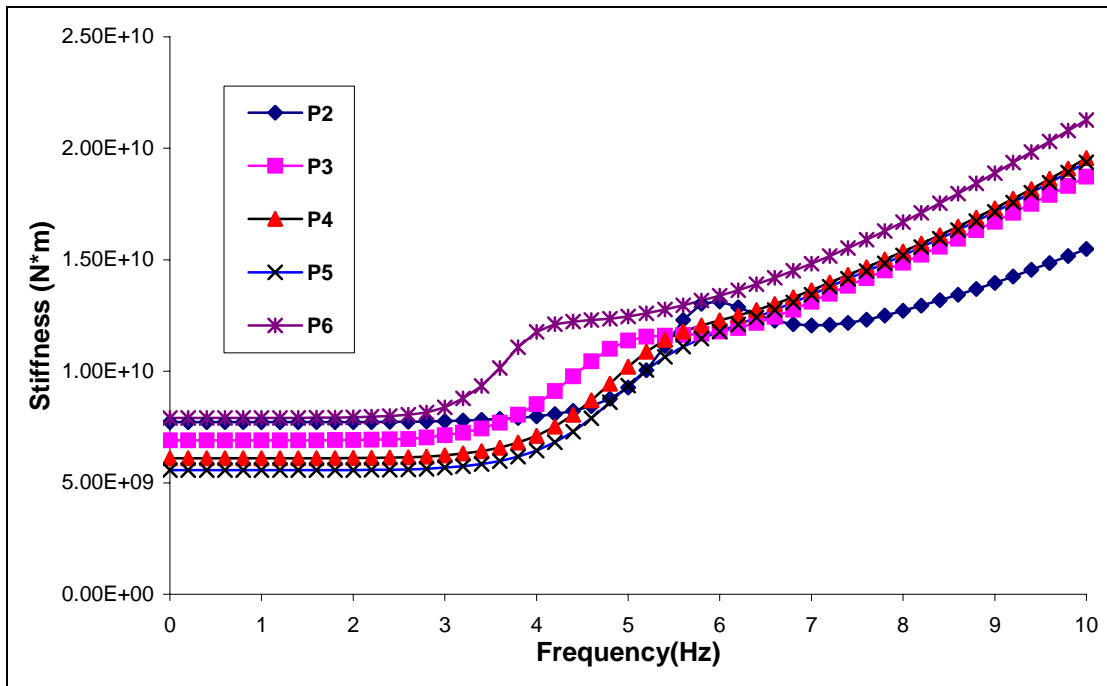


Figure IV. 32 New Imaginary Part of Rocking Stiffness around Y Axis

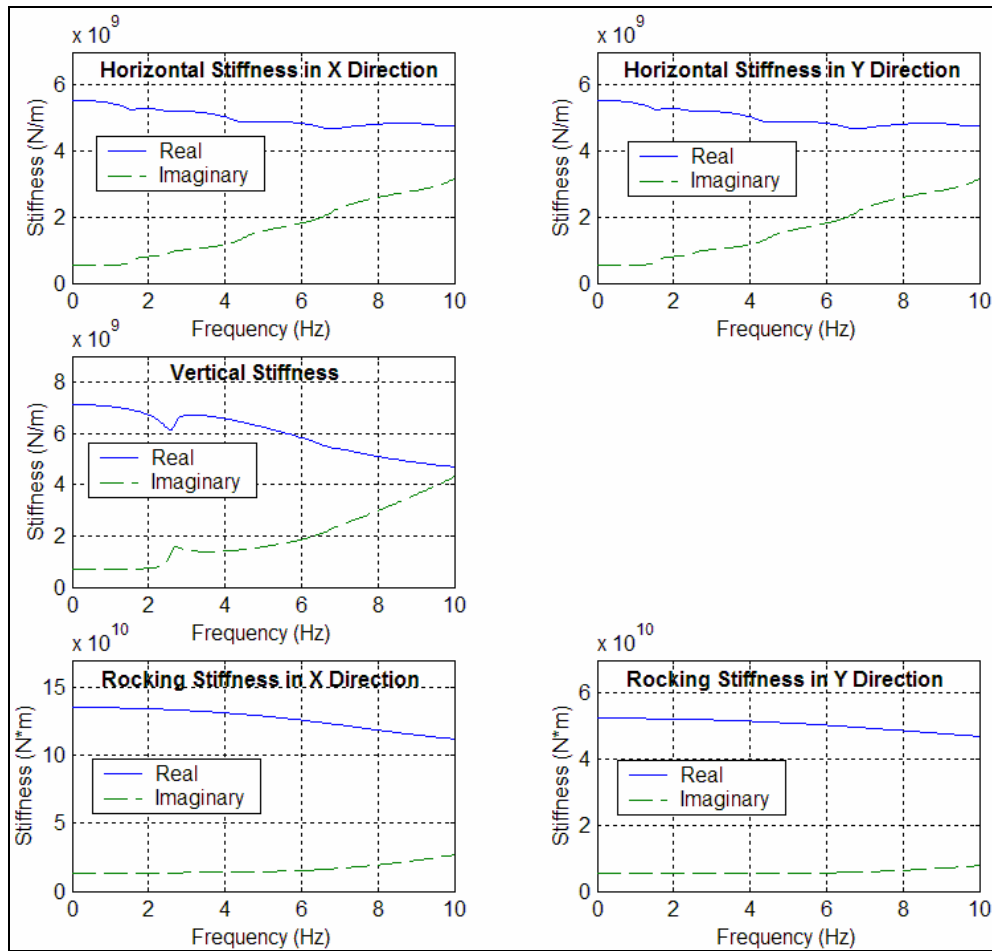


Figure IV. 33 New Stiffness of Mat under Pier #1 and Pier #7

CHAPTER V

EFFECT OF RUBBER PADS' STIFFNESS

The formulation and computer software described in Chapter II were applied to the Marga-Marga bridge to estimate its frequency response characteristics due to base motions, ignoring first soil-structure interaction effects. The main objective was to study the effect of the stiffness of the rubber pads on the dynamic response of the bridge.

5.1 Properties of Structure

5.1.1 Deck

The Marga-Marga bridge is shown schematically in Figure V.1.

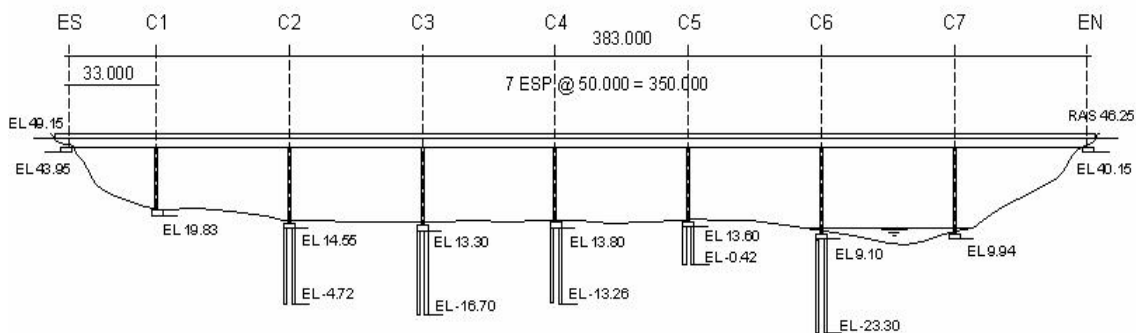


Figure V. 1 Overview of Marga-Marga Bridge

The deck of the bridge consists of 8 spans, which are all 50 meters long except the span connecting the north abutment and pier 1, which is 33 meters long. The deck is composite with a concrete slab over 4 steel I-beams. It is modeled as an equivalent beam with a mass density, Poisson's ratio and Young's modulus of 2940kg/m³, 0.245 and

3.3×10^{10} Pa, respectively. The centroid of the equivalent beam cross section is 2.65 meters above the top of the base isolators (rubber pads) and 0.45 meters below the upper surface (as shown in Figure V.2).

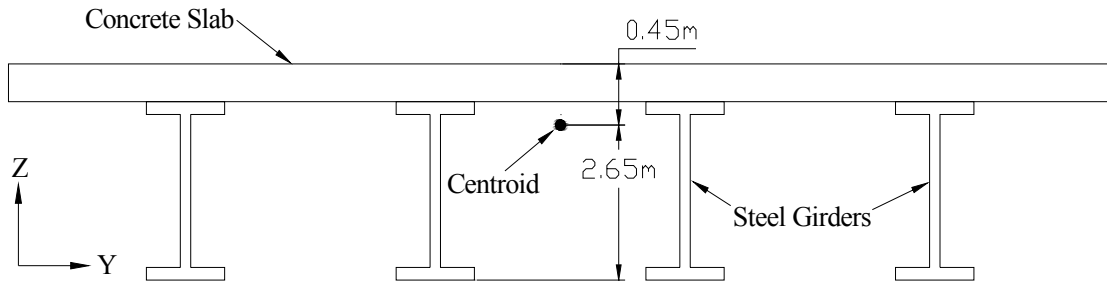


Figure V. 2 Cross Section of Deck

The properties of the deck cross section are:

$$\left\{ \begin{array}{l} A = 8.13(\text{m}^2) \\ A_{s_y} = 3.85(\text{m}^2) \\ I_z = 238.6(\text{m}^4) \\ A_{s_z} = 2.25(\text{m}^2) \\ I_y = 5.98(\text{m}^4) \\ J = 0.116(\text{m}^4) \end{array} \right.$$

in which A is the area of the deck's cross section; A_{s_y} and A_{s_z} are the shear areas of the composite cross section in the Y and Z direction, respectively; I_z and I_y are the bending moments of inertia in the Z and Y direction, respectively, and J is the torsional moment of inertia.

5.1.2 Piers

The piers and their dimensions are illustrated in Figure V.3. The formulation of the dynamic stiffness of prismatic members assumes a constant cross section. Each pier was therefore divided into three members according to the variation of the cross section.

As shown in Figures V.3 and V.4, the top and bottom parts (members) are solid, while the long member in between is hollow. The mass density, Poisson's ratio and Young's modulus used in the analysis for the piers are 2500 kg/m^3 , 0.2 and $3.3 \times 10^{10} \text{ Pa}$, respectively.

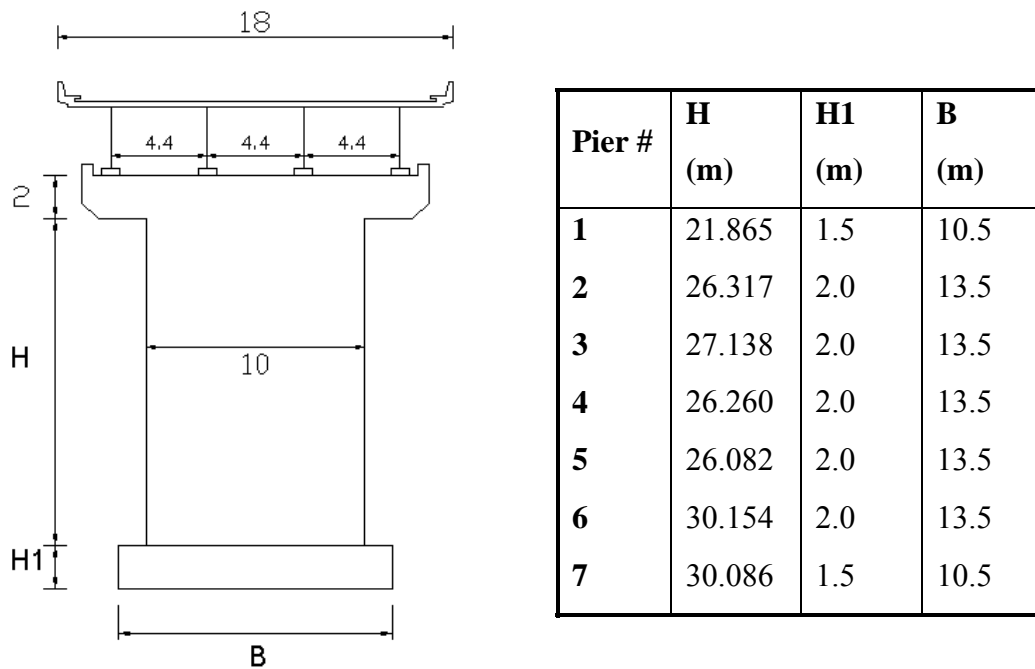


Figure V. 3 Transverse View of Pier and Its Dimensions

The properties of the pier cross sections are:

$$\left\{ \begin{array}{l} A = 31.6(\text{m}^2) \\ A_{yy} = 26.86(\text{m}^2) \\ I_x = 657.385(\text{m}^4) \\ A_{xx} = 26.86(\text{m}^2) \\ I_y = 10.533(\text{m}^4) \\ J = 37.92(\text{m}^4) \end{array} \right. \text{ and } \left\{ \begin{array}{l} A = 6.38(\text{m}^2) \\ A_{yy} = 4.17(\text{m}^2) \\ I_z = 63.33(\text{m}^4) \\ A_{zz} = 1.25(\text{m}^2) \\ I_y = 4.18(\text{m}^4) \\ J = 12.658(\text{m}^4) \end{array} \right.$$

for the top member and the middle member, respectively.

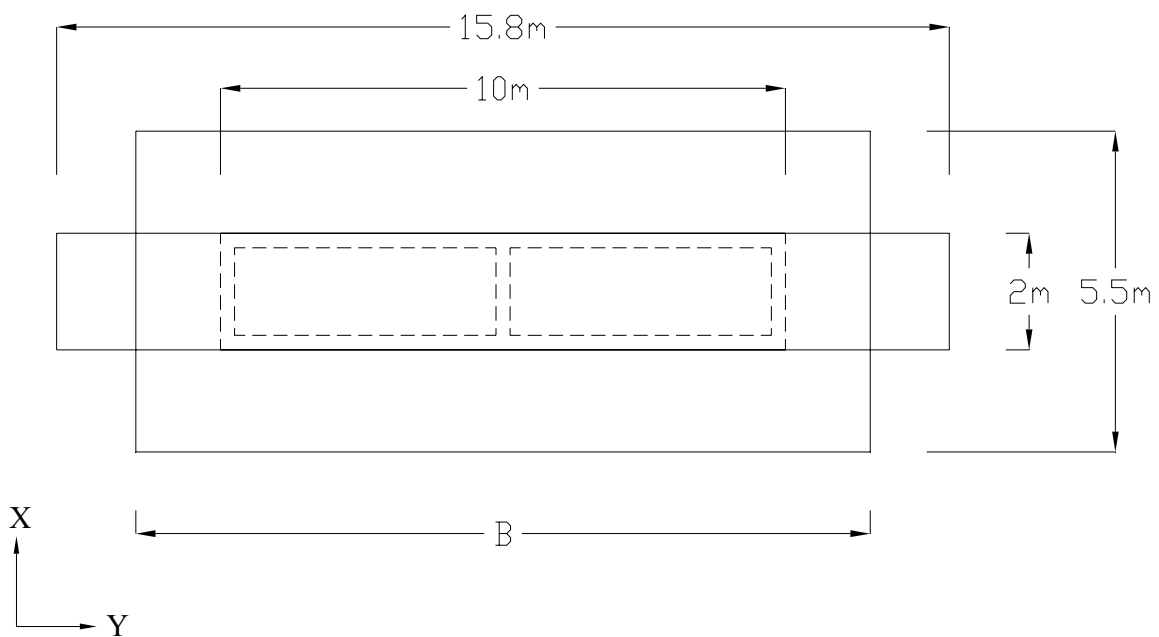


Figure V. 4 Cross Sections of Pier

The properties of the bottom members' cross-sections are:

$$\left\{ \begin{array}{l} A = 74.25(\text{m}^2) \\ A_{yy} = 63.113(\text{m}^2) \\ I_x = 1127.672(\text{m}^4) \\ A_{xx} = 63.113(\text{m}^2) \\ I_y = 187.172(\text{m}^4) \\ J = 552.531(\text{m}^4) \end{array} \right. \text{ and } \left\{ \begin{array}{l} A = 57.75(\text{m}^2) \\ A_{yy} = 49.088(\text{m}^2) \\ I_x = 530.578(\text{m}^4) \\ A_{xx} = 49.088(\text{m}^2) \\ I_y = 145.578(\text{m}^4) \\ J = 396.555(\text{m}^4) \end{array} \right.$$

for piers 2~6 and piers 1 & 7, respectively, where A_{xx} is the shear area in the X direction and I_x is the bending moment of inertia around the X axis.

5.1.3 Rubber Pads

The rubber pads in the structure act as base isolators to mitigate the motion of the deck due to earthquakes. On the top of each pier, four rubber pads (each under one of the four steel I-beams) were placed in a line, separately, along the Y axis, as shown in Figure V.5. They were combined into one structural member in the analysis.

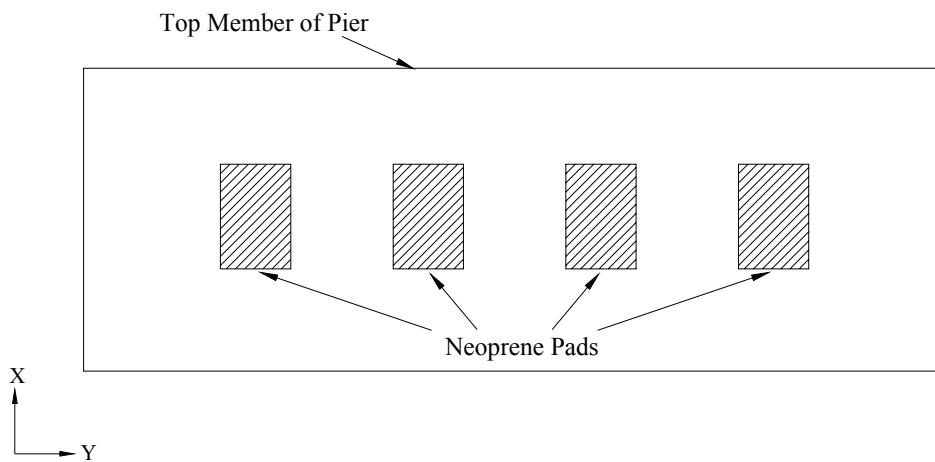


Figure V. 5 Rubber Pads on Top of Pier

The rubber pads were made of alternating layers of rubber and steel, so they have a relatively high axial stiffness and lower shear stiffness. To model this, we selected equivalent Young's modulus, E_{eqvl} and shear modulus, G_{eqvl} to match the axial and shear stiffness according to

$$\left\{ \begin{array}{l} S_{axial} = \frac{1}{\sum_i \frac{L_i}{E_i A}} = \frac{E_{eqvl} A}{\sum_i L_i} \\ S_{shear} = \frac{1}{\sum_j \frac{L_j}{G_j A_s}} = \frac{G_{eqvl} A_s}{\sum_j L_j} \end{array} \right.$$

where E_k , G_k and L_k represent the Young's modulus, shear modulus and thickness of the k th layer; A and A_s are the area and shear area of the cross section; i denotes all rubber and steel layers while j only denotes the rubber layers.

Rubber is a non-linear material, so E_k and G_k of the rubber pads actually depend on the magnitude of the deformation. The equivalent Young's modulus and shear modulus of the rubber pads corresponding to 5% shear deformation is 1.8×10^9 Pa and 1.85×10^6 Pa. V.M. Daza (2003) suggested a variation of the shear modulus with shear strain given by $G = 6.0 \times 10^5 \cdot \gamma^{-0.3764}$.

The length of the rubber pad members is 0.2 m and the mass density is 3000 kg/m^3 .

The cross section properties of the rubber pad members are summarized as:

$$\left\{ \begin{array}{l} A = 1.738(\text{m}^2) \\ A_{sy} = 1.477(\text{m}^2) \\ I_x = 168.269(\text{m}^4) \\ A_{sx} = 1.477(\text{m}^2) \\ I_y = 0.099(\text{m}^4) \\ J = 35.845(\text{m}^4) \end{array} \right. , \left\{ \begin{array}{l} A = 0.906(\text{m}^2) \\ A_{sy} = 0.770(\text{m}^2) \\ I_x = 87.747(\text{m}^4) \\ A_{sx} = 0.770(\text{m}^2) \\ I_y = 0.017(\text{m}^4) \\ J = 18.672(\text{m}^4) \end{array} \right. \text{ and } \left\{ \begin{array}{l} A = 1.109(\text{m}^2) \\ A_{sy} = 0.943(\text{m}^2) \\ I_x = 107.387(\text{m}^4) \\ A_{sx} = 0.943(\text{m}^2) \\ I_y = 0.037(\text{m}^4) \\ J = 22.856(\text{m}^4) \end{array} \right.$$

for rubber pads on top of the piers, at the north abutment and at the south abutment, respectively.

5.2 Numbering of Structure

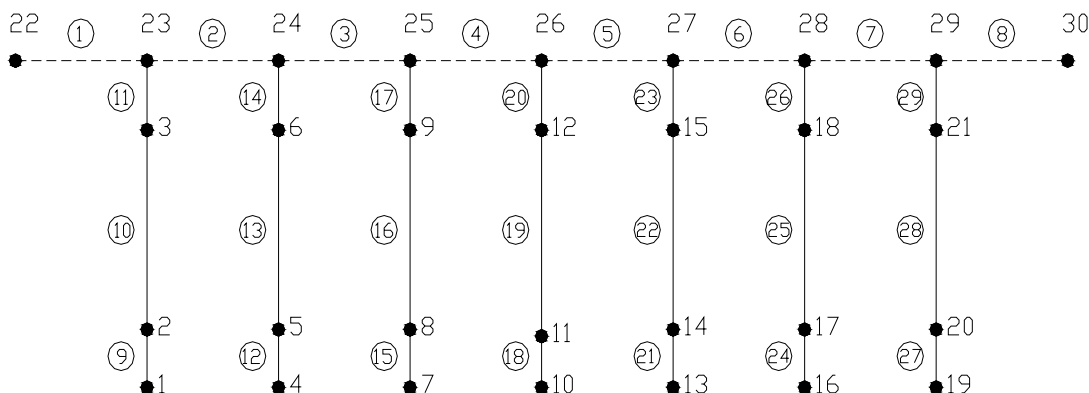


Figure V. 6 Elements and Nodal Numbering of Marga-Marge Bridge (without Rubber Pads)

Figure V.6 shows the numbering of the nodes and members of the model of the Marga Marga bridge without rubber pads while Figure V.7 shows the numbering with rubber pads. In these two figures, dashed lines represent the deck; solid normal lines and solid bold lines represent piers and rubber pads, respectively. The bridge is initially fixed at the bottom of all piers. (In the next chapter, the stiffness of the foundations is included.)

The left end of the deck (node 22 in Figure V.6) is fixed in all directions and the right end (node 30 in Figure V.6) is fixed in the transverse and vertical direction; for the model with rubber pads, the bottom faces of the two rubber pads (nodes 1 and 30 in Figure V.7) under the two ends of the deck are fixed in all directions.

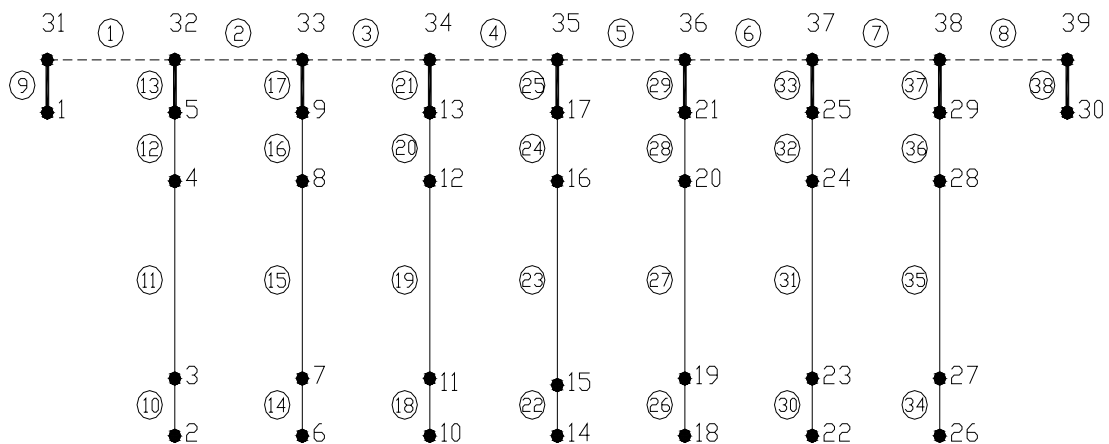


Figure V. 7 Elements and Nodal Numbering of Marga-Marge Bridge (with Rubber Pads)

5.3 Results

Running the program Bridge.for for the structural models of Figures V.6 & V.7, one can get the transfer functions of the displacements of each node due to a unit harmonic motion at the base of each pier or any combination of these motions.

In the figures in this chapter and the next chapter, transfer functions of node 26 (top of pier 4) in Figure V.6 due to unit harmonic motion at base of pier 4 or of all piers will be illustrated for the case without rubber pads and transfer functions of node 17 (top of pier 4) and node 35 (deck at pier 4) for the case with rubber pads.

A number of dynamic studies were conducted by students at the University of Chile using different structural models for the bridge. Their results provided natural frequencies and mode shapes rather than transfer functions as done here.

The original design had assumed that under the design earthquake the shear deformation of the rubber pads might reach 30%. This yielded a first natural frequency in the longitudinal direction of 0.49 Hz and in the transverse direction 0.59 Hz.

Table V. 1 Natural Frequencies of Marga-Marga Bridge from Former Studies (Hz)

		Longitudinal				Transverse			Vertical		
Experimental Data 1	May 1996	1.86				1.17	1.42	2.1			
Experimental Data 2	July 1996	1.71				1.07	1.27	1.9			
M.E. Segovia (1997)	no Rubber Pads	3.85				2	2.22	2.7			
	5% Deformation	1.54				0.71	1.02	1.85			
D. Romo (1999)	no Rubber Pads	2.01	2.13	2.39	2.77	1.29	1.79	2.67	3.36		
	Free Deck	0.65	2.09	2.24		0.93	2.18		1.87		
	Constrained Deck	2.01	2.03	2.1	2.25	0.93	1.28	2.18			
V.M. Daza (2003)		0.67	2.5	2.8		0.96	1.5		1.88	2.1	2.56

The other studies gave some recommended values of the natural frequencies of the Marga-Marga bridge, as shown in Table V.1. Different studies used different models and assumptions and therefore yielded different results.

The models of D. Romo and V.M. Daza used a finite element idealization of the bridge (with shell elements), so they may provide us better results. It can be seen from Romo's results that whether or not the deck is constrained the first transverse natural frequency is the same as long as the amount of the shear deformation in the pads is the same.

5.3.1 Longitudinal Direction (X direction)

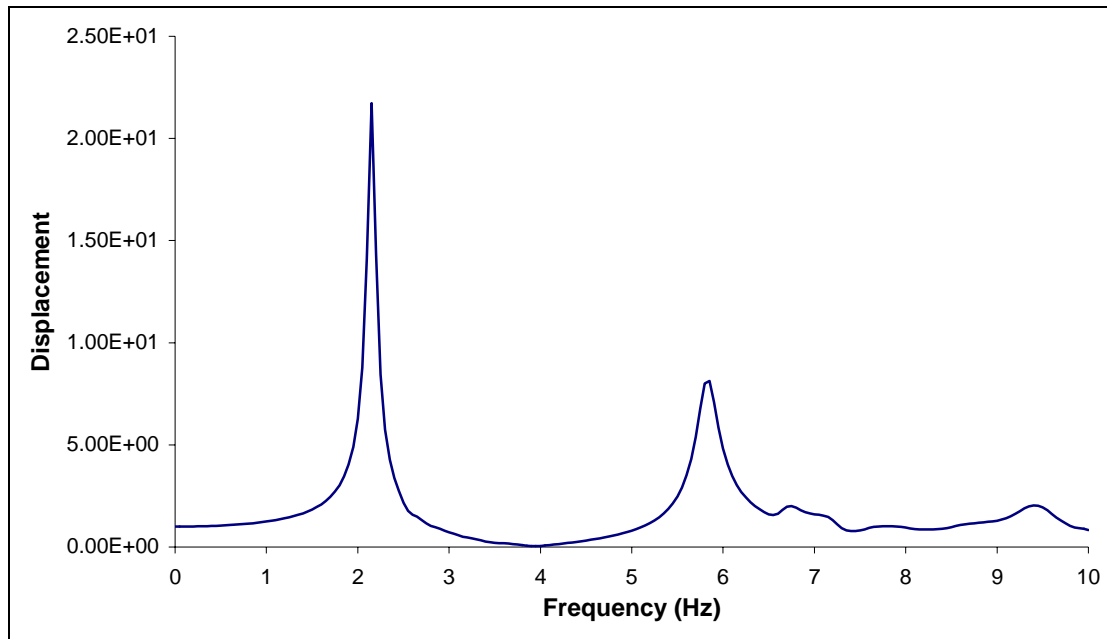
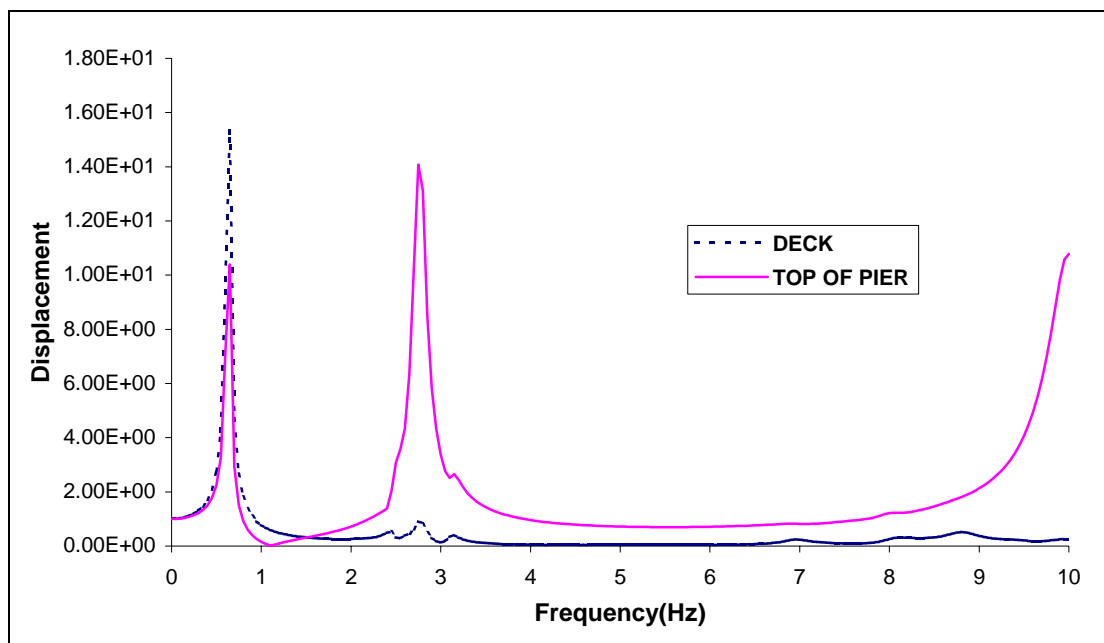


Figure V. 8 Displacement in X Direction at Top of Pier 4 due to Unit Motion at Base of All Piers (without Rubber Pads)

Figure V.8 shows the transfer function of the top of pier 4 for the structure without rubber pads due to a unit harmonic motion in the longitudinal direction (X direction) at the bottom of all piers. It can be seen that, in the longitudinal direction, the first two significant peaks of the transfer function due to the same unit harmonic base motion at all piers are 2.15 Hz and 5.85 Hz, respectively. The first one is very similar to the first two modes reported by D. Romo (2.01Hz and 2.13Hz) for the same case.

The use of rubber pads will change the frequency response characteristics of the structure. Figure V.9 shows the transfer functions of the deck and the top of pier 4 for the structure with rubber pads. In this case, the equivalent tangent shear modulus of the rubber pads is 6.0 Mpa, which corresponds to a shear deformation of 0.23% according to

the result of a regression analysis of experimental data ($G = 6.0 \times 10^5 \cdot \gamma^{-0.3764}$). It can be seen from Figure V.9 that the first two significant peaks have been reduced to 0.65 Hz and 2.75 Hz. It should be noted that, the peak at 0.65Hz is larger for the deck than for the top of the pier, whereas at 2.75 Hz, the displacement at the deck has been greatly reduced compared with that at the top of the pier, showing the effect of the rubber pads. The third peak for this case is around 10 Hz. The first significant peak agrees well with the first natural frequency reported by both V.M. Daza and D. Romo (for a free deck). The second peak occurs at a frequency in between the second and third natural frequencies of V.M. Daza's model.



**Figure V. 9 Displacement in X Direction due to Unit Motion at Base of All Piers
(with Rubber Pads, $G = 6.0 \times 10^6$ Pa, Free Deck)**

It appears that some of the natural modes reported by D. Romo are not excited by an equal base motion of all the piers in the longitudinal direction.

Figure V.10 shows the transfer function due to motion only at the base of pier 4. For this case the first peak is much smaller. The amplitudes of the second peak are however very similar for both cases, implying the response at this frequency (particularly on top of the pier) is essentially controlled by the motion at the base of pier 4. Figures V.11 and V.12 show the transfer functions due to unit motions at the bottom of all piers with smaller shear modulus of the rubber pads of 1.8Mpa and 1.0 Mpa, which correspond to shear deformations of 5% and 26%, respectively. The first two significant peaks occur now at 0.45 Hz, 1.95Hz and 0.35Hz, 1.7Hz, respectively. The displacements at the deck are always smaller than those at the top of the pier for all frequencies except at the first peak.

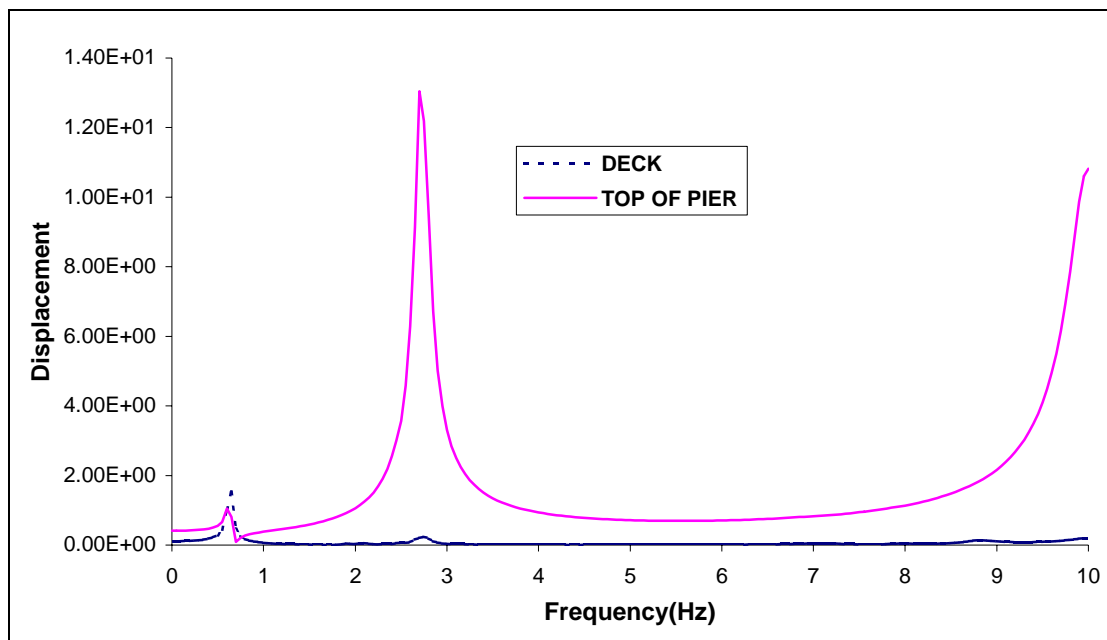
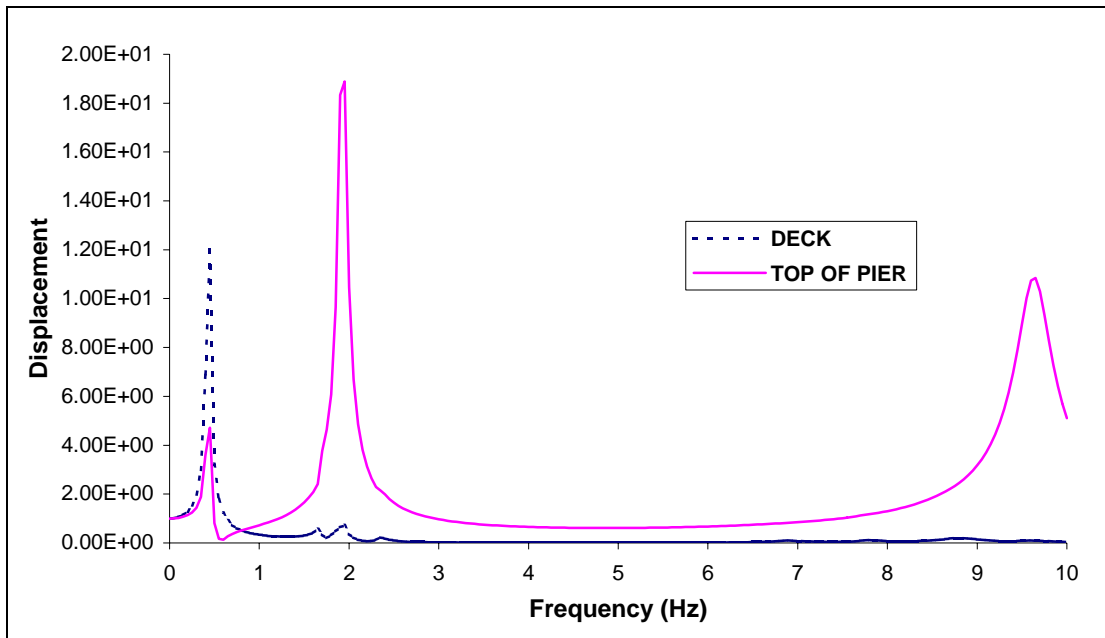
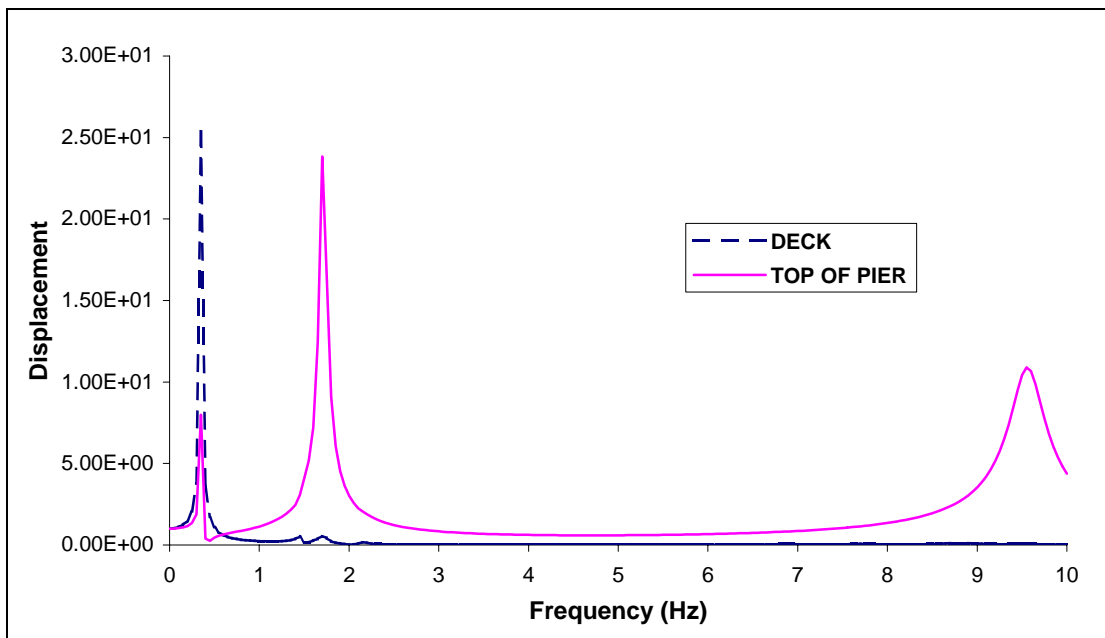


Figure V. 10 Displacement in X Direction due to Unit Motion at Base of Pier 4

(with Rubber Pads, $G = 6.0 \times 10^6$ Pa, Free Deck)



**Figure V. 11 Displacement in X Direction due to Unit Motion at Base of All Piers
(with Rubber Pads, $G = 1.8 \times 10^6$ Pa, Free Deck)**



**Figure V. 12 Displacement in X Direction due to Unit Motion at Base of All Piers
(with Rubber Pads, $G = 1.0 \times 10^6$ Pa, Free Deck)**

In all these cases it was assumed that the deck was free to displace at the ends in both directions on top of the rubber pads. A more realistic assumption is that the motions of the ends of the deck are partly prevented. The results obtained fixing the left end of the deck (node 1 in Figure V.7) in both longitudinal and transverse directions and the right end (node 30 in Figure V.7) in the transverse direction are shown in Figures V.13 to V.16. The true situation is likely somewhere in between these 2 extreme cases.

For the case of rubber pads with a shear modulus of 6.0Mpa and a constrained deck, the first significant peak occurs at 1.7 Hz (rather than the 0.65Hz for free deck). This value agrees well with some experimental data. It is followed by two small peaks at 2.5Hz and 2.85Hz at the top of pier 4, as shown in Figure V.13. But the motion of the deck is apparently amplified at 6.5Hz in this case. When the motion of the deck is constrained at the ends the amplitude of the first peak is again dramatically reduced when only the base of pier 4 is excited and the amplitude of the second peak on top of the deck at 2.85Hz is amplified (compare Figures V.13 and V.14). It should be noticed that the frequency and amplitude of this peak are essentially unaffected by the boundary conditions at the ends of the deck.

Figures V.15 and V.16 also show the results for rubber pads with shear modulus of 1.8Mpa and 1.0Mpa. In these two cases, the transfer functions of both the deck and the top of the pier have several peaks between 1.5Hz and 2.0Hz.

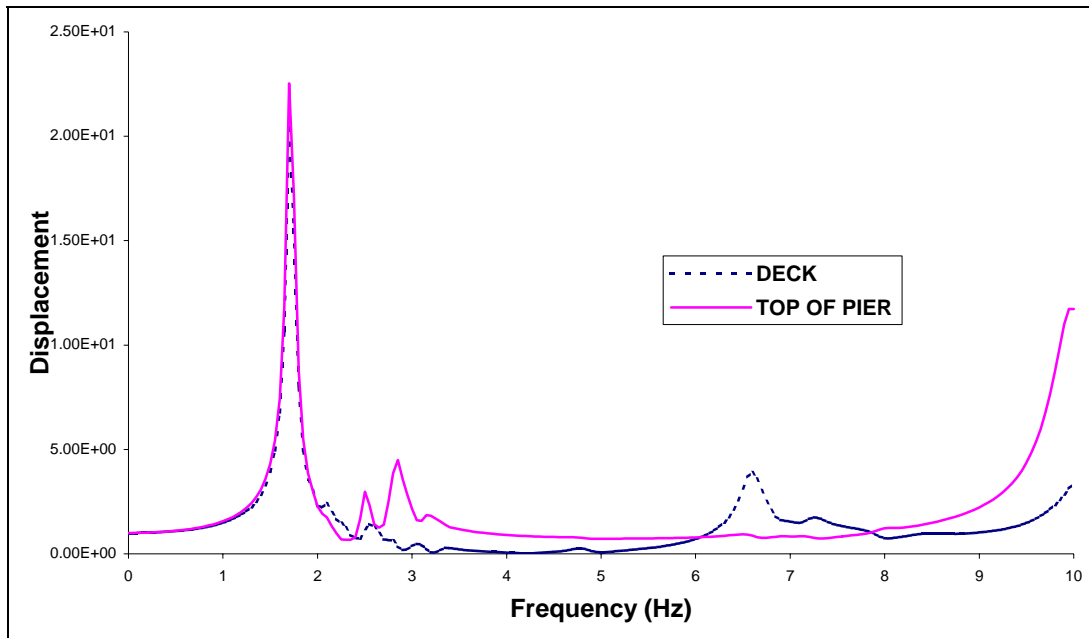


**Figure V. 13 Displacement in X Direction due to Unit Motion at Base of All Piers
(with Rubber Pads, $G = 6.0 \times 10^6$ Pa, Constrained Deck)**

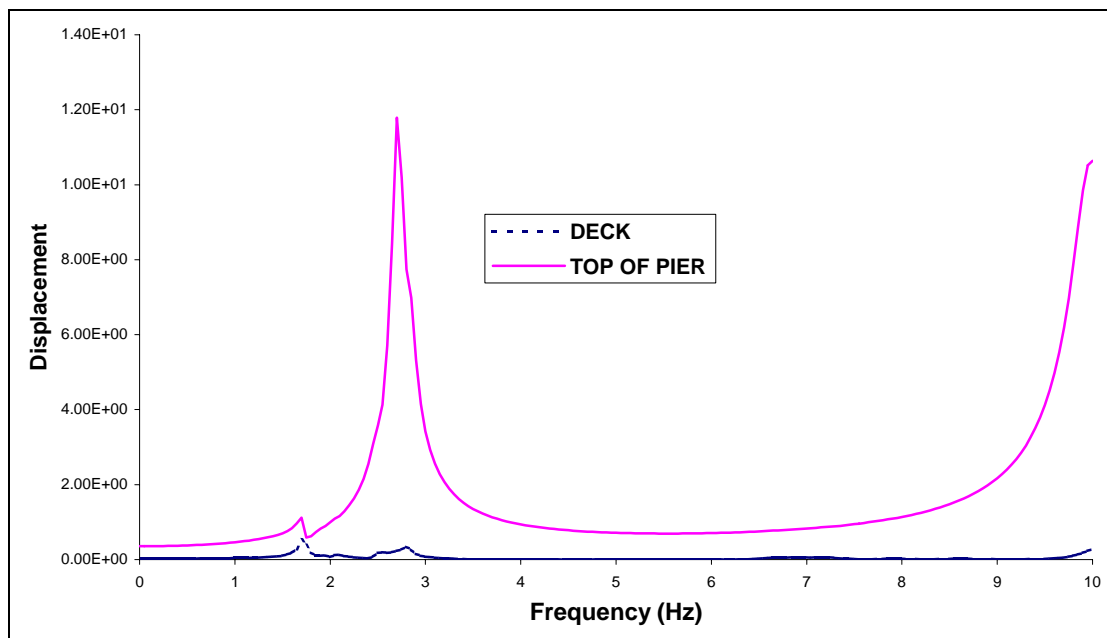


**Figure V. 14 Displacement in X Direction due to Unit Motion at Base of Pier 4
(with Rubber Pads, $G = 6.0 \times 10^6$ Pa, Constrained Deck)**

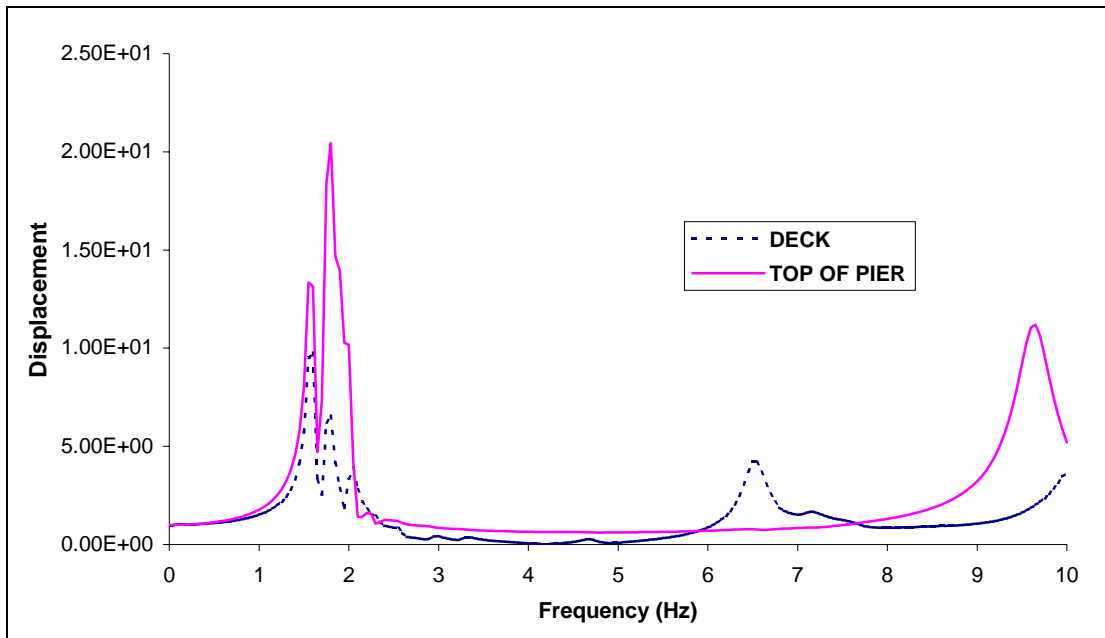


**Figure V. 15 Displacement in X Direction due to Unit Motion at Base of All Piers
(with Rubber Pads, $G = 1.8 \times 10^6$ Pa, Constrained Deck)**

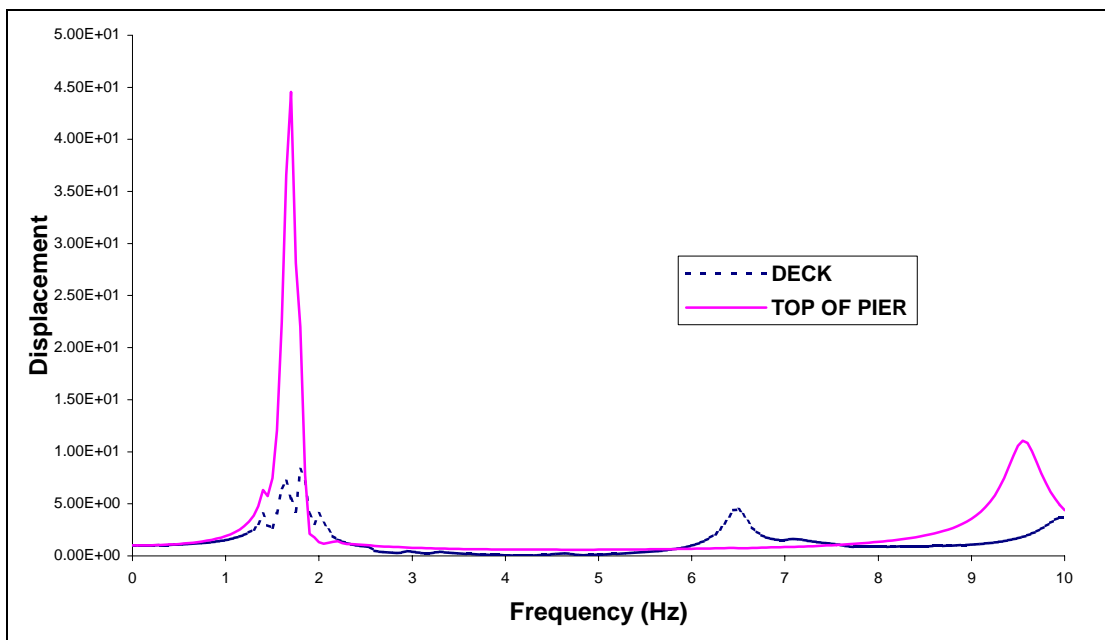


**Figure V. 16 Displacement in X Direction due to Unit Motion at Base of All Piers
(with Rubber Pads, $G = 1.0 \times 10^6$ Pa, Constrained Deck)**

5.3.2 Transverse Direction (Y direction)

In the transverse direction, without rubber pads, the first three significant peaks would be at 1.85Hz, 2.70Hz and 4.90Hz, respectively, as shown in Figure V.17, which illustrates the transfer function at the top of pier 4 due to a unit harmonic motion in the transverse direction at the bottoms of all the piers. The first two significant peaks are in relatively good agreement with those of the second and third mode in D. Romo's model for the same case (1.79Hz and 2.67Hz).

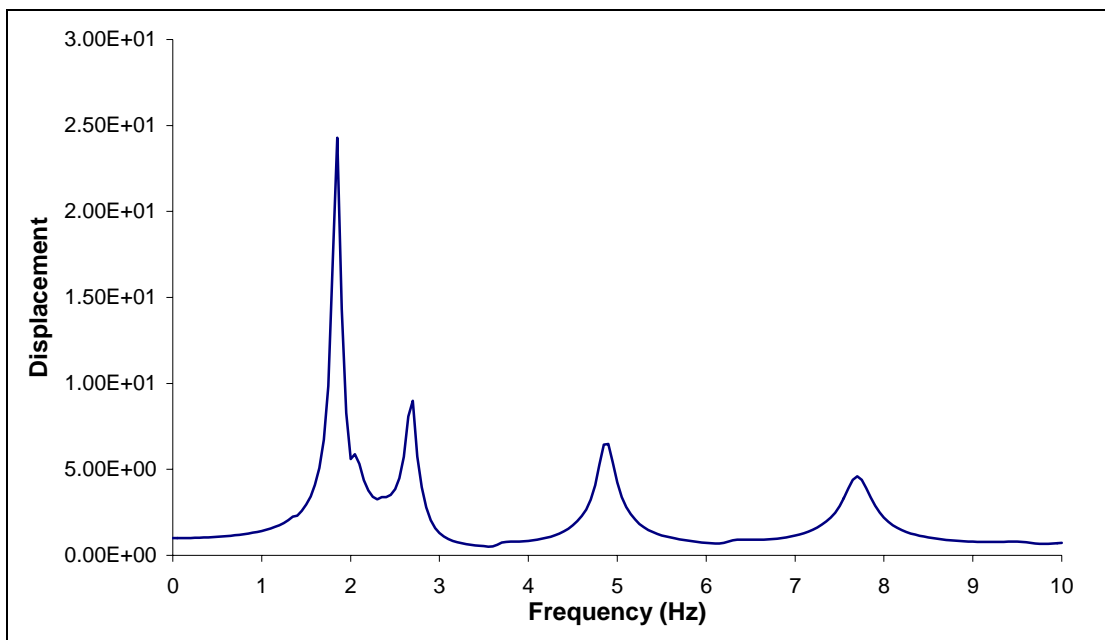
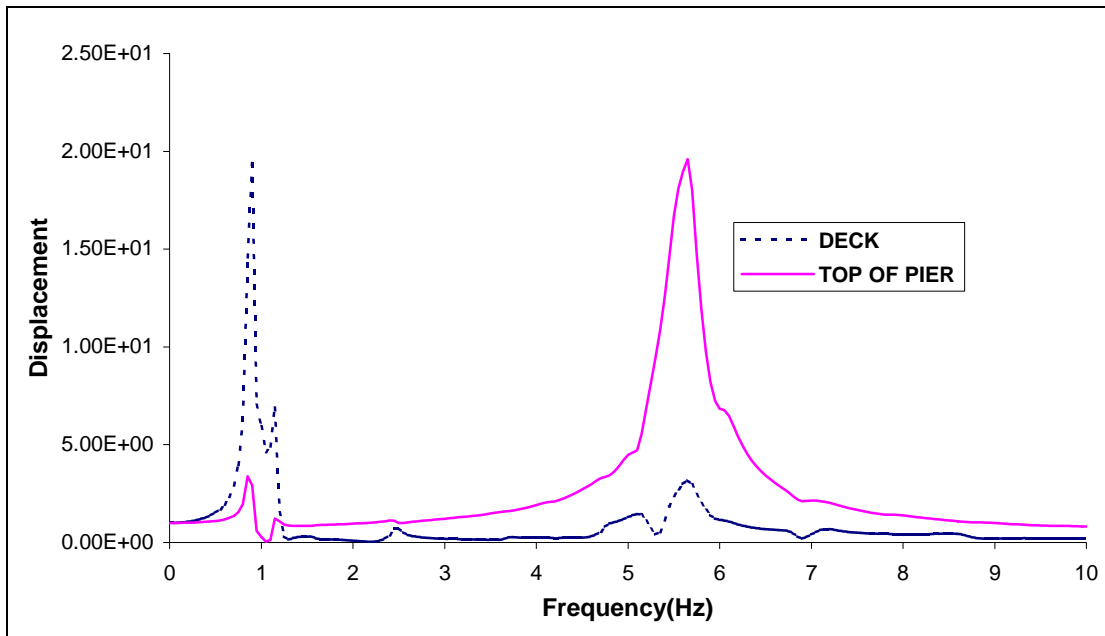


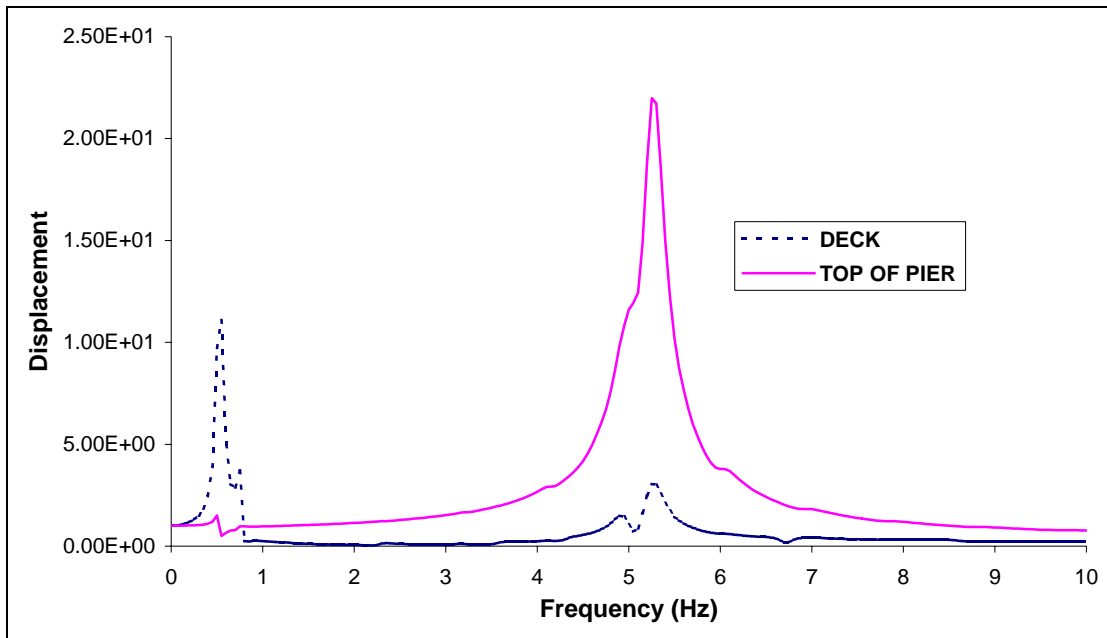
Figure V. 17 Displacement in Y Direction at Top of Pier 4 due to Unit Motion at Base of All Piers (without Rubber Pads)

Figure V.18 shows the transfer functions for a free deck and a shear modulus of the rubber pads of 6.0Mpa. It can be seen that the motion of the deck has a significant peak at 0.90 Hz and two small peaks at 1.15Hz and 5.7Hz, while the motion of the top of the pier has a significant peak at 5.7Hz and a small one at 0.9Hz. As the shear modulus reduces to 1.8Mpa and 1.0Mpa as shown in Figure V.18 and Figure V.19, the significant

peak for the deck decreases to 0.55Hz and 0.45Hz, respectively; while that of the top of the deck takes place at 5.3Hz and 5.25Hz, respectively. The peak at 0.90Hz frequency agrees with the results of D. Romo and the V.M. Daza (0.93Hz and 0.96Hz) while the 1.15Hz frequency agrees with the experimental data (1.17Hz and 1.07Hz).



**Figure V. 18 Displacement in Y Direction due to Unit Motion at Base of All Piers
(with Rubber Pads, $G = 6.0 \times 10^6$ Pa, Free Deck)**



**Figure V. 19 Displacement in Y Direction due to Unit Motion at Base of All Piers
(with Rubber Pads, $G = 1.8 \times 10^6$ Pa, Free Deck)**

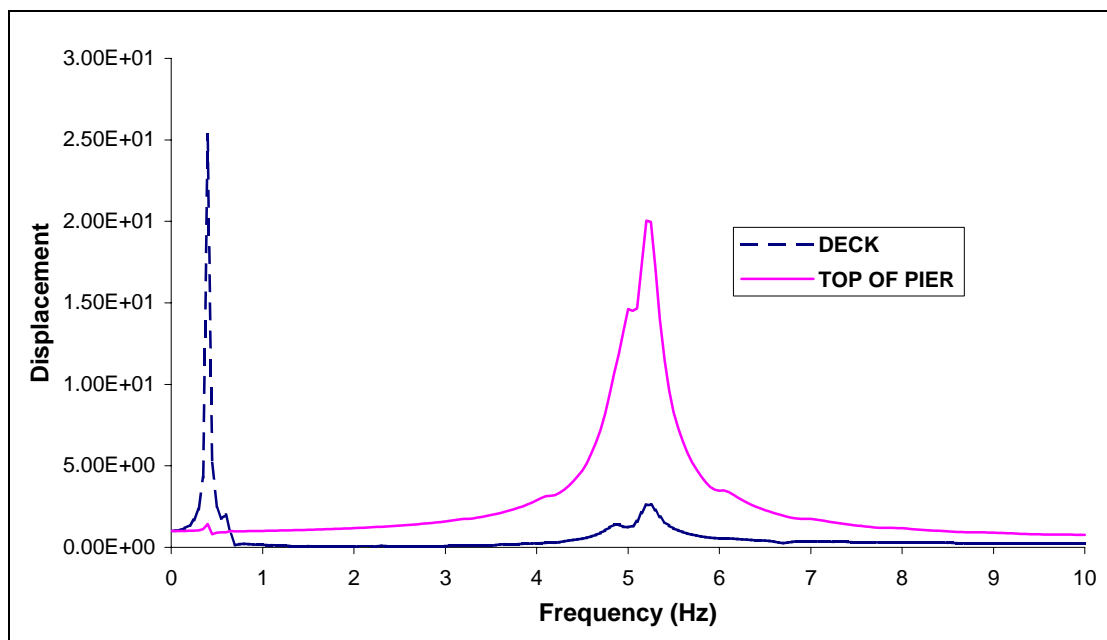


**Figure V. 20 Displacement in Y Direction due to Unit Motion at Base of All Piers
(with Rubber Pads, $G = 1.0 \times 10^6$ Pa, Free Deck)**

If the motion of the deck is constrained at the ends, the transfer function of the motion of the deck exhibits more peaks. With the shear modulus of the rubber pads equal to 6.0Mpa as shown in Figure V.21, the peaks for the deck are at 0.9Hz, 1.85Hz and 4.30Hz. The frequencies of these peaks change to 0.55Hz, 1.75Hz, 4.30Hz and 0.45Hz, 1.70Hz, 4.30Hz for 1.8Mpa and 1.0Mpa rubber pads, as shown in Figure V.22 and Figure V.23, respectively. But the peaks for the transfer functions of the motion at the top of the pier occur at almost the same frequency as in the case of a free deck.

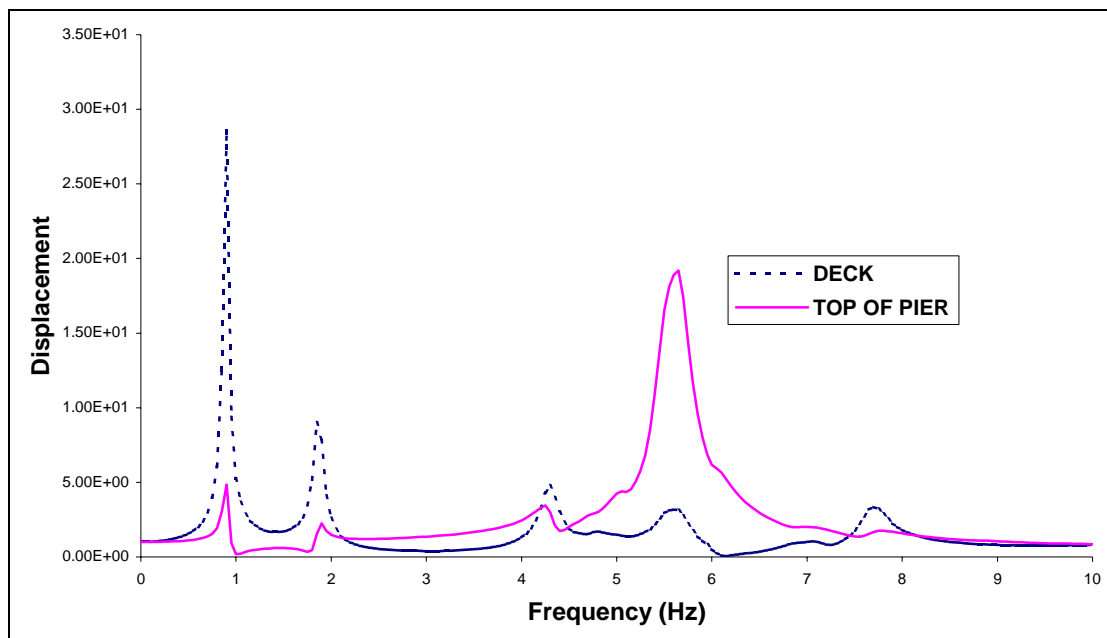
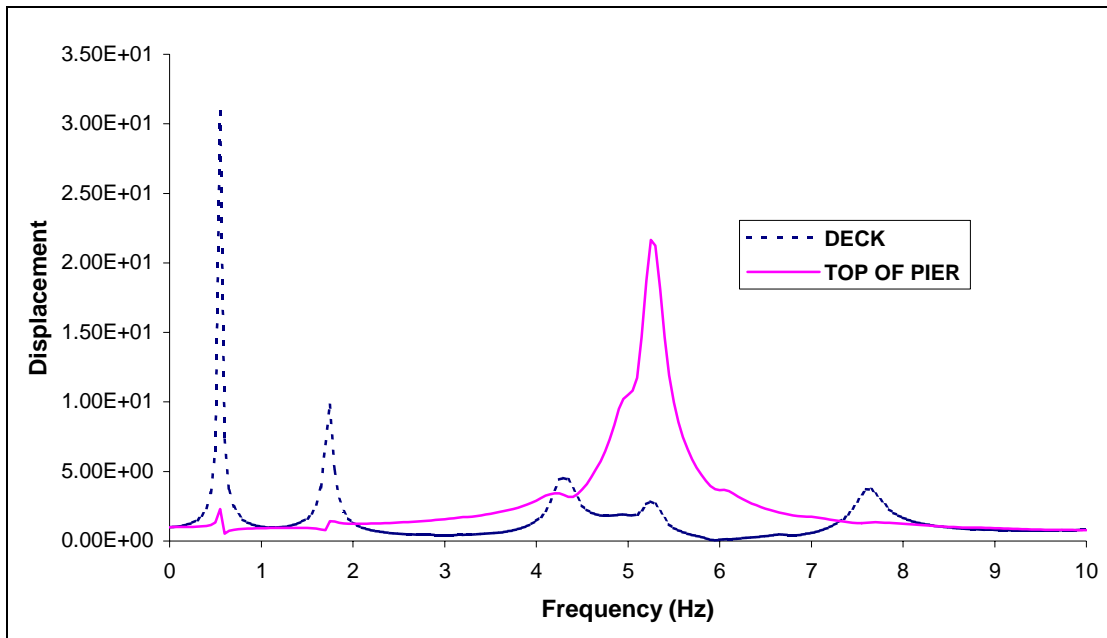
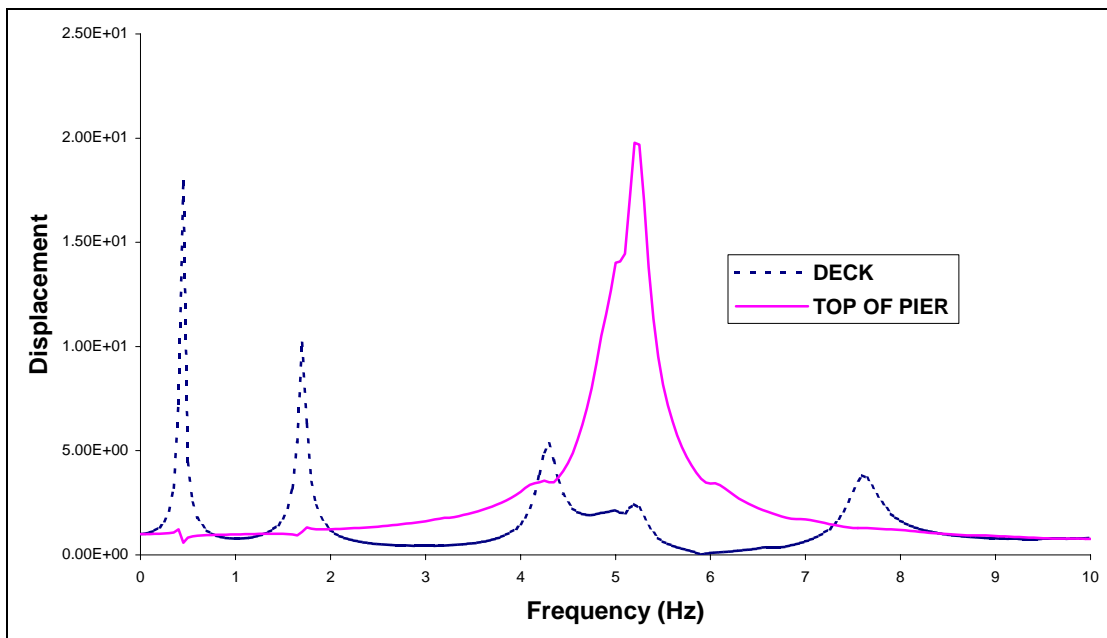


Figure V. 21 Displacement in Y Direction due to Unit Motion at Base of All Piers

(with Rubber Pads, $G = 6.0 \times 10^6$ Pa, Constrained Deck)



**Figure V. 22 Displacement in Y Direction due to Unit Motion at Base of All Piers
(with Rubber Pads, $G = 1.8 \times 10^6$ Pa, Constrained Deck)**



**Figure V. 23 Displacement in Y Direction due to Unit Motion at Base of All Piers
(with Rubber Pads, $G = 1.0 \times 10^6$ Pa, Constrained Deck)**

5.3.3 Vertical Direction (Z direction)

The frequency response in the vertical direction depends on the Young's modulus of the rubber pads rather than their shear modulus. Since the rubber pads are made of alternating layers of rubber and steel, they are not isotropic. Some studies indicated that the rubber pads used in the Marga-Marga bridge have a Young's modulus between 1.35Gpa and 2.40Gpa.

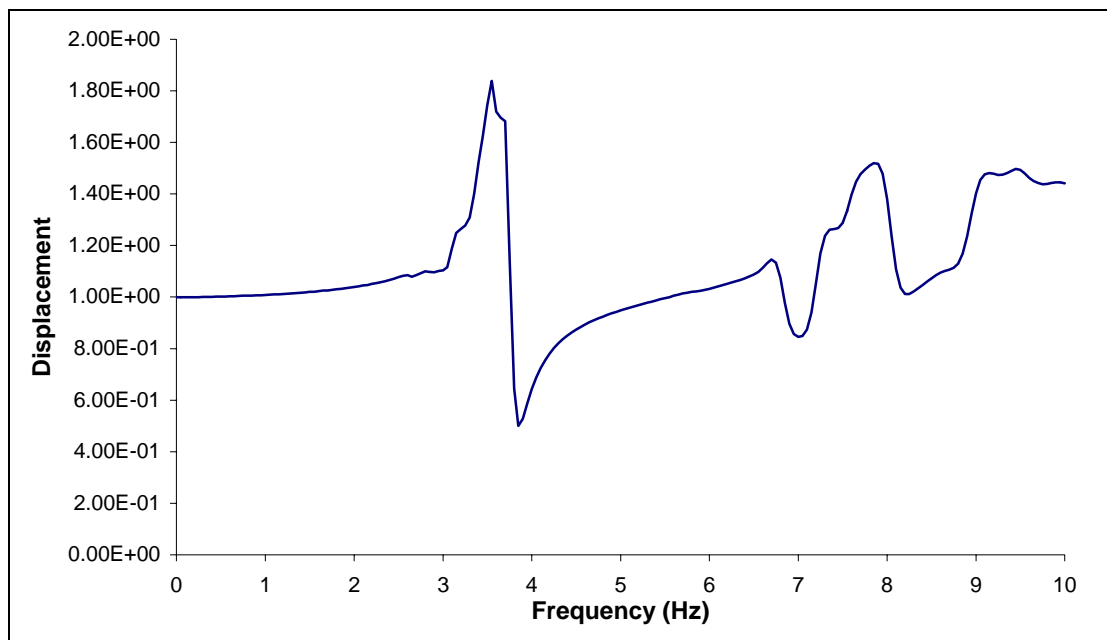


Figure V. 24 Displacement in Z Direction at Top of Pier 4 due to Unit Motion at Base of All Piers (without Rubber Pads)

Without rubber pads, the transfer function of the displacement at the top of pier 4 due to a unit vertical harmonic motion at the bottoms of all piers is shown in Figure V.24. It can be seen that the first significant peak occurs around 3.55Hz. This value agrees well with the first natural frequency of 3.36Hz reported by D. Romo for the same case.

With the introduction of rubber pads with a Young's modulus of 6.0Gpa or 1.8Gpa, the first significant peak still happens around 3.55Hz although there are some small fluctuations between 2.20Hz and 2.80Hz, as shown in Figures V.25 and V.26. A peak at 2.20Hz would be consistent with the natural frequency of 2.18Hz reported by D. Romo and frequencies of 1.88Hz and 2.10Hz obtained by V.M. Daza. The largest amplification occurs however at 3.55Hz, a frequency not reported in their studies. It can be concluded that the frequency at which the significant peak happens is almost independent of the introduction of the rubber pads or their Young's modulus. But as the Young's modulus decreases, the amplitude of the peak corresponding to the displacement at the deck increases.

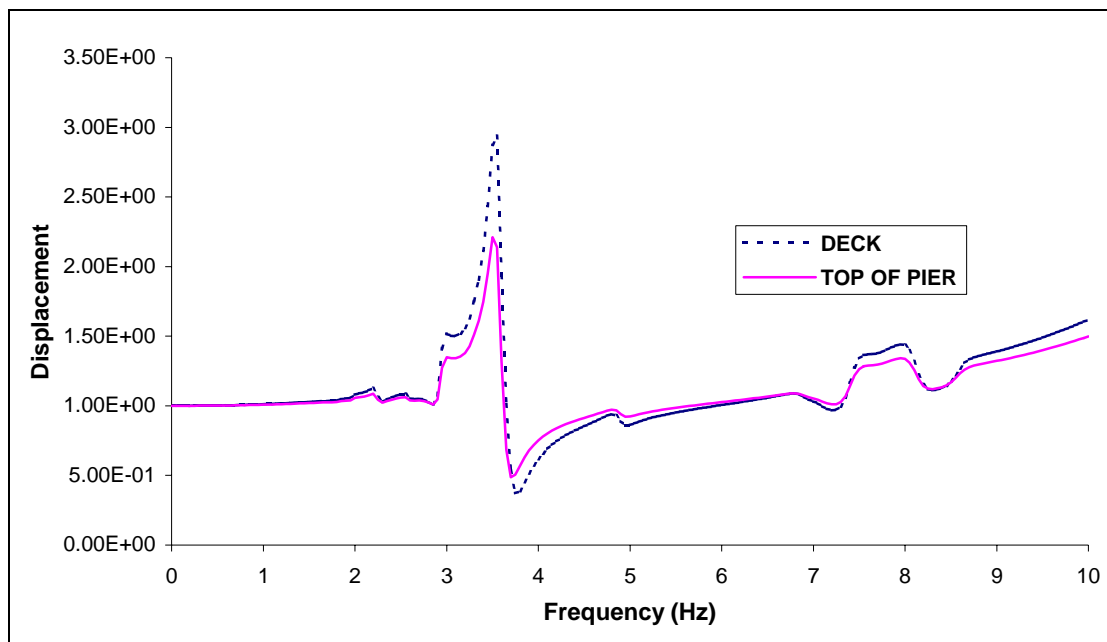
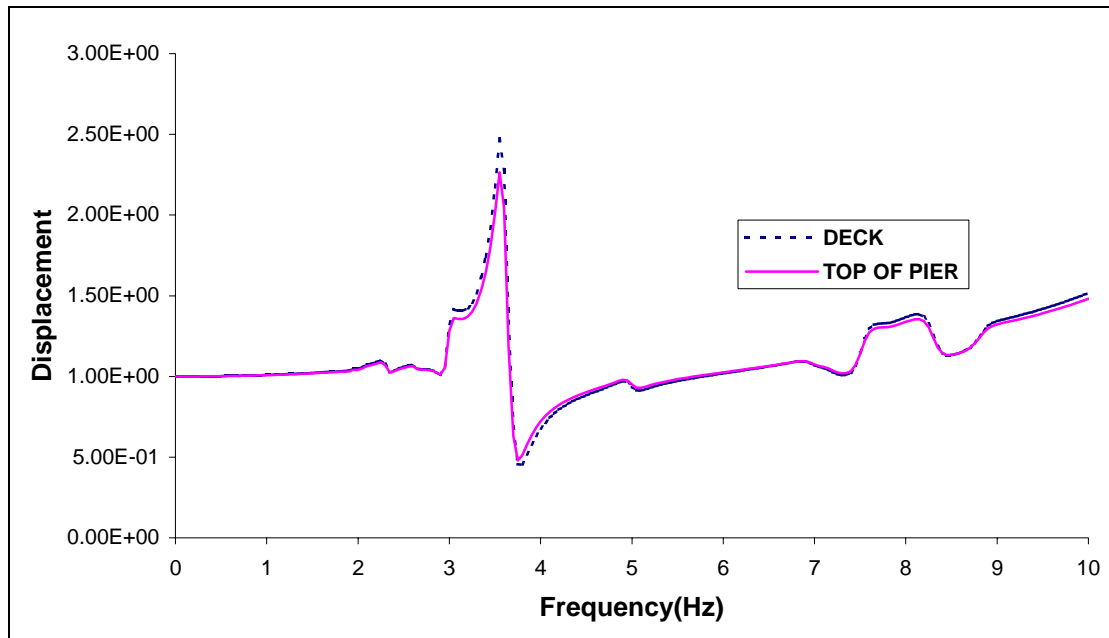


Figure V. 25 Displacement in Z Direction due to Unit Motion at Base of All Piers

(with Rubber Pads, $E = 1.8 \times 10^9$ Pa, Free Deck)



**Figure V. 26 Displacement in Z Direction due to Unit Motion at Base of All Piers
(with Rubber Pads, $E = 6.0 \times 10^9$ Pa, Free Deck)**

5.4 Conclusions

1. When comparing the results of the present study to those reported by previous researchers at the University of Chile one should take into account that, in addition to the difference in the structural models, the results presented here are transfer functions reflecting the natural frequencies and also the participation factors of various modes, while the previous studies provided the natural frequencies of all the modes. Some of these modes might have a very small participation factor, not get excited by the assumed base motions, and not show as a result in the transfer functions;
2. In the longitudinal direction, this study yields results very similar to those of D. Romo, except that if the deck is free and the rubber pads have a 5% shear

deformation, the first natural frequency from this work (0.45Hz) is much lower than that from the model of D. Romo (0.65Hz). This study has 0.65Hz as the first longitudinal natural frequency when the shear modulus of the rubber pads is 6.0Mpa, which corresponds to a shear deformation of only 0.23%;

3. In the transverse direction, this research gives smaller natural frequencies than the model of D. Romo. But when the shear modulus of the rubber pads is 6.0Mpa (0.23% shear deformation), the results from this research are again very similar to the model of D.Romo with 5% shear deformation;
4. For the cases with rubber pads, the transfer function at the top of the pier assuming a constrained deck are almost the same as for a free deck. This implies that the constraints on the ends of the deck will not change the motion at the top of the pier very much. Actually, the two ends of the deck are neither entirely fixed in the two horizontal directions, nor absolutely free. The abutments will restrain the motion of the deck but the deck can still slide over the abutments;
5. The constraints on the two ends of the deck will not change the first transverse natural frequency, in which mode the deck slides over the relatively soft rubber pads. This is because the deck is very long so the bending strain energy in the first mode (half harmonic shape) is very small if the two ends of the deck are fixed transversely compared with the strain energy associated with the shear deformation of the rubber pads. For smaller values of the shear modulus of the rubber pads, restraining the motion of the deck at the ends will have a larger effect on the first natural frequency.

CHAPTER VI

EFFECT OF SOIL STRUCTURE INTERACTION

The transfer functions in the previous chapter were obtained assuming rigid foundations. This assumption may not be very realistic in some cases, especially for soft soils. To account for the finite stiffness of the foundations, soil structure interaction (SSI) analyses are conducted in this chapter.

The numbering of the structure's model is the same as shown in Figures V.6 & V.7. The nodes on the south and north abutment (nodes 22 and 30 in Figure V.6 or nodes 1 and 30 in Figure V.7) are still fixed for all 6 degrees of freedom, while the nodes under each pier (nodes 1, 4, 7, 10, 13, 16 and 19 in Figure V.6 or nodes 2, 6, 10, 14, 18, 22 and 26 in Figure V.7) are fixed against rotation around the Z axis but supported by springs with finite stiffness for the other 5 degrees of freedom to model the finite stiffness of the foundation. The properties and stiffness of the pile foundations (at the pile heads) of the Marga-Marga bridge were obtained in Chapter IV. The properties of the deck, piers and rubber pads are the same as those used in Chapter V.

The computer software described in previous chapters was applied again to the Marga-Marga bridge, but including the stiffness of the pile foundations, to compare the results with those without SSI and, to evaluate its potential importance.

6.1 Assumptions

Two important assumptions were made to calculate the transfer functions of the system in this chapter. First, each pile cap has 6 degrees of freedom (DoFs), and the application of a unit force in any direction may cause displacements in the others. This is known as the coupling between the different DoFs, such as the coupling between the horizontal

and the rocking stiffness. In this study, the coupling terms were neglected because they are relatively unimportant. (The coupling term between the horizontal and the rocking stiffness is very small compared with the horizontal or rocking stiffness themselves.) The stiffness matrix of a pile foundation used here is a diagonal matrix, and all the non-diagonal terms are zero, as shown in equation VI.1.

$$[K_{pile}(\omega)] = \begin{bmatrix} S_x(\omega) & 0 & 0 & 0 & 0 & 0 \\ 0 & S_y(\omega) & 0 & 0 & 0 & 0 \\ 0 & 0 & S_z(\omega) & 0 & 0 & 0 \\ 0 & 0 & 0 & R_x(\omega) & 0 & 0 \\ 0 & 0 & 0 & 0 & R_y(\omega) & 0 \\ 0 & 0 & 0 & 0 & 0 & T_z(\omega) \end{bmatrix} \dots\dots\dots(VI.1)$$

in which S_x , S_y , S_z , R_x and R_y denote the horizontal dynamic stiffness in the X and Y directions, the vertical stiffness in the Z direction, and the rocking stiffness around the X axis and around the Y axis, respectively; T_z represents the torsional stiffness around the Z axis, assumed to be infinite in this case.

The other simplifying assumption is that in calculating the dynamic stiffness of one pile group, the existence of the other pile groups can be neglected, because the distance between two pile groups (about 50 meters for the Marga-Marga bridge) is much larger than the horizontal dimension of the pile groups themselves (5.5 meters in the X direction).

6.2 Loads

In the previous chapter, for the structure with rigid foundations, a unit harmonic displacement was applied at the bottom of each pier. In this chapter, the bottoms of the piers are not fixed any more due to the finite stiffness of the pile foundations. The unit displacement would be applied at the bottom of the equivalent springs representing the

foundation. Because we neglect the coupling effect between different DoFs, this is equivalent to applying a harmonic load at the bottom of each pier with magnitude equal to the dynamic stiffness of the pile foundation in that direction. For example, in the vertical direction, the equivalent vertical force is applied at the bottom of each pier with a magnitude of S_z , which is the vertical stiffness of the pile foundation under that pier.

6.3 Results

6.3.1 Longitudinal Direction (X direction)

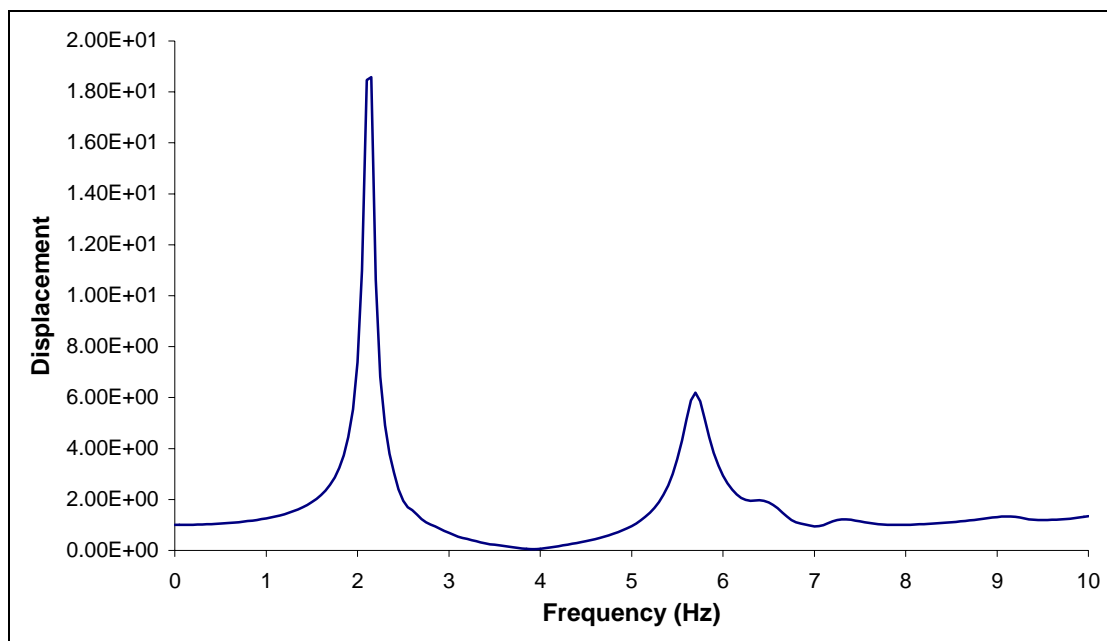


**Figure VI. 1 Displacement in X Direction at Top of Pier 4
due to Unit Motion at Bottom of All Foundations (without Rubber Pads)**

Table VI. 1 Effect of SSI on Peaks of Transfer Function in Longitudinal Direction (Hz)

Shear Modulus of Rubber Pads	Without SSI			With SSI		
	First Peak	Second Peak	Third Peak	First Peak	Second Peak	Third Peak
No Rubber Pads	2.15	5.85		2.13	5.75	
6.0Mpa(free deck)	0.65	2.75		0.60	2.65	
1.8Mpa(free deck)	0.45	1.95		0.40	1.80	
1.0Mpa(free deck)	0.35	1.70		0.35	1.60	
6.0Mpa(constrained deck)	1.70	2.50	2.85	1.70	2.45	2.60
1.8Mpa(constrained deck)	Between 1.5 and 2.0			Between 1.5 and 2.0		
1.0Mpa(constrained deck)	Between 1.5 and 2.0			Between 1.5 and 2.0		

Due to the finite stiffness of the foundations, the natural frequencies of the soil structure system are expected to be smaller than those of the structure on rigid foundations.

Figure VI.1 shows the transfer function at the top of pier 4 in the X direction without rubber pads. It can be seen that the two significant peaks are at 2.13Hz and 5.75Hz, which are only slightly smaller than those of the case without SSI (2.15Hz and 5.85Hz). Figures VI.2 to VI.9 show the transfer functions at the top of pier 4 and the deck for the case with rubber pads and SSI. The change in the frequencies of the significant peaks due to the consideration of the SSI is summarized in Table VI.1.

It can be concluded that the effect of SSI is very small in the longitudinal direction in relation to the first few natural frequencies of the structure because the positions of the peaks change very little. Even some small peaks appear at the same frequencies as in the case without SSI. (For example, there is also a small peak for the motion of the deck around 6.6Hz for the constrained deck.)

The SSI effects are more pronounced for high frequencies. Whether the deck is constrained or not, the motion at the top of the pier has a large peak around 10.0Hz

without SSI. This peak is greatly de-amplified and shifted to a value between 8Hz to 9Hz (shown in Figures VI.2 to VI.9) when the SSI effect is included. Figures VI.10 & VI.11 show the transfer functions for the motion at the base of pier 4 in the longitudinal direction when the same harmonic motion is applied at the base of all foundations. It can be seen that the motion is a function of the frequency, rather than a constant of 1 as would be obtained without SSI effect. The base motion of the pier can be amplified up to 30% or de-amplified up to 40%. Between 0.0 and 3.0 Hz the SSI effect results in small changes in the frequencies of the peaks resulting in a relatively sharp peak followed by a valley. The motion increases smoothly between 3.0 and 7.5 Hz. Between approximately 8.0 and 10.0 Hz there is a significant reduction in the amplitude of the motions. This is the range of frequencies over which the flexibility of the foundations would have the most significant effect in the longitudinal direction.

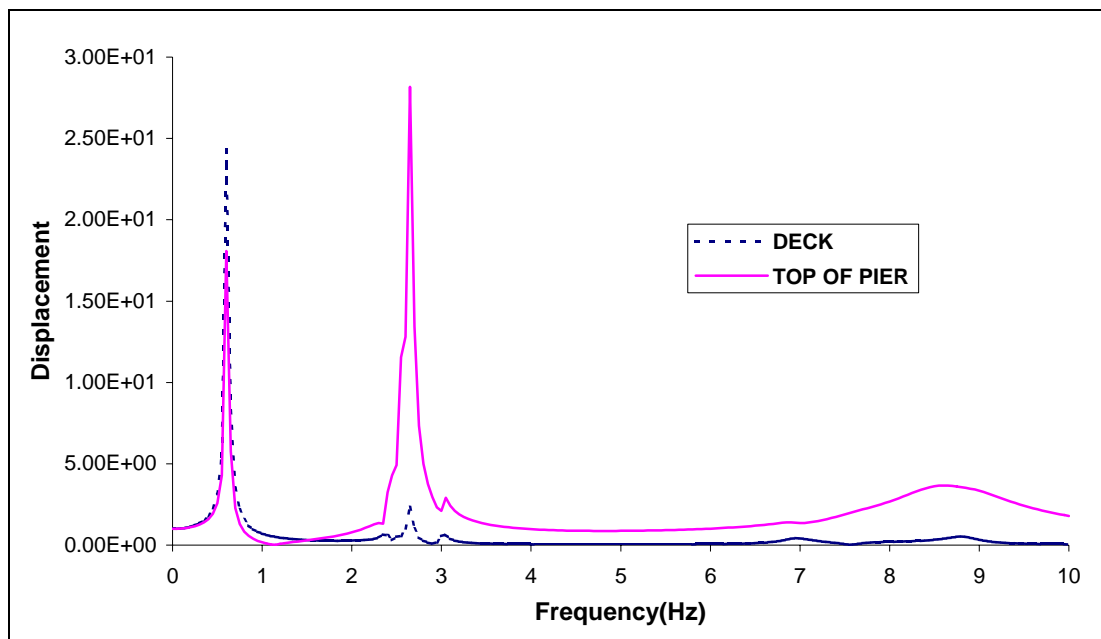
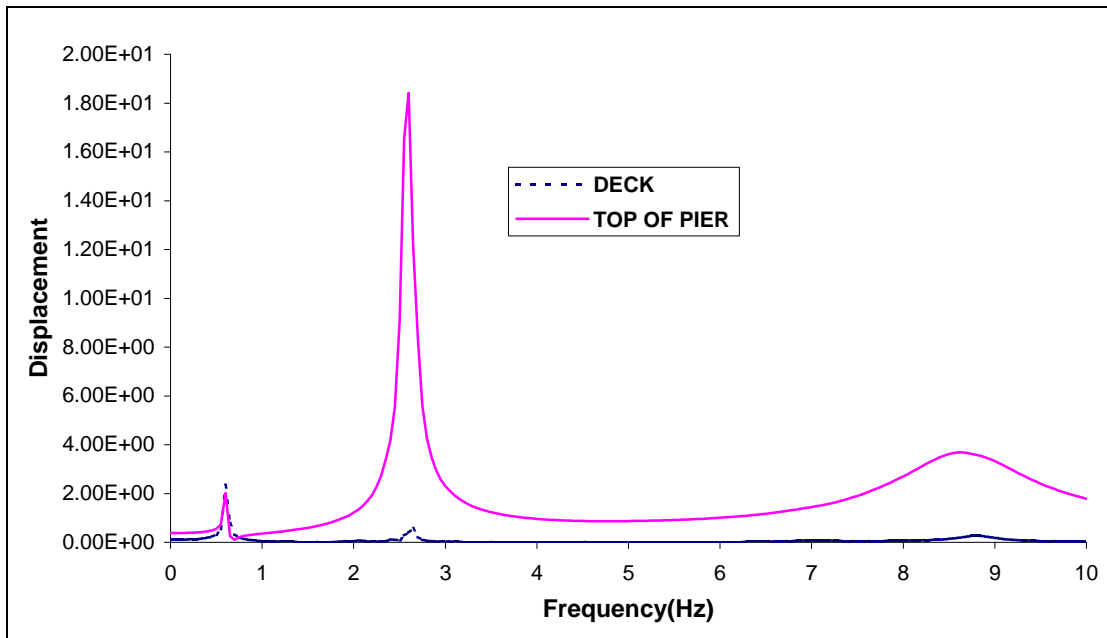
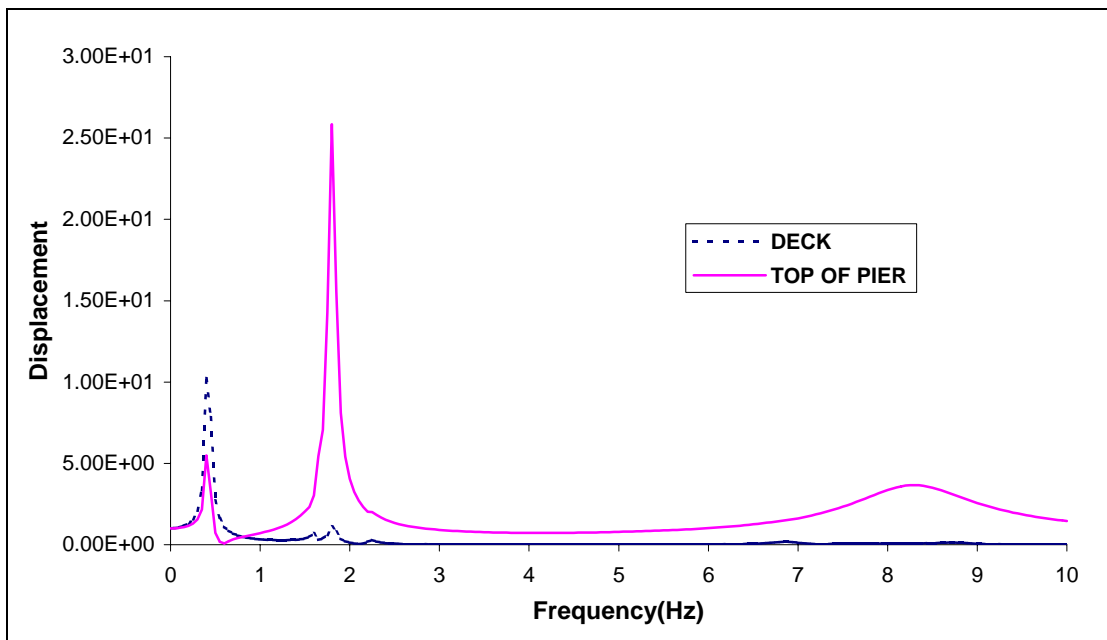


Figure VI. 2 Displacement in X Direction due to Unit Motion at Base of All Foundations

(with Rubber Pads, $G = 6.0 \times 10^6$ Pa, Free Deck)



**Figure VI. 3 Displacement in X Direction due to Unit Motion at Base of Foundation under Pier 4
(with Rubber Pads, $G = 6.0 \times 10^6$ Pa, Free Deck)**



**Figure VI. 4 Displacement in X Direction due to Unit Motion at Base of All Foundations
(with Rubber Pads, $G = 1.8 \times 10^6$ Pa, Free Deck)**

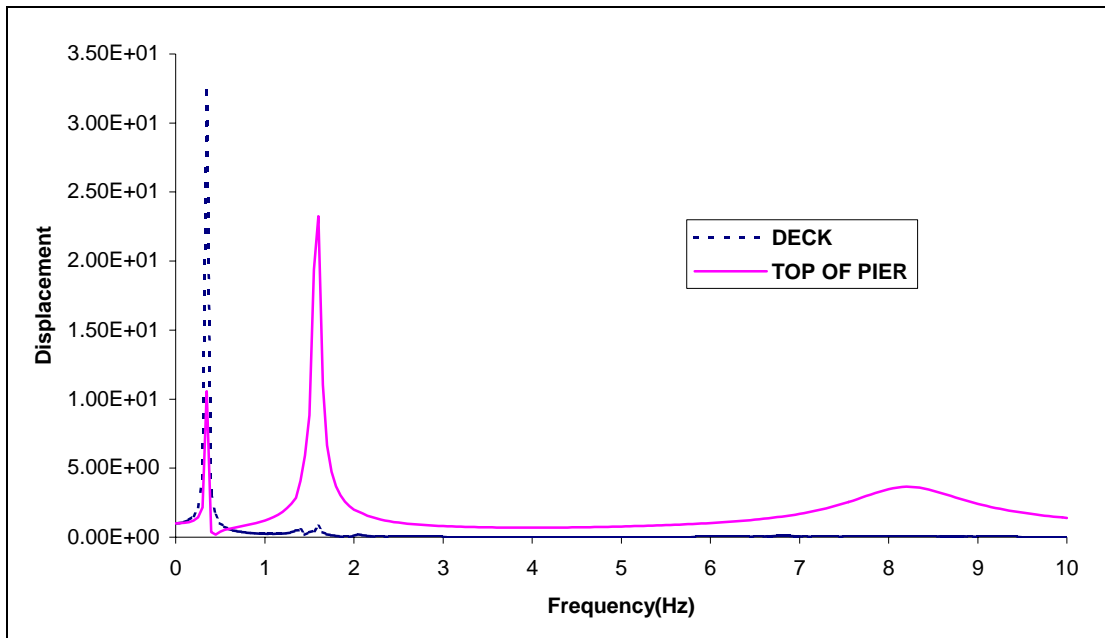


**Figure VI. 5 Displacement in X Direction due to Unit Motion at Base of All Foundations
(with Rubber Pads, $G = 1.0 \times 10^6$ Pa, Free Deck)**

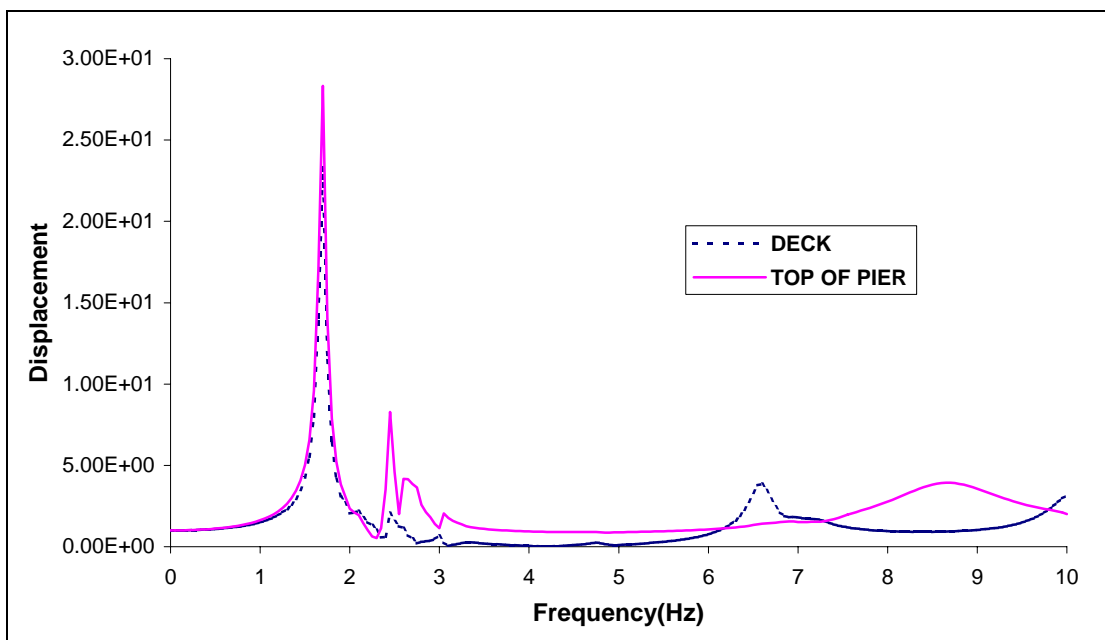


**Figure VI. 6 Displacement in X Direction due to Unit Motion at Base of All Foundations
(with Rubber Pads, $G = 6.0 \times 10^6$ Pa, Constrained Deck)**

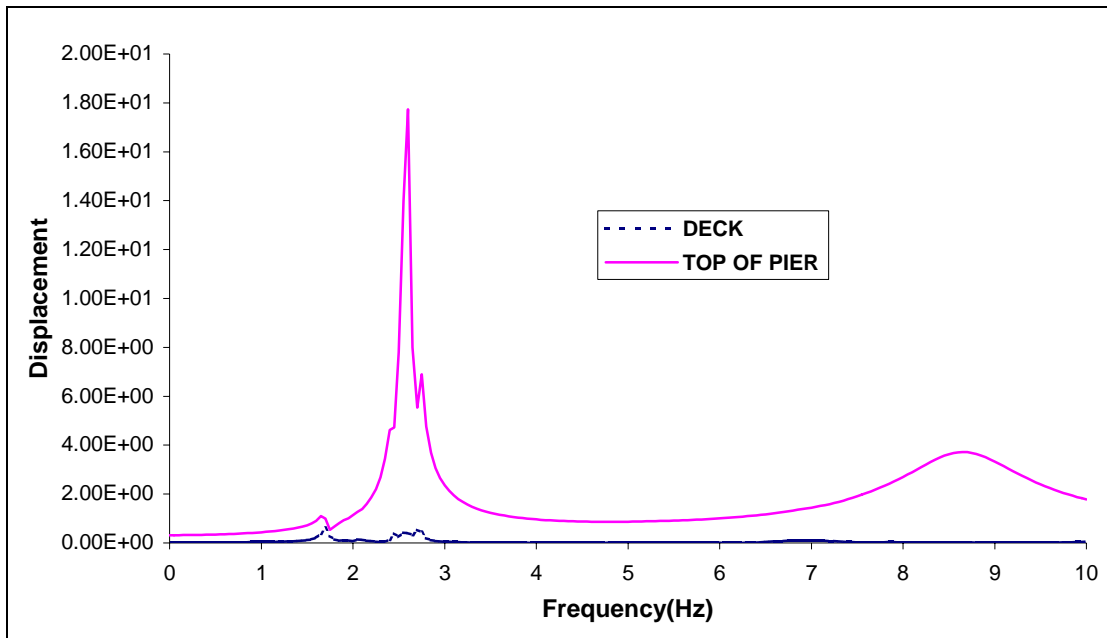


**Figure VI. 7 Displacement in X Direction due to Unit Motion at Base of Foundation under Pier 4
(with Rubber Pads, $G = 6.0 \times 10^6$ Pa, Constrained Deck)**

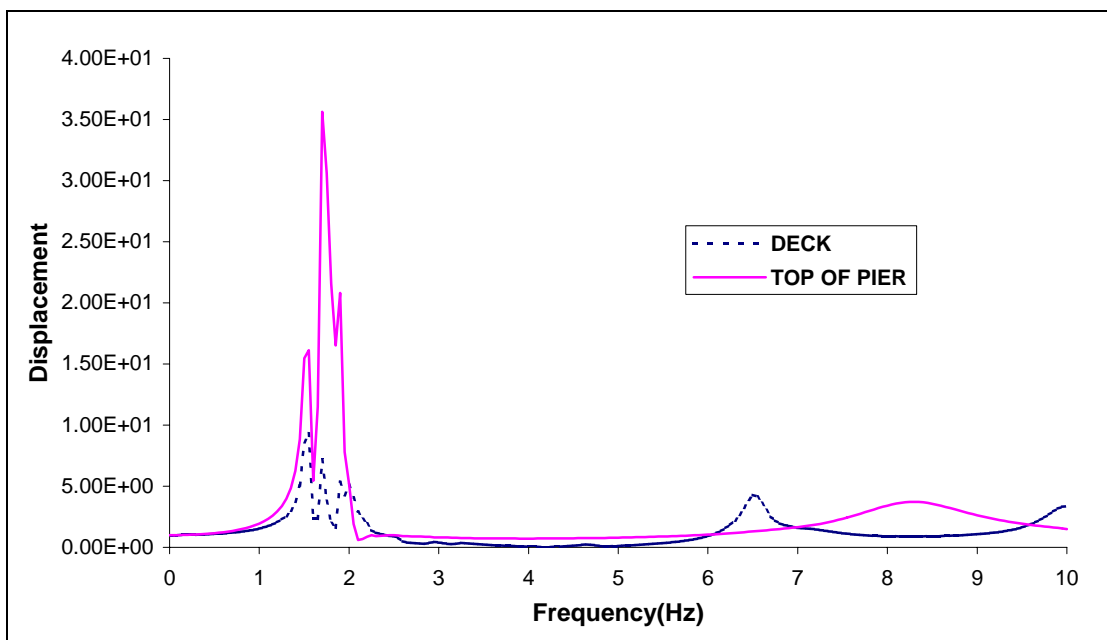


**Figure VI. 8 Displacement in X Direction due to Unit Motion at Base of All Foundations
(with Rubber Pads, $G = 1.8 \times 10^6$ Pa, Constrained Deck)**

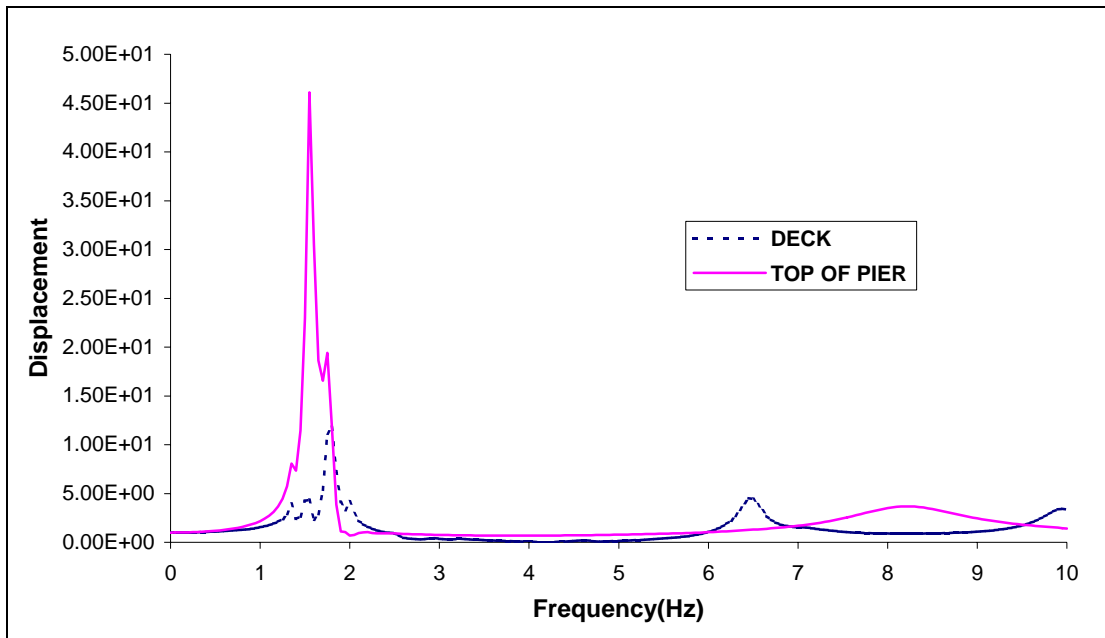


**Figure VI. 9 Displacement in X Direction due to Unit Motion at Base of All Foundations
(with Rubber Pads, $G = 1.0 \times 10^6$ Pa, Constrained Deck)**

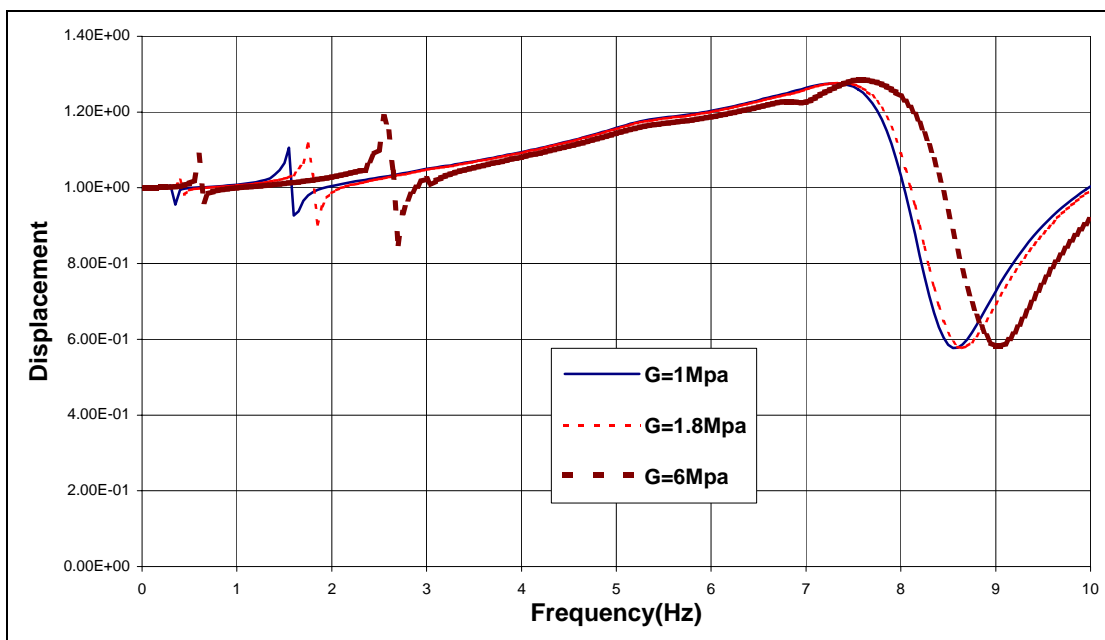


**Figure VI. 10 Motion of the Base of Pier 4 When All Foundations Are Excited in the X Direction
(Free Deck)**

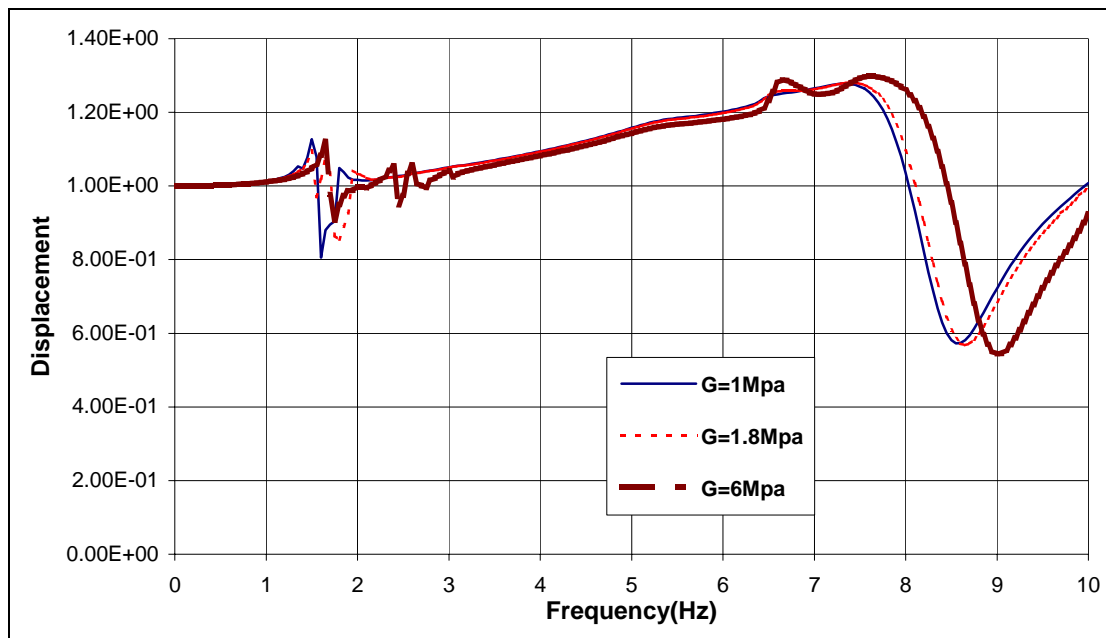
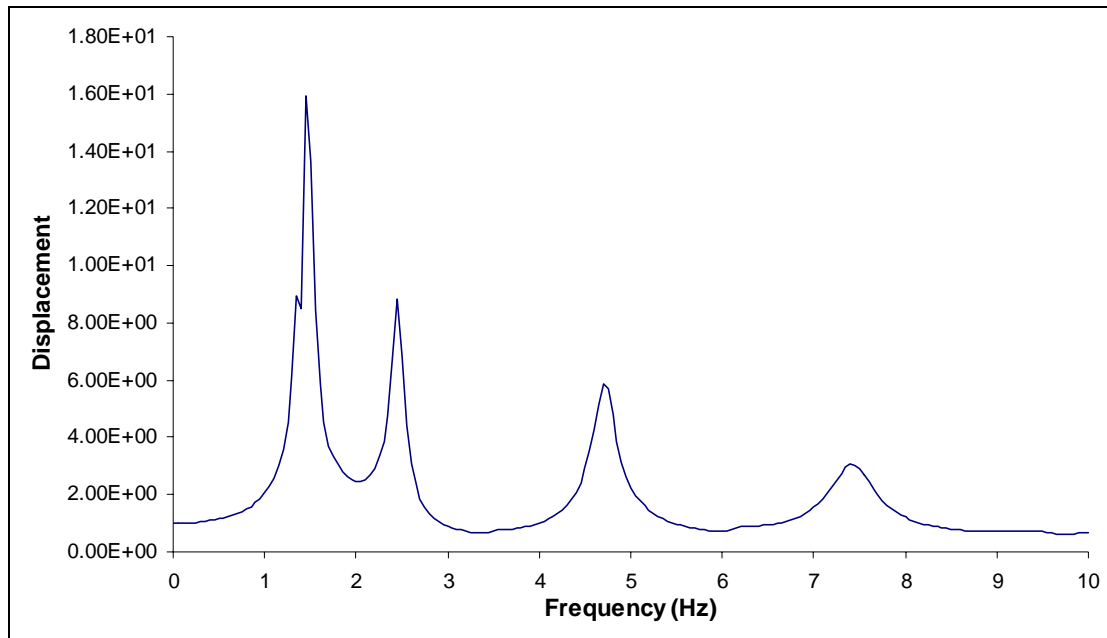


Figure VI. 11 Motion of the Base of Pier 4 When All Foundations Are Excited in the X Direction (Constrained Deck)

6.3.2 Transverse Direction (Y direction)

The effects of the SSI on the frequencies of the peaks of the transfer functions in the transverse direction are summarized in Table VI.2 and illustrated in Figures VI.12 to VI.18. It is somewhat larger than in the longitudinal direction. The reason is that the bending stiffness of the 7 piers is larger transversely than longitudinally.

For the structure without rubber pads, the effect is very clear. The first three significant peaks change from 1.85Hz, 2.70Hz and 4.90Hz to 1.45Hz, 2.45Hz and 4.75Hz. With the introduction of the rubber pads, the effect of soil structure interaction is less pronounced. Table VI.2 shows that the change in the frequency of the peaks for the isolated system is very small for the first peak (about 10% with a free deck and less when the deck is restrained). It is more significant on the motion and peaks of the pier than those of the deck (comparing the fourth peak without SSI and the third peak with SSI). Both for the



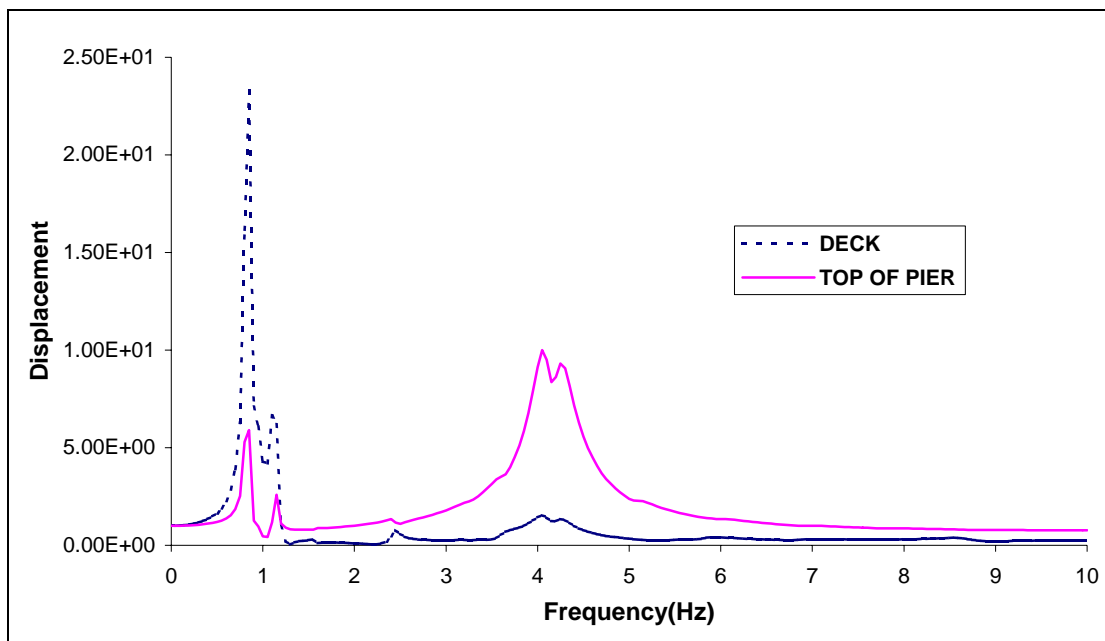
**Figure VI. 12 Displacement in Y Direction at Top of Pier 4
due to Unit Motion at Bottom of All Foundations (without Rubber Pads)**

Table VI. 2 Effect of SSI on Peaks of Transfer Function in Transverse Direction (Hz)

Shear Modulus of Rubber Pads	Without SSI				With SSI			
	1 st Peak	2 nd Peak	3 rd Peak (Deck)	4 th Peak (Pier)	1 st Peak	2 nd Peak	3 rd Peak (Pier)	4 th Peak (Deck)
	No Rubber Pads	1.85	2.70	4.90		1.45	2.45	
6.0Mpa(free deck)	0.90			5.70	0.85	1.12	4.05	
1.8Mpa(free deck)	0.55			5.30	0.50		3.70	
1.0Mpa(free deck)	0.45			5.25	0.40		3.60	
6.0Mpa(constrained deck)	0.90	1.85	4.30	5.70	0.85	1.85	4.05	4.45
1.8Mpa(constrained deck)	0.55	1.75	4.30	5.30	0.55	1.75	3.70	4.30
1.0Mpa(constrained deck)	0.45	1.70	4.30	5.25	0.45	1.70	3.60	4.27

pier and the deck the main interaction effects in the transverse direction occur in the frequency range between 3 and 6Hz, whereas in the longitudinal direction the range was 8 to 11Hz.

From Figures VI.19 & VI.20, it can also be seen that the SSI effect is more prominent in the transverse direction than in the longitudinal direction, because the base motion of pier 4 is amplified or de-amplified more in the transverse than in the longitudinal direction.



**Figure VI. 13 Displacement in Y Direction due to Unit Motion at Base of All Foundations
(with Rubber Pads, $G = 6.0 \times 10^6$ Pa, Free Deck)**

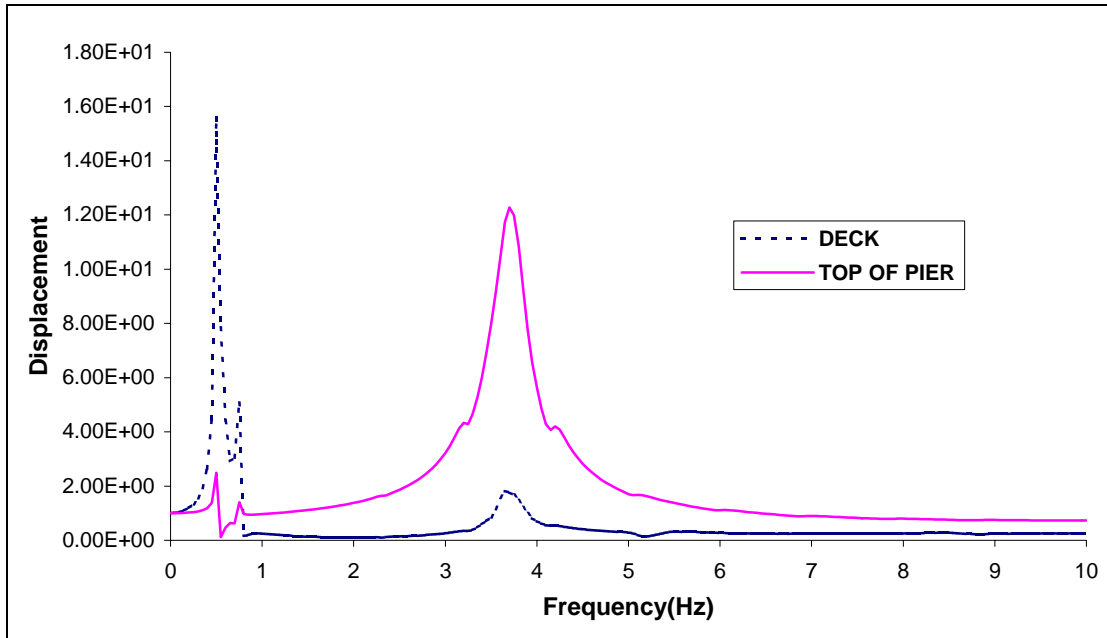


**Figure VI. 14 Displacement in Y Direction due to Unit Motion at Base of All Foundations
(with Rubber Pads, $G = 1.8 \times 10^6$ Pa, Free Deck)**

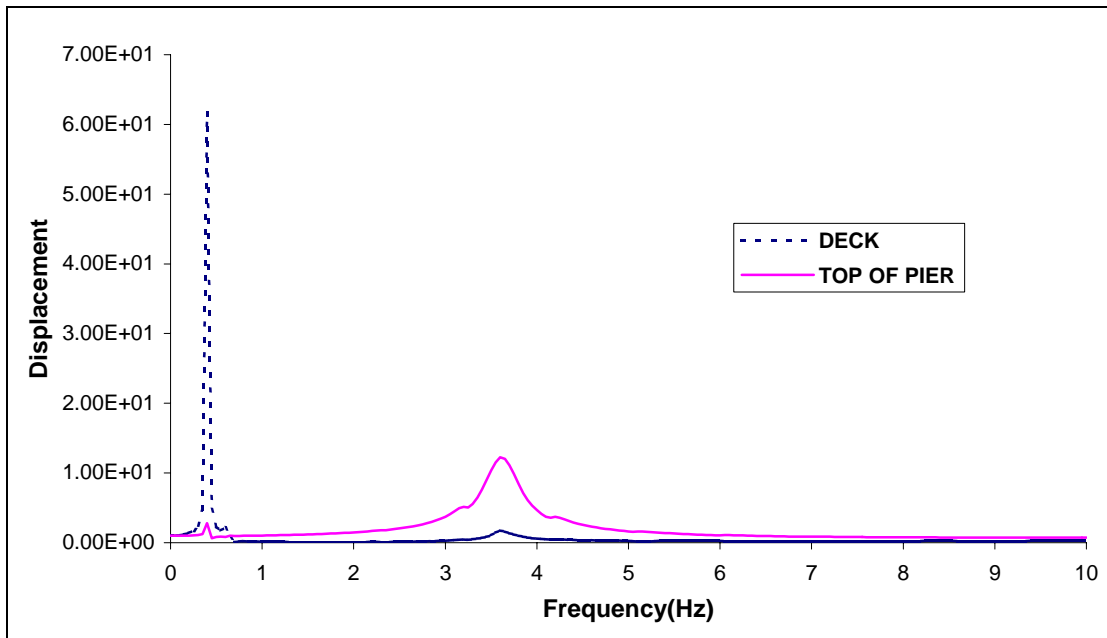


**Figure VI. 15 Displacement in Y Direction due to Unit Motion at Base of All Foundations
(with Rubber Pads, $G = 1.0 \times 10^6$ Pa, Free Deck)**

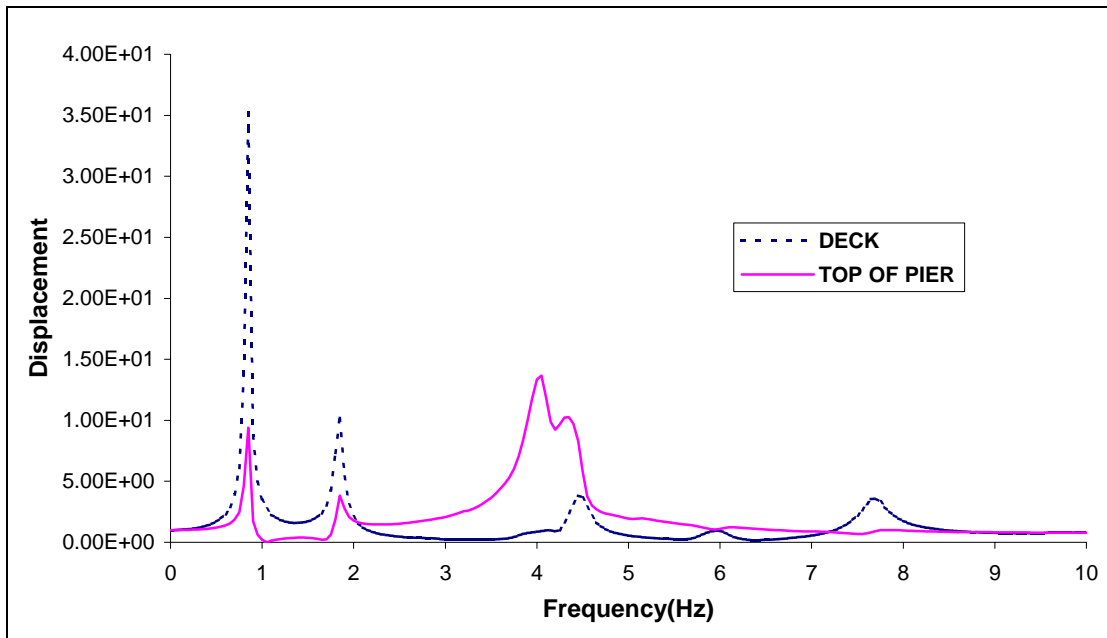


**Figure VI. 16 Displacement in Y Direction due to Unit Motion at Base of All Foundations
(with Rubber Pads, $G = 6.0 \times 10^6$ Pa, Constrained Deck)**

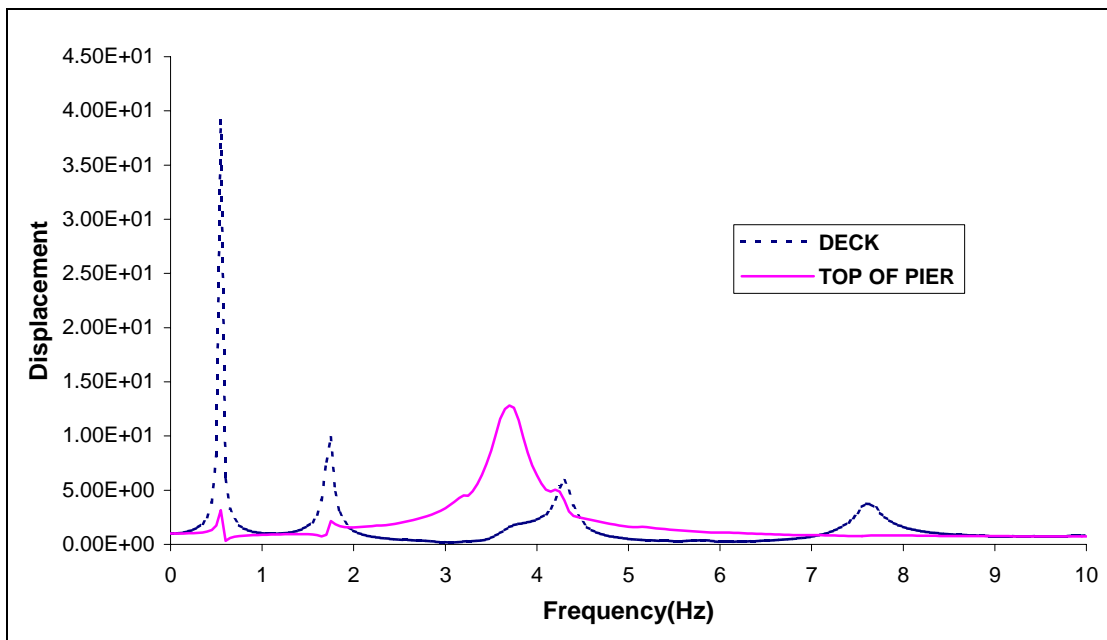


**Figure VI. 17 Displacement in Y Direction due to Unit Motion at Base of All Foundations
(with Rubber Pads, $G = 1.8 \times 10^6$ Pa, Constrained Deck)**

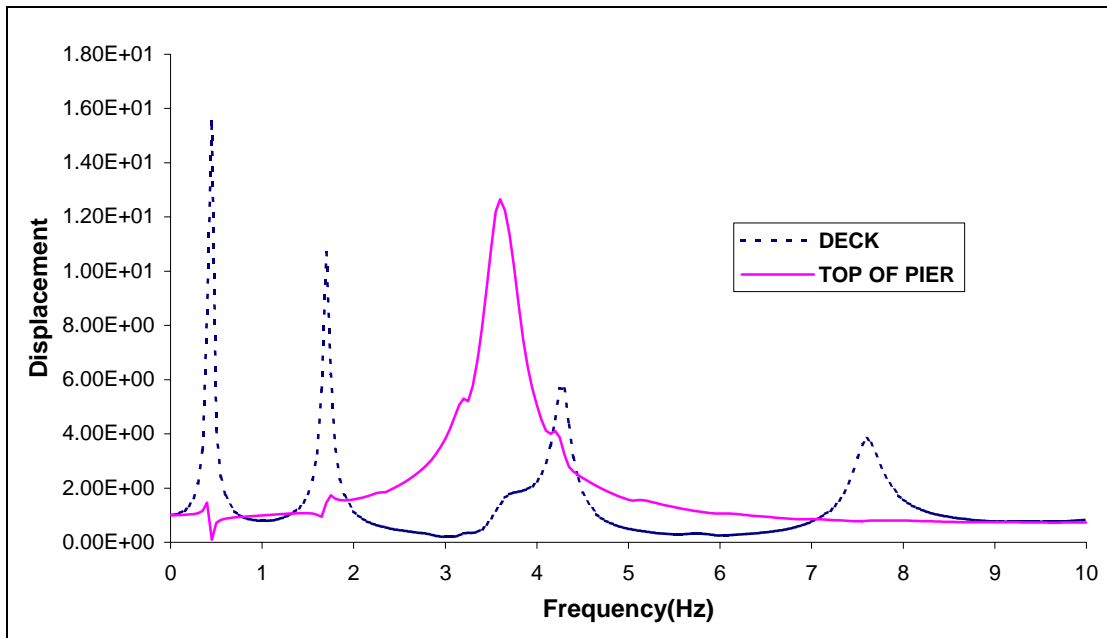


Figure VI. 18 Displacement in Y Direction due to Unit Motion at Base of All Foundations
(with Rubber Pads, $G = 1.0 \times 10^6$ Pa, Constrained Deck)

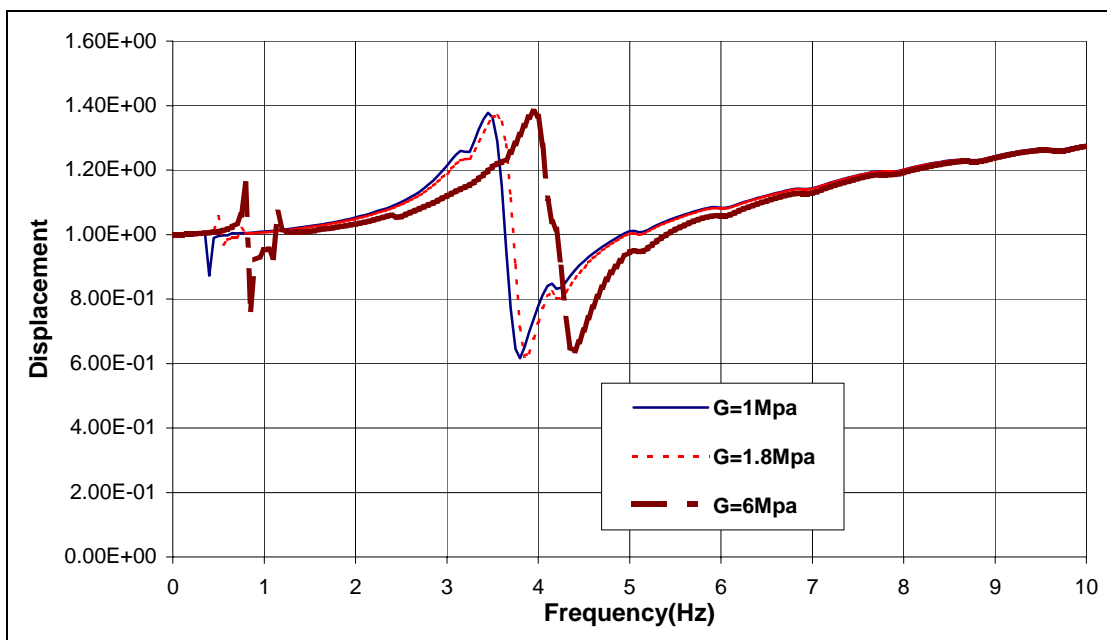


Figure VI. 19 Motion of the Base of Pier 4 When All Foundations Are Excited in the Y Direction
(Free Deck)

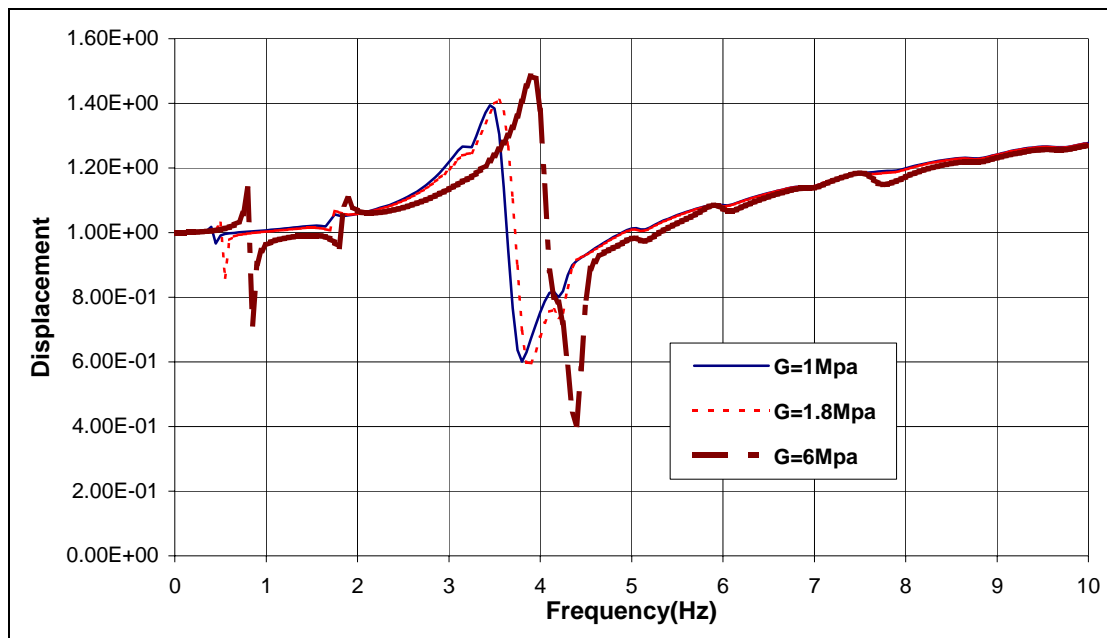


Figure VI. 20 Motion of the Base of Pier 4 When All Foundations Are Excited in the Y Direction (Constrained Deck)

6.3.3 Vertical Direction (Z direction)

As shown in Figures VI.21 to VI.23, the effect of SSI in the vertical direction is still very small. The position of the only significant peak decreases from 3.55Hz to 3.45Hz due to the effect of SSI, and the introduction of the rubber pads has a negligible effect on it. The major effect of SSI is to increase the amplification ratio, an effect very similar to that of the rubber pads. For the case without rubber pads the ratio increases from 1.8 to 2.4 due to SSI. As the Young's modulus of the rubber pads decreases, the effect of SSI becomes smaller.

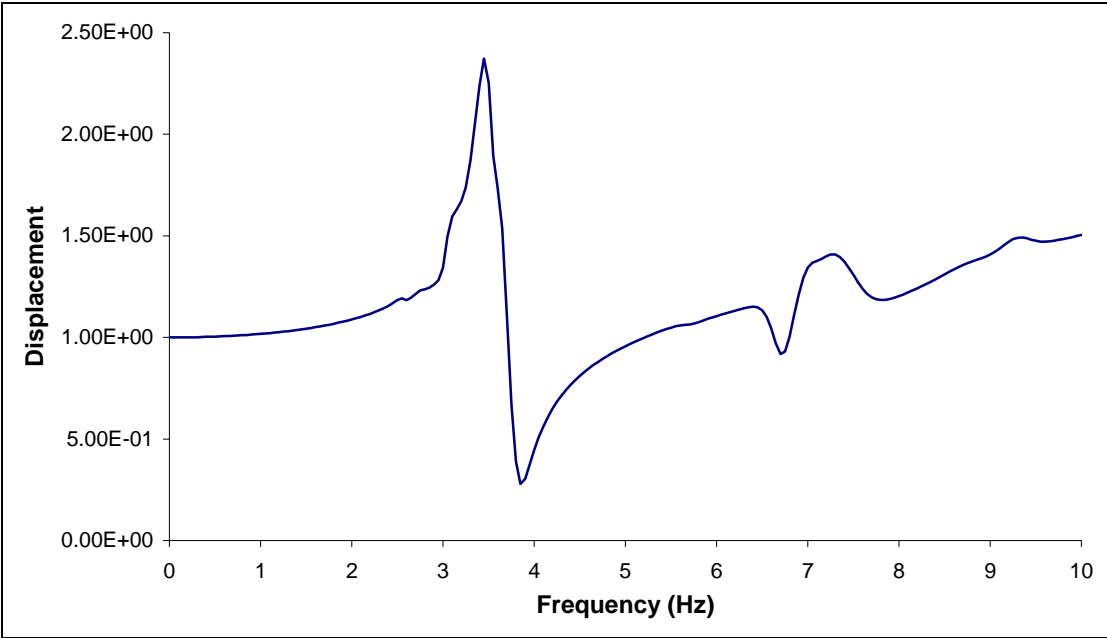


Figure VI. 21 Displacement in Z Direction at Top of Pier 4 due to Unit Motion at Bottom of All Foundations (without Rubber Pads)

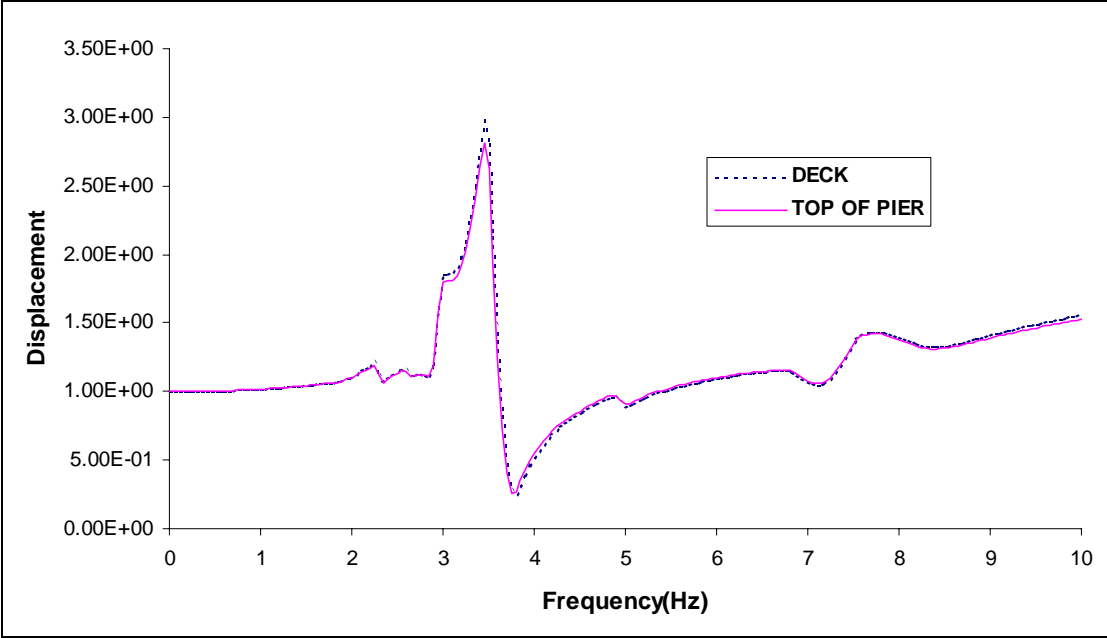
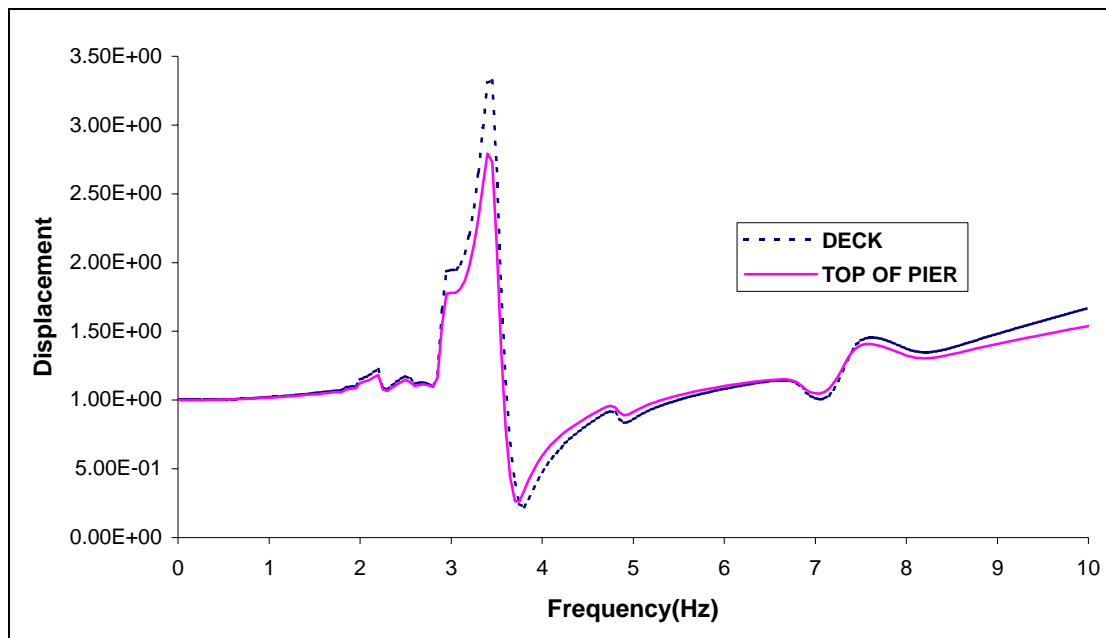


Figure VI. 22 Displacement in Z Direction due to Unit Motion at Base of All Foundations (with Rubber Pads, $E = 6.0 \times 10^9$ Pa, Free Deck)



**Figure VI. 23 Displacement in Z Direction due to Unit Motion at Base of All Foundations
(with Rubber Pads, $E = 1.8 \times 10^9$ Pa, Free Deck)**

6.3.4 Effect of Soil Properties

To study further the potential SSI effects, the soil properties were reduced over the top 12 meters to simulate some nonlinear soil behavior. The foundation stiffness terms were calculated again for this case. The assumed properties and the calculated foundation stiffness were shown in Tables IV.7 ~ IV.10 and Figures IV.23 ~ IV.33. The new foundation stiffness terms with reduced soil shear modulus were discussed in §4.4.

Tables VI.3 & VI.4 show the change of the frequencies of the peaks of the transfer functions due to the new soil profile. The decrease in the frequencies for the structure on the new, softer, soils is larger than that on the original soils, as could be expected but it is still very small in the longitudinal direction and only a little larger in the transverse direction.

Table VI. 3 Effect of SSI on Peaks of Transfer Function in Longitudinal Direction (Hz)
(with New Soil Properties)

Shear Modulus of Rubber Pads	Without SSI			With SSI (New Soil Properties)		
	1 st Peak	2 nd Peak	3 rd Peak	1 st Peak	2 nd Peak	3 rd Peak
No Rubber Pads	2.15	5.85		2.10	5.62	
6.0Mpa(free deck)	0.65	2.75		0.60	2.60	
1.8Mpa(free deck)	0.45	1.95		0.40	1.75	
1.0Mpa(free deck)	0.35	1.70		0.35	1.55	
6.0Mpa(constrained deck)	1.70	2.50	2.85	1.70	2.40	2.60
1.8Mpa(constrained deck)	Between 1.5 and 2.0			Between 1.5 and 2.0		
1.0Mpa(constrained deck)	Between 1.5 and 2.0			Between 1.5 and 2.0		

Table VI. 4 Effect of SSI on Peaks of Transfer Function in Transverse Direction (Hz)
(with New Soil Properties)

Shear Modulus of Rubber Pads	Without SSI				With SSI (New Soil Properties)			
	1 st Peak	2 nd Peak	3 rd Peak (Deck)	4 th Peak (Pier)	1 st Peak	2 nd Peak	3 rd Peak (Pier)	4 th Peak (Deck)
No Rubber Pads	1.85	2.70	4.90		1.30	2.35		4.60
6.0Mpa(free deck)	0.90			5.70	0.80	1.10	3.85	
1.8Mpa(free deck)	0.55			5.30	0.50		3.40	
1.0Mpa(free deck)	0.45			5.25	0.40		3.35	
6.0Mpa(constrained deck)	0.90	1.85	4.30	5.70	0.80	1.80	3.85	4.30
1.8Mpa(constrained deck)	0.55	1.75	4.30	5.30	0.55	1.75	3.40	4.30
1.0Mpa(constrained deck)	0.45	1.70	4.30	5.25	0.45	1.70	3.35	4.27

6.4 Conclusions

- 1) Generally, soil structure interaction (SSI) changes the frequencies of the peaks of the transfer functions. The effects of SSI on the first natural frequencies are very small for the conditions of the Marga-Marga bridge. These conclusions had also been reached by V.M. Daza in his work. They are somewhat larger in the transverse than in the longitudinal direction;
- 2) For the structure without rubber pads, the effect of soil structure interaction is more pronounced. The frequencies of the peaks of the transfer functions decrease clearly;
- 3) For the structure with rubber pads, SSI has some small effects on the motion at the top of the pier, but since the deck has been isolated by rubber pads, the motions of the deck are affected much less;
- 4) The main SSI effects are in the range of frequencies between 3.0 and 5.0 Hz in the transverse direction and above 8.0Hz in the longitudinal direction.

CHAPTER VII

CONCLUSIONS AND RECOMMENDATIONS

7.1 General Observations

The studies carried out and described in Chapters V and VI indicate that:

- 1) The presence of the isolation pads reduces considerably the amplitude of the longitudinal deck motions with respect to those at top of the pier except at the first natural frequency of the system, which varies from 0.35Hz to 1.7Hz depending on the assumed conditions at the ends of the deck (free deck or constrained deck). At this frequency the motion of the deck seems to be larger than that of the top of the pier for a free deck (the frequency is that of the deck vibrating as a free body on top of the rubber pads). For a constrained deck, the amplitude of the motion of the deck is much smaller than that of the pier for the smaller values of the assumed shear modulus (as the level of excitation and therefore the level of deformation of the rubber pads increase). The only other exception is at around 6.5Hz when the deck is constrained and the same motion is applied at the base of all the piers.

Comparing the transfer functions for the motion of the deck in Figures VI.2 ~ VI.9 with that for the case without rubber pads (Figure VI.1) one can reach the same conclusion. The inclusion of the rubber pads will reduce the motions of the deck over most ranges of frequencies (except for the fundamental frequency).

If the energy of the earthquake is not around the fundamental frequency of the deck (Chilean earthquakes tend to have predominant frequencies of 3.0Hz to 4.0Hz) the effect of the rubber pads on the seismic motions of the deck in the longitudinal direction will be very beneficial. Comparing on the other hand the

transfer functions of the motion on the top of pier 4 with and without rubber pads (same figures) it can be seen that the main effect is in the change in the natural frequencies but there is no longer a reduction over most of the frequency range: the amplitudes decrease at the frequencies of the structure without rubber pads and increase instead at the frequencies (more than one) of the structure with rubber pads;

- 2) The effect of the rubber pads on the motion of the deck in the transverse direction is less pronounced than in the longitudinal direction. While there are important reductions in amplitude with respect to the top of the pier or with respect to the deck without rubber pads, there are now several frequency ranges over which the motion of the deck may be larger than that of the pier (several peaks associated with the motion of the deck);
- 3) Comparing the motion at the top of the pier without rubber pads with that with rubber pads, one can conclude that the presence of the rubber pads increases the amplitude of the transfer functions around the first vertical natural frequency (about 3.3Hz for the Marga-Marga bridge). Over the other frequency ranges, the value of the transfer functions is almost 1. Around the first vertical natural frequency, the amplitude of the motion at the deck with rubber pads is always larger than that at the top of the pier.

7.2 Data from a Real Earthquake

Figures VII.1, VII.2 and VII.3 show the Power spectra (square of the amplitude Fourier spectra of the motions) recorded on the Marga-Marga bridge in the longitudinal, transverse and vertical directions under an earthquake that occurred on July 24, 2001. In these three figures, the motion at the free field (on rock at the left of the left abutment) is shown at the upper-left corner, the motion at the bottom of pier 4 at the upper-right

corner, the motion at the top of pier 4 at the lower-left corner, and the motion on top of the deck at the lower-right corner.

These experimental data show:

- 1) In the longitudinal direction:
 - a) A considerable reduction in the motion above 3.0Hz at the three locations (compared to the free field);
 - b) A significant peak at about 1.5Hz in the base motion of the pier, which is considerably reduced on top of the pier and on the deck (square of the amplitude is 1.5×10^8 at the base, 2.0×10^7 at the top of the pier and 6.0×10^6 on the deck. (a reduction in amplitude by factors of $\sqrt{7.5} = 2.74$ at the top of the pier and $\sqrt{25} = 5.0$ on the deck);
 - c) A significant amplification at about 2.7Hz on top of the pier, which is not present on the deck. (amplification ratio of the amplitude is about $\sqrt{(4 \times 10^8)/(4 \times 10^7)} \approx 3.2$ from the base to the top of the pier). The amplitude at the base of the pier at this frequency was slightly smaller than in the free field;

The first natural frequency in shear of the soil deposit itself is about 1.4Hz from the analysis in Chapter IV, which explains the peak at about 1.5Hz in the base motion of the pier. As for the amplification at 2.7Hz, one can find from Figures VI.2 or VI.3 that this is a natural frequency of the structure and the motion at the top of pier 4 is amplified very much while the motion of the deck is not. The analysis conducted cannot explain, on the other hand, the large reductions in motion above 3Hz.

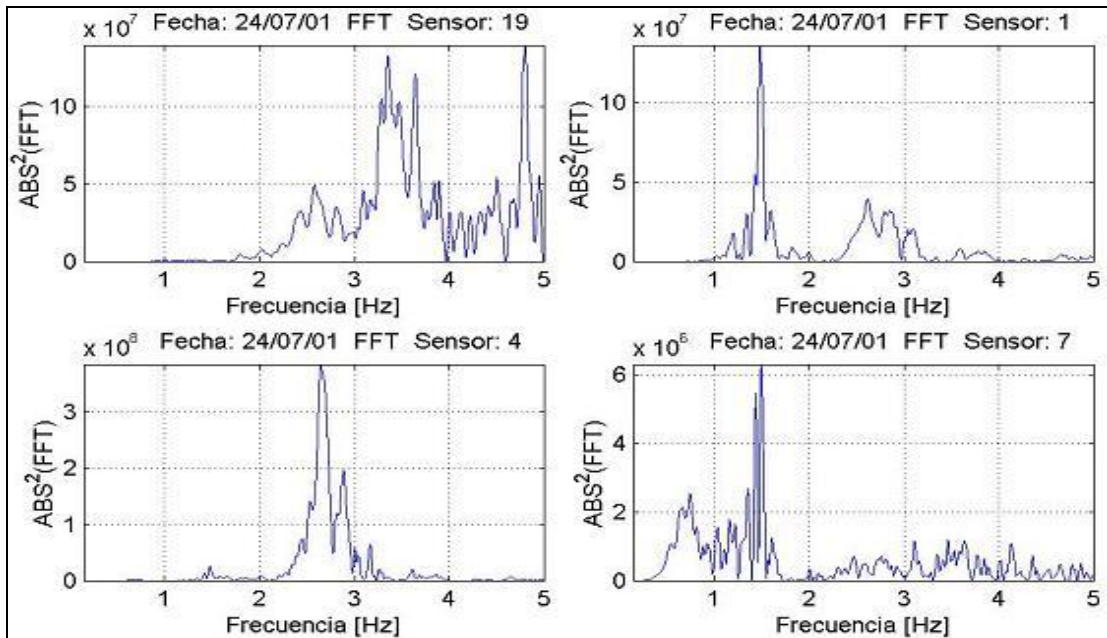


Figure VII. 1 FFT of Recorded Longitudinal (X) Motion of Marga-Marga Bridge during the Earthquake of July 24, 2001

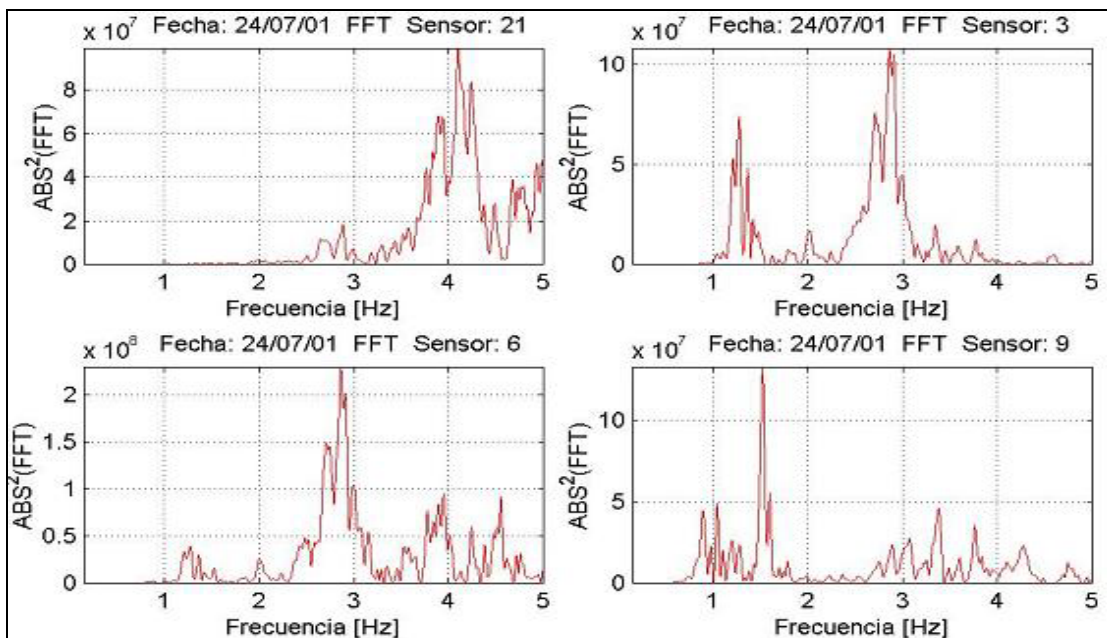


Figure VII. 2 FFT of Recorded Transverse (Y) Motion of Marga-Marga Bridge during the Earthquake of July 24, 2001

- 2) In the transverse direction,
- a) A considerable reduction in the motion above 3.5Hz (especially around 4.0Hz) at the base of the pier and on the deck (compared to the free field). On the top of the pier the amplitude of motion around 4Hz is similar to that in the free field;
 - b) A peak at about 1.3Hz at the base of the pier with an amplitude squared of 7.5×10^7 . It is only 4.0×10^7 at the top of the pier and 2.0×10^7 on the deck, a reduction in amplitude by factors of $\sqrt{7.5/4.0} \approx 1.37$ at the top of the pier and $\sqrt{7.5/2.5} \approx 1.73$ on the deck;
 - c) A number of small peaks around 1.0Hz and a more significant peak at 1.5Hz on the deck motions with an amplitude squared of 1.5×10^8 . This peak is not present on the motion on top of the pier;
 - d) A peak at the base and on top of the pier at about 2.8~2.9Hz, with amplification ratios with respect to the motion at the free field of $\sqrt{11/2} \approx 2.35$ (for the base of the pier) and $\sqrt{22/2} \approx 3.32$ (for the top of the pier), while the motion is greatly de-amplified on the deck.

The reduction in the motions between 3.5 and 4.5Hz at the base of the pier is consistent with the reported SSI effect in the transverse direction, but the reduction above 4.5Hz is not explained by this research. The peak in the base motion at 1.3Hz is also very close to the shear natural frequency of the soil deposit calculated in Chapter IV (1.4Hz). For the case with a constrained deck, Figures VI.16 ~ VI.18 show that the structure has a natural frequency at about 1.7~1.85Hz, where the motion of the deck is greatly amplified (not too far from the 1.5Hz of the data). From Figure VII.4, which shows the transfer function for one-dimensional soil amplification, one can find that around 2.8~2.9Hz the

amplification ratio of the motion from the outcrop of rock to the free surface is about 2.2. As one can find from Figures VI.13 ~ VI.20, the amplification ratio at this frequency from the free surface to the bottom of the pier is about 1.1, to the top of the pier 2.0 to 2.5 and to the deck 0.25 to 0.35, depending on the shear modulus of the rubber pads. So the amplification from rock outcrop to the base of the pier is about 2.4 to 2.7, to the top of the pier about 4.0 and to the deck about 0.55. While these figures do not coincide exactly with those reported from the experimental data, they follow the same general trend. It should be noticed that the amplification values will depend on the assumed values of damping.

- 3) In the vertical direction,
 - a) These are peaks in the free field motion at 4.0Hz and 4.8Hz. These two peaks have a very similar amplitude in the motions recorded at the base and on top of the pier but are amplified on the deck by factors of $\sqrt{6/1.5} \approx 2.0$ (for 4.0Hz) or $\sqrt{9/3.5} \approx 1.6$ (for 4.8Hz);
 - b) A peak at about 2.6Hz at the base, the top of pier and the deck with an amplitude square of 1.5×10^7 .

The soil deposit has a dilatational natural frequency of about 2.4Hz as stated in Chapter IV. The amplitude of the transfer functions at this frequency is nearly equal at all three locations in the bridge, as shown in Figures VI.22 & VI.23. The amplification in the motion of the deck at 4Hz and 4.8Hz cannot be explained in the studies conducted.

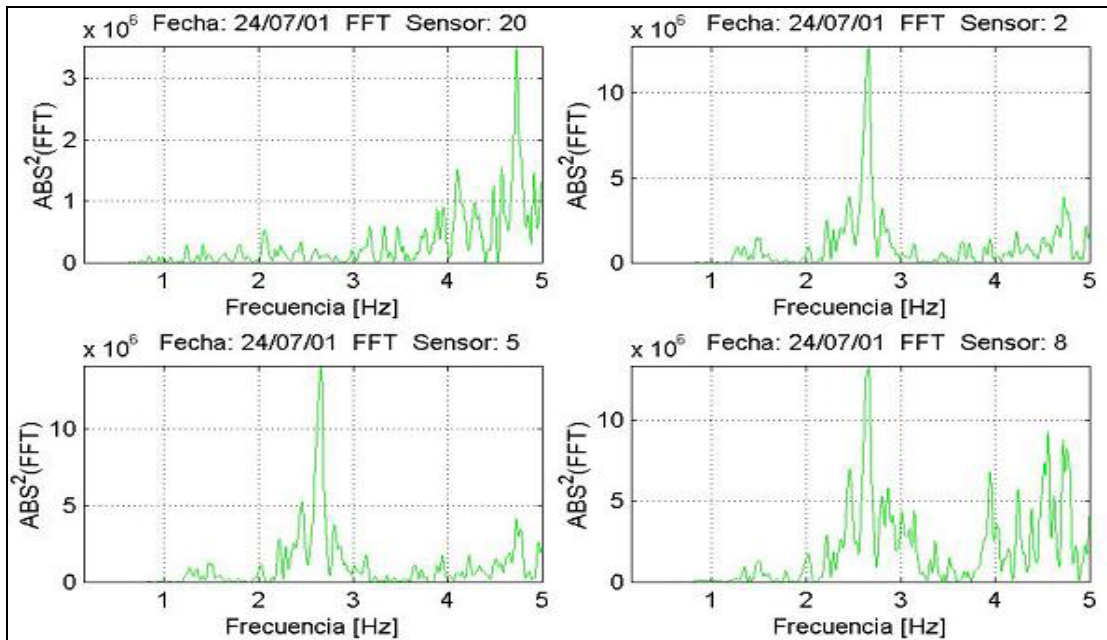


Figure VII. 3 FFT of Recorded Vertical (Z) Motion of Marga-Marga Bridge during the Earthquake of July 24, 2001

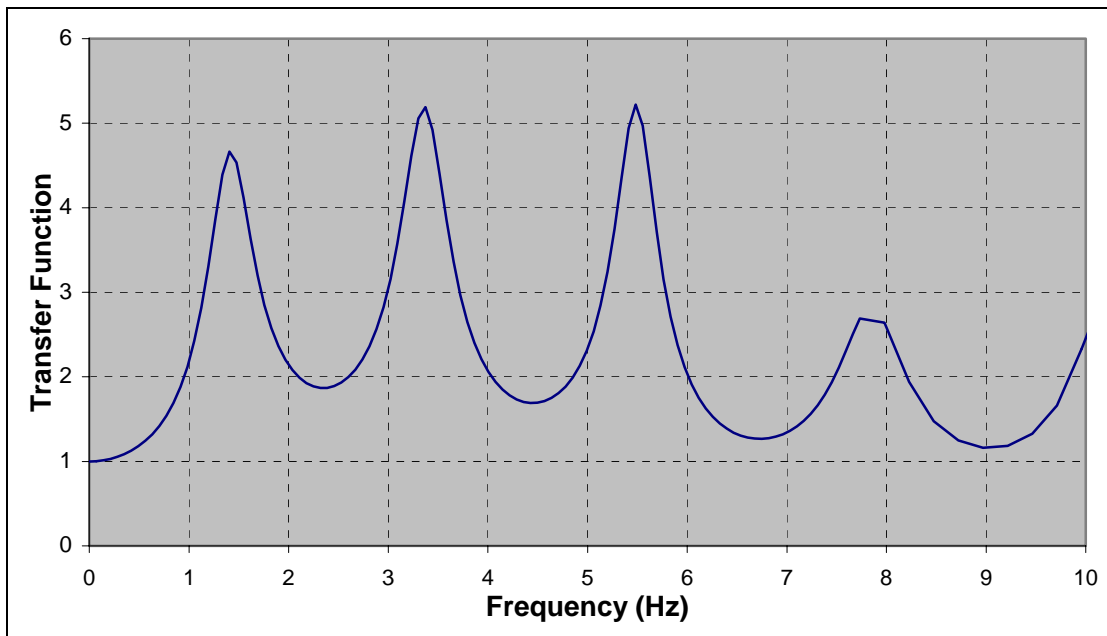


Figure VII. 4 One-dimensional Horizontal Soil Amplification of the Soil Deposit

7.3 Recommendation for Future Studies

- 1) Nonlinear one-dimensional or two dimensional soil amplification analyses in the time domain may be needed to give a better estimate of the natural frequencies of the soil deposit and soil amplification effects;
- 2) Because the amplification ratio depends strongly on the damping, iterations may be needed in a linearized analysis of the complete soil-structure-rubber pads system to get better estimates of the effective hysteretic damping and shear modulus;
- 3) The transfer functions are sensitive to the modeling of the rubber pads, which means that more realistic, nonlinear models of the rubber pads and time domain nonlinear analyses would improve the prediction of the structural response;
- 4) The transfer functions can change substantially if the motions at the base of the various piers are different. In this study it was assumed in most cases that all supports had the same motion although the program allowed to consider and combine different motions. One would need however more information on the potential variations in the motions of the supports.

REFERENCES

- Banerjee, J. R. and William, F. W. (1985). "Exact Bernoulli-Euler dynamic stiffness matrix for a range of tapered beams." *International Journal for Numerical Methods in Engineering*, 21, 2289-2302.
- Banerjee, J. R. and William, F. W. (1994a). "An exact dynamic stiffness matrix for coupled extentional-torsional vibration of structural members." *Computers and Structures*, 50, 161-166.
- Banerjee, J. R. and William, F. W. (1994b). "Coupled bending-torsional dynamic stiffness matrix for an axially loaded Timoshenko beam element." *International Journal of Solids and Structures*, 31, 749-762.
- Betti, R. (1995). "Dynamic soil-bridge interaction." *Proceedings of Engineering Mechanics*, 1, 82-85.
- Billings, L. J. (1993). "Finite element modeling of elastomeric seismic isolation bearings." Ph.D. Dissertation, University of California, Irvine, California.
- Carrubba, P., Massimino, M. R. and Maugeri, M. (2003). "Soil nonlinear stiffnesses for SSI involving embedded foundations." *Computational Engineering*, 4, 53-62.
- Casas, J.R. (1997). "Horizontal bridge-soil interaction assessment by dynamic testing." *Experimental Mechanics*, 37(1), 69-77.
- Chang C. H. (2002). "Modeling of laminated rubber bearings using an analytical stiffness matrix." *International Journal of Solids and Structures* 39, 6055-6078.
- Chaudhary, M.T.A., Abe, M. and Fujino, Y. (2001a). "Identification of soil-structure interaction effect in base-isolated bridges from earthquake records." *Soil Dynamics and Earthquake Engineering*, 21(8), 713-725.
- Chaudhary, M.T.A., Abe, M. and Fujino, Y. (2001b). "Performance evaluation of base-isolated Yama-age bridge with high damping rubber bearings using recorded seismic data." *Engineering Structures*, 23(8), 902-910.
- Chaudhary, M. T. A., Abe, M. and Fujino, Y. (2002a). "Investigation of atypical seismic response of a base-isolated bridge." *Engineering Structures*, 24(7), 945-953.

- Chaudhary, M.T.A., Abe, M. and Fujino, Y. (2002b). "Role of structural details in altering the expected seismic response of base-isolated bridges." *Mechanical Systems and Signal Processing*, 16(2-3), 413-428.
- Chaudhary, M. T. A., Abe, M., Fujino, Y. and Yoshida, J. (2000). "System identification of two base-isolated bridges using seismic records." *Journal of Structural Engineering*, 126(10), 1187-1195.
- Chaudhry, M. S. and Prakash, S. (1998). "Dynamic soil structure interaction for bridge abutments on piles." *Geotechnical Special Publication*, 2, 1247-1258.
- Chen, Y. H. and Sheu, J. T. (1993). "Axial loaded damped Timoshenko beam on viscoelastic foundation." *International Journal for Numerical Methods in Engineering*, 36, 1013-1027.
- Chen, Y.-H. and Sheu, J.-T. (1996). "Beam length and dynamic stiffness." *International Computer Methods in Applied Mechanics and Engineering*, 129, 311-318.
- Consolazio, G. R., Lehr, G. B. and McVay, M. C. (2003). "Dynamic finite element analysis of vessel-pier-soil interaction during barge impact events." *Transportation Research Record*, 1849(03-3230), 81-90.
- Crouse, C. B. and Price, T. (1993). "Dynamic soil-foundation interaction at the Meloland Road overcrossing." *Engineering in Natural Hazards Mitigation*, 355-360.
- Crouse, C. B., Hushmand, B. and Martin, G. R. (1987). "Dynamic soil structure interaction of a single-span bridge." *Earthquake Engineering & Structural Dynamics*, 15(6), 711-729.
- Crouse, C.B. and McGuire, J. (2001). "Energy dissipation in soil-structure interaction." *Earthquake Spectra*, 17(2), 235-259.
- Daza, V. M. (2003). "Interaccion sismica suelo-estructura en el Puente Marga-Marga." Engineering Thesis, Civil Engineering Department, University of Chile, Santiago, Chile.
- Dendrou, B., Werner, S. and Toridis, T. (1984). "Three-dimensional response of a concrete bridge system to traveling seismic waves." *Computers and Structures*, 20(1-3), 593-6.

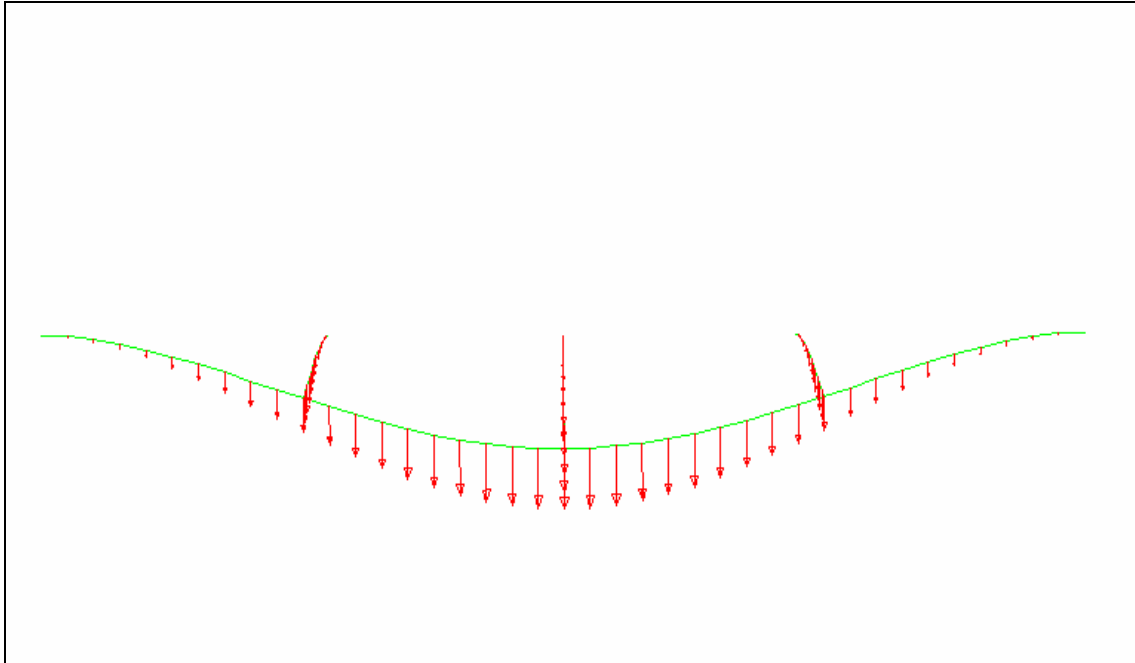
- Doyle, J. F. (1989a). *Wave propagation in structures – an FFT-based spectral analysis methodology*, Springer, Verlag, New York.
- Doyle, J. F. (1989b). *Wave propagation in structures – spectral analysis using fast discrete fourier transform*, 2nd Ed. Springer, Verlag, New York.
- Elsabee F. and Morray J. P. (1977). “Dynamic behavior of embedded foundations.” *Research Report R77-33*, Department of Civil Engineering, MIT, Cambridge, Massachusetts.
- Gomez R. (1982). “Rigideces dinamicas de grupos de pilotes.” Tesis de Doctorado Presentada en la Universidad Autonoma de Mexico, Mexico City.
- Gopalakrishnan, S. and Doyle, J. F. (1994). “Wave propagation in connected waveguides of varying cross-section.” *Journal of Sound and Vibration*, 175, 374-363.
- Guin, J. and Banerjee, P.K. (1998). “Coupled soil-pile-structure interaction analysis under seismic excitation.” *Journal of Structural Engineering*, 124(4), 434-444.
- Harada, T., Yamashita, N. and Sakanashi, K. (1994). “Theoretical study on fundamental period and damping ratio of bridge pier-foundation system.” *Doboku Gakkai Rombun-Hokokushu/Proceedings of the Japan Society of Civil Engineers*, 489(1-27), 227-234.
- Haringx J. A. (1949). “On highly compressible helical springs and rubber rods, and their application for vibration-free mountings.” *III. Philips Research Reports 4*, 206–220.
- Hino, K. and Tanabe, T. A. (1986). “Nonlinear dynamic response analysis of RC structures on the ground with infinite boundaries.” *Transactions of the Japan Concrete Institute*, 8, 443-450.
- Hutchinson, T.C., Chai, Y.H., Boulanger, R.W. and Idriss, I.M. (2004). “Inelastic seismic response of extended pile-shaft-supported bridge structures.” *Earthquake Spectra*, 20(4), 1057-1080.
- Iwasaki, T., Kawashima, K., Takagi, Y. and Aizawa, K. (1984). “Dynamic soil-structure interaction analysis of Kaihoku Bridge.” *Transactions of the Japan Society of Civil Engineers*, 14, 67-68.

- Kaito, K., Abe, M, Fujino, Y and Chaudhary, M. T. A. (1999). "Performance evaluation of a base-isolated bridge using complex modal analysis." *Proceedings of the International Modal Analysis Conference - IMAC*, 2, 1749-1755.
- Kausel E. (1974). "Forced vibrations of circular foundations on layered media." *Research Report R74-11*, Department of Civil Engineering, MIT, Cambridge, Massachusetts.
- Kolousěk, V. (1973). *Dynamics in engineering structures*, Butterworth, London.
- Kuribaya, E. and Iida, Y. (1974). "Application of finite element method to soil-foundation interaction analysis." *Radio Engineering and Electronic Physics*, 151-158.
- Latona, R. W. (1969). "Analysis of building frames for natural frequencies and natural mode shapes." Inter American Program, Civil Engineering Department, MIT, Cambridge, Massachusetts.
- Lee, L. J. and Dasgupta, G. (1984). "Finite element formulation of nonlinear structure-soil interacting system for seismic response analysis." *American Society of Mechanical Engineers, Pressure Vessels and Piping Division (Publication) PVP*, 80, 133-146.
- Levine, M. B. and Scott, R. F. (1989). "Dynamic response verification of simplified bridge-foundation model." *Journal of Geotechnical Engineering*, 115(2), 246-260.
- Makris, N., Badoni, D., Delis, E. and Gazetas, G. (1994). "Prediction of observed bridge response with soil-pile-structure interaction." *Journal of Structural Engineering*, 120(10), 2992-3011.
- Makris, N., Gazetas, G. and Delis, E. (1996). "Dynamic soil-pile-foundation-structure interaction: Records and predictions." *Geotechnique*, 46(1), 33-50.
- Matsuda, A. (1999). "Three-dimensional finite element analysis of laminated rubber bearings using the selective integration method." *JSME Int. J., Ser. A*, 42(1), 40-48.

- Matsuda, A. (2001). "Evaluation for mechanical properties of laminated rubber bearings using nonlinear finite element analysis with hyperelasticity." Ph.D. Dissertation, Tsukuba University, Japan.
- McGuire, J. W., Cannon, I. B. S., Cofer, W. F. and McLean, D. I. (1998). "Seismic evaluation of pile-founded highway bridge on saturated peat." *Journal of Structural Engineering*, 124(1), 71-79.
- Mylonakis, G., Nikolaou, A. and Gazetas, G. (1997). "Soil-pile-bridge seismic interaction: kinematic and inertial effects. Part I: soft soil." *Earthquake Engineering & Structural Dynamics*, 26(3), 337-359.
- Papaleontiou, C. G. (1992). "Dynamic analysis of building structures under combined horizontal and vertical vibrations." Ph.D. Dissertation, University of Texas, Austin, Texas.
- Park, K. S., Jung, H. J. and Lee, I. W. (2002). "A comparative study on seismic performances of base isolation systems for multi-span continuous bridge." *Engineering Structures*, 24(8), 1001-1013.
- Poulos H. G. (1971). "Behavior of laterally loaded piles II-piles groups." *Journal of the Soil Mechanics and Foundations Division, ASCE*, 97(5), 733-751.
- Romo, D. (1999). "Análisis de registros sísmicos y microambientales en el Puente Marga-Marga." Engineering Thesis Civil Engineering Department, University of Chile, Santiago, Chile.
- Saadeghvaziri, M. A., Yazdani-Motlagh, A. R. and Rashidi, S. (2000). "Effects of soil-structure interaction on longitudinal seismic response of MSSS bridges." *Soil Dynamics and Earthquake Engineering*, 20(1-4), 231-242.
- Segovia, M. E. (1997). (reference of Daza V. M. (2003)).
- Seki, W., Fukahori, Y., Iseda, Y. and Matsunaga, T. (1987). "A large deformation finite element analysis for multilayer elastomeric bearings." *Transaction of the Meeting of the Rubber Division*, 856-870.

- Shinozuka, M., Chung, H. C., Ichitsubo, M. and Liang, J. (2001). "System identification by video image processing." *Proceedings of SPIE - The International Society for Optical Engineering*, 4330, 97-107.
- Skinner, R. I., Robinson, H. W. and McVerry, H. C. (1993). *An introduction to seismic isolation*, Wiley, Chichester, England.
- Spyrakos, C. C. (1990). "Assessment of SSI on the longitudinal seismic response of short span bridges." *Engineering Structures*, 12(1), 60-66.
- Spyrakos, C. C. and Loannidis, G. (2003). "Seismic behavior of a post-tensioned integral bridge including soil-structure interaction (SSI)." *Soil Dynamics and Earthquake Engineering*, 23(1), 53-63.
- Su L., Ahmadi G. and Tadjbakhsh I. G. (1989). "A comparative study of performances of various base isolation systems, part I: shear beam structures." *Earthquake Engineering and Structural Dynamics*, 18, 11-32.
- Su L., Ahmadi G. and Tadjbakhsh I. G. (1990). "A comparative study of performances of various base isolation systems, Part II: Sensitivity analysis." *Earthquake Engineering and Structural Dynamics*, 19, 21-33.
- Takayama, M., Tada, H. and Tanaka, R. (1990). "Finite element analysis of laminated rubber bearing used in base-isolation system." *Transaction of the Meeting of the Rubber Division*, American Chemical Society, Washington, D.C., 46-62.
- Takemiya, H. (1985). "Seismic analysis and design of multi-span continuous high-pier bridges with emphasis on soil-structure interaction." *Transactions of the Japan Society of Civil Engineers*, 15, 553-556.
- Takemiya, H. and Yamada, Y. (1981). "Layered soil-pile-structure dynamic interaction." *Earthquake Engineering & Structural Dynamics*, 9(5), 437-457.
- Tan, R.Y. and Cheng, W.M. (1993). "System identification of a non-classically damped linear system" *Computers and Structures*, 46(1), 67-75.
- Tan, R.Y. and Huang, M.C. (2000). "System identification of a bridge with lead-rubber bearings." *Computers and Structures*, 74(3), 267-280.

- Tan, R.Y. and Weng, I.W. (1996). "Identification of dynamic properties of isolated structures." *Engineering Structures*, 18(3), 240-246.
- Tongaonkar, N. P. and Jangid, R. S. (2003). "Seismic response of isolated bridges with soil-structure interaction." *Dynamics and Earthquake Engineering*, 23(4), 287-302.
- Wolf, J. P. (1988). *Soil-structure-interaction analysis in time domain*, Prentice Hall, Englewood Cliffs, New Jersey.
- Yamada, Y. and Kawano, K. (1979). "Efficiency of the FEM in the analysis of dynamic soil structure interaction." *Proceedings of the Technical Program, INTERNEPCON: International Electronic Packaging and Production Conferences*, 541-551.
- Yu, C. P. (1995). "Determination of pile lengths using flexural waves." *Report GR95-3*, Geotechnical Engineering Center, Civil Engineering Department, University of Texas, Austin, Texas.
- Yu, C. P. (1996). "Effect of vertical earthquake components on bridge response." Ph.D. Dissertation, University of Texas, Austin, Texas.
- Yu, C. P. and Roësset, J. M. (1998). "Dynamic analysis of structures using continuous solutions in frequency domain." *Proceedings of EASEC-6 Conference on Structural Engineering & Construction*, Taipei, Taiwan, 2, 1369-1375.
- Yu C. P. and Roësset J. M. (2001). "Dynamic stiffness matrix for linear members with distributed mass." *Tamkang Journal of Science and Engineering*, 4(4), 253-263.
- Zechlin, E. T. and Chai, J. (1998). "Nonlinear dynamic analysis of large diameter pile foundations for the Bay Bridge." *Geotechnical Special Publication*, 2, 1223-1234.
- Zheng, J. Z. and Takeda, T. (1995). "Effects of soil-structure interaction on seismic response of PC cable-stayed bridge." *Soil Dynamics and Earthquake Engineering*, 14(6), 427-43.

APPENDIX**MODE SHAPES OF THE BRIDGE IN FIGURE II.5****Figure A.1 The 1st Mode Shape of the Bridge in Figure II.5**

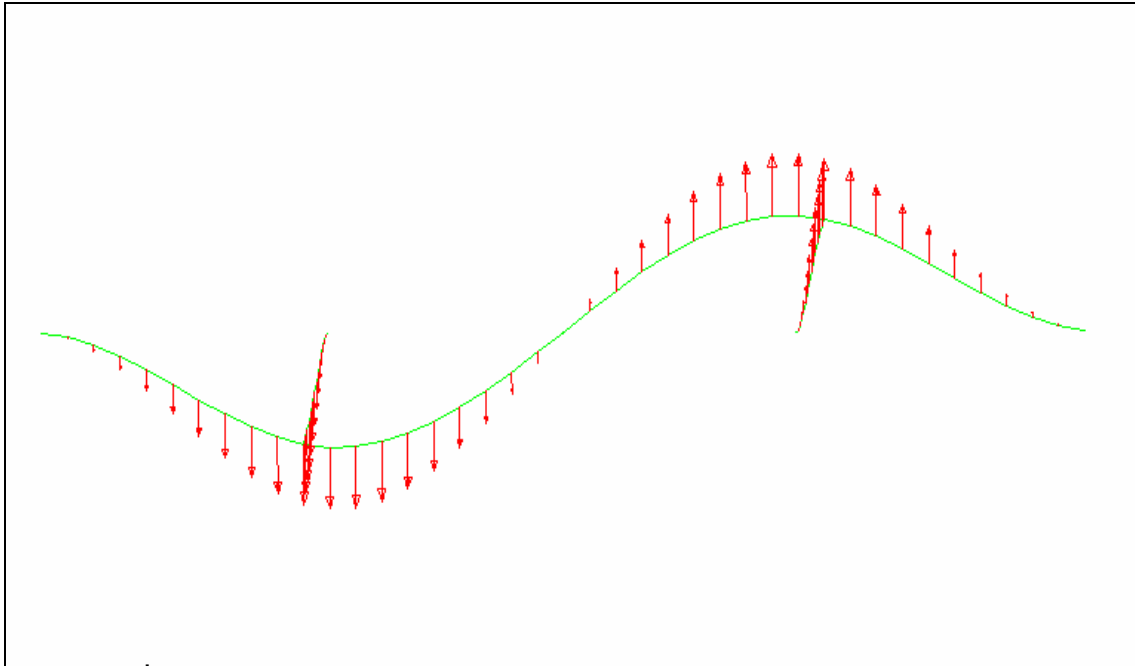


Figure A.2 The 2nd Mode Shape of the Bridge in Figure II.5

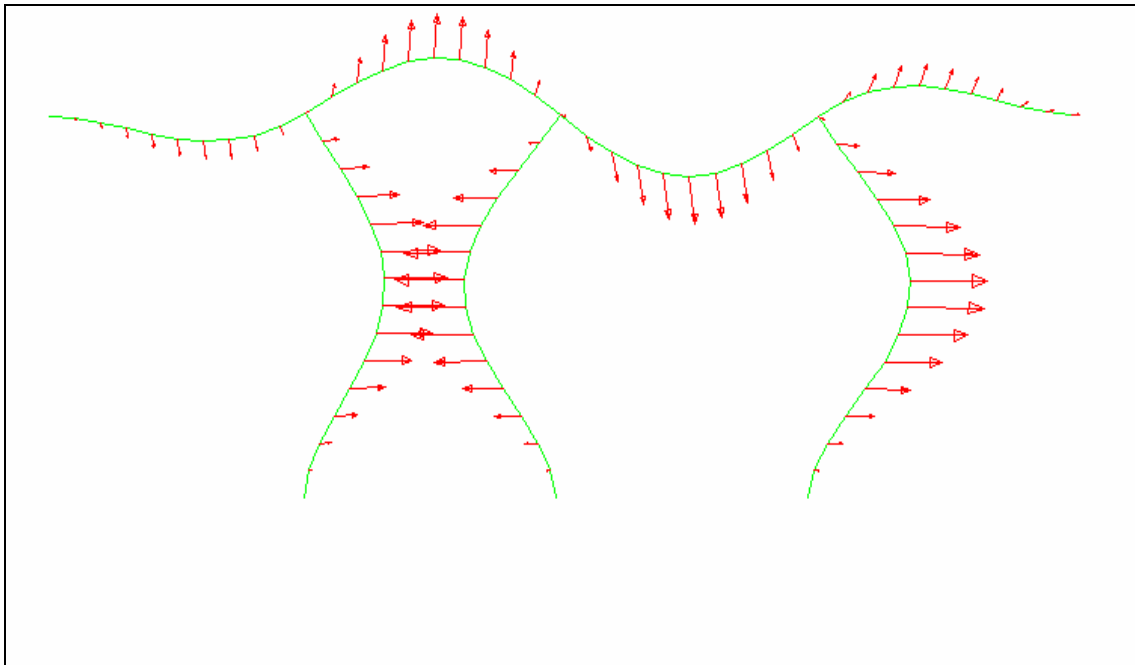


Figure A.3 The 3rd Mode Shape of the Bridge in Figure II.5

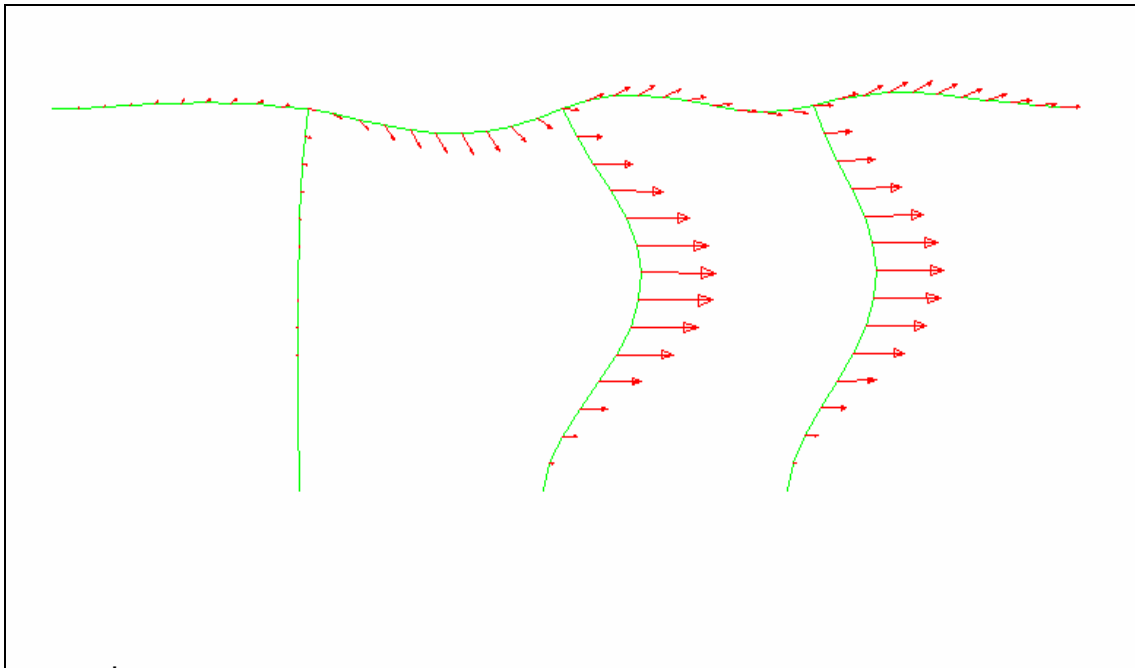


Figure A.4 The 4th Mode Shape of the Bridge in Figure II.5

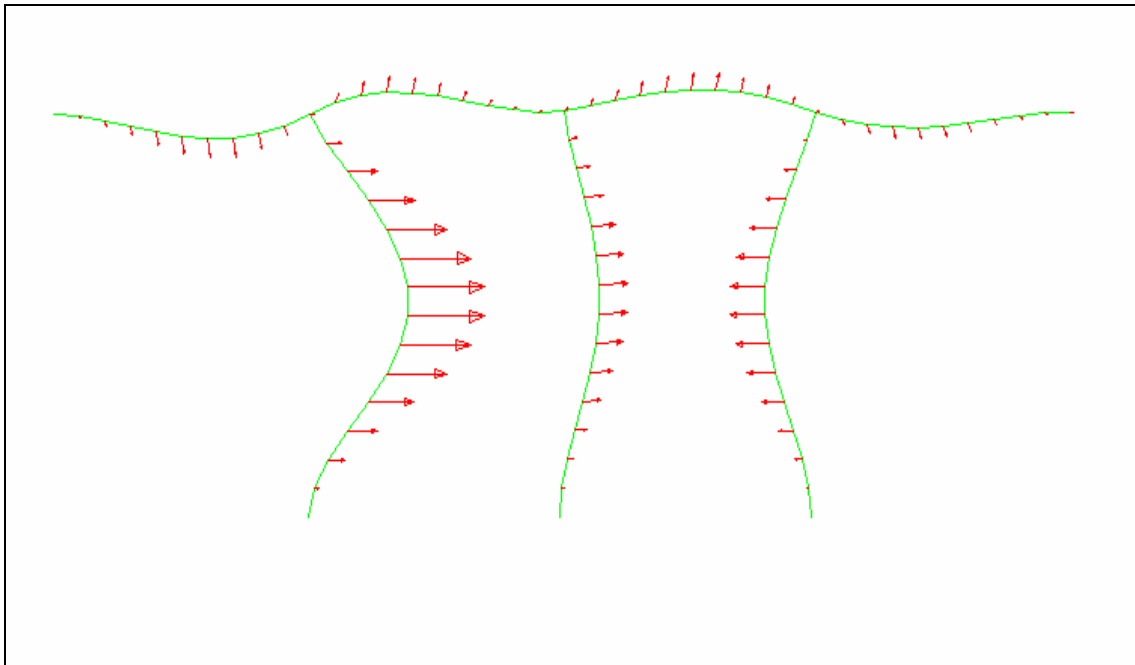


Figure A.5 The 5th Mode Shape of the Bridge in Figure II.5

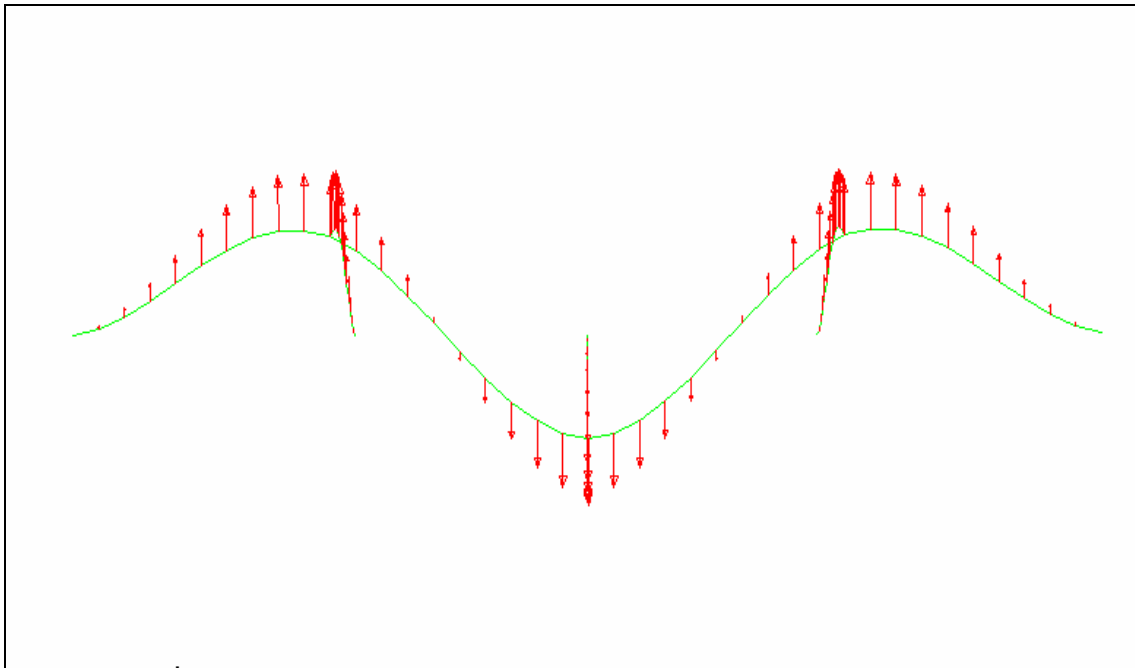


Figure A.6 The 6th Mode Shape of the Bridge in Figure II.5

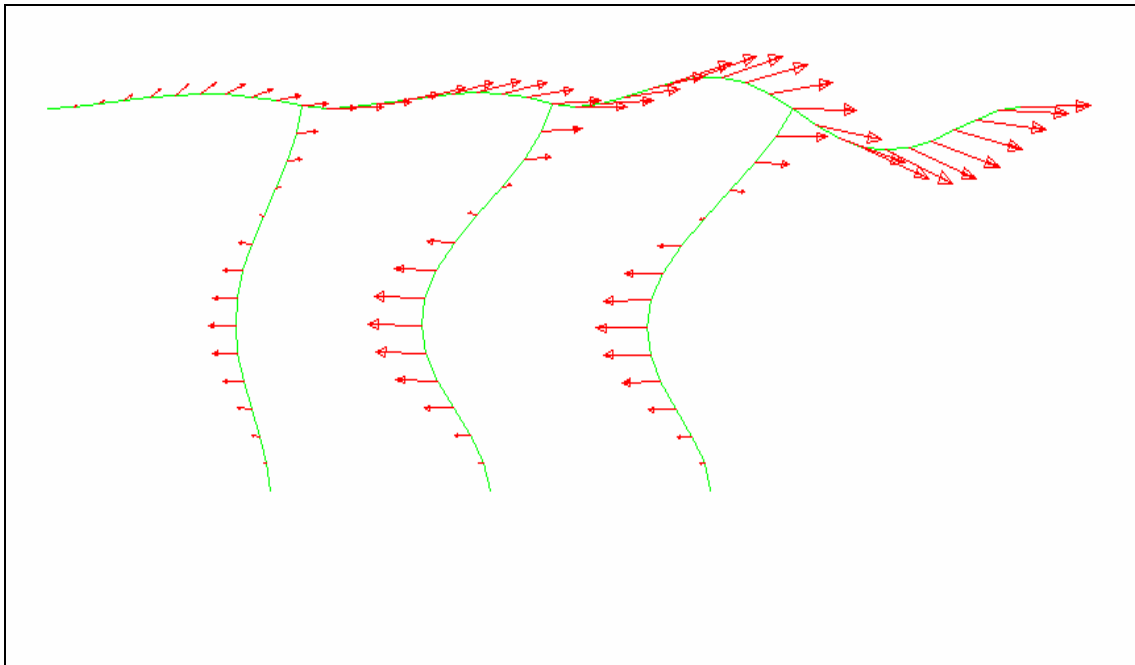


Figure A.7 The 7th Mode Shape of the Bridge in Figure II.5

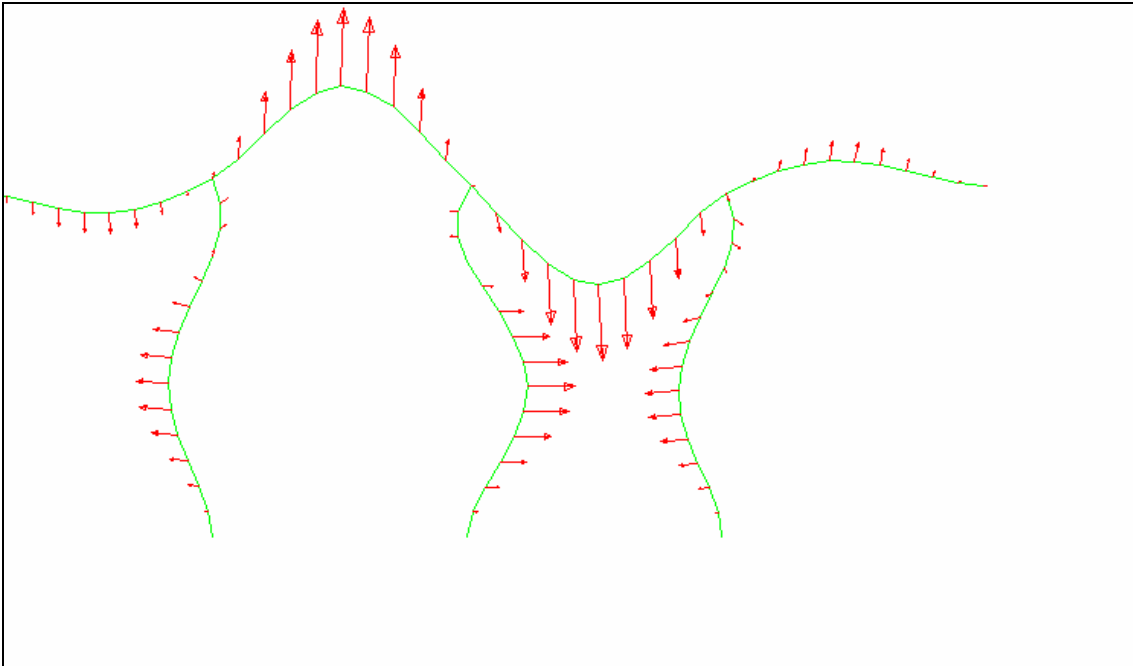


Figure A.8 The 8th Mode Shape of the Bridge in Figure II.5

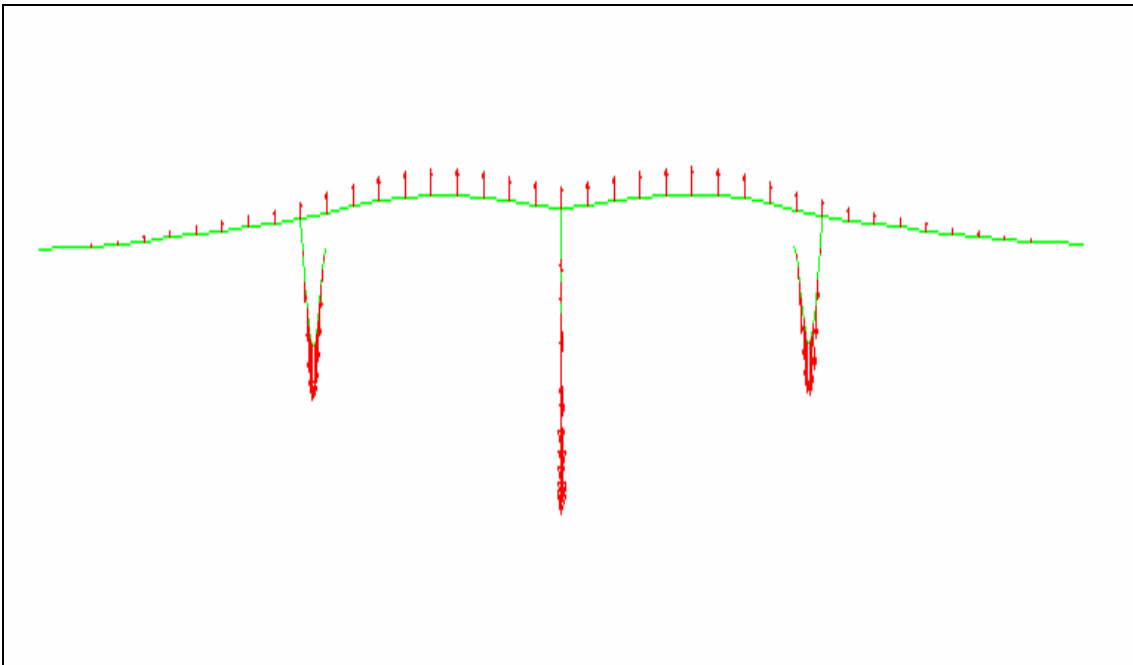


Figure A.9 The 9th Mode Shape of the Bridge in Figure II.5

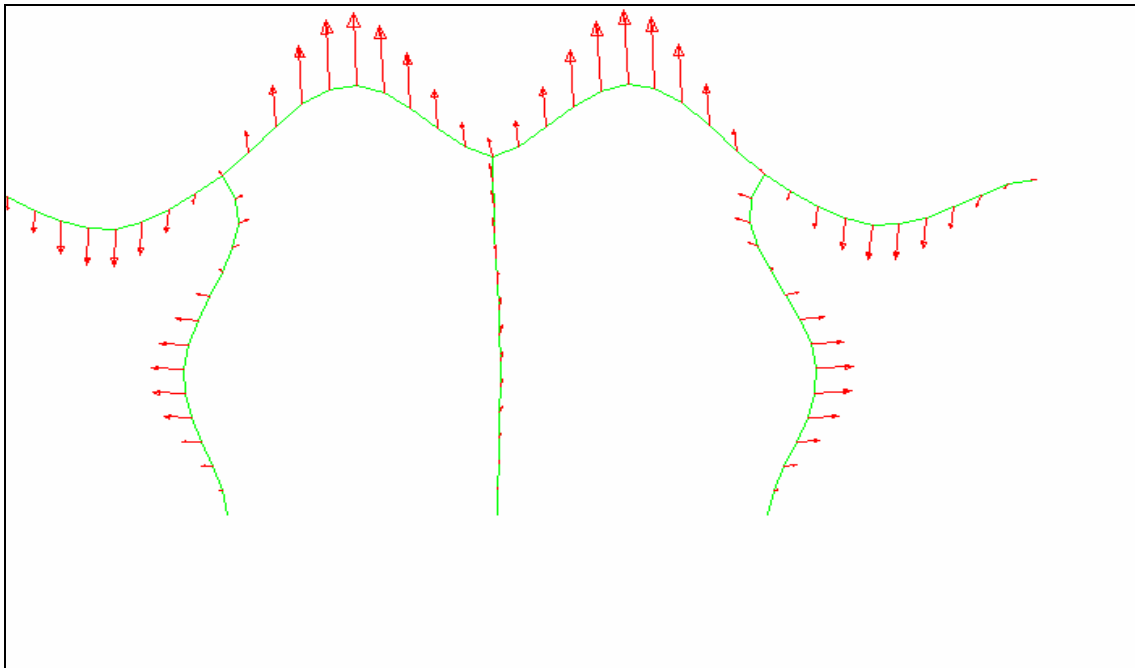


Figure A.10 The 10th Mode Shape of the Bridge in Figure II.5

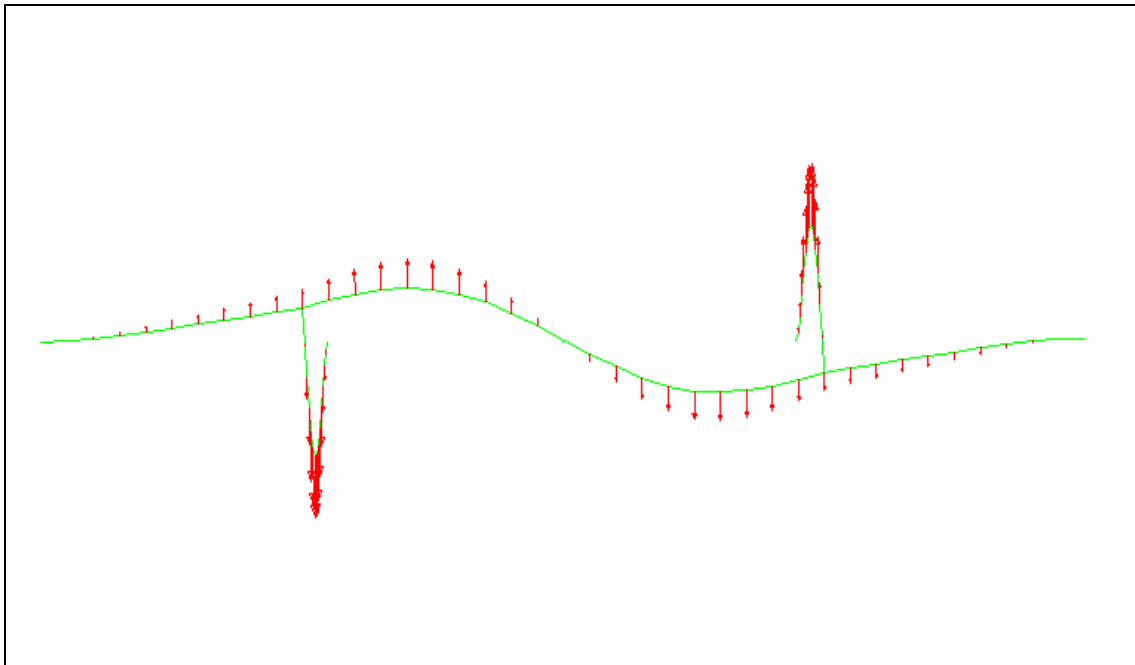


Figure A.11 The 11th Mode Shape of the Bridge in Figure II.5

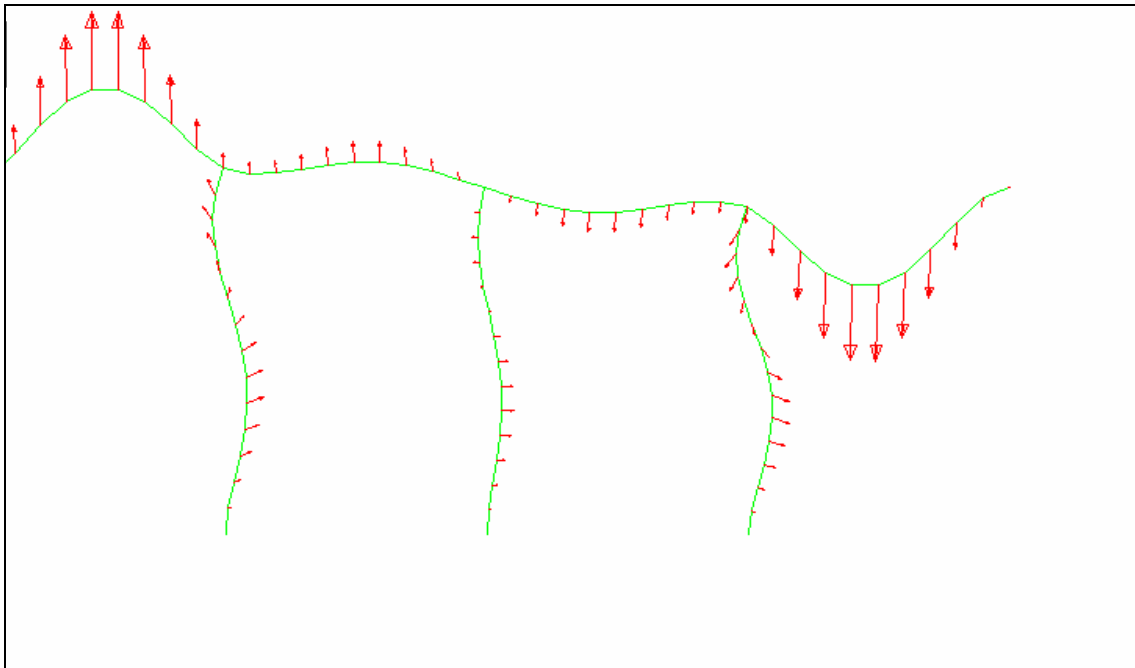


Figure A.12 The 12th Mode Shape of the Bridge in Figure II.5

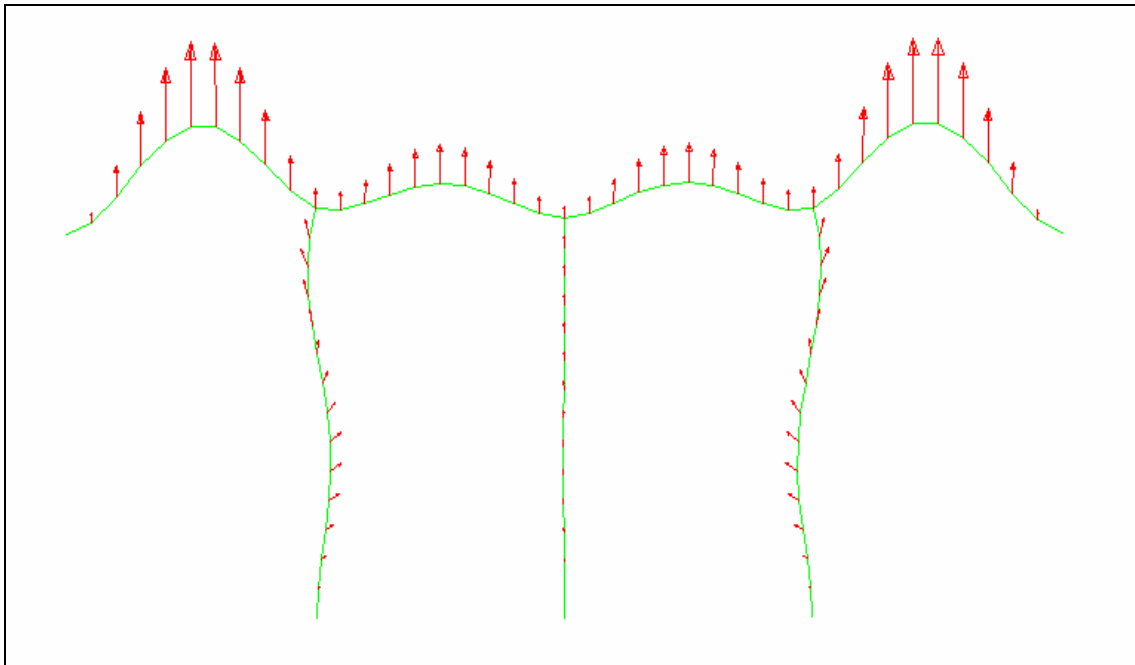


Figure A.13 The 13th Mode Shape of the Bridge in Figure II.5

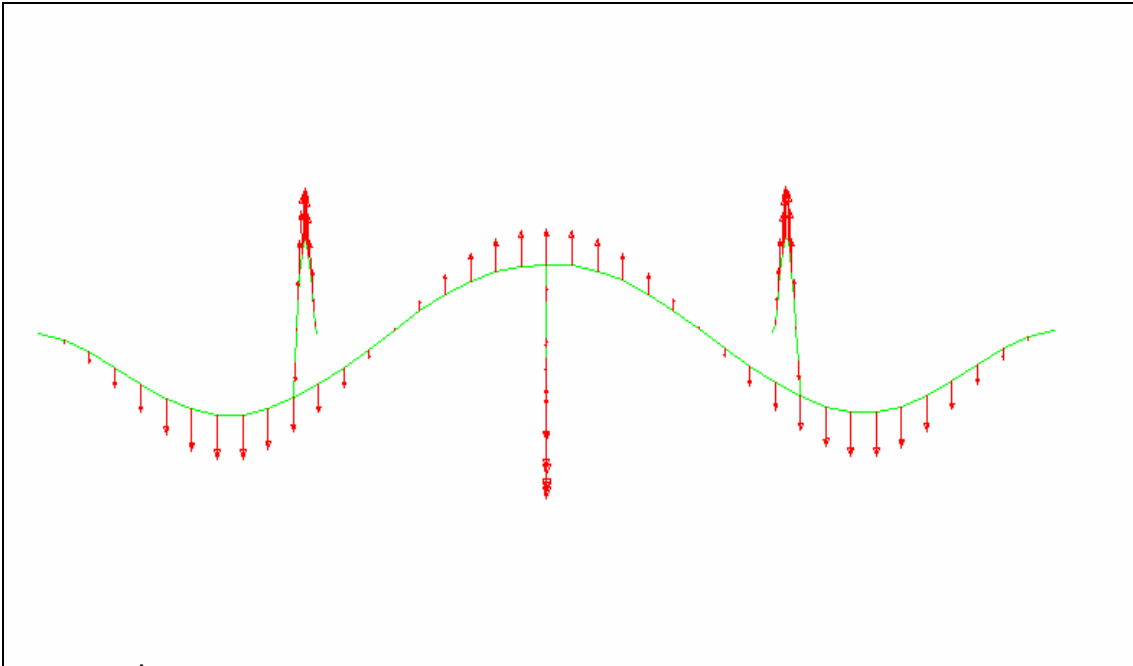


Figure A.14 The 14th Mode Shape of the Bridge in Figure II.5

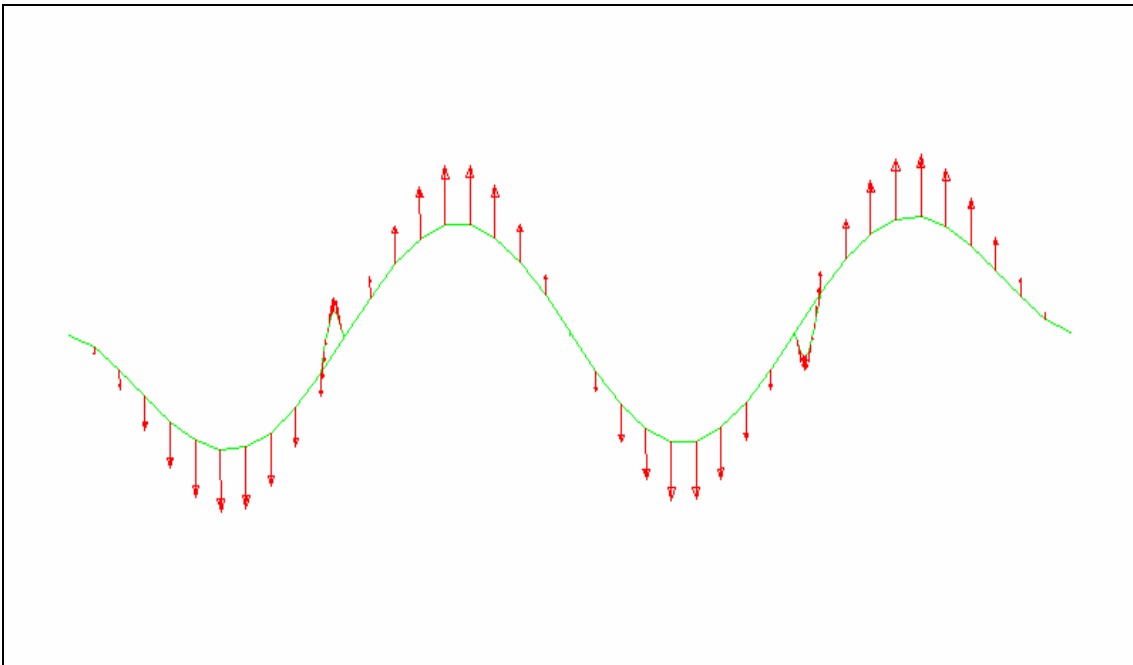


Figure A.15 The 15th Mode Shape of the Bridge in Figure II.5

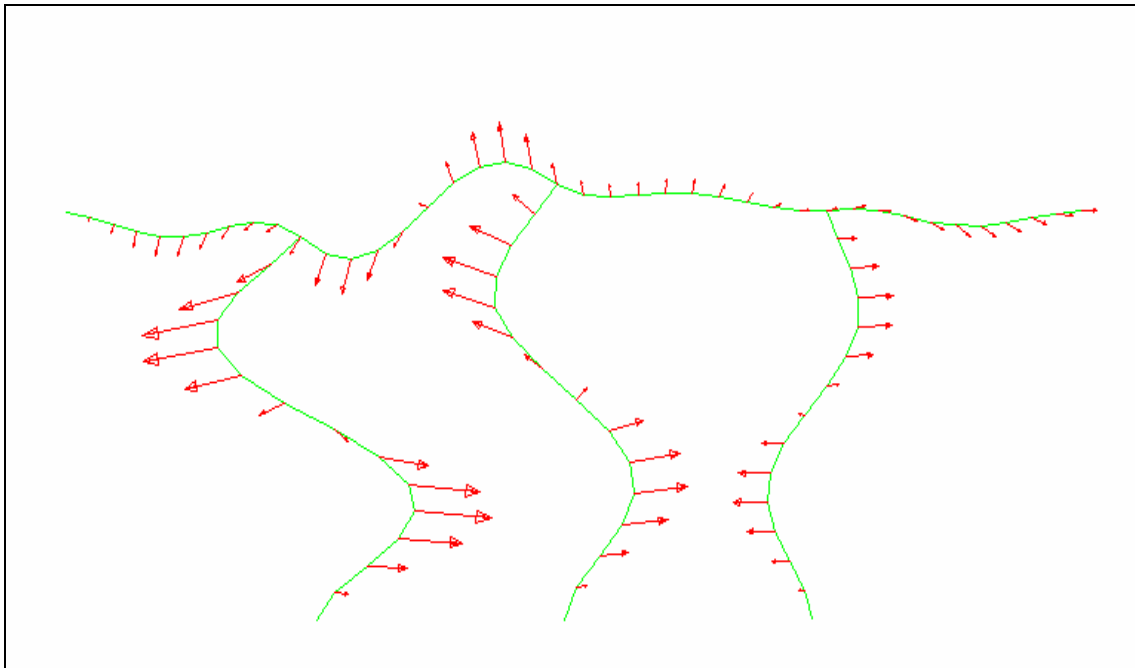


Figure A.16 The 16th Mode Shape of the Bridge in Figure II.5

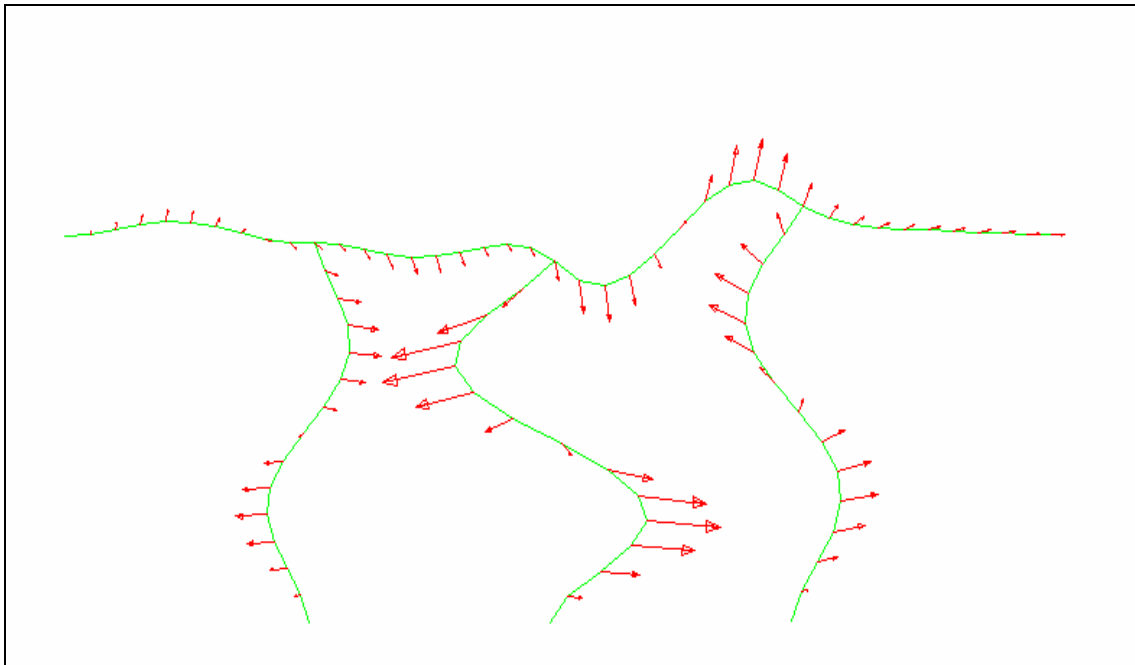


Figure A.17 The 17th Mode Shape of the Bridge in Figure II.5

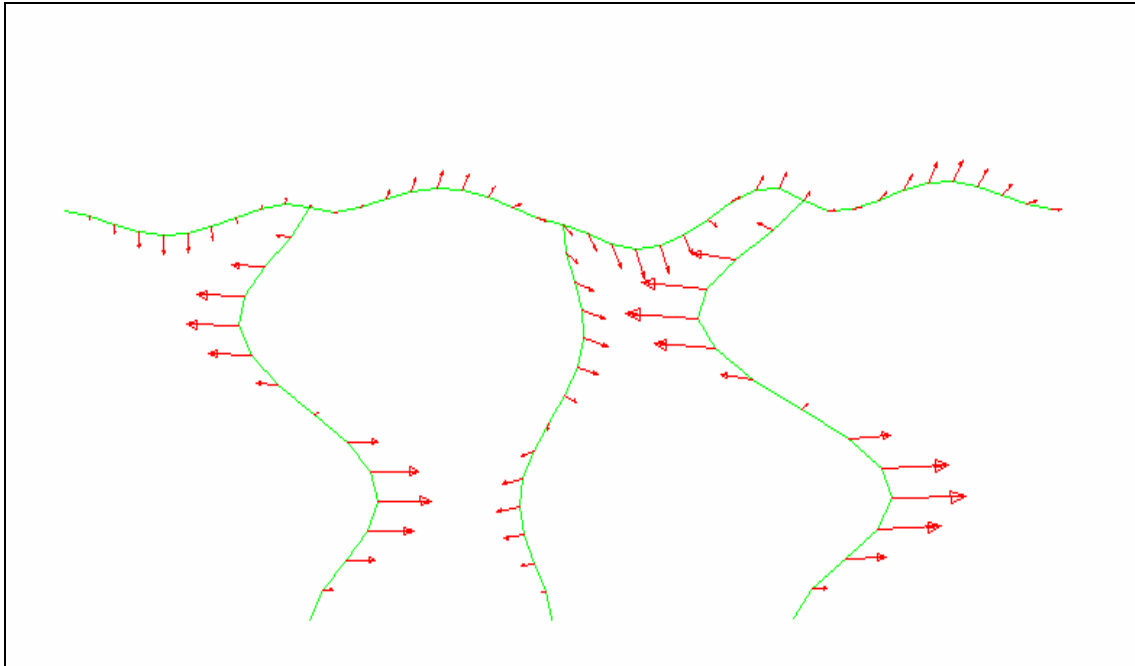


Figure A.18 The 18th Mode Shape of the Bridge in Figure II.5

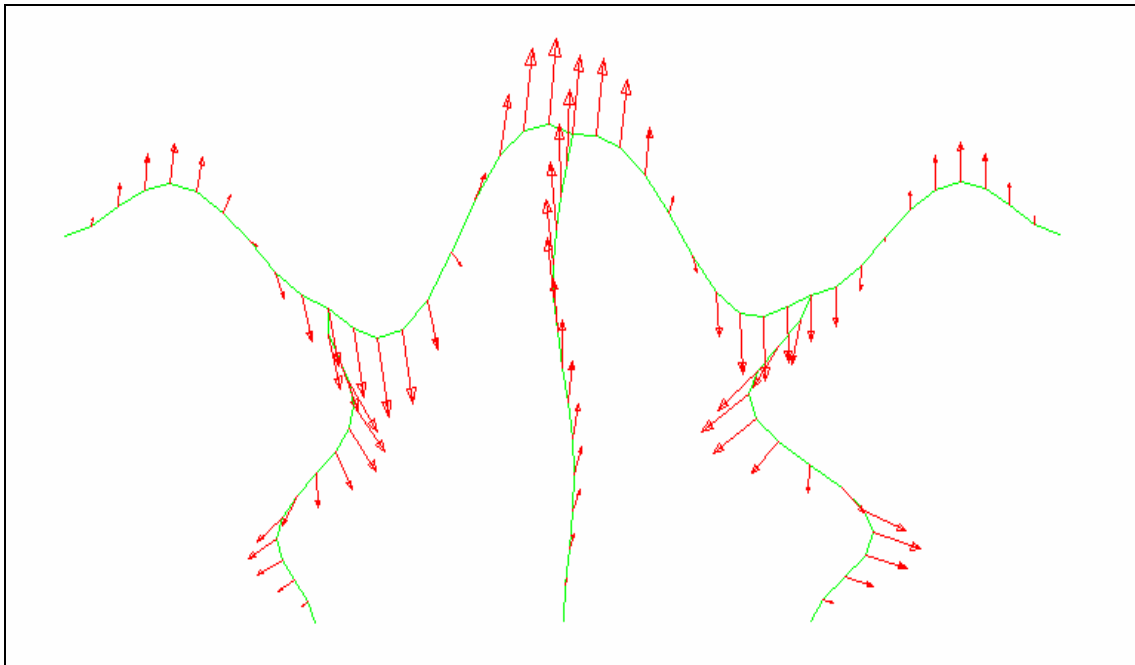


Figure A.19 The 19th Mode Shape of the Bridge in Figure II.5

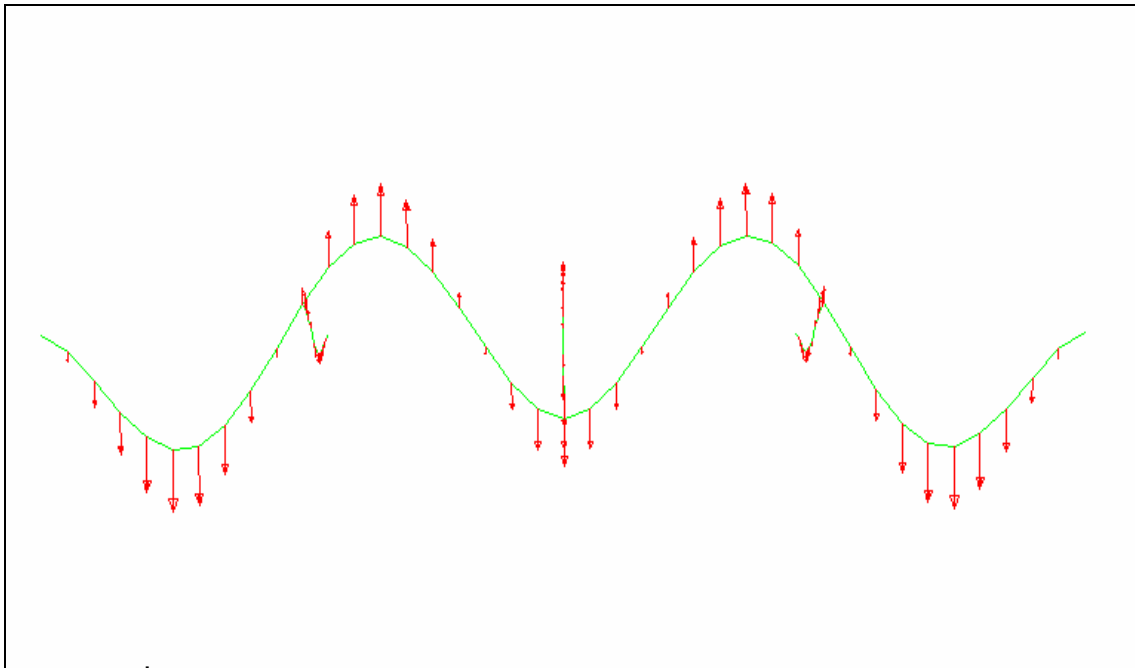


Figure A.20 The 20th Mode Shape of the Bridge in Figure II.5

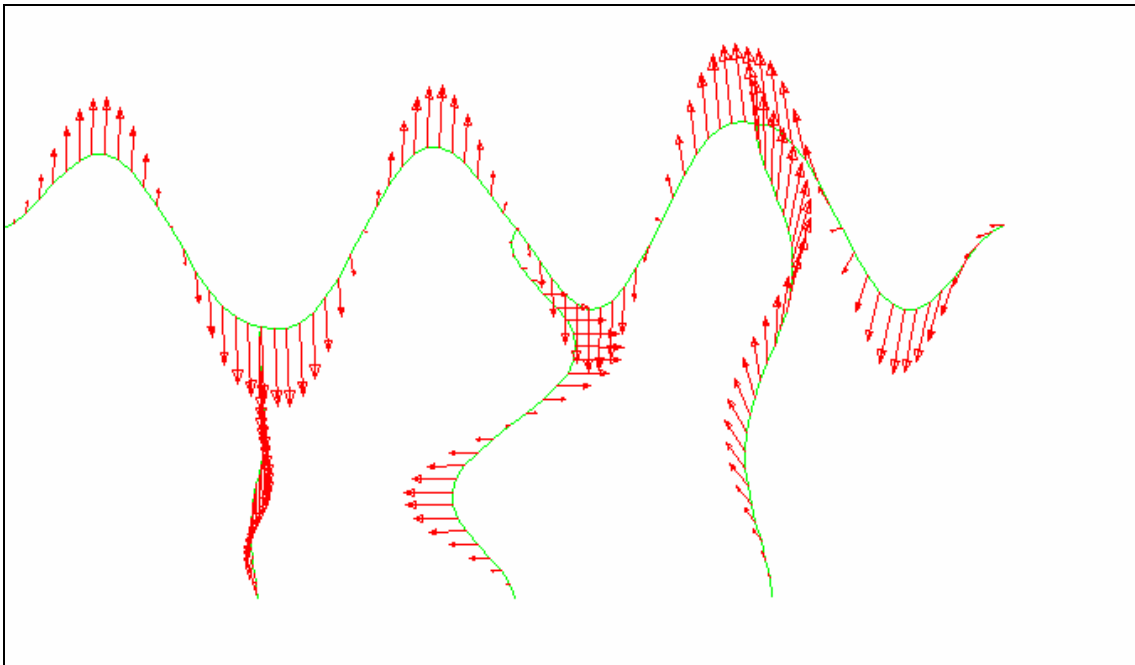


Figure A.21 The 21st Mode Shape of the Bridge in Figure II.5

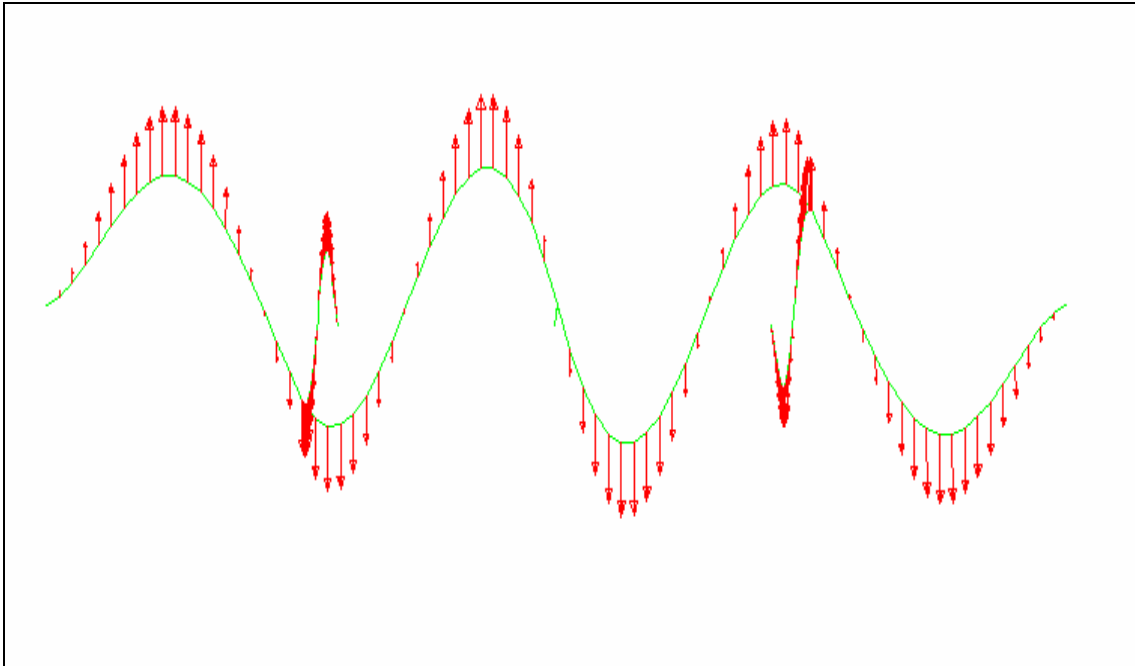


Figure A.22 The 22nd Mode Shape of the Bridge in Figure II.5

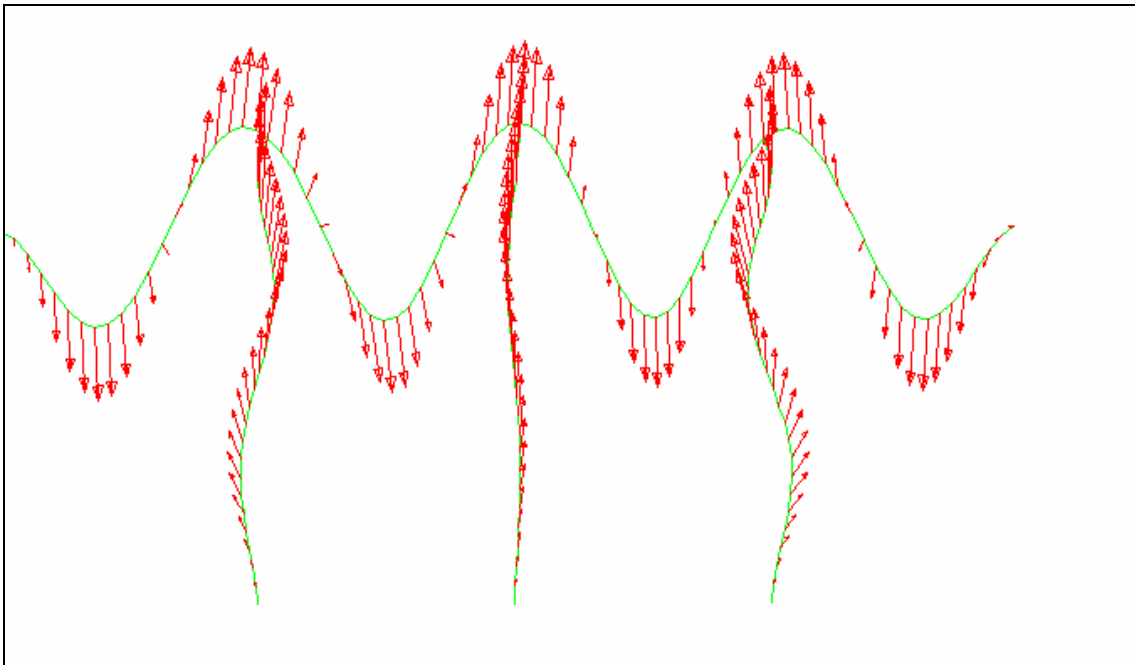


Figure A.23 The 23rd Mode Shape of the Bridge in Figure II.5

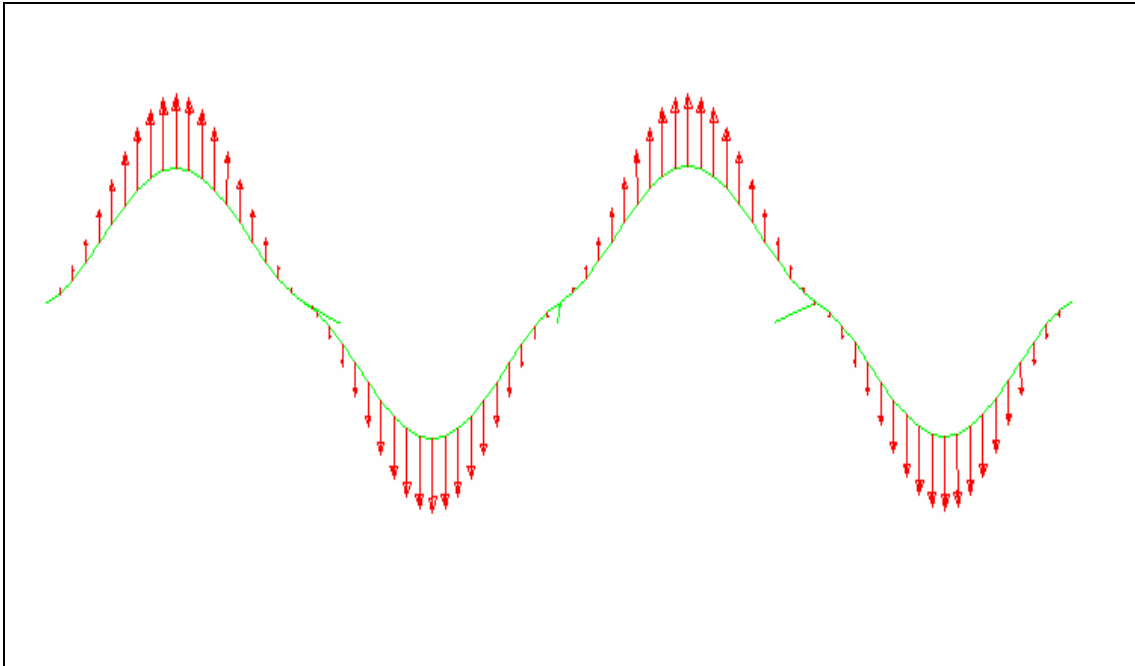


Figure A.24 The 24th Mode Shape of the Bridge in Figure II.5

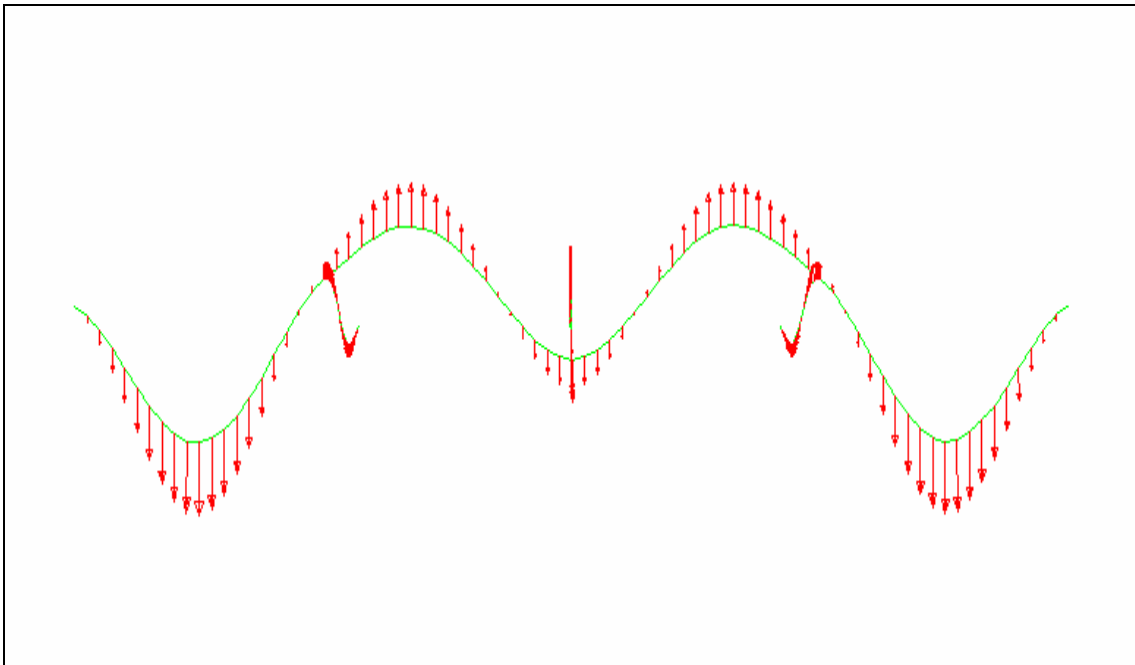


Figure A.25 The 25th Mode Shape of the Bridge in Figure II.5

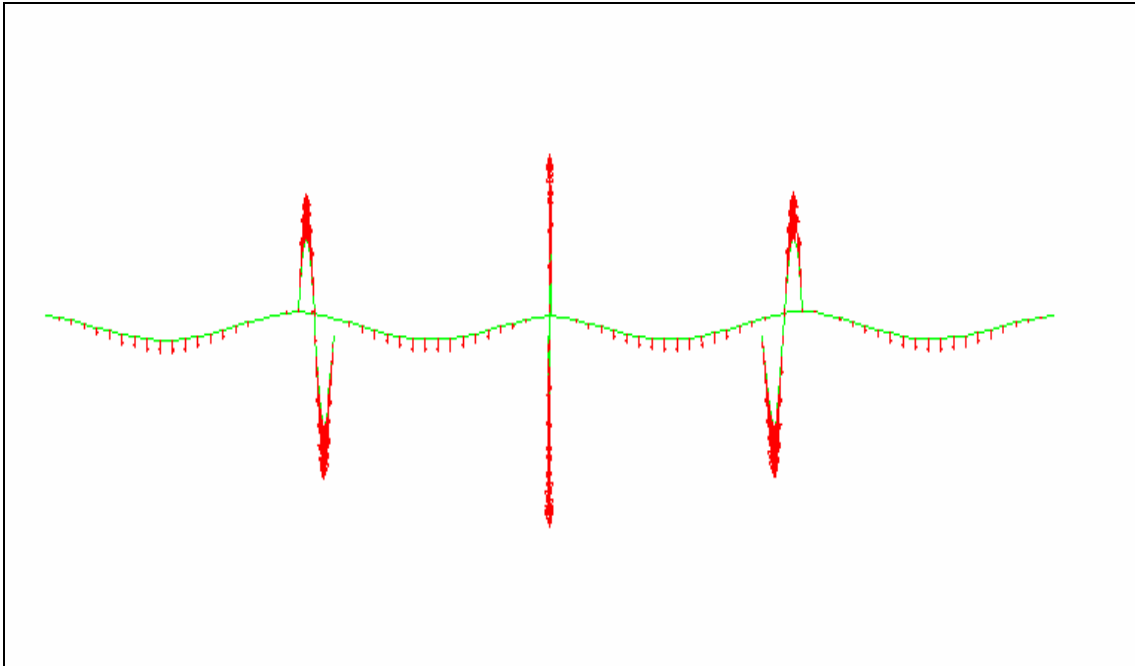


Figure A.26 The 26th Mode Shape of the Bridge in Figure II.5

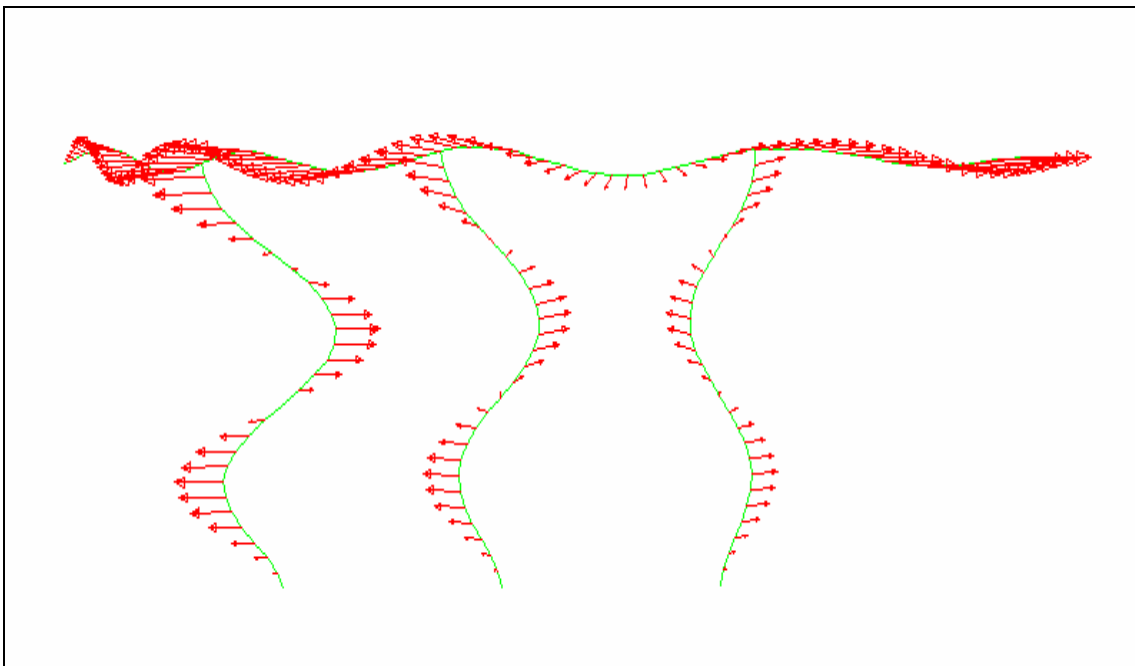


Figure A.27 The 27th Mode Shape of the Bridge in Figure II.5

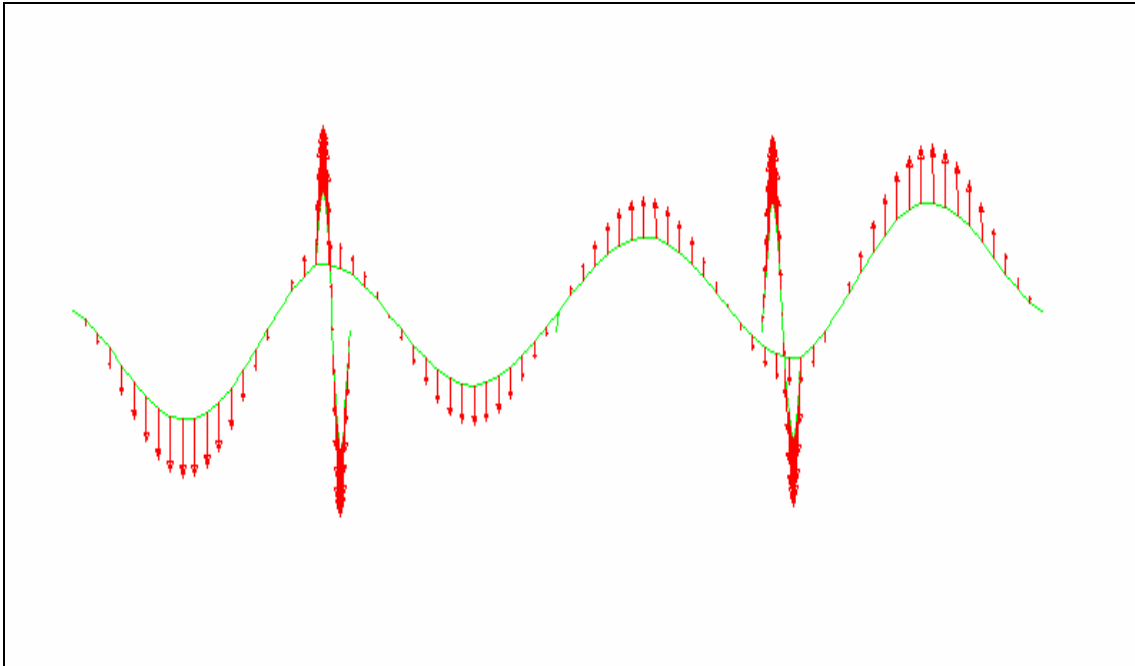


Figure A.28 The 28th Mode Shape of the Bridge in Figure II.5

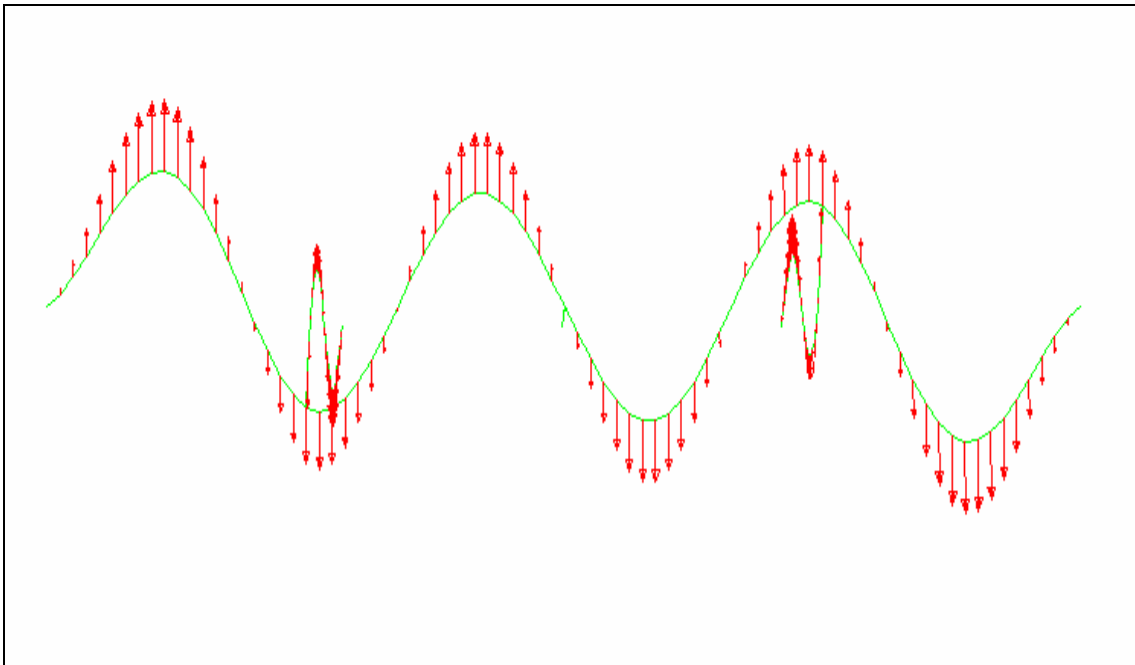


Figure A.29 The 29th Mode Shape of the Bridge in Figure II.5

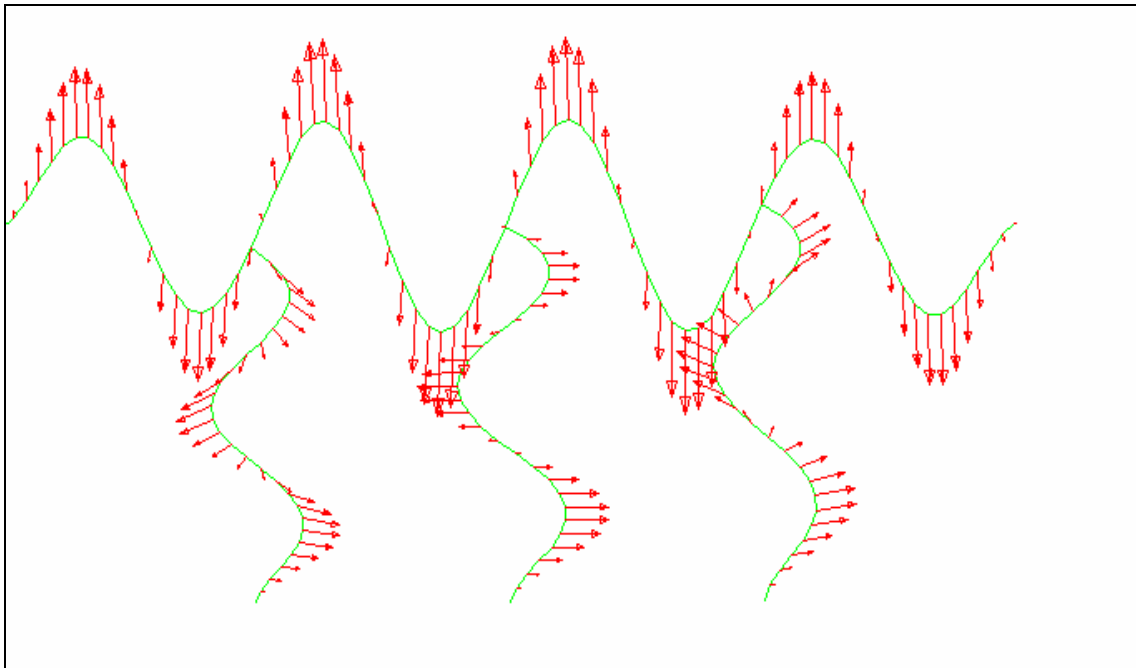


Figure A.30 The 30th Mode Shape of the Bridge in Figure II.5

VITA

Wentao Dai was born in Qingdao, China in August 1976. He received his B.En. and M.S. degrees in civil engineering from Tongji University, Shanghai, China in July 1999 and March 2002, respectively.

His permanent address and email address are:

4 Le An Er Rd. Apt. 2-302, Qingdao, Shandong 266044, China

daiwentao@gmail.com.